Entropy Generation in a Nanofluid Flow Through Ducts with Magnetic Effect

A Thesis Submitted to
NATIONAL INSTITUTE OF TECHNOLOGY WARANGAL, (T.S.)
for the award of the degree of
DOCTOR OF PHILOSOPHY
in
MATHEMATICS

by
SHAFEEURRAHMAN MD.
(Roll No. 714049)

under the supervision of
Dr. D. SRINIVASACHARYA

Department of Mathematics
National Institute of Technology Warangal
Telangana State, India

July 2017

C E R T I F I C A T E

This is to certify that the thesis entitled " **Entropy Generation in a Nanofluid Flow Through Ducts with Magnetic Effect** " submitted to National Institute of Technology Warangal, for the award of the degree of ***Doctor of Philosophy***, is the bonafide research work done by **Mr. SHAFEEURRAHMAN MD.** under my supervision. The contents of this thesis have not been submitted elsewhere for the award of any degree.

Dr. D. Srinivasacharya
Associate Professor
Department of Mathematics
National Institute of Technology,
Warangal - 506004, T.S., INDIA

.

Dedicated to

My Family & My Supervisor

ACKNOWLEDGEMENTS

It is a rare privilege and boon that I could associate myself for pursuing my research work with Dr. D. Srinivasacharya, Associate Professor of Mathematics, National Institute of Technology Warangal, India. I sincerely record my gratitude for his invaluable guidance and constant encouragement throughout the preparation of this thesis and his involvement and meticulous supervision while my work was in progress. With his inimitable qualities as a good teacher, he chiseled my path towards perfection. Ever since I met him, he has been a perpetual source of inspiration, divine guidance, encouragement and enlightenment. He is responsible for making the period of my research work as an educative and enjoyable learning experience. He has been a great source of motivation and inspiration. The thesis would not have seen the light of the day without his unrelenting support and cooperation. I deem it a privilege to have worked under his amiable guidance. My vocabulary is inadequate to express my gratitude.

I am grateful to Prof. Debashis Dutta, Head of the Department, Prof. G. Radhakrishnamacharya, Prof. Y. N. Reddy and Prof. K. N. S. Kasi Viswanadham, Professors of the Department of Mathematics, for providing necessary help and support throughout the period of my research work.

I take this opportunity to thank the members of the Doctoral Scrutiny Committee, Prof. J. V. Ramana Murthy and Dr. Ch. Ramreddy, Department of Mathematics and Dr. S. Srinath, Department of Chemical Engineering for their valuable suggestions, moral support and encouragement while my work was in progress.

I place on record my gratitude to all the Faculty members of the Department of Mathematics, for their constant encouragement. Also, I am grateful to Prof. D. S. Kesava Rao, Head, Department of Humanities and Social Sciences and Dr. M. Raja Vishwanathan for their kind support.

I express my sincere thanks and gratitude to the Director, National Institute of Technology, Warangal for awarding me Institute Fellowship (QIP) to carry out my research work. I thank him for his kind support and encouragement at every stage of this endeavor.

I owe my special thanks to Dr. K. Kaladhar, N I T Pondicherry, Dr. M. Krishna Prasad, N I T Raipur, Dr. O. Surender, N I T Mizoram, Dr. G. Swamy Reddy, Dr. M. Upendar, Dr. P. Vijay Kumar, Dr. G. Madhava Rao, Dr. K. Himabindu for their continuous support. I thank Mrs. T. Pradeepa, Mr. P. Jagadeeshwar, Mr. G. Venkata Suman, Mr. Ch. Venkata Rao, Mr. I. Sreenath, Mr. P. Naveen and my friends, who helped me during my Ph.D and all other Research colleagues in the Department for being cooperative and also for making my stay in the NIT campus fruitful and enjoyable every moment.

I am very much grateful to my parents Md. Jillurrahaman and Tahera begum, my in-laws Md Ghalib and Faheem Shaheda my sister Tasleem Jahan and my brother Md. Faizurrahman whose encouragement gave me the determination to complete my work ahead of time. Their love and affection has been motivating force behind what I am today.

Last but not least, I would like to thank my better half Sufiya Naheed and my innocent daughters Shaafiya and Shaaziya for their prayers, patience, encouragement and understanding that were vital to complete this dissertation. Without their help and encouragement, I would not have been finished this thesis.

. SHAFEEURRAHMAN MD.

A B S T R A C T

Entropy and entropy generation are fundamental quantities. They play essential role in understanding the performance of engineering devices. Minimizing entropy generation is important to improving the efficiency of any system. To optimize the performance of engineering systems containing devices the irreversibilities of individual devices must be minimized. Since the total irreversibility of a system is the sum of the component irreversibilities, this procedure improves the system performance. In order to preserve the quality of energy in a fluid flow process or at least to reduce the entropy generation, it is important to study the distribution of the entropy generation within the fluid volume. Nanofluids are fluids that contain small volumetric quantities of nanoparticles. Nanofluid is the nanotechnology based that exhibit thermal properties superior to those of their base fluids. These are more susceptible to the influence of magnetic field than the conventional base fluids. The study of entropy generation due to nanofluid flows in different geometries has important applications in physics and engineering. Hence, this thesis describes the entropy generation due to nanofluid flow through vertical channels, cylindrical annulus and infinite rotating parallel disks in the presence of Hall, ion-slip, Joule heating, radiation and chemical reaction effects.

The thesis consists of FIVE parts and TEN chapters. Part-I consists of a single chapter (Chapter - 1), which provides an introduction to the concepts and a review of the pertinent literature. Second part contains three chapters (i.e. Chapters 2, 3 and 4). Chapters 2 deals with Hall and ion-slip effects on natural and mixed convection heat transfer flow of nanofluid in vertical channel, Chapters 3 and 4 are extensions of chapters 2 in which the effect of thermal radiation Joule heating and chemical reaction on entropy generation and Bejan number are studied. The third part contains three Chapters (Chapters 5, 6 and 7) and deals with convective heat transfer flow of a nanofluid in between concentric cylinders with Hall, ion-slip, thermal radiation, Joule heating and chemical reaction effects. Fourth part contains two chapters (Chapters 8 and 9) and deals with the entropy generation due to nanofluid flow through the parallel disks in the presence of Hall, ion-slip, Joule heating, radiation and chemical reaction effects. In all the above chapters, the governing equations and the corresponding boundary conditions are initially cast into dimensionless form by using suitable transformations. The resulting system of equations are solved using Homotopy Analysis Method. The effects of Hall, ion-slip, Joule heating, radiation and chemical reaction on the velocity, temperature, nanofluid concentration as well as entropy generation rate and Bejan number are presented through graphs. The fifth part contains only one chapter (Chapter - 10) which gives summary and overall conclusions and scope for future work.

NOMENCLATURE

A	constant pressure gradient
a	radius of the inner cylinder
b	radius of the outer cylinder
Be	Bejan number
B_0	uniform magnetite field
Br	Brinkman number
C_p	specific heat at constant pressure
D	Mass diffusivity
D_B	Brownian diffusion coefficient
D_T	Thermophoretic diffusion coefficient
d	channel width
f	dimensionless transverse velocity
g	Indused velocity
Gr	Grashof number
g^*	acceleration due to gravity
h	channel width
Ha	Hartman number
J	Joule heating parameter
k	thermal conductivity
K	chemical reaction parameter
k_1	rate of chemical reaction
K_f	thermal conductivity of the fluid
Le	Lewis number
M	magnetic parameter
Nb	Brownian motion parameter
Nh	entropy generation due to heat transfer
$N\vartheta$	entropy generation due to viscous dissipation
Nm	entropy generation due to magnetic effect
Nr	Buoyancy ratio is
Ns	dimensionless entropy generation number
Nt	Thermophoresis parameter
p	Pressure
Pr	Prandtl number
qr	Radiation heat flux
R	suction or injection Reynolds number
Rd	Radiation parameter
Re	Reynolds number
Ru	universal gas constant
S	dimensionless nanoparticle concentration

S_G	entropy generation volumetric rate
T	dimensional temperature
T_m	Mean fluid temperature
u	dimensional axial velocity
v	dimensional transverse velocity
U_0	characteristic velocity
V_0	injection velocity
V_1	suction velocity

Greek Symbols

α	effective thermal diffusivity
βh	Hall parameter
βi	ion-slip parameter
β_T	coefficients of thermal expansion
γ	rotating rate parameter
ρ	density of the fluid
χ	mean absorption coefficient
θ	dimensionless temperature
μ	viscosity of the fluid
ϕ	nanoparticle concentration
υ	kinematic viscosity coefficient
σ	electrical conductivity
σ^*	Stefan-Boltzman constant
Ω	angular velocities
Ω_1, Ω_2	rotating speeds of lower and upper disks
Ω_3, Ω_4	temperature and concentration ratios

Contents

[1]Type - I: Published in "**Frontiers in Heat and Mass Transfer, (2017), Vol.8,11**", Type - II: Published in "**Journal of Nanofluids, Vol. 5 (2016), 982–992**"

[2]Published ins "**International Journal of Engineering and Technology, Vol.9, No. 4(2017)** "

[3]Communicated to "**Chemical Industry and Chemical Engineering Quarterly, (2017)**"

[4]Type - I: Published in "**Journal of the Association of Arab Universities for Basic and Applied Sciences,Vol. 24(2017), 223–231**", Type - II: Communicated to "**Propulsion and Power Research**"

[5] Published in "**Journal of Nanofluids, Vol. 6(2017), 1227–1237**"

[6] Published in "**International Journal of Heat and Technology, Vol. 35, No. 3(2017), 487–497**"

[7] Communicated to "**Journal of the Brazilian Society of Mechanical Sciences and Engineering**"

[8] Communicated to "**Journal of King Saud University - Science**"

Part I

INTRODUCTION

Chapter 1

Introduction

The problems on laminar flow of a fluid between vertical parallel plates, concentric cylinders and rotating circular disks are of interest to researchers, as they constitute a good approximation to the flows that are commonly encountered in an engineering and technology. The vertical channel configuration is relevant to solar energy collectors, transpiration cooling, gaseous diffusion technology, cooling of rocket, mechanized irrigation and filtration processes, thermal insulation engineering, etc. A commonly occurring geometry in electrical machineries, microelectronic devices, industrial heat exchangers, a growth of single silicon crystals, motion of a planetary atmosphere, etc., is the annulus between concentric cylinders, in which one or both the cylinders are rotating. The geometry of rotating disks has special technical importance in rotating machinery, crystal growth process, computer storage devices, chemical engineering, agricultural engineering, etc.

The improvement of thermal systems have gained a growing interest due to the relations with the problems of material processing, energy conversion and environmental effects. Efficient energy utilization during any fluid flow is one of the fundamental problems of the engineering processes to improve the system. One of the powerful tools used for the improve-

ment of performance of the engineering processes are the minimization of entropy generation.. Hence, the contemporary trend in the field of heat transfer and thermal design is to perform analysis of the entropy generation and its minimization. This new trend is important and, at the same time, it is necessary to contribute to a viable engineering solution to the energy problems.

One of the frequently encountered challenge by the technological industries, such as microelectronics, defense, metrology, nuclear reactors, power generation, thin film solar energy collectors, manufacturing etc., is cooling. Liquid cooling is necessary when the heat flux is more in electronic devices. The phenomenal increase in the thermal conductivity of fluids with an addition of small volumes of nanoparticles has created tremendous interest in the techniques of heat transfer enhancement. Nanofluids are referred to as safe coolants for nuclear reactors and smart coolants for computers, i.e. next generation coolants. When nanofluids are used to improve the design and performance of thermal management systems, they offer several benefits, including improved reliability, reduction in cooling system size, decreased pumping-power needs, increased energy and fuel efficiencies, and lower pollution. Thus, nanofluids can have a significant impact in cooling a number of high-heat-flux devices and systems used in the consumer, industrial and defense industries. The full heat transfer potential of these nanofluids may be exploited with the acquaintance of underlying mechanism of heat transfer in these fluids.

1.1 Nanofluids

The utilization of regular fluids, for example, water, ethylene glycol and engine oil in numerous engineering and industrial applications restricts the heat transfer abilities because of their poor heat transfer properties. The low thermal conductivity of the ordinary heat transfer liquids is an essential restriction in upgrading the performance and the compactness of many designing electronic gadgets. The proposed traditional approach to upgrade heat transfer in thermal system frameworks is to expand the heat transfer surface area of cooling gadgets and the flow velocity or to scatter solid particles in heat transfer liquids.

The idea of utilizing suspensions of solid particles to improve thermal conductivity of traditional heat transfer liquids was originated by Maxwell [56]. By scattering millimeter or micrometer-sized particles in fluids, Maxwell could improve the thermophysical properties of base liquids. However, significant issues, for example, abrasion, clogging micro channel and high pressure drop prevented the usual microparticle slurries to be utilized as heat transfer liquids. On account of these reasons, the millimeter or micrometer particles suspension was rejected in heat transfer application. After a century, Maxwell's thought was re-examined by Choi [21] and he utilized the suspensions of nanoparticle in conventional base liquids with no dispersants.

Nanofluid is the term initially coined by Choi [21] to define another class of heat transfer liquids that display thermal properties better than those of their base liquids. Nanofluids are fluids that contain little volumetric amounts of nanometer-sized particles, called nanoparticles. Choi [21] experimentally checked that the inclusion of nanoparticles in ordinary base liquids significantly improved the thermal conductivity. Nanofluid is the nanotechnology based heat transfer fluid that can be prepared by stably suspending nanometer-sized particles in regular liquids. Nanofluids have higher thermophysical properties, such as, viscosity, thermal diffusivity, thermal conductivity, and convective heat transfer coefficients contrasted with those of base liquids. Typical thermal conductivity improvements are in the scope of $15\% - 40\%$ over the base liquid and heat transfer coefficient improvements have been found up to 40% *et al* [95]. The objective of nanofluids is to accomplish the most elevated conceivable thermal properties at the littlest conceivable concentrations (ideally < 1 by volume) by uniform scattering and stable suspension of nanoparticles (ideally $< 10nm$) in host liquids. Additionally, the presence of nanoparticles improves the electrical conductivity of the nanofluids, henceforth are more vulnerable to the impact of magnetic field than the traditional base fluids.

Several models and methods have been suggested in the literature to investigate the convective flows of nanofluids. Among them, Tiwari-Das model [88] and Buongiorno model [13] are often used by researchers to study the heat transfer improvement in nanofluids.

Tiwari-Das Model

Tiwari and Das [88] developed a model to analyze the behaviour of nanofluids by taking the volumetric fraction of nanparticles into consideration. Using this model, the basic governing equations are given by

$$\nabla \cdot \bar{\mathbf{V}} = 0 \tag{1.1}$$

$$\rho_{nf}(\bar{\mathbf{V}} \cdot \nabla)\bar{\mathbf{V}} = -\nabla p - (\rho\beta)_{nf}(T - T_\infty)]\bar{\mathbf{g}} + \mu_{nf}\,\nabla^2\bar{\mathbf{V}} \tag{1.2}$$

$$\bar{\mathbf{V}} \cdot \nabla T = \alpha_{nf}\nabla^2 T \tag{1.3}$$

where $\bar{\mathbf{V}}$ is the velocity vector, T is the temperature of the nanofluid, $\rho\beta_{nf}$ is the buoyancy coefficient of the nanofluid, $\bar{\mathbf{g}}$ is the acceleration due to gravity, μ_{nf} is the viscosity of the nanofluid, α_{nf} is the thermal diffusivity of the nanofluid and ρ_{nf} is the density of the nanofluid, which are given by

$$\begin{aligned} \mu_{nf} = \frac{\mu_f}{(1-\phi)^{2.5}},\ \rho_{nf} = (1-\phi)\rho_f + \phi\rho_s,\ \rho C_{p_{nf}} = (1-\phi)\rho C_{p_f} + \phi\rho C_{p_s} \\ \alpha_{nf} = \frac{k_{nf}}{\rho C_{p_{nf}}},\ \frac{k_{nf}}{k_f} = \frac{(k_s + 2k_f) - 2\phi(k_f - k_s)}{(k_s + 2k_f) + \phi(k_f - k_s)} \end{aligned} \tag{1.4}$$

here ϕ is the solid volume fraction of the nanofluid, ρ_s and ρ_f are the density of the solid particle and base fluid, respectively, μ_f is the viscosity of the base fluid, k_f and k_s are the thermal conductivity of the base fluid and nanoparticle, respectively and k_{nf} is the effective thermal conductivity of the nanofluid approximated by the Maxwell-Garnett model (see Oztop and Abu-Nada [2]).

Buongiorno Model

Buongiorno [13] proposed a new model based on the mechanics of nanoparticle/base-fluid relative velocity. He identified seven slip mechanisms namely, Brownian diffusion, inertia, thermophoresis, fluid drainage, diffusiophoresis, magnus effect and gravity. They can generagte a relative velocity between the base fluid and nanoparticles and inferred that, of these

seven just thermophoresis and Brownian motion are critical slip mechanisms in nanofluids. Based on this study, he has finally developed an acceptable two-component four-equation non-homogeneous equilibrium model for mass, momentum, and heat transfer in nanofluids. This is the model which is being used to study the heat transfer problems theoretically. The basic governing equations for this model are given by

$$\nabla \cdot \bar{\mathbf{V}} = 0 \tag{1.5}$$

$$\rho_f \left(\bar{\mathbf{V}} \cdot \nabla \bar{\mathbf{V}}\right) = -\nabla p + [\phi\, \rho_s \ + (1-\phi)\rho_f \,(1-\beta)(T - T_\infty)]\bar{\mathbf{g}} + \mu\, \nabla^2 \bar{\mathbf{V}} \tag{1.6}$$

$$\bar{\mathbf{V}} \cdot \nabla T = \alpha\, \nabla^2 T + \tau \left[D_B \left(\nabla \phi . \nabla T\right) + \frac{D_T}{T_m} \left(\nabla T . \nabla T\right) \right] \tag{1.7}$$

$$\bar{\mathbf{V}} \cdot \nabla \phi = D_B \left(\nabla^2 \phi\right) + \frac{D_T}{T_m} \left(\nabla^2 T\right) \tag{1.8}$$

where ν is the kinematic viscosity of the nanofluid, α is the thermal diffusivity of the nanofluid, D_B is the Brownian diffusion coefficient, D_T is the thermophoretic diffusion coefficient and $\tau = (\rho c)_s/(\rho c)_f$, with $(\rho c)_f$ and $(\rho c)_s$ being the heat capacity of nanofluid and the effective heat capacity of the nanoparticle material, respectively.

1.2 Magnetohydrodynamics

Magnetohydrodynamics (MHD) deals with the dynamics of matter moving in an electromagnetic field, particularly where currents created in the matter by induction change the field. MHD is the study of magnetic properties of electrically conducting fluids. This subject has attracted numerous scientists and engineers for the last few decades because of its fascination and importance in various technological devices and in understanding the diverse cosmic phenomena. The applications MHD flows include droplets sprays, lubricant, polymer technology, power generation from two-phase mixtures, medical diagnostic devices, extrusion of molten polymers, cooling systems with liquid metals etc. MHD describes the frontier area combining classical fluid mechanics and electrodynamics. MHD phenomena are outcome of

mutual interaction between magnetic field and electrically conducting fluid flowing across it.

Consider an incompressible and electrically conducting fluid in the presence of an arbitrary magnetic field. A magnetic field in the medium will be induced due to the motion of a conducting liquid in an applied magnetic field. The total magnetic field is the sum of the induced and applied magnetic fields ($\overline{B} = \overline{B_0} + \overline{b}$, $\overline{b}$ is induced magnetic field). The assumption of electric field ($\vec{E}$) is of the same order of magnitude as the induced electric field ($\vec{q} \times \vec{B}$) allows to assume that the induced magnetic field is much smaller than the externally applied magnetic field. The magnetic Reynolds number characterizes the relative strength of the induced field. Assume that the electric energy is negligible compared to the magnetic energy. Since the displacement current and electric field energy are neglected, the main interaction is between the magnetic field and the fluid. Further, a force called Lorenz force ($\overline{J} \times \overline{B}$, where $\overline{J}$ is the current density) will act on the fluid and alter its motion when currents are induced by a motion of a conducting fluid through a magnetic field. The magnetic field, then interacts with the fluid by means of body force and body couple per unit mass. The current density vector $\vec{J}$ is approximately the same in any inertial frame. This means, using Ohm's law

$$\vec{J} = \sigma\Big[\vec{E} + \vec{q} \times \vec{B}\Big].$$

If gravitational effects are not present, then a regular magneto-fluid dynamics assumption is $\rho\overline{f} = \rho_e E + \overline{J} \times \overline{B}$, where ρ_e is the free charge density. Since, the electric force density $\rho_e E$ is smaller than $\overline{J} \times \overline{B}$, the electric force density can be neglected. Hence, the fluid dynamical aspects of MHD are handled by adding an electromagnetic force term to the momentum equation of the fluid.

1.3 Basic Terminology

Convection

The mechanism of exchange of heat energy as a result of a temperature gradient or temperature differences is determined by heat transfer. Heat transfer happens in three modes: conduction, convection and radiation. The heat transfer due to the movement of fluid from one region to the other region in the medium is called convection. The heat transfer by convection together with conduction is known as convective heat transfer. Convective heat transfer is further classified as *Forced Convection*, *Free Convection* and *Mixed Convection*.

Free/Natural Convection

Free convection flow is caused by buoyancy forces which emerge from the density changes in the fluid due to temperature and concentration gradients.

Forced Convection

If the external agent (such as pump, fan, etc.) causes the motion of the fluid flow, then the process is termed as forced convection.

Mixed Convection

The fluid flow in which the influence of forced flow in free convection or the buoyancy force in forced convection turn out to be significant then it is called mixed convection.

Brownian Motion

The arbitrary motion of nanoparticles within the base fluid is called Brownian motion, and this results from continuous collisions between the nanoparticles and the molecules of the base fluid.

Thermophoresis

Particles can diffuse under the influence of a temperature gradient. This phenomenon is called thermophoresis, and is the particle equivalent of the renowned Soret effect for gaseous or liquid mixtures.

Boussinesq Approximation

For sufficiently small isobaric changes in temperature and concentration, the fluid density depends linearly on temperature and concentration differences, which is called as a linear Boussinesq approximation (discussed in detail by Tritton [90]) and is given by

$$\rho = \rho_\infty[1 - \beta_T(T - T_\infty) - \beta_C(C - C_\infty)] \tag{1.9}$$

where ρ_∞ is the fluid density, T_∞ is the ambient temperature,C_∞ is the ambient concentration at some reference point in the medium, β_T is the coefficient of thermal expansion and β_C is the coefficient of solutal expansion, which are given by

$$\beta_T = -\frac{1}{\rho}\left(\frac{\partial \rho}{\partial T}\right)_{p,C} \tag{1.10a}$$

$$\beta_C = -\frac{1}{\rho}\left(\frac{\partial \rho}{\partial C}\right)_{p,T} \tag{1.10b}$$

Equation (1.10) is a good approximation for the variation of density. This states that

i. all variations in fluid properties can be completely ignored except for density in mo-

mentum equation.

ii. the density is considered to vary with temperature and concentrations only, and its variations can be ignored everywhere except where they give rise to buoyancy force.

Hall and Ion-slip Effects

"The presence of a magnetic field, in the flow of electric current through a conductor, applies a transverse force on the moving charge carriers that tends to push them to one side of the conductor. All accumulation of charge along the edges of conductors will adjust this magnetic effect, producing a quantifiable voltage between two sides of the conductor. The existence of quantifiable transverse voltage is known as a Hall effect" named after E. H. Hall who discovered it in 1879.

"In view of non-homogeneous distributions of charge carriers, Lorentz forces generate voltage gradients in all conducting liquids moving through magnetic fields. In plasma, electrons are stripped from the molecules, leaving a fuming mass of free electrons and positive ions. These carriers can be isolated by Lorentz forces in the conventional manner. The electrons tend to move faster than the ions when the plasma moves at high speed. The difference of the velocities is called ion-slip". Ion-slip creates a voltage that is axial to the direction of the flow.

The study of fluid flow with Hall currents and ion-slip effects has important engineering applications in problems of magnetohydrodynamics generators and Hall accelerators as well as in flight magnetohydrodynamics. If the electron-atom collision frequency is assumed to be relatively high, the Hall and ion-slip effects cannot be neglected in which a current is induced in the direction normal to both the electric and magnetic fields. In this case, the generalized ohms law (current density) is given by [83]

$$\bar{J} = \sigma\left[\bar{E} + \vec{q} \times \bar{B} - \eta(\bar{B} \times \bar{J}) + \frac{\eta\beta_i}{B_0}(\bar{B} \times \bar{J}) \times \bar{B}\right] \tag{1.11}$$

where η is the Hall factor and β_i is the ionic slip parameter, the total electric field current

which is neglected in this study by the assumption that the induced magnetic field is very small.

Joule Heating Effect

The Joule heating is produced by inter communication among the atomic ions that compose the body of the conductor and moving charged particles that form the current. It is because of the collision between the moving particles. In this process, some of the kinetic energy is converted into the heat and as a result temperature of the body increases. In recent years, the engineers and scientists are interested to increase the efficiency of various mechanical systems and industrial machineries. Such kinds of difficulties can be handled to decrease the temperature produced due to Ohmic dissipation or Joule heating. Numerous researches have been carried out for Joule heating effect on fluid flow and heat transfer at various conditions and found that it plays notable effect on MHD flow and heat transfer.

Chemical Reaction

Chemical reaction effect on the fluid flow is of considerable significance in chemical technology, materials processing systems and hydrometallurgical industries. The research on fluid flow with thermophoresis and chemical reaction effects can help to design the chemical processing equipment, chemical diffusion in the disk electrode modelling, carbon monoxide reactions in metallurgical mass transfer and kinetics, optical materials processing, and formation and dispersion of fog, etc. Several investigators have analyzed the impact of chemical reaction on the flow, heat and mass transfer through channels, pipes and an annular region.

Chemical reaction is the reaction in which the rate of reaction is directly proportional to the species concentration. Depending on the occurrence at an interface or as a single-phase volume reaction, the chemical reaction can be termed as either heterogeneous or

homogeneous. With first order chemical reaction, the equation (1.8) can be written as

$$\bar{\mathbf{V}} \cdot \nabla\phi = D_B \left(\nabla^2\phi\right) + \frac{D_T}{T_m}\left(\nabla^2 T\right) - k_1(C - C_0) \tag{1.12}$$

where k_1 is the rate of chemical reaction.

Radiation

The influence of thermal radiation is very important when the temperature difference between the surface and atmosphere is large. The study of radiative and magnetic field effects has important applications in physics and engineering.

Heat transfer due to emission of electromagnetic waves is known as thermal radiation. The importance of radiation becomes intensified at high absolute temperature levels. It is well known that the thermal radiation heat transfer does not require any intermediate medium by electromagnetic waves, or photons, which may travel a long distance without interacting with medium. Thus thermal radiation is of great importance in vacuum and space applications. The transfer of energy by radiation depends on differences of the individual absolute temperature of the bodies. In the presence of thermal radiation, the energy equation (1.7) reduce to

$$\bar{\mathbf{V}} \cdot \nabla T = \alpha\, \nabla^2 T + \tau \left[D_B \left(\nabla\phi.\nabla T\right) + \frac{D_T}{T_m}\left(\nabla T.\nabla T\right)\right] + \nabla q_r \tag{1.13}$$

The radiation heat flux is q_r, under the Rosseland approximation can be written as

$$q_r = -\frac{4\sigma^*}{3\chi}\frac{\partial T^4}{\partial y} \tag{1.14}$$

where σ^* is a Stefan-Boltzman constant and χ is the coefficient of mean absorption. We assume the variation in the fluid phase temperature inside the flow to be appropriately minimum such that T^4 may be shown as a linearly continuous function of the temperatures and enlarged in a Taylor Series around T_m and removing highest order terms, we get $T^4 =$

$4T_m^3\,T - 3T_m^4$.

Homotopy Analysis method

The basic idea of the homotopy in topology is employed by Liao [47] in 1992 to develop a general analytic method for nonlinear problems, called homotopy analysis method (HAM). It provides a great freedom to express solution by means of different base functions. Also, it provides a convenient way to control the rate and region of convergence of the series solution of nonlinear problems. It can be applied to ordinary differential equations, partial differential equations, integro-differential equations, delay-differential equation, integral equations etc. This method is based on the following assumptions:

- There exists the solution of zero-order deformation in the whole region of the embedding parameter $p \in [0, 1]$.
- All the high-order deformation equations have solutions.
- All Taylor series, expanded in the embedding parameter p, converge at $p = 1$.

Afterward, Liao [49] presented an optimal homotopy analysis approach for strongly nonlinear differential equations. The optimality of auxilary parameters and HAM are the advancements of HAM discussed by Turkyilmazoglu [92, 93].

1.4 Entropy Generation

Entropy and entropy generation are fundamental quantities. They play essential role in understanding of many diverse phenomena ranging from cosmology to biology. A physical quantity termed entropy defined in the second law of thermodynamics is a measure of irreversibility of systems. Entropy generation is not a property because it depends upon the process path. To comprehend the function of entropy generation mechanism, it makes practicality to concentrate on the irreversibility of fluid flow and heat transfer procedures. To

optimize the performance of engineering systems containing devices in which simultaneous heat and mass exchange occur, their irreversibilities of individual devices must be minimized. Since the total irreversibility of a system is the sum of the component irreversibilities, this procedure improves the system performance. The factors that cause irreversibilities include friction, inelastic deformation of solids, unrestrained expansion, heat transfer across a finite temperature difference, electric resistance, mixing of two fluids, and chemical reactions.

The second law of thermodynamics can be combined with the principles of fluid mechanics and heat transfer to acquire knowledge about irreversibilities that influence the working efficiency of the system and processes. All the real processes related to thermal convection system are associated with thermal gradient and frictional effects and hence some amount of available energy is destroyed during the process due to irreversibilities. The optimization may, therefore, be carried out by minimizing the irreversibilities present in the system. This approach of thermodynamic optimization known as Entropy Generation Minimization (EGM) was first reported by Bejan [9]. Entropy generation minimization (EGM)is a method of "modeling and optimization". Since then the theories based on these foundations have rapidly developed. However, the entropy generation consequential from temperature differences has stayed untreated by traditional thermodynamics, which persuades numerous scientists to investigate the applied and fundamental engineering problems in light of the second law of thermodynamics. Bejan [10, 11, 12] presented the following expression for the volumetric entropy generation rate

$$S_{gen} = \frac{K_f}{T_1^2}[\nabla T]^2 + \frac{1}{T_1}\Phi \tag{1.15}$$

where the first term on the right hand side of the above equation represents the entropy generation due to heat transfer and the second term represents the entropy generation due to viscous dissipation or friction.

It can be noted that second law analysis makes possible to compare many different interactions in a process or system and to identify the major sources of exergy distributions or losses. This enables us to exactly identify the region where the entropy generation rate is

maximum in the entire fluid regime. This study facilitated through the entropy generation number introduced by Bejan. Consequently, the relative effects of heat transfer and fluid friction can be determined successfully by Bejan number.

1.5 Aim and Scope of the Thesis

The aim of the present thesis is to study entropy generation analysis due to convective flow of a nanofluid in different geometries under various physical effects. Buongiorno [13] model is the basis of the present study. The geometries considered in this thesis are vertical parallel plates, concentric cylinders and infinite rotating parallel disks. The governing equations (which are nonlinear) along with the corresponding boundary conditions are initially converted into dimensionless form using non-dimensional transformations. The obtained system of ordinary differential equations is solved using Homotopy Analysis Method (HAM), which is one of the most efficient methods in solving diverse types of system of nonlinear differential equations such as homogeneous, non-homogeneous, coupled and decoupled. The effecs of Hall, ion-slip, magnetic, Joule Heating, thermal radiation, chemical reaction parameters, and Brinkman number on the flow characteristics such as the velocity, temperature, nanoparticle concentration, entropy generation and Bejan number are analyzed.

1.6 Literature Review

Convective flow of a fluid in a vertical channel and an annulus between two concentric cylinders has been the concentration of examination for a long time because of their extensive variety of practical applications. Several researchers have studied analytically and numerically the problems on fluid flow and heat transfer between vertical parallel plates. Cheng *et al* [20] investigated the problem of the flow reversal and heat transfer of fully developed mixed convective flow in a vertical channels. Further, the flow in an annulus between concentric cylinders induced by a relative rotating motion or axial movement is applicable to journal bearings, rotating electrical machines, standard commercial rheometers and swirl nozzles.

Williams [96] was the first to investigate numerically the free convection in a rotating annulus. He presented a very good analysis of axisymmetric flows in an annular geometry for various combinations of physical parameters. The exactness of the numerical computations was further substantiated by experimental observations [97] for the same geometry. The convective flow of a fluid between rotating disks is an important topic in view of its applications in rotating machinery, crystal growth processes, lubrication and computer storage devices. Soong [75] presented the theoretical analysis for axisymmetric mixed convective flow between rotating coaxial disks.

The study of convective flow of a nanofluid has received considerable theoretical and practical interest in view of its use in a wide variety of engineering applications. These applications include cooling of nuclear reactor, power generating systems, automobile engines, welding equipment, heat exchanging in electronics devices and computers. The detailed introduction and applications of nanofluids can be found in Das *et al* [23]. Buongiorno [13] has investigated the factors which contribute to abnormal thermal conductivity increase relative to base fluids and viscosity. He developed an analytical model for convective transport in a nanofluid, which takes Brownian diffusion and thermophoresis effects into account. The literature on nanofluids has been reviewed by Daungthongsuk and Wongwises [24], Eastman *et al* [27] and Lee [46] among several others. These reviews examine in detail the work done on convective transport in nanofluids. Number of studies were conducted in recent years, on A vertical channel filled with nanofluid by considering distinct types of convectional base fluids with particular nanoparticles. Hang and Pop [41] verified the mixed convective nanofluids flow in a vertical channel and observed that nanoparticle volume fraction plays an essential role for developing the heat and mass transfer properties of the fluids. Hang *et al* [40] studied the mixed convective nanofluid flow in a vertical channel using the Buongiorno method. Several studies were also conducted on the convective heat transfer and nanofluid flow through concentric cylinders. Sheikhzadeh *et al* [73] analyzed the mixed convective flow of a nanofluid in an annulus between concentric cylinders. Togun *et al* [89] presented a detailed review on heat transfer of mixed, forced and natural and convective nanofluid flow through various annular passage configurations. On the other hand, the heat transfer

and fluid flow between rotating disks is an important topic in view of its wider applications in rotating machinery, crystal growth processes, lubrication and computer storage devices. Feng and Kleinstreuer [33] examained the convective heat transfer of nanofluid in parallel disks system.

The flow in an electrically conducting nanofluid with magnetic effects has attracted several researchers in view of its applications in an engineering technology and science. After the pioneering works of Hartman and Lazarus [42] in connection to the impact of magnetic field on the laminar flow of viscous liquids between parallel plates, several researchers have investigated the impacts of magnetic field on the Newtonian and non-Newtonian flows through different geometries when the fluid is an electrically conducting. Chamkha *et al* [15] presented a review on various research work done on the MHD convection of a nanofluid in various geometries and applications. In order to simplify the mathematical analysis of most of the MHD flow problems, the Hall current and ion-slip effects in Ohms law were ignored. However, the impact of Hall current and ion-slip is necessary in the presence of strong magnetic field. Therefore, in several physical situations it is required to include the effects of Hall and ion-slip terms in the magnetohydrodynamic (MHD) equations. The effects of Hall current on an electrically conducting viscous steady fluid in a channels is studied by Tani [86]. Since then several researchers have studied the Hall and ion-slip effects on the flow through different geometries. Srinivasacharya and Kaladhar [78] analyses the impact of Hall and ion-slip on MHD natural convective flow of a couple stress fluid in an annulus. Srinivasacharya and Kaladhar [80] studied the effects of Hall current and ion-slip on mixed convection flow of a couple stress fluid between parallel plates. Hayat *et al* [84] examained the unsteady flow due to non-coaxially rotating disk with Hall effects. It is well known that the Joule heating plays notable effect on MHD flow and heat transfer. Zhang *et al* [31] conducted a numerical study on MHD fluid flow and heat transfer under different levels of thermal radiation considering Joule heating effect. Hayat *et al* [70] explored the mixed convective Jeffrey nanofluid flow in a compliant walls channel by taking Joule heating along with viscous dissipation and thermal radiation into account.

Several authors examined the effect of radiation on convective flow of a nanofluid with

heat and mass transfer from bodies of different geometries under various physical conditions. Sheikholeslami and Ganji [72] investigated the effect of thermal radiation and magnetic field on the unsteady flow of a nanofluid flow and heat transfer. Srinivasacharya and Vijay Kumar [82] considered the mixed convective flow of a nanofluid in a non-Darcy porous medium considering radiation effect. Chen *et al* [18] studied the effects of thermal radiation on laminar forced and free convection along a wavy surface. Hady *et al* [39] reported that an increase in thermal radiation parameter reduces the nanofluid temperature which leads to increase the rate of heat transfer. Rahman [1] investigated numerically the problem of thermal radiation and unsteady MHD flow of a nanofluid in a stretching porous medium. Turkyilmazoglu and Pop [94] considered the problem of unsteady natural convective flow of some nanofluids past a vertical infinite plate with radiation effect. El-Kabeir *et al* [30] investigated the effect of thermal radiation on boundary flow and heat transfer by non-Darcy natural convection from a vertical cylinder embedded in a porous medium saturated with nanofluid. Agha *et al* [3] studied the influence of thermal radiation on natural convective boundary layer flow for heat and mass transfer in a porous medium saturated by a nanofluid past a semi-infinite vertical plate, via a model in which Brownian motion and thermophoresis are taken into account.

The role of chemical reaction on heat and mass transfer are of great influence in chemical technology and industries of hydrometallurgy. In most of the cases of chemical reactions, the reaction rate depends on the concentration of the species itself. Chemically reacting nanofluid may play a significant role in many processing systems and materials. Several investigators have focused on the effect of chemical reaction on the heat and mass transfer flow passing through an annular region between concentric cylinders, channels and parallel disks. Habibis *et al*[69] studied the flow reversal of chemical reacting fully developed mixed convective flow in a vertical channel. Kothandapani and Prakash [52] investigated the chemical reaction effect on flow of a nanofluid in a vertical channel in presence of inclined magnetite field. Babulal and Dulalpal [26] discussed the combination of chemical reaction and Joule heating effects on MHD mixed convective flow of a viscous dissipating fluid on a vertical parallel plates. Mridulkumar *et al* [61] analysed the effect chemical reaction on MHD boundary

layer flow with Joule heating effect over the stretching sheet. Poulomi *et al* [64] examined the significance of mixed convective chemically reacting nanofluid flow with internal heat generation and thermal radiation.

Entropy generation, a measure of the destruction of available energy in a system, plays an important role in the design and development of engineering processes. Entropy generation is a powerful and useful optimization tool for a high range of thermal applications. Entropy generation is directly proportion to the thermodynamic irreversibility in a system. Bejan [11, 12] developed the entropy generation minimization method and introduced its applications in engineering sciences. Thereafter, many authors such as Baytas [8], Tasnim and Mahmud [87], Ganji *et al* [35], Esfahani and Shahabi [32], Tshehla *et al*[91], Heidary *et al* [44], Chauhan and Kumar [16], Ramakrishna *et al* [65], etc., have studied the entropy generation and irreversibility profiles for different geometries in different types of Newtonian and non-Newtonina fluids. The majority of entropy generation analysis deal with convection processes in which the entropy generation is the result of fluid friction and heat transfer. Haddad *et al* [38] presented the entropy generation due to laminar forced convection in the entrance region of a concentric cylindrical annulus. It was found that the thermal entropy generation is relatively dominant over viscous entropy generation. Yilbas *et al* [98] concluded a study on the entropy analysis for non-Newtonian fluid flow in an annular Pipe. They found that the rate of entropy generation can be reduced by reducing both non-Newtonian parameter and Brinkman number. Rashid and Mehr [66] examained the effects of the velocity slip and temperature jump conditions on the entropy generation in the MHD flow over a porous rotating disk. Mahian *et al* [53, 54, 55] determined the influence MHD flow on the entropy generation of a nanofluid flow through a vertical annulus. Entropy generation due to a nanofluid flow through a channel with convective cooling/heating was investigated by [22, 17, 51, 58]. Eegunjobi and Makinde [29] presented the effects of slip and convection heating on entropy generation in a vertical channel. Gyftopoulos and Beretta [37] studied the entropy generation due to chemically reacting system. Imen *et al* [45] analyzed the entropy generation analysis of a chemical reaction process. The entropy generation on the MHD blood flow of a nanofluid influenced by thermal radiation is presented by Rashidi *et al* [68]. Fersadou

et al [34] analyzed numerically the entropy generation and magnetohydrodynamic mixed convective nanofluid flow in a vertical channel. Srinivasacharya and Hima Bindu [77] explored the entropy generation due to micropolar fluid flow between concentric cylinders.

1.7 Outline of the Thesis

The main aim of this thesis is to present entropy generation analysis in a nanofluid flow through a vertical channels, concentric cylinders and parallel disk. A quantitative analysis has been performed based on numerical computations in order to know the effects of certain physical parameters on entropy generation and Bejan number through graphs.

This thesis consists of FIVE parts and TEN chapters.

Part-I consists of a single chapter (Chapter - 1). This chapter is introductory in nature and presents the motivation for the investigations carried out in the thesis. A survey of pertinent literature is presented. The basic equations governing the flow, heat and mass transfers of a nanofluid along with the nanoparticle volume fraction are given.

Part-II deals with the mixed convective flow of a nanofluid with Hall, ion-slip, Joule heating and radiation effects in a vertical channel. This part consists of three chapters (Chapters 2, 3 and 4). In all these chapters, the nonlinear governing equations and their associated boundary conditions are initially cast into dimensionless form. The resulting system of equations is then solved using well established method, namely, homotopy analysis method (HAM). The convergence of the solution is established through error analysis. The obtained numerical results are compared wherever possible with the available results and found to be in good agreement.

In chapter 2, the steady convective flow of a nanofluid with Hall and ion-slip effects in a vertical channel is investigated. The effects of magnetic, Hall, ion-slip, thermophoresis, Brownian motion and Buoyancy ratio parameters on the non-dimensional velocities, temperature and nanoparticle concentration are discussed.

The effects of Joule heating and radiation on the entropy generation for steady incompressible mixed convective nanofluid flow in a vertical channel is considered in chapter - 3. The non-dimensional velocities, temperature, nanoparticle concentration, entropy generation and Bejan number profiles are presented graphically for different values of thermal radiation, magnetic and Joule heating parameters.

In chapter 4, the entropy generation due to laminar mixed convective flow of an incompressible chemically reacting nanofluid in a vertical channel is studied by taking Joule heating effect in to consideration. The entropy generation and Bejan number are computed numerically by utilizing the velocity and temperature.

Part-III deals with the convective flow of a nanofluid between two concentric cylinders by considering Hall, ion-slip, Joule heating and radiation effects. This part consists of three chapters (Chapters 5, 6 and 7). Using suitable transformation, the governing equations are transformed to non-linear ordinary differential equations. Homotopy analysis method is used to solve the resulting system of equations in order to explore the usefulness of the present study.

The steady, laminar convective flow of nanofluid with Hall and ion-slip effects in between two concentric cylinders in presence of magnetic field is studied in chapter 5. The outer cylinder is rotating with an angular velocity ω and the inner cylinder is at rest. The flow is generated due to the rotation of this cylinder. The effects of magnetic, Hall, ion-slip, thermophoresis and Brownian motion parameters on the non-dimensional velocities, temperature and nanoparticle concentration are discussed. In this chapter, two types (cases) of problems are considered. The first type is of natural convective flow and the second type is of mixed convective flow of a nanofluid.

Chapter6 presents the effects of radiation and Joule heating on entropy generation due to the laminar mixed convective flow of a nanofluid in an annulus between two concentric cylinders. The effects of magnetic, Joule heating, radiation parameters and Brinkman number on the velocity in flow direction, dimensionless temperature, nanoparticle concentration, Bejan number and entropy generation are analyzed and presented graphically.

In chapter7, the laminar mixed convective flow of an incompressible chemically reacting nanofluid in an annulus between two concentric cylinders is investigated by considering Joule heating effect. The non-linear governing equations are non-dimensionalized and then solved by using HAM. The entropy generation rate and Bejan number are calculated numerically. The effects of magnetic, Joule heating, chemical reaction parameters and Brinkman number on the velocity, temperature and nanoparticle concentration are investigated and presented graphically.

Part-IV deals with the mixed convective flow of a nanofluids between rotating parallel circular disks considering Hall, ion-slip, Joule heating and radiation effects. This part consists of two chapters (Chapters 8 and 9).

Chapter8 analyzes the Hall and ion-slip effects on entropy generation in a mixed convective an electrically conducting nanofluid flow between two parallel coaxial disks by considering Joule heating effect. The entropy generation rate and Bejan number are calculated numerically. The effects of Joule heating and relative rotating rate parameters on the axial and tangential velocities, temperature, nanoparticle concentration, entropy generation and Bejan number are presented graphically.

In chapter9, the Joule heating effect on entropy generation due to laminar mixed convective flow of an incompressible chemically reacting nanofluid between two parallel coaxial disks is discussed. The entropy generation and Bejan number are computed numerically by utilizing the velocity and temperature. The effects of chemical reaction, radiation, thermophoresis parameters and Brinkman number on the velocity, temperature and nanoparticle concentration are investigated and presented geometrically.

Part-V consists of a single chapter (Chapter - 10). This chapter summarizes the main conclusions of the earlier chapters and the directions in which further investigations may be carried out are indicated.

List of references is given at the end of the thesis. The references are numbered in a sequence in which they appear in the text.

Considerable part of the work in the thesis is published/accepted for publication in the reputed journals. The remaining part is communicated for possible publications. The details are presented below.

List of Papers Published

1. " Hall and ion-slip effects on natural convection flow in a vertical channel filled with a nanofluid ", *"Journal of Nanofluids"*, Vol. 5, (2016), pp. 982–992.

2. " Mixed convection flow of a nanofluid in a vertical channel with Hall and ion-slip effects", *"Frontiers in Heat and Mass Transfer"*, Vol. 8, 11,(2017), DOI NO: 10.5098/hmt.8.11.

3. " Hall and ion-slip effects on mixed convection flow of a nanofluid between two concentric cylinders", *"Journal of the Association of Arab Universities for Basic and Applied Sciences"*, Vol. 24, (2017), pp. 223–231.

4. "Entropy generation due to MHD mixed convection of a nanofluid between two concentric cylinders with radiation and Joule heating effects" *"Journal of Nanofluids"*, Vol. 6,(2017), pp. 1227–1237.

5. " Entropy generation due to MHD mixed convection of a nanofluid in a vertical channel with Joule heating and radiation effects", *"International Journal of Engineering and Technology"*,Vol. 9, No. 4,(2017), DOI: 10.21817/ijet/2017/v9i4/170904403.

6. " Joule heating effect on entropy generation in MHD mixed convection flow of chemically reacting nanofluid between two concentric cylinders", *"International Journal of Heat and Technology"*,Vol. 35, No. 3,(2017), pp. 487–497.

List of Papers Communicated

1. " Joule heating effect on entropy in MHD mixed convection flow of a chemically reacting nanofluid in a vertical channel", *"Chemical Industry and Chemical Engineering Quarterly"*.

2. " Entropy generation in MHD mixed convection flow of a nanofluid between parallel disks with Joule heating, Hall and ion-slip effects", *"Journal of the Brazilian Society of Mechanical Sciences and Engineering"*.

3. " Entropy generation in mixed convection flow of a chemically reacting nanofluid between parallel disks with radiation effect", *"Journal of King Saud University - Science"*.

4. " Free convection of a nanofluid flow in an annulus with Hall and ion-slip effects, *"Propulsion and Power Research"*.

Part II

ENTROPY GENERATION IN MIXED CONVECTIVE FLOW OF A NANOFLUID IN A VERTICAL CHANNEL

Chapter 2

Hall and ion-slip effects on convective flow in a vertical channel filled with nanofluid [1]

2.1 Introduction

Convective transport in a nanofluid through a vertical channel, a frequently encountered geometry in the thermal engineering equipment, has been the subject of investigation for many years. This is because of its wide range of applications in the structure of cooling devices for electronics and microelectronic equipment, solar energy collection, etc. On the other hand, the study of convective heat transfer and fluid flow problems with the interaction of magnetite field has increased enormously because of many engineering and industrial applications. In most of the investigations concerned with MHD convective flows, the Hall and ion-slip terms in Ohm's law were ignored in order to simplify the mathematical analysis of the problem. However, the impact of Hall and ion-slip are essential in the presence of a strong magnetite field. Therefore, in several physical situations it is required to include

[1] Type - I: Published in "**Frontiers in Heat and Mass Transfer, (2017), Vol.8,11**", Type - II: Published in "**Journal of Nanofluids, Vol. 5 (2016), 982–992**"

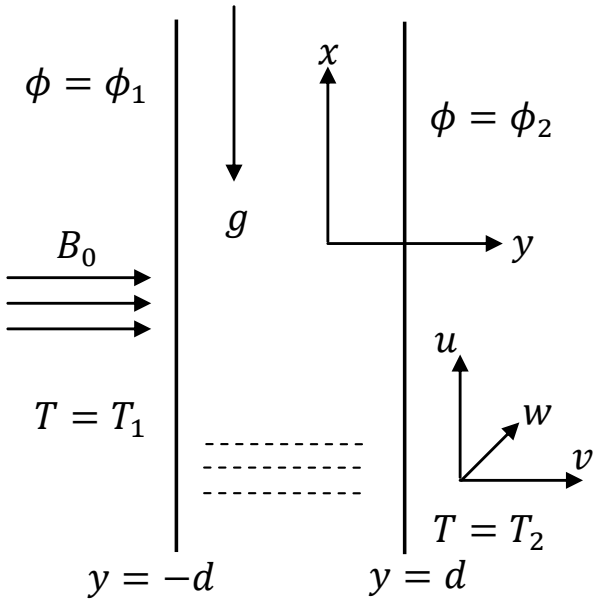

Figure 2.1: Physical model and coordinate system.

the significance of Hall and ion-slip parameters in MHD flow problems. Several researchers investigated the influence of Hall current and ion-slip on the convective transport in Newtonian and non-Newtonian fluid flows through channels. Tani [86] analyzed the effect of Hall current on the electrically conducting viscous fluid flow in a vertical channel. Srinivasacharya and Kaladhar [79] explored the significance of Hall current and ion-slip effects on natural convection in a couple stress fluid flow through a vertical parallel plates.

The aim of this chapter is to analyze the significance of Hall and ion-slip on the steady mixed/natural convective flow of a nanofluid in a vertical channel. The homotopy analysis method (HAM) is used to solve the governing nonlinear ordinary differential equations. The effect of flow parameters on the dimensionless velocity, temperature, and nanoparticle concentration are examined.

2.2 Mathematical Formulation

Consider a steady, laminar and electrically conducting flow of a nanofluid passing through a vertical channel. The distance between the plates of a channel is $2d$. The x-axis is taken in the direction of flow vertically upward through the central line of a vertical channel, $y-$axis is in the direction orthogonal to the flow as shown in figure 2.1. The plate $y = -d$ is maintained at a temperature T_1 and nanoparticle volume fraction ϕ_1, while plate $y = d$ is maintained at a temperature T_2 and nanoparticle volume fraction ϕ_2. A uniform magnetic field B_0 is applied in $y-$direction. The Hall current and ion-slip effects are considered in view of relatively high electron-atom collision frequency. This assumption causes a cross flow in the z-direction, therefore the flow becomes three dimensional. The induced magnetic field is negligible comparison to the applied magnetic field. A uniform pressure gradient is applied in x-direction. Further, all the characteristics of fluid are considered as constant apart from the density in the buoyancy term. Assume that the plates along the x and z-direction are extended infinitely. Hence, the velocity vector of a fluid is taken as $(u(y), v(y), w(y))$. The temperature and nanoparticle volume fraction are respectively denoted by $T(y)$ and $\phi(y)$.

Under these assumptions, the equations governing a nanofluid flow, as proposed by Buongiorno [13], under the significance of uniform transverse magnetite field with Hall and ion-slip effects are as follows

$$\frac{\partial v}{\partial y} = 0 \tag{2.1}$$

$$\rho_f\, v\frac{\partial u}{\partial y} = -\frac{\partial p}{\partial x}+\mu\frac{\partial^2 u}{\partial y^2}+(1-\phi_0)\rho_{f_0} g^*\,\beta_T(T-T_1)-(\rho_s-\rho_{f_0})\,g^*(\phi-\phi_1)-\frac{\sigma\, B_0^2}{(\alpha e^2+\beta h^2)}\,(\alpha e\, u+\beta h\, w) \tag{2.2}$$

$$\rho_f\, v\frac{\partial w}{\partial y} = \mu\frac{\partial^2 w}{\partial y^2}+\frac{\sigma\, B_0^2}{(\alpha e^2+\beta h^2)}\,(\beta h\, u-\alpha e\, w) \tag{2.3}$$

$$v\frac{\partial T}{\partial y} = \alpha\frac{\partial^2 T}{\partial y^2}+\frac{2\mu}{(\rho c)_p}\left[\left(\frac{\partial u}{\partial y}\right)^2+\left(\frac{\partial w}{\partial y}\right)^2\right]+\tau\left[D_B\frac{\partial T}{\partial y}\frac{\partial \phi}{\partial y}+\frac{D_T}{T_0}\left(\frac{\partial T}{\partial y}\right)^2\right] \tag{2.4}$$

$$v\frac{\partial \phi}{\partial y} = D_B\frac{\partial^2 \phi}{\partial y^2}+\frac{D_T}{T_0}\frac{\partial^2 T}{\partial y^2} \tag{2.5}$$

where βh is the Hall parameter, βi is the ion-slip parameter, ρ is the density, g^* is the

acceleration due to gravity, μ is the viscosity coefficient, C_p is the specific heat capacity, σ is the electrical conductivity, $\alpha e = 1 + \beta h\, \beta i$ is a constant, β_T is the coefficients of thermal expansion, α is the effective thermal diffusivity, D_B is the Brownian diffusion coefficient, D_T is the thermophoretic diffusion coefficient, k is the coefficient of thermal conductivity, D is the mass diffusivity and $\tau = \dfrac{(\rho\, C)_P}{(\rho\, C)_f}$.

The conditions on the boundary are

$$\begin{aligned} \phi = \phi_1 \quad u = 0, \quad v = v_0, \quad w = 0, \quad T = T_1, \quad \text{on} \quad y = -d, \\ \phi = \phi_2 \quad u = 0, \quad v = v_0, \quad w = 0, \quad T = T_2, \quad \text{on} \quad y = d. \end{aligned} \tag{2.6}$$

It is to be noted from (2.1) and (2.6) that $v = v_0$.

In this chapter, two types of convection i.e., mixed (type - I) and free (type - II) convection are considered.

2.2.1 Mixed Convection

Assume that the mixed convective flow is taking place in the presence of thermal buoyancy and uniform pressure gradient in the x-direction. Introducing the following non-dimensional variables

$$\eta = \frac{y}{d},\ f = \frac{u}{u_0},\ g = \frac{w}{u_0},\ \theta = \frac{T - T_1}{T_2 - T_1},\ S = \frac{\phi - \phi_1}{\phi_2 - \phi_1},\ P = \frac{d^2 p}{\mu\, u_0} \tag{2.7}$$

in Eqs.(2.1) - (2.5), we get the nonlinear differential equations as

$$f'' - Rf' + \frac{Gr}{Re}\,(\theta - NrS) - \frac{Ha^2}{(\alpha e^2 + \beta h^2)}\,(\alpha e\, f + \beta h\, g) - A = 0 \tag{2.8}$$

$$g'' - Rg' + \frac{Ha^2}{(\alpha e^2 + \beta h^2)}\,(\beta h\, f - \alpha e\, g) = 0 \tag{2.9}$$

$$\theta'' - R\, Pr\, \theta' + Pr\, Nb\, \theta' S' + Pr\, Nt\, \theta'^2 + 2\, Br\, Gr^2 \left[(f')^2 + (g')^2\right] = 0 \tag{2.10}$$

$$S'' - R\, Le\, S' + \frac{Nt}{Nb}\,\theta'' = 0 \tag{2.11}$$

where prime indicate the derivative with respect to η, υ is the kinematic viscosity coefficient, $Pr = \dfrac{\mu\, C_P}{k_f}$ is Prandtl number, $Le = \dfrac{\upsilon}{D_B}$ is Lewis number, $R = \dfrac{v_0 d}{\upsilon}$ is the suction/injection parameter, $Gr = \dfrac{(1-\phi)\, g^*\, \beta_T (T_2 - T_1) d^3}{\upsilon^2}$ is Grashof number, $Re = \dfrac{u_0 d}{\upsilon}$ is Reynold's number, $Ha^2 = \dfrac{{B_0}^2\, d^2\, \sigma}{\mu}$ is Hartman number, $A = \dfrac{d^2}{\mu\, u_0}\dfrac{\partial p}{\partial x}$ is a constant pressure gradient, $Br = \dfrac{\mu\, {u_0}^2}{k_f (T_2 - T_1)}$ is Brinkman number, $Nb = \dfrac{\tau\, D_B (\phi_2 - \phi_1)}{\upsilon}$ is the Brownian motion parameter, $Nt = \dfrac{\tau\, D_T (T_2 - T_1)}{\upsilon}$ is the thermophoresis parameter and $Nr = \dfrac{(\rho_p - \rho_{f_0})(\phi_2 - \phi_1)}{\rho_{f_0} \beta_T (T_2 - T_1)(1-\phi)}$ is the buoyancy ratio.

The corresponding dimensionless boundary conditions are

$$\begin{aligned} f = 0, \quad g = 0, \quad \theta = 0, \quad S = 0 \quad \text{at} \quad \eta = -1 \\ f = 0, \quad g = 0, \quad \theta = 1, \quad S = 1 \quad \text{at} \quad \eta = 1 \end{aligned} \tag{2.12}$$

2.2.2 Natural convection

In this case, we assume that the flow is to be natural convective and there is no external pressure gradient ($\frac{\partial p}{\partial x} = 0$).

Introducing the following non-dimensional varaibles

$$\eta = \frac{y}{d},\ f = \frac{ud}{\nu\, Gr},\ g = \frac{wd}{\nu\, Gr},\ \theta = \frac{T - T_1}{T_2 - T_1},\ S = \frac{\phi - \phi_1}{\phi_2 - \phi_1} \tag{2.13}$$

in Eqs.(2.1) - (2.5), we get

$$f'' - Rf' + \frac{Gr}{Re}(\theta - NrS) - \frac{Ha^2}{(\alpha e^2 + \beta h^2)}(\alpha e\, f + \beta h\, g) = 0 \tag{2.14}$$

$$g'' - Rg' + \frac{Ha^2}{(\alpha e^2 + \beta h^2)}(\beta h\, f - \alpha e\, g) = 0 \tag{2.15}$$

$$\theta'' - R\, Pr\, \theta' + Pr\, Nb\, \theta' S' + Pr\, Nt\, \theta'^2 + 2\, Br\, Gr^2 \left[(f')^2 + (g')^2\right] = 0 \tag{2.16}$$

$$S'' - R\,Le\,S' + \frac{Nt}{Nb}\,\theta'' = 0 \tag{2.17}$$

The corresponding dimensionless boundary conditions are

$$\begin{aligned} f = 0, \quad g = 0, \quad \theta = 0, \quad S = 0 \quad \text{at} \quad \eta = -1 \\ f = 0, \quad g = 0, \quad \theta = 1, \quad S = 1 \quad \text{at} \quad \eta = 1 \end{aligned} \tag{2.18}$$

2.3 Solution of the Problem

2.3.1 Mixed Convection

The governing Eqs. (2.8) - (2.11) along with (2.12) are solved by using homotopy analysis method (HAM). (For more details on HAM, see the works of Liao [47, 48, 49, 50]). The first step in HAM is, to choose the initial approximations of $f(\eta)$, $g(\eta)$, $\theta(\eta)$ and $S(\eta)$ and auxiliary linear operators. Therefore, we choose the initial approximations as

$$f_0(\eta) = 0, \quad g_0(\eta) = 0, \quad \theta_0(\eta) = \frac{(\eta+1)}{2} \quad \text{and} \quad S_0(\eta) = \frac{(\eta+1)}{2} \tag{2.19}$$

and the auxiliary linear operators as $L_i = \dfrac{\partial^2}{\partial \eta^2}$ for $i = 1, 2, 3, 4$ such that

$$L_1(c_1 + c_2\eta) = 0,\ L_2(c_3 + c_4\eta) = 0,\ L_3(c_5 + c_6\eta) = 0 \quad \text{and} \quad L_4(c_7 + c_8\eta) = 0 \tag{2.20}$$

where $c_i, (i = 1, 2, \cdots 8)$, are constants.

The second step in HAM is to define the zeroth order deformation, which is given by

$$(1-p)L_1[f(\eta;p) - f_0(\eta)] = ph_1N_1[f(\eta;p)], \quad (1-p)L_2[g(\eta;p) - g_0(\eta)] = ph_2N_2[g(\eta;p)],$$

$$(1-p)L_3[\theta(\eta;p) - \theta_0(\eta)] = ph_3N_3[\theta(\eta;p)], \quad (1-p)L_4[S(\eta;p) - S_0(\eta)] = ph_4N_4[S(\eta;p)] \tag{2.21}$$

where

$$\left.\begin{aligned} N_1[f(\eta,p),g(\eta,p),\theta(\eta,p),S(\eta,p)] &= f''-Rf'+\frac{Gr}{Re}\left(\theta-NrS\right)-\frac{Ha^2}{(\alpha e^2+\beta h^2)}\left(\alpha e\, f+\beta h\, g\right)-A \\ N_2[f(\eta,p),g(\eta,p),\theta(\eta,p),S(\eta,p)] &= g''-Rg'+\frac{Ha^2}{(\alpha e^2+\beta h^2)}\left(\beta h\, f-\alpha e\, g\right) \\ N_3[f(\eta,p),g(\eta,p),\theta(\eta,p),S(\eta,p)] &= \theta''-R\,Pr\,\theta'+PrNb\theta'S'+PrNt\,\theta'^2+2\,Br\,Gr^2\left[(f')^2+(g')^2\right] \\ N_4[f(\eta,p),g(\eta,p),\theta(\eta,p),S(\eta,p)] &= S''-R\,Le\,S'+\frac{Nt}{Nb}\,\theta'' \end{aligned}\right\} \tag{2.22}$$

where $p\in[0,1]$ is the embedded parameter and h_i, $(i=1,2,3,4)$, are the non-zero auxiliary parameters.

The equivalent boundary conditions are

$$\begin{aligned} f(-1;p)=0,\quad g(-1;p)=0,\quad \theta(-1;p)=0,\quad S(-1;p)=0,\\ f(1;p)=0,\quad g(1;p)=0,\quad \theta(1;p)=1,\quad S(1;p)=1 \end{aligned} \tag{2.23}$$

From $p=0$ to $p=1$, we can have

$$\begin{aligned} f(\eta;0)=f_0,\quad g(\eta;0)=g_0,\quad \theta(\eta;0)=\theta_0,\quad S(\eta;0)=S_0,\\ f(\eta;1)=f(\eta),\quad g(\eta;1)=g(\eta),\quad \theta(\eta;1)=\theta(\eta),\quad S(\eta;1)=S(\eta) \end{aligned}$$

Thus, as p varying from 0 to 1, f, g, θ and S varies continuously from the initial guess f_0, g_0, θ_0 and S_0 to the final solution $f(\eta)$, $g(\eta)$, $\theta(\eta)$ and $S(\eta)$ respectively. Using the Taylor's

series, f, g, θ and S can be written as

$$\begin{aligned}
f(\eta;p) &= f_0 + \sum_{m=1}^{\infty} f_m(\eta)p^m, \quad f_m(\eta) = \frac{1}{m!}\frac{\partial^m f(\eta;p)}{\partial p^m}\bigg|_{p=0}, \\
g(\eta;p) &= g_0 + \sum_{m=1}^{\infty} g_m(\eta)p^m, \quad g_m(\eta) = \frac{1}{m!}\frac{\partial^m g(\eta;p)}{\partial p^m}\bigg|_{p=0}, \\
\theta(\eta;p) &= \theta_0 + \sum_{m=1}^{\infty} \theta_m(\eta)p^m, \quad \theta_m(\eta) = \frac{1}{m!}\frac{\partial^m \theta(\eta;p)}{\partial p^m}\bigg|_{p=0}, \\
S(\eta;p) &= S_0 + \sum_{m=1}^{\infty} S_m(\eta)p^m, \quad S_m(\eta) = \frac{1}{m!}\frac{\partial^m S(\eta;p)}{\partial p^m}\bigg|_{p=0}.
\end{aligned} \tag{2.24}$$

The values of the auxiliary parameters are chosen in such a way that the series (2.24) converge at $p = 1$ i.e.,

$$\begin{aligned}
f(\eta) &= f_0 + \sum_{m=1}^{\infty} f_m(\eta), \quad g(\eta) = g_0 + \sum_{m=1}^{\infty} g_m(\eta), \\
\theta(\eta) &= \theta_0 + \sum_{m=1}^{\infty} \theta_m(\eta), \quad S(\eta) = S_0 + \sum_{m=1}^{\infty} S_m(\eta).
\end{aligned} \tag{2.25}$$

Next, the m^{th}-order deformation equations are given by

$$\begin{aligned}
&L_1[f_m(\eta) - \chi_m f_{m-1}(\eta)] = h_1 R_m^f(\eta), \quad L_2[g_m(\eta) - \chi_m g_{m-1}(\eta)] = h_2 R_m^g(\eta), \\
&L_3[\theta_m(\eta) - \chi_m \theta_{m-1}(\eta)] = h_3 R_m^\theta(\eta), \quad L_4[S_m(\eta) - \chi_m S_{m-1}(\eta)] = h_4 R_m^S(\eta).
\end{aligned} \tag{2.26}$$

where

$$\begin{aligned}
\chi_m &= 0 \quad \text{for} \quad m \leq 1 \\
&= 1 \quad \text{for} \quad m > 1
\end{aligned}$$

here m is an integer and

$$\left.\begin{aligned} R_m^f(\eta) &= f'' - Rf' + \frac{Gr}{Re}(\theta - NrS) - \frac{Ha^2}{(\alpha e^2 + \beta h^2)}(\alpha e\, f + \beta h\, g) - A \\ R_m^g(\eta) &= g'' - Rg' + \frac{Ha^2}{(\alpha e^2 + \beta h^2)}(\beta h\, f - \alpha e\, g) \\ R_m^\theta(\eta) &= \theta'' - R\,Pr\,\theta' + PrNb\theta' S' + PrNt\,\theta'^2 + 2\,Br\,Gr^2\left[\sum_{n=0}^{m-1} f'_{m-1-n} f'_n + \sum_{n=0}^{m-1} g'_{m-1-n} g'_n\right] \\ R_m^S(\eta) &= S'' - R\,Le\,S' + \frac{Nt}{Nb}\theta'' \end{aligned}\right\} \tag{2.27}$$

2.3.2 Natural convection

In this case also, the governing Eqs.(2.14) - (2.17) along with the boundary conditions (2.18) are solved by using homotopy analysis method (HAM). The procedure of obtaining the solution is similar to that of the mixed convection case and hence details of the solution procedure for this case are not presented here to avoid repetition.

2.4 Convergence

2.4.1 Mixed convection

In HAM, it is essential to see that the series solution converges. Also, the rate of convergence of the HAM solution strongly depends on the values of auxiliary parameter h. To find the admissible range of the auxiliary parameters, h-curves are plotted for 20^{th}-order of approximation and are shown in figure (2.2). It is evident from these figures that the admissible range for h_1, h_2, h_3 and h_4 are $-0.6 < h_1 < -0.3$, $-0.65 < h_2 < -0.4$, $-1.5 < h_3 < -0.3$ and $-1.6 < h_4 < -0.15$ respectively.

Order	Optimal of h_1		Optimal of h_2		Optimal of h_3		Optimal of h_4	
	h_1	Min. of E_m	h_2	Min. of E_m	h_3	Min. of E_m	h_4	Min. of E_m
10	-0.59	4.50×10^{-6}	-0.51	8.43×10^{-8}	-0.2	2.13×10^{-8}	-1.56	6.26×10^{-8}
15	-0.59	8.81×10^{-8}	-0.52	4.71×10^{-10}	-0.2	4.80×10^{-9}	-1.6	5.41×10^{-11}
20	-0.6	4.51×10^{-8}	-0.51	8.52×10^{-11}	-1.6	2.30×10^{-9}	-1.6	8.69×10^{-10}

Table 2.1: "Optimal values of h_1, h_2, h_3 and h_4 at different order of approximations (mixed convection case)".

The following average residual errors (Ref. Liao [49]) are computed to obtain the optimal value of auxiliary parameters

$$\begin{aligned} E_{f,m} &= \frac{1}{2K}\sum_{i=-K}^{K}\left(N_1\left[\sum_{j=0}^{m} f_j(i\triangle t)\right]\right)^2, \quad E_{g,m} = \frac{1}{2K}\sum_{i=-K}^{K}\left(N_2\left[\sum_{j=0}^{m} g_j(i\triangle t)\right]\right)^2, \\ E_{\theta,m} &= \frac{1}{2K}\sum_{i=-K}^{K}\left(N_3\left[\sum_{j=0}^{m} \theta_j(i\triangle t)\right]\right)^2, \quad E_{S,m} = \frac{1}{2K}\sum_{i=-K}^{K}\left(N_4\left[\sum_{j=0}^{m} S_j(i\triangle t)\right]\right)^2. \end{aligned} \tag{2.28}$$

where $\triangle t = 1/K$ and $K = 5$. At different order of approximations (m), the least average residual errors are shown in table (2.1). From this, we see that the average residual errors are least at h_1=-0.59, h_2=-0.51, h_3=-0.20 and h_4=-1.6. Therefore, the optimum values of convergence control parameters are taken as h_1=-0.59, h_2=-0.51, h_3=-0.20 and h_4=-1.6. The series solutions for different values of m are computed and presented in table (2.2). It is found from this table that the series (2.25) converges in the whole region of η. The graphs of the following ratio's

$$\beta f = \left|\frac{f_m(h)}{f_{m-1}(h)}\right|, \quad \beta g = \left|\frac{g_m(h)}{g_{m-1}(h)}\right|, \quad \beta\theta = \left|\frac{\theta_m(h)}{\theta_{m-1}(h)}\right|, \quad \beta S = \left|\frac{S_m(h)}{S_{m-1}(h)}\right|. \tag{2.29}$$

against the number of terms m in the homotopy series are presented in figure (2.3). These figures indicate that the series expansion in (2.25) converge to the exact solution.

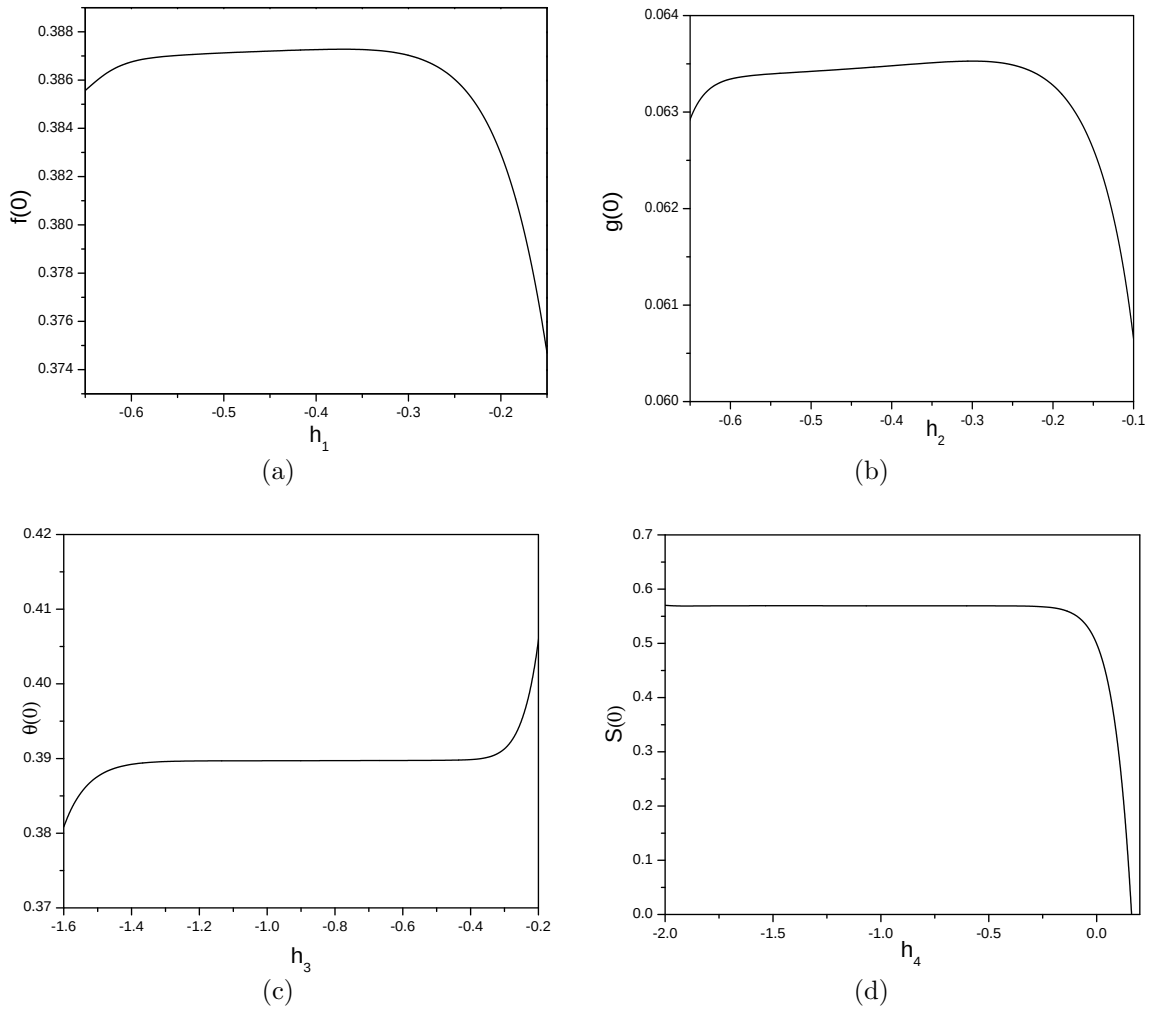

Figure 2.2: "h-curves for (a) $f(\eta)$, (b) $g(\eta)$, (c) $\theta(\eta)$ and (d) $S(\eta)$ when $Nr = 1.0, Nt = 0.5, Gr = 10.0, Ha = 5.0, R = 1.0, A = 1.0, Pr = 1.0, \beta i = 2.0, Re = 2, \beta h = 2.0, Le = 1.0$ and $Br = 0.5$ (mixed convection case)".

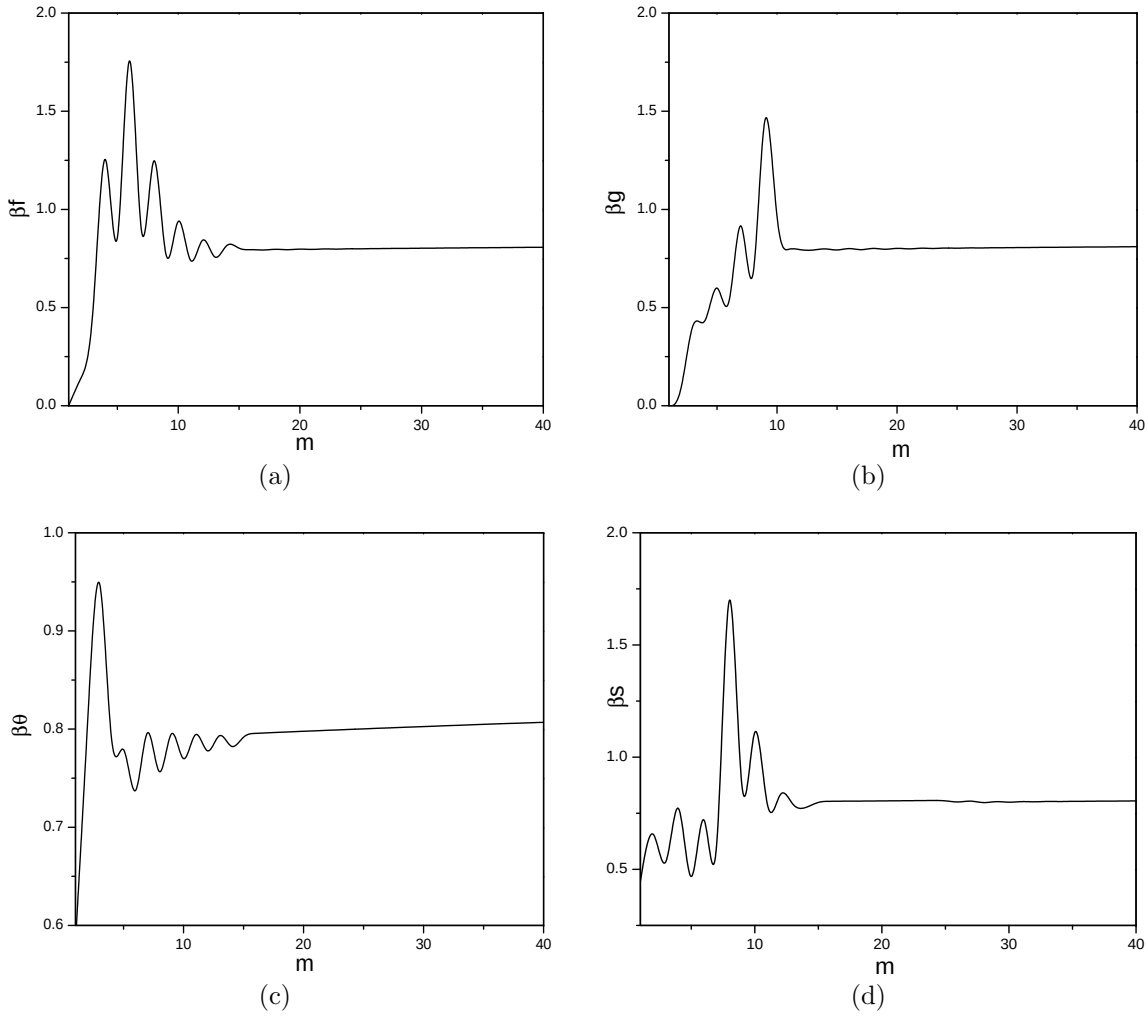

Figure 2.3: "The ratios of βf, βg, $\beta\theta$ and βs to reveal the convergence of the HAM solutions (mixed convection case)".

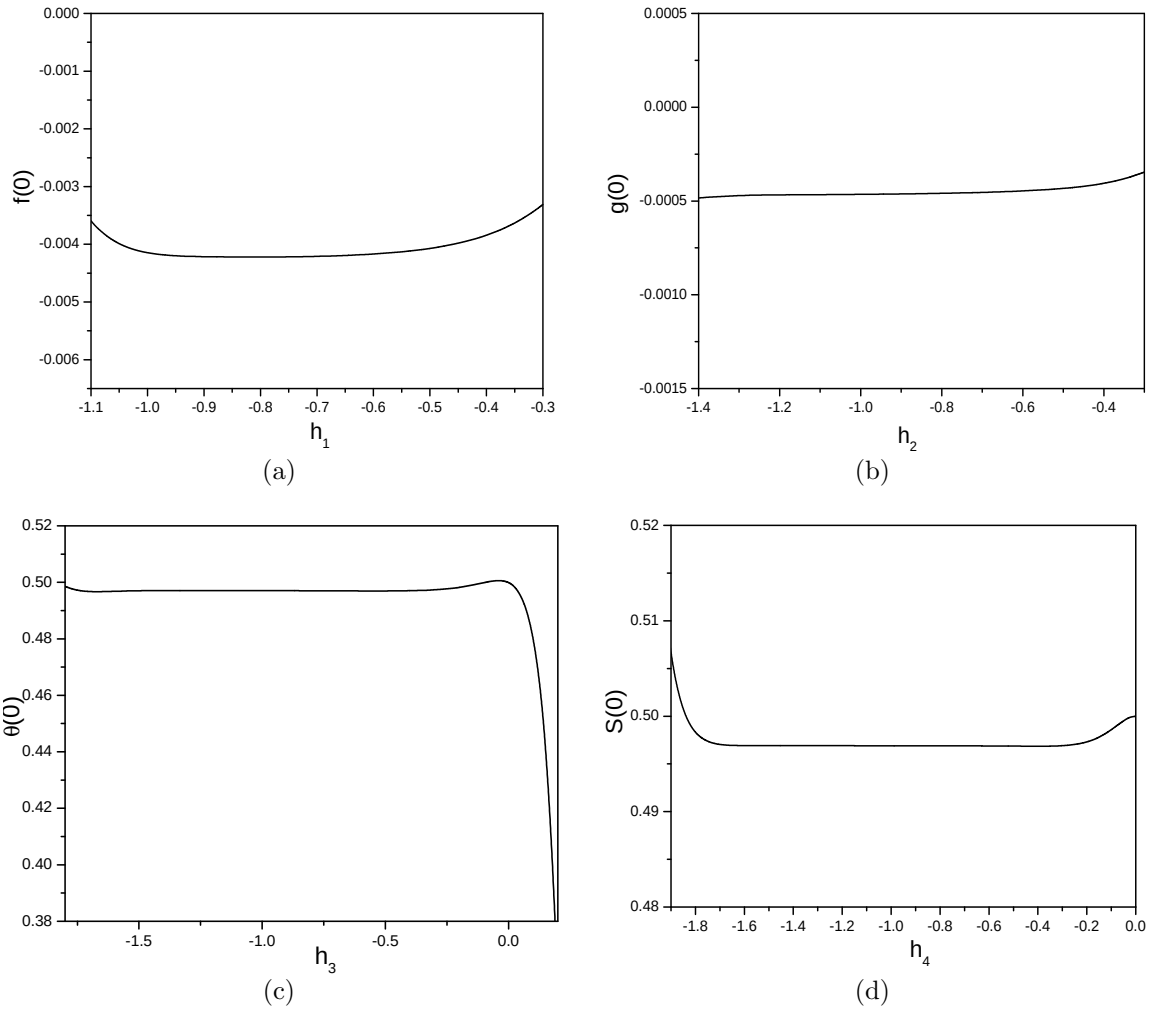

Figure 2.4: "h-curves for (a) $f(\eta)$, (b) $g(\eta)$, (c) $\theta(\eta)$ and (d) $S(\eta)$ when $Nr = 1.0, Nt = 0.5, Gr = 10.0, Ha = 4.0, R = 1.0, Nb = 0.5, Pr = 1.0, \beta i = 2.0, Re = 2, Le = 1.0, \beta h = 2.0$ and $Br = 0.5$(natural convection case)".

Order	f(0)	g(0)	$\theta(0)$	S(0)
5	0.10620400	0.031283400	0.53412318	0.46716189
10	0.10621315	0.030166000	0.54427627	0.46723565
15	0.10621472	0.029013511	0.54731928	0.46734612
20	0.10622485	0.029015717	0.54731934	0.46735634
25	0.10622487	0.029016788	0.54731936	0.46735657
30	0.10622495	0.029023823	0.54732937	0.46735667
35	0.10622496	0.029025837	0.54732938	0.46736671
40	0.10622497	0.029025838	0.54732938	0.46736774
45	0.10622498	0.029026893	0.54732939	0.46736775
50	0.10622498	0.029026893	0.54732939	0.46736879
55	0.10622498	0.029026893	0.54732939	0.46736879

Table 2.2: "Convergence of HAM solutions for different order of approximations (mixed convection case)."

2.4.2 Natural convection

To find the admissible range of the auxiliary parameters, h-curves are plotted for 20^{th}-order of approximation and shown in figure (2.4). It is evident from this figure that the admissible ranges for h_1, h_2, h_3 and h_4 are $-1.0 < h_1 < -0.4$, $-1.4 < h_2 < -0.45$, $-1.7 < h_3 < -0.1$ and $-1.8 < h_4 < -0.2$ respectively. The average residual errors given by (2.28), at different orders of approximations (m), are computed. It is found that the average residual errors are least at $h_1 = -0.49$, $h_2 = -1.2$, $h_3 = -0.22$ and $h_4 = -1.58$. Therefore, the optimum values of convergence control parameters are taken as $h_1 = -0.49$, $h_2 = -1.2$, $h_3 = -0.22$ and $h_4 = -1.59$. Further, the series solutions for different values of m are computed. It is observed from these computed values that the series (2.25) converge in the whole region of η. The graphs of the ratio are shown in figure (2.5) against the number of terms m in the homotopy series and it indicates that the series (2.25) converges to the exact solution.

Order	Optimal of h_1		Optimal of h_2		Optimal of h_3		Optimal of h_4	
	h_1	Min. of E_m	h_2	Min. of E_m	h_3	Min. of E_m	h_4	Min. of E_m
10	-0.49	6.68×10^{-7}	-1.20	4.51×10^{-8}	-0.24	1.89×10^{-5}	-1.58	1.88×10^{-7}
15	-0.49	8.28×10^{-8}	-1.20	1.46×10^{-9}	-0.22	1.98×10^{-5}	-1.60	3.08×10^{-8}
20	-0.50	1.35×10^{-8}	-1.32	7.45×10^{-11}	-0.22	2.05×10^{-5}	-1.58	9.15×10^{-8}

Table 2.3: "Optimal values of h_1, h_2, h_3 and h_4 at different order of approximations (natural convection case)".

Order	f(0)	g(0)	$\theta(0)$	S(0)
5	0.001062040	0.0004656312	0.436658412	0.449041671
10	0.106547215	0.0008211301	0.415106427	0.454270672
15	0.113062142	0.0010397013	0.410628731	0.455023673
20	0.120618062	0.0010598529	0.410337319	0.455477867
25	0.120612487	0.0024016788	0.410546319	0.467356575
30	0.120612495	0.0029023823	0.410546329	0.534617356
35	0.120624963	0.0390258370	0.410546352	0.534657367
40	0.120628976	0.0390283896	0.410546793	0.546723674
45	0.120632449	0.0390293790	0.410547931	0.546723677
50	0.120632498	0.0390296893	0.410547932	0.546732687
55	0.120632498	0.0390296893	0.410547932	0.546736287

Table 2.4: "Convergence of HAM solutions for different order of approximations (natural convection case)".

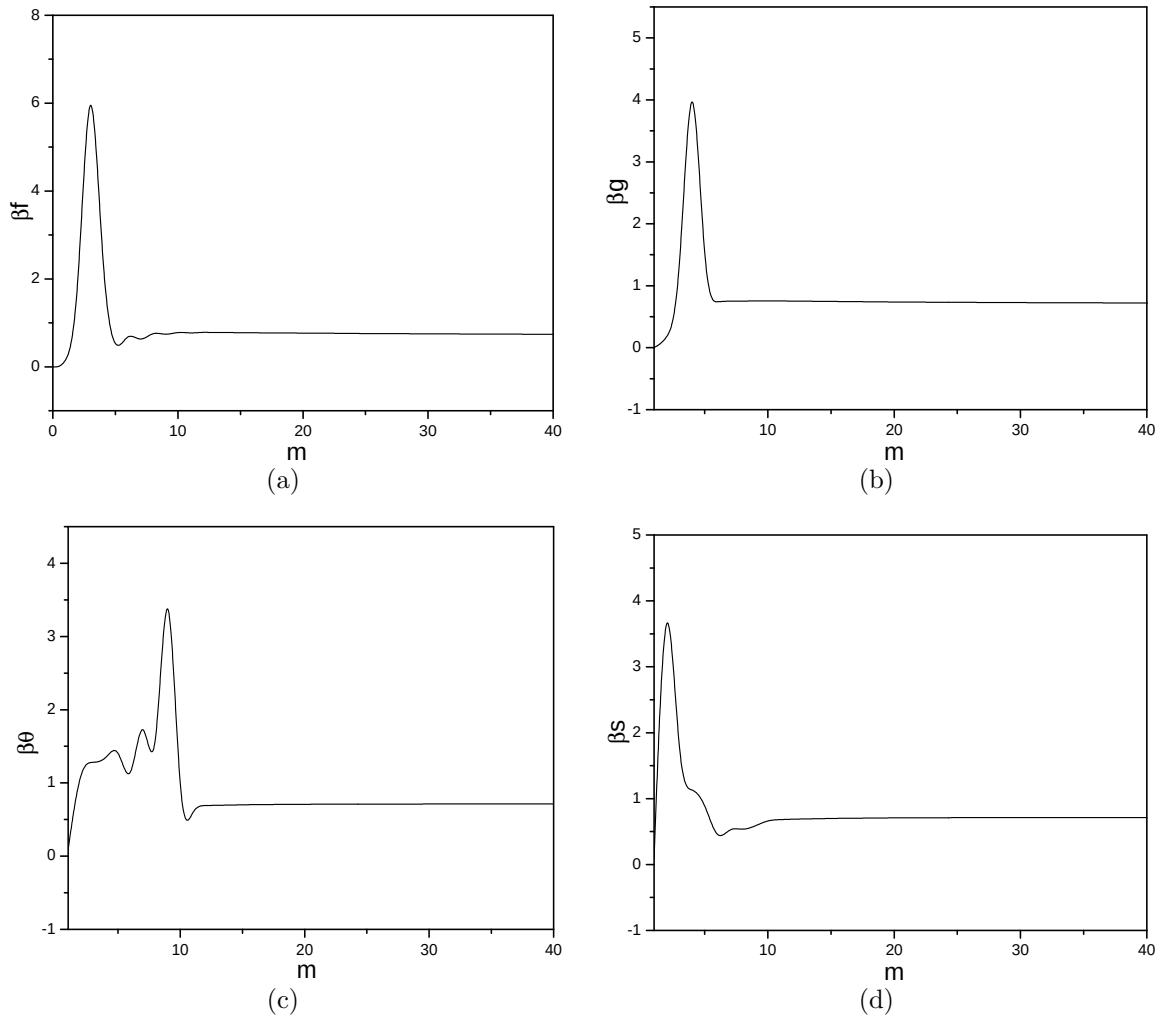

Figure 2.5: "The ratios of βf, βg, $\beta\theta$ and βs to reveal the convergence of the HAM solutions (natural convection case)".

2.5 Results and Discussion

2.5.1 Mixed convection

An influence of magnetic parameter Ha, Hall parameter βh, ion-slip parameter βi, buoyancy ratio parameter Nr and thermophoresis parameter Nt on $f(\eta), g(\eta), \theta(\eta)$ and $S(\eta)$ are presented graphically in figures (2.6) - (2.10). To study the effect of these parameters, the computations were carried out by taking $Le = 1.0$, $Br = 0.5$, $Pr = 1.0$, $Gr = 10$, $R = 1$, $Re = 2$, $Nb = 0.5$ and $A = 1$.

Figure (2.6) exhibits the impact of the magnetic parameter Ha on the velocity in flow direction, induced flow velocity, temperature and nanoparticle concentration. Figure 2.6(a) reveals that the velocity in flow direction is decreasing with an increase in Ha. The transverse magnetic field, which is orthogonal to the flow direction, gives a resistance force called as Lorentz force. This Lorentz force resists the fluid flow and due to this, the velocity in flow direction decreases. The influence of Ha on induced velocity is presented in figure 2.6(b). It is depicted from this figure that the induced velocity is increasing with a rise in Ha. Figure 2.6(c) explains the changes of dimensionless temperature with Ha. It is seen from this figure that the temperature decays with a growth in Ha. Figure 2.6(d) interprets the variations of nanoparticle concentration with Ha. The nanoparticle concentration is reduced with an enhancement in the magnetic parameter. The resistance, created by the Lorentz force, increases the friction between its fluid layers and hence, the temperature and nanoparticle concentration decrease.

The variations of velocity in the flow direction $f(\eta)$, induced flow velocity $g(\eta)$, temperature $\theta(\eta)$ and nanoparticle concentration $S(\eta)$ with βh are presented in figure (2.7). It is identified from figure 2.7(a) that the velocity is increasing with a rise in βh . Figure 2.7(b) reveals that the induced flow in the z-direction ($g(\eta)$) is decreasing as the value of Hall parameter increases. From figure 2.7(c). It is noticed that the temperature $\theta(\eta)$ is diminishing with a rise in βh. The nanoparticle concentration is decreasing with an increase in βh, as depicted in figure 2.7(d). The inclusion of Hall current reduces the effective conductivity

and it drops the resisting force enforced by the magnetic field. Hence the increase in the Hall parameter enhances the velocity component and temperature.

The variations of velocity in the flow direction, cross flow velocity, temperature and nanoparticle concentration with βi are shown in figure (2.8). It is seen from figure 2.8(a) that the velocity in flow direction is increasing with an enhancement in βi. Figure 2.8(b) reveals that the induced flow velocity decays with an enhancement in ion-slip parameter. From figure 2.8(c), it is noticed that the temperature is diminishing with a rise in βi. There is a decay in the nanoparticle concentration with growth in βi, as depicted in figure 2.8(d).

Figure (2.9) represents the influence of Nr on the velocity in flow direction, induced flow velocity, temperature and nanoparticle concentration. From figure 2.9(a), it is identified that the velocity is increasing with a rise in Nr. Figure 2.9(b) explains that the induced flow in the direction of z-axis is diminishing with a rise in Nr. The dimensionless temperature is rising with a rise in Nr, as shown in figure 2.9(c). From figure 2.9(d), it is noticed that the nanoparticle concentration is decreasing with an enhancement in Nr.

The impact of Nt on the velocity in the flow direction, induced flow velocity, temperature and nanoparticle concentration is represented in figure (2.10). The velocity is increasing with a rise in Nt as shown in figure 2.10(a). An increase in Nt leads to increase in the effective conductivity, which in turn, decreases the damping force. It is observed from figure 2.10(b) that the induced flow in the direction of the z-axis is diminishing with an enhancement in Nt. Figure 2.10(c) reveals that the temperature is increasing with an increase in Nt. From figure 2.10(d), it is noticed that the nanoparticle concentration is decays with an enhancement in Nt.

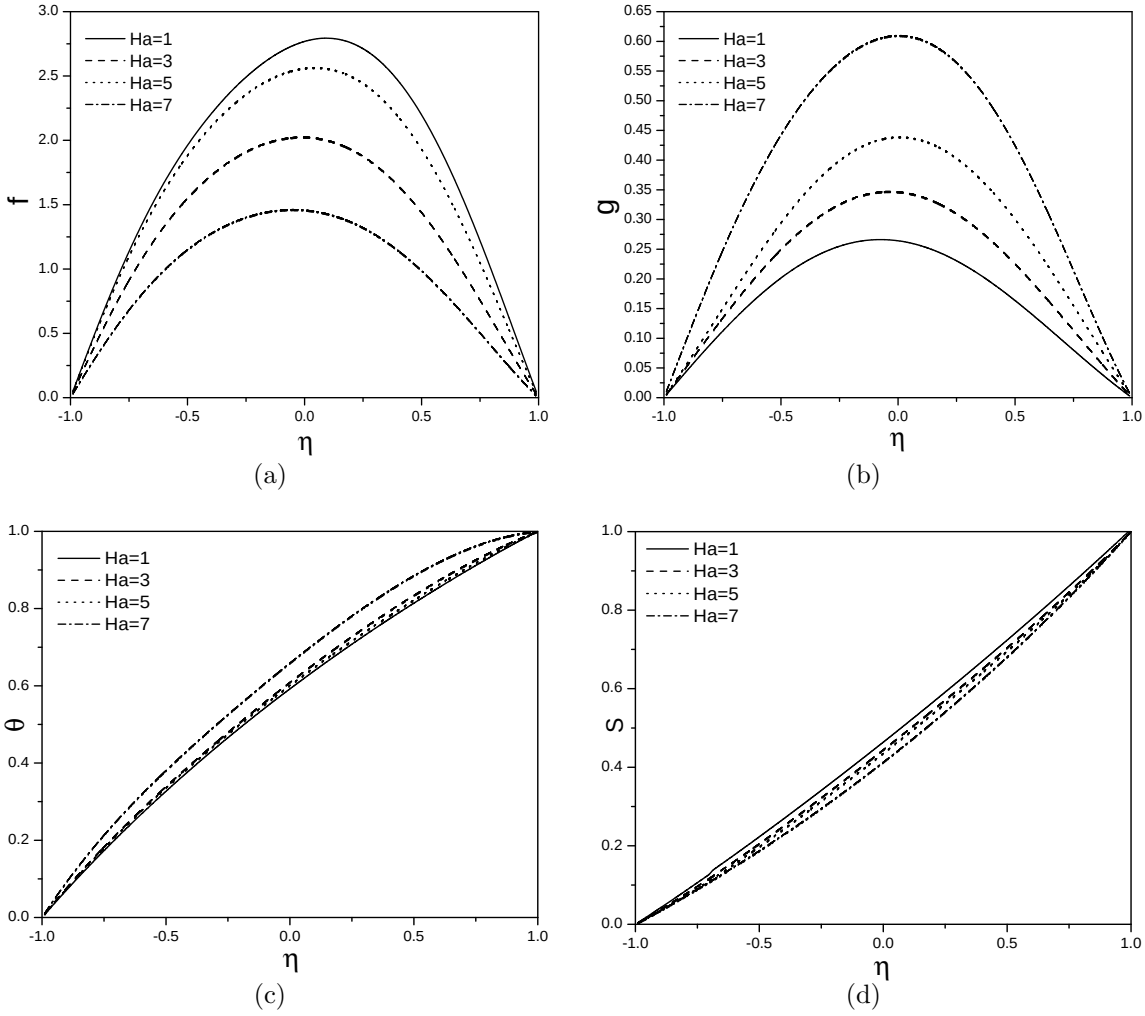

Figure 2.6: "Effect of Ha on (a) $f(\eta)$, (b) $g(\eta)$, (c) $\theta(\eta)$ and (d) $S(\eta)$ for $\beta i = 2.0, Nr = 1.0, Nt = 0.5, Nb = 0.5, \beta h = 2.0, Gr = 10.0, Re = 2.0, R = 1.0, A = 1.0, Le = 1.0, Pr = 1.0$ and $Br = 0.5$ (mixed convection case)".

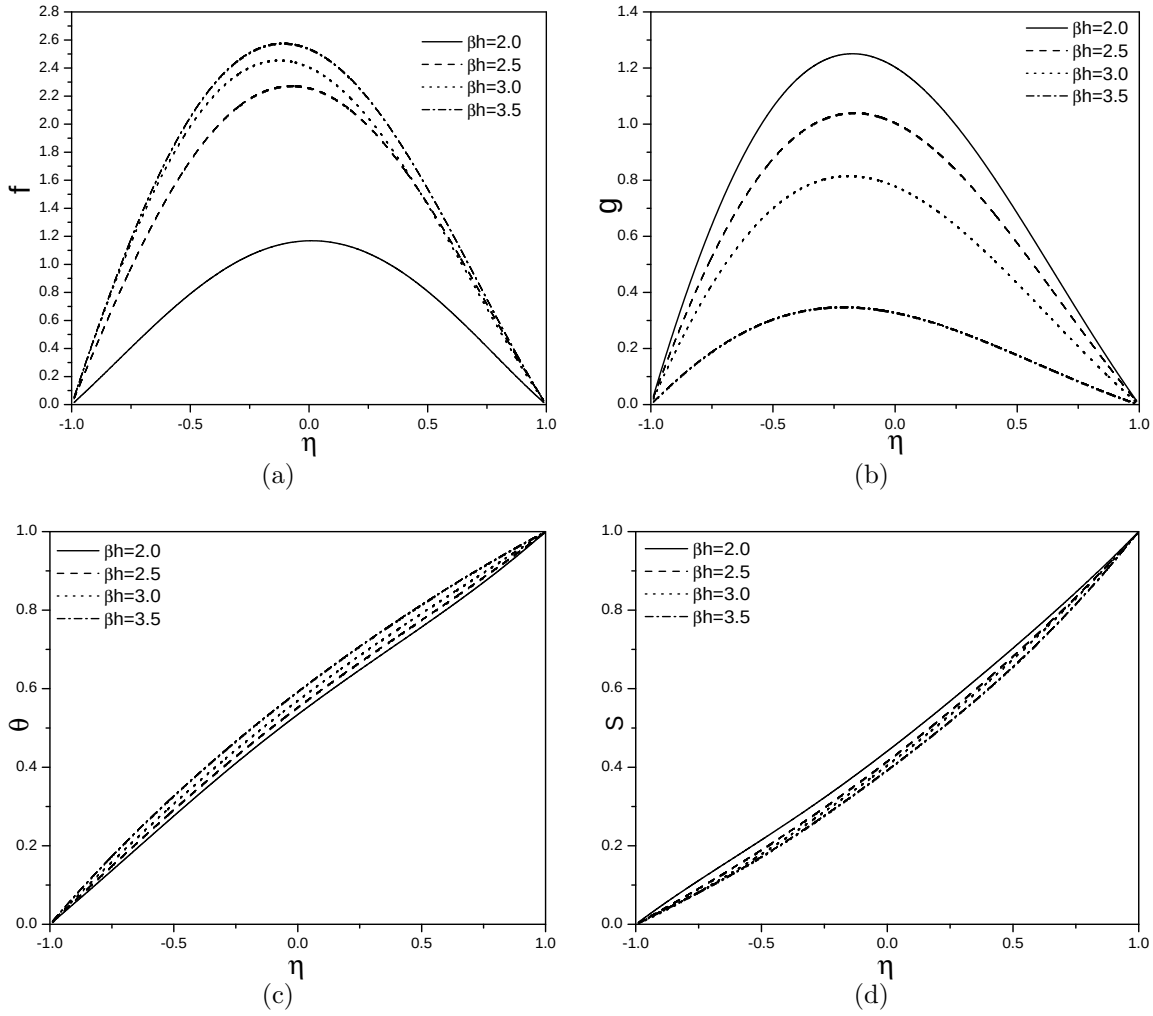

Figure 2.7: "Effect of βh on (a) $f(\eta)$, (b) $g(\eta)$, (c) $\theta(\eta)$ and (d) $S(\eta)$ for $Nr = 1.0, Nt = 0.5, Nb = 0.5, Gr = 10.0, Re = 2.0, R = 1.0, A = 1.0, Pr = 1.0, \beta i = 2.0, Ha = 5.0, Le = 1.0$ and $Br = 0.5$ (mixed convection case)".

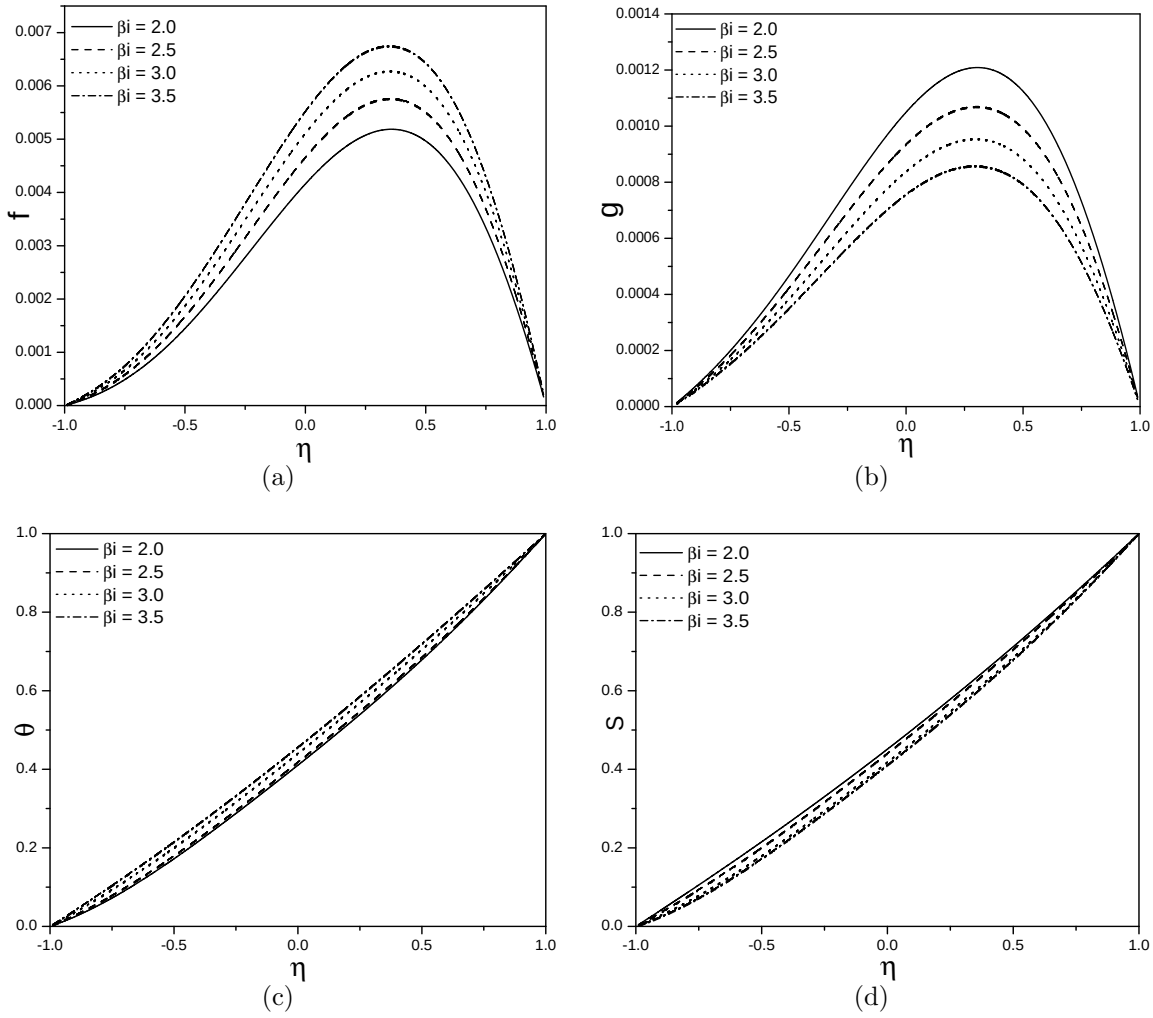

Figure 2.8: "Effect of βi on (a) $f(\eta)$, (b) $g(\eta)$, (c) $\theta(\eta)$ and (d) $S(\eta)$ for $\beta h = 2.0, Nr = 1.0, Nt = 0.5, Nb = 0.5, Gr = 10.0, Re = 2.0, R = 1.0, A = 1.0, Pr = 1.0, Le = 1.0, Ha = 5.0$ and $Br = 0.5$ (mixed convection case)".

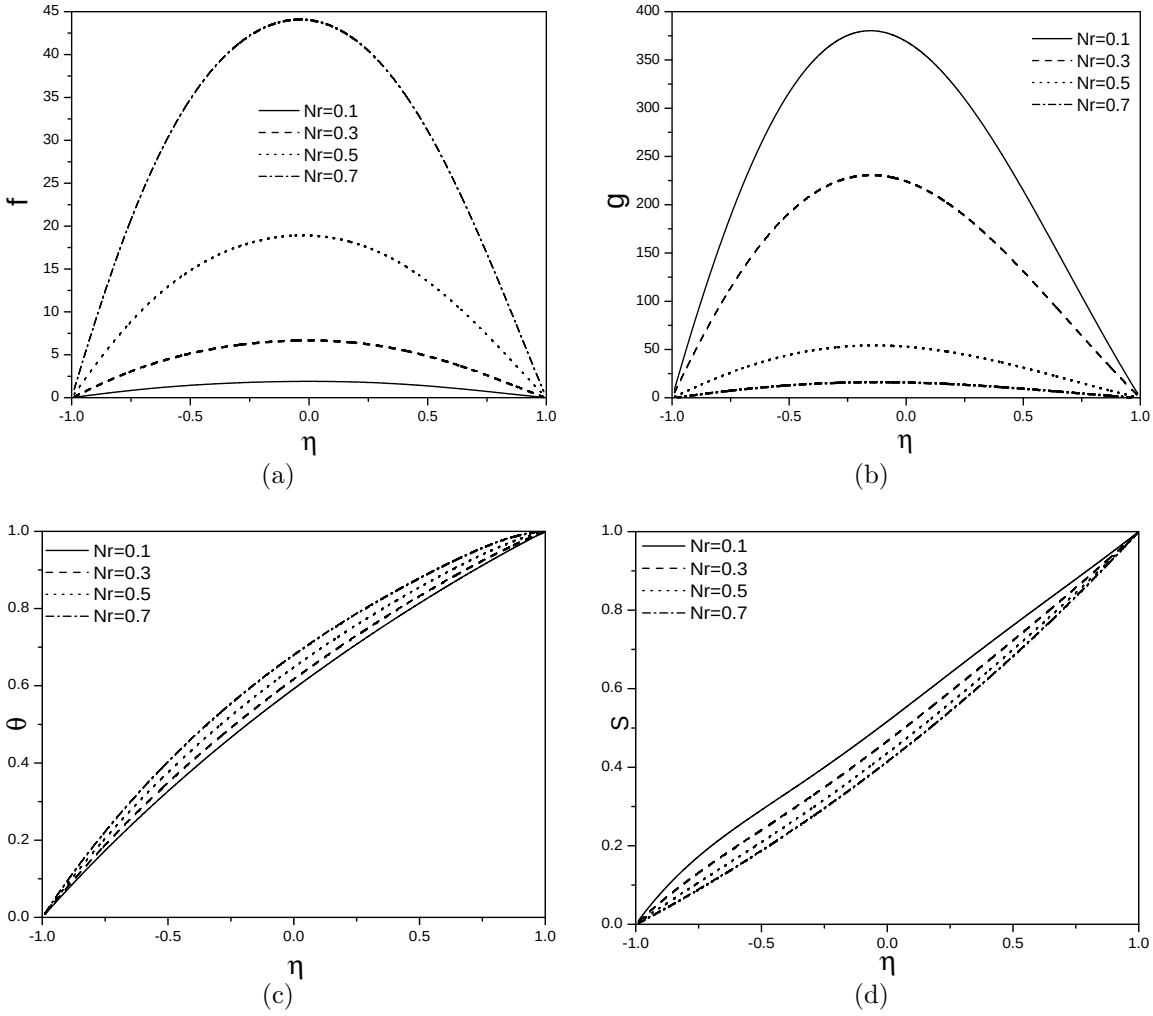

Figure 2.9: "Effect of Nr on (a) $f(\eta)$, (b) $g(\eta)$, (c) $\theta(\eta)$ and (d) $S(\eta)$ for $\beta h = 2.0, Nt = 0.5, Nb = 0.5, Gr = 10.0, Re = 2.0, R = 1.0, A = 1.0, Pr = 1.0, \beta i = 2.0, Le = 1.0, Ha = 5.0$ and $Br = 0.5$ (mixed convection case)."

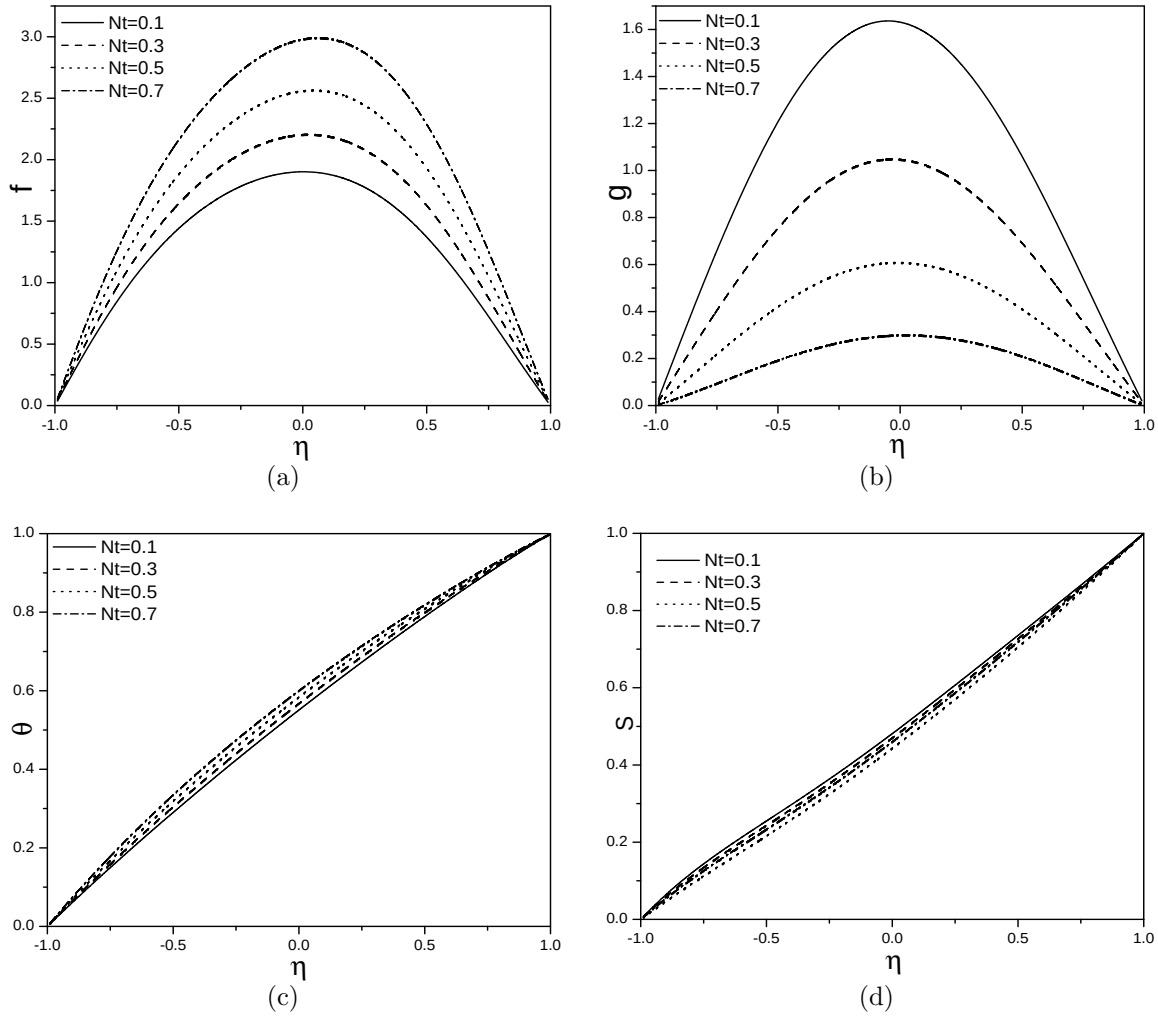

Figure 2.10: "Effect of Nt on (a) $f(\eta)$, (b) $g(\eta)$, (c) $\theta(\eta)$ and (d) $S(\eta)$ for $Nr = 1.0, Nb = 0.5, \beta h = 2.0, Gr = 10.0, Re = 2.0, R = 1.0, A = 1.0, Pr = 1.0, \beta i = 2.0, Ha = 5.0$ and $Br = 0.5$ (mixed convection case)".

2.5.2 Natural convection

The effects of magnetic parameter Ha, Hall parameter βh, ion-slip parameter βi, thermophoresis parameter Nt and Brownian motion Nb on $f(\eta)$, $g(\eta)$, $\theta(\eta)$ and $S(\eta)$ are shown graphically in figures (2.11) - (2.15). To study the effects of these parameters, the computations were carried out by taking $Le = 1.0$, $Br = 0.5$, $Pr = 1.0$, $Gr = 10$, $R = 1$, $Re = 2$ and $Nr = 1.0$.

Figure (2.11) shows the impact of magnetic parameter Ha on the velocity in flow direction, cross flow velocty, temperature and nanoparticle concentration. Figure 2.11(a) reveals that the velocity in flow direction diminishes with an enhancement in Ha. The transverse magnetic field which is applied normal to the flow direction gives rise to a resistive force known as Lorentz force. This Lorentz force resists the flow and hence, the velocity in flow direction decreases. The impact of Ha on the $g(\eta)$ is shown in figure 2.11(b). It is seen from this figure that $g(\eta)$ increases with an enhancement in Ha. Figure 2.11(c) presents the variation of non-dimensional temperature with Ha. It shows that the temperature drops with an intensification in Ha. Figure 2.11(d) shows the variation of nanoparticle concentration with Ha. The nanoparticle concentration $S(\eta)$ increases with an increase in Ha as shown in figure 2.11(d). The resistance, created by Lorentz force, increases the friction between its fluid layers and thus decreases its temperature and increases nanoparticle concentration.

The variations of velocity in flow direction $f(\eta)$, cross flow velocty $g(\eta)$, temperature $\theta(\eta)$ and nanoparticle concentration $S(\eta)$ with βh are presented in figure (2.12). It is noticed from figure 2.12(a) that the velocity in flow direction increases with an increase in βh. Figure 2.12(b) reveals that the induced flow in the z-direction $g(\eta)$ decreases as Hall parameter increases. From figure 2.12(c), it is noticed that the temperature $\theta(\eta)$ increases with a rise in βh. There is an increase in the nanoparticle concentration $S(\eta)$ with an increase in βh as depicted in figure 2.12(d). The inclusion of Hall parameter reduces the effective conductivity then it drops the resistive force imposed by the magnetic field. Hence an increase in Hall parameter increases the velocity component $f(\eta)$ and temperature $\theta(\eta)$.

The variations of velocity in flow direction $f(\eta)$, induced flow velocty $g(\eta)$, temperature

$\theta(\eta)$ and nanoparticle concentration $S(\eta)$ with βi are shown in figure (2.13). It is observed from figure 2.13(a) that the dimensionless velocity in flow direction increases with an increase in βi. Figure 2.13(b) reveals that the induced flow in the z-direction $g(\eta)$ decreases as ion-slip parameter increases. From figure 2.13(c), it is noticed that the temperature $\theta(\eta)$ rises with a rise in βi. There is a decrease in the nanoparticle concentration $S(\eta)$ with an increase in βi as depicted in figure 2.13(d).

Figure (2.14) represent the impact of Nb on the velocity in flow direction $f(\eta)$, induced flow velocity $g(\eta)$, temperature $\theta(\eta)$ and nanoparticle concentration $S(\eta)$. From figure 2.14(a), it is identified that the velocity $f(\eta)$ increases with a rise in Nb. Figure 2.14(b) explains that the induced flow in the direction of $z-$axis, increases with a rise in Nb. The dimensionless temperature $\theta(\eta)$ increases with an increase in Nb as shown in figure 2.14(c). From figure 2.14(d), it is noticed that the nanoparticle concentration $S(\eta)$ decreases with an enhancement in Nb.

The effect of Nt on the velocity in flow direction $f(\eta)$, induced flow velocity $g(\eta)$, temperature $\theta(\eta)$ and nanoparticle concentration $S(\eta)$ are presented in figure (2.15). The velocity $f(\eta)$ increases with a rise in Nt as shown in figure 2.15(a). Increase in Nt leads to an increase in the effective conductivity, which in turn, increase in the damping force on the velocity component $f(\eta)$. It is observed from figure 2.15(b) that the induced flow in the direction of $z-$axis increases with an enhancement in Nt. Figure 2.15(c) reveals that the temperature $\theta(\eta)$ increasing with an enhancement in Nt. From figure 2.15(d), it is noticed that the nanoparticle concentration $S(\eta)$ is increasing with an enhancement in Nt.

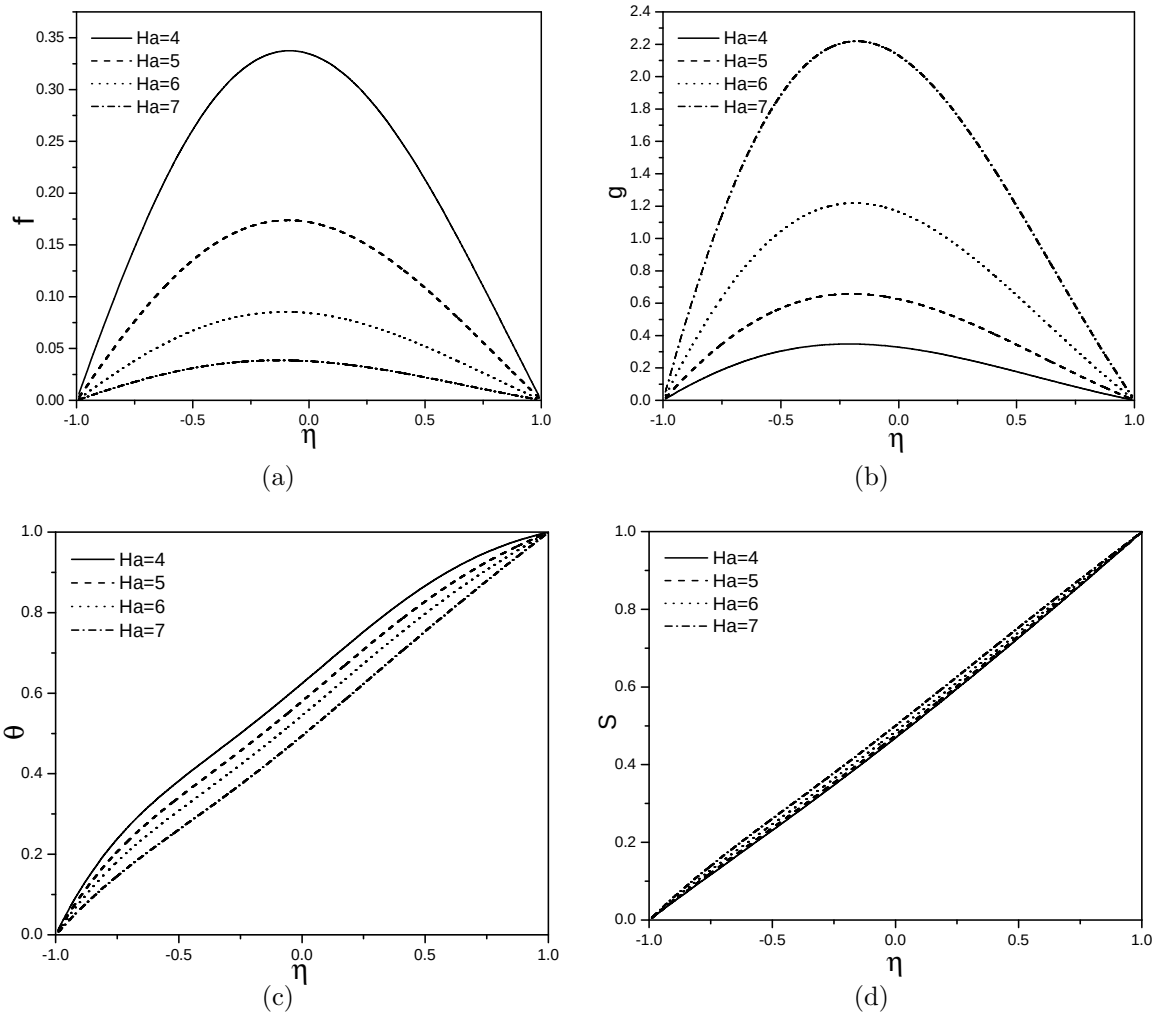

Figure 2.11: "Effect of Ha on (a) $f(\eta)$, (b) $g(\eta)$, (c) $\theta(\eta)$ and (d) $S(\eta)$ for $Nr = 1.0, Gr = 10, Re = 2.0, R = 1.0, Pr = 1.0, \beta i = 2.0, Le = 1.0, \beta h = 2.0$ and $Br = 0.5$ (natural convection case)".

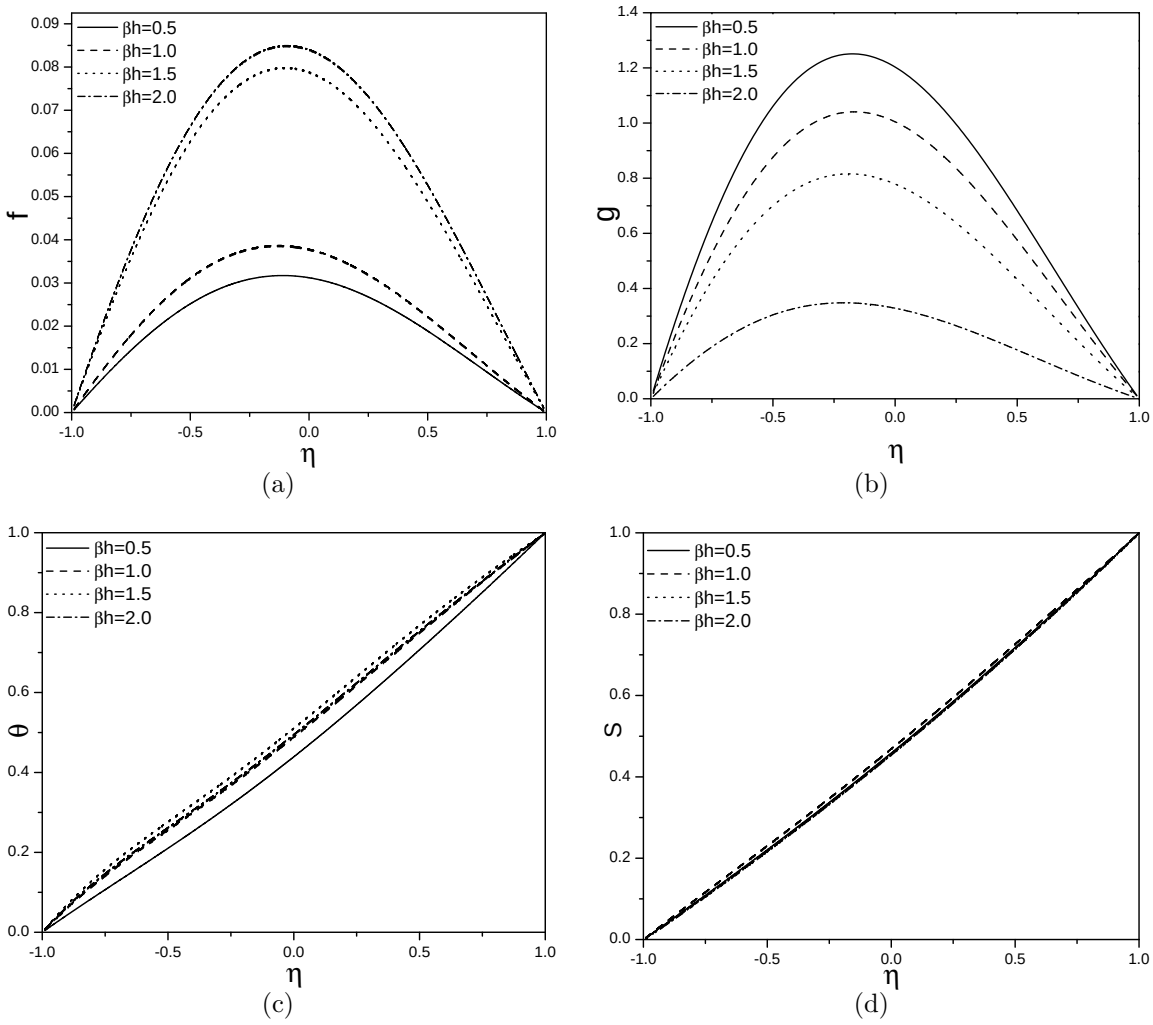

Figure 2.12: "Effect of βh on (a) $f(\eta)$, (b) $g(\eta)$, (c) $\theta(\eta)$ and (d) $S(\eta)$ for $Nr = 1.0, Gr = 10, Re = 2.0, R = 1.0, Pr = 1.0, \beta i = 2.0, Le = 1.0, Ha = 4.0$ and $Br = 0.5$ (natural convection case)".

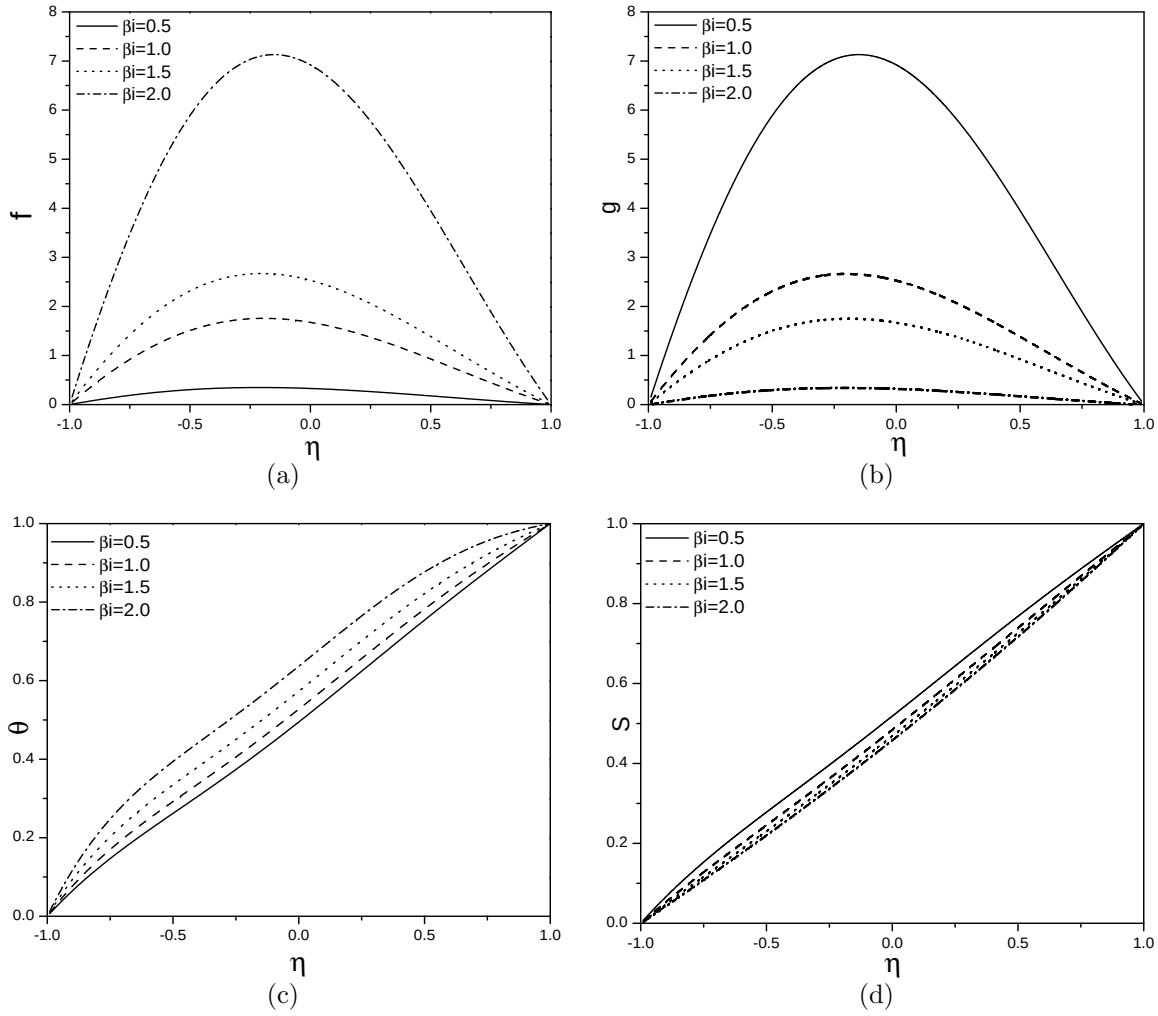

Figure 2.13: "Effect of βi on (a) $f(\eta)$, (b) $g(\eta)$, (c) $\theta(\eta)$ and (d) $S(\eta)$ for $Nr = 1.0, Gr = 10, Ha = 4.0, Re = 2.0, R = 1.0, Pr = 1.0, Le = 1.0, \beta h = 2.0$ and $Br = 0.5$ (natural convection case)".

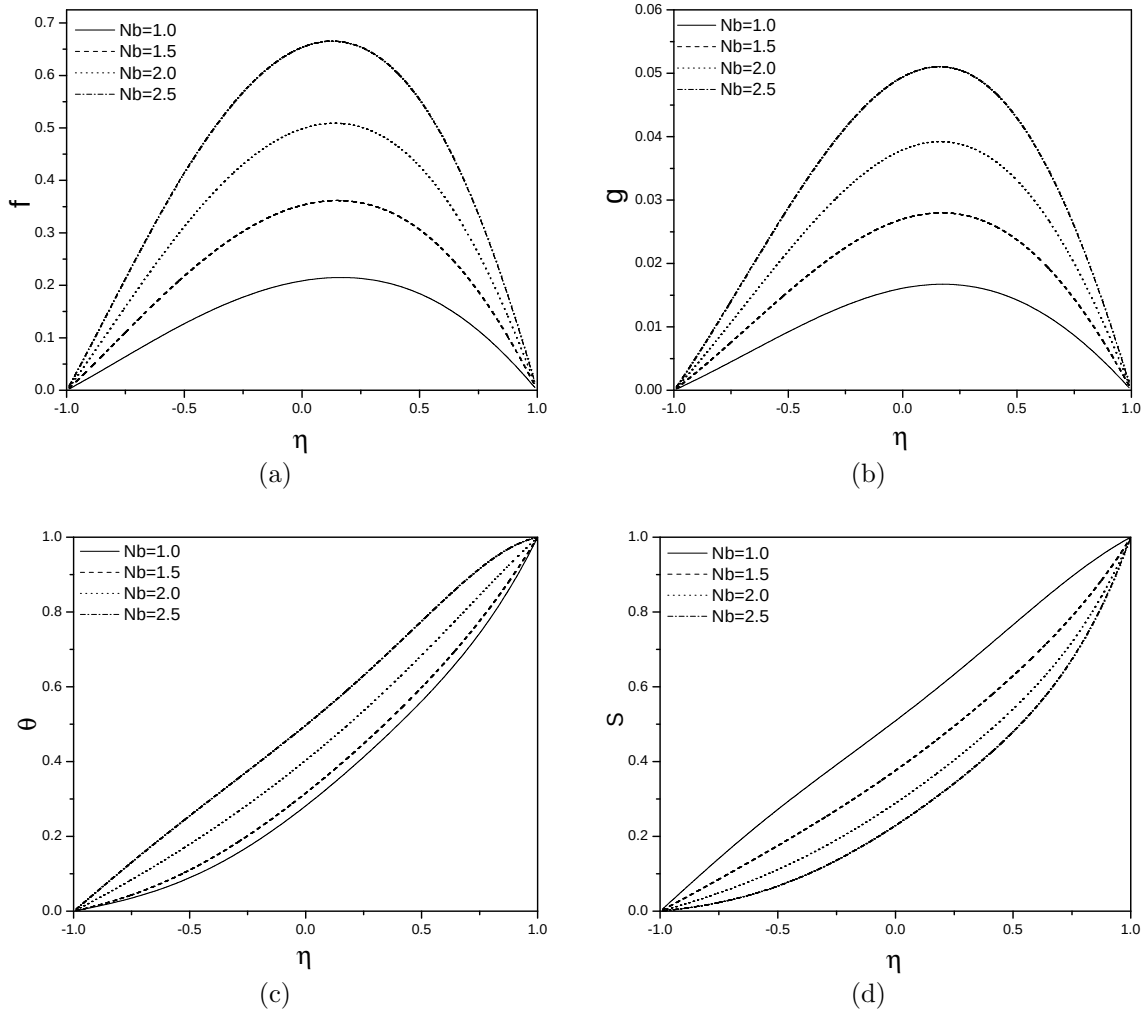

Figure 2.14: "Effect of Nb on (a) $f(\eta)$, (b) $g(\eta)$, (c) $\theta(\eta)$ and (d) $S(\eta)$ for $Nr = 1.0, Gr = 10, Ha = 4.0, Re = 2.0, R = 1.0, Pr = 1.0, \beta i = 2.0, Le = 1.0, \beta h = 2.0$ and $Br = 0.5$ (natural convection case)".

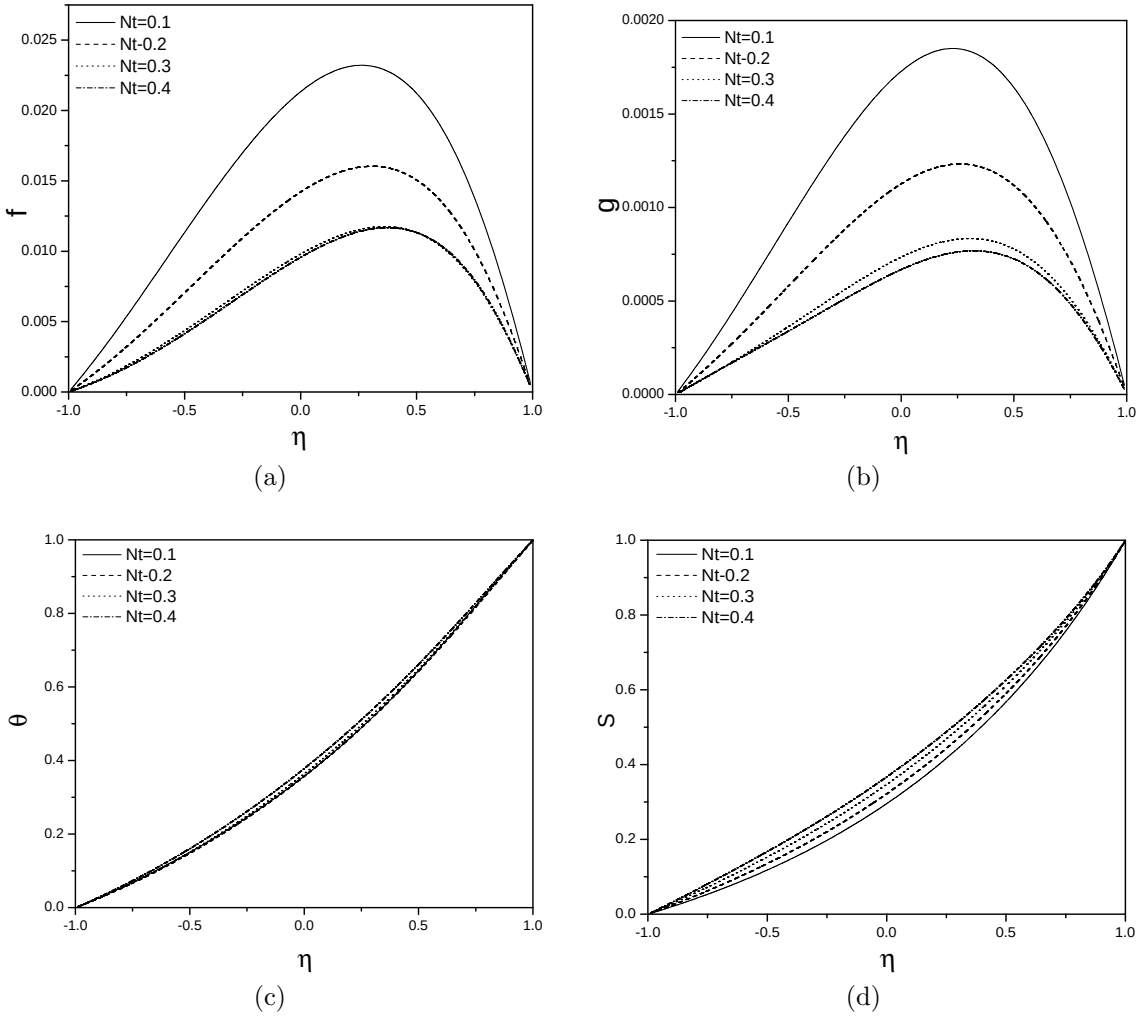

Figure 2.15: "Effect of Nt on (a) $f(\eta)$, (b) $g(\eta)$, (c) $\theta(\eta)$ and (d) $S(\eta)$ for $Nr = 1.0, Gr = 10, Ha = 4.0, Re = 2.0, R = 1.0, Pr = 1.0, \beta i = 2.0, Le = 1.0, \beta h = 2.0$ and $Br = 0.5$ (natural convection case)".

2.6 Conclusions

In this chapter, the steady, laminar and an incompressible flow of a nanofluid passing through a vertical channel has been investigated in the presence of MHD, Hall and ion-slip effects with the natural and mixed convective flows. From the analysis, the following are the major observations in both cases.

With an increase in the magnetic parameter, the velocity in flow direction and the temperature decrease, whereas the velocity in z-direction increases in both the cases, but the nanoparticle concentration increases in case of natural convection, whereas it decreases in case of mixed convection. As Hall parameter increases, the dimensionless temperature and velocity in the flow direction increase, whereas the induced flow velocity decreases in both the cases, but the nanoparticle concentration increases in case of natural convection, whereas it decreases in case of mixed convection. The dimensionless temperature and the velocity in the flow direction increase, but the nanoparticle concentration and the flow velocity in z-direction decrease in both the cases with an ion-slip parameter increases. As the Brownian motion parameter increases, the dimensionless temperature and the velocity in the flow direction increase, but the nanoparticle concentration decreases in case of natural convection.

Chapter 3

Radiation and Joule heating effects on entropy generation due to MHD mixed convective flow of a nanofluid in a vertical channel [1]

3.1 Introduction

The study of mixed convective heat transfer and nanofluid flow in a vertical channel has a wide range of applications in thermal engineering equipment. Grosan and Pop [36] analyzed the fully developed and mixed convective nanofluid flow in a vertical channel. Further, the radiation effect on convective flow of a nanofluid under different geometries have a vast range of applications involving a high temperatures such as gas turbines, missiles, satellites, nuclear power plant, aircraft, space vehicles etc. Chamkha *et al* [14] studied numerically the effects of thermal radiation on mixed convective flow around a cone inscribed in a porous medium filled with a nanofluid. Numerous studies have been carried out to explore the effect of Joule heating on fluid flow and heat transfer at various conditions and found that, it plays

[1] Published ins "**International Journal of Engineering and Technology, Vol.9, No. 4(2017)** "

a significant role on MHD flow and heat transfer. Anand *et al* [4] analyzed the thermal radiation and Joule heating effect on magnetohydrodynamic flow of a nanofluid in boundary layer. Hayat *et al* [70] presented a model for Joule heating and solar radiation in MHD convective flow of a nanofluid.

Also, the optimal design criteria for thermal systems by minimizing their entropy generation has been a topic of great interest in recent times. In the energy optimization problems and in the design of many traditional heat removal engineering devices, it is necessary to minimize the entropy generation due to heat transfer and fluid friction. Bejan [9] introduced the entropy generation minimization method and developed its applications in an engineering sciences. Since then several researchers have been studying the entropy generation analysis for different types of geometries with diverse fluids. Omid *et al* [63, 62] analyzed the significance of radiation effect on entropy generation within nanofluids. Dehsara *et al* [25] analyzed numerically the entropy generation in a nanofluid flow in the presence of variable magnetic field, viscous dissipation and solar radiation.

The present chapter concentrates on the investigation of characteristics of mixed convective flow of a nanofluid through a vertical channel with Joule heating and thermal radiation effect. The homotopy analysis method is used to solve the governing nonlinear differential equations. The effects of radiation, Joule heating and magnetic parameter on the velocity along the fluid direction, temperature, nanoparticle concentration, Bejan number and entropy generation are investigated.

3.2 Mathematical Formulation

Consider a laminar, steady, incompressible and electrically conducting nanofluid flow through a vertical channel of width $2d$. The physical model and coordinate system is given in figure (2.1). The fluid is considered to be absorbing/emitting radiation, but non-scattering medium. T descibe the radiative heat flux, Rosseland approximation [76] is used in an energy equation. Apart from the uniform magnetic field B_0 applied in $y-$direction, the Joule heating effect is

also considered.

The governing equations of the fluid flow, under the assumption of low magnetic Reynolds number and Boussinesq approximation, are as follows

$$\frac{\partial v}{\partial y} = 0 \tag{3.1}$$

$$\rho_f \, v \frac{\partial u}{\partial y} = -\frac{\partial p}{\partial x} + \mu \frac{\partial^2 u}{\partial y^2} + (1 - \phi_m)\rho_{f_0} g^* \, \beta_T (T - T_1) - (\rho_s - \rho_{f_0}) \, g^* (\phi - \phi_1) - \sigma \, B_0^2 \, u \tag{3.2}$$

$$v \frac{\partial T}{\partial y} = \alpha \frac{\partial^2 T}{\partial y^2} - \frac{1}{\rho c_p} \frac{\partial q_r}{\partial y} + \frac{2\mu}{\rho c_p} \left(\frac{\partial u}{\partial y} \right)^2 + \tau \left[D_B \frac{\partial T}{\partial y} \frac{\partial \phi}{\partial y} + \frac{D_T}{T_m} \left(\frac{\partial T}{\partial y} \right)^2 \right] + \frac{1}{\rho c_p} \, \sigma \, B_0^2 \, u^2 \tag{3.3}$$

$$\frac{\partial \phi}{\partial y} v = \frac{D_T}{T_m} \frac{\partial^2 T}{\partial y^2} + D_B \frac{\partial^2 \phi}{\partial y^2} \tag{3.4}$$

The conditions on the boundary are

$$\begin{aligned} u = 0, \quad v = v_0, \quad T = T_1, \quad \phi = \phi_1 \quad \text{on} \quad y = -d, \\ u = 0, \quad v = v_0, \quad T = T_2, \quad \phi = \phi_2 \quad \text{on} \quad y = d \end{aligned} \tag{3.5}$$

Radiation heat flux q_r, using Rosseland approximation, is taken as

$$q_r = -\frac{4\sigma^*}{3\chi} \frac{\partial T^4}{\partial y} \tag{3.6}$$

where σ^* is a Stefan-Boltzman constant and χ is the coefficient of mean absorption. We assume the variation in fluid phase temperature inside the flow to be appropriately minimum such that T^4 may be expressed as a linearly continuous function of the temperature and expanding in a Taylor series around T_m and removing highest order terms, we get $T^4 = 4T_m^3 \, T - 3T_m^4$.

It is to be noted from (3.1) and the boundary conditions (3.5) that $v = v_0$ (a constant).

Introducing the following non-dimensional varaibles

$$\eta = \frac{y}{d},\ f = \frac{u}{u_0},\ p = \frac{\mu\, u_0}{d^2}\, P,\ \theta = \frac{T - T_1}{T_2 - T_1},\ S = \frac{\phi - \phi_1}{\phi_2 - \phi_1} \tag{3.7}$$

in Eqs. (3.1) - (3.4), we get

$$f'' - Rf' + \frac{Gr}{Re}\,(\theta - NrS) + Ha^2\, f - A = 0 \tag{3.8}$$

$$\theta''(1 + \frac{4}{3}Rd) - R\,Pr\,\theta' + PrNb\,\theta' S' + PrNt\,\theta'^2 + 2\,Br(f')^2 + J\,f^2 = 0 \tag{3.9}$$

$$S'' - R\,Le\,S' + \frac{Nt}{Nb}\theta'' = 0 \tag{3.10}$$

where $J = \dfrac{{u_0}^2 \sigma\, B_0^2\, d^2}{(T_2 - T_1)k_f}$ is Joule heating parameter and $Rd = \dfrac{4\sigma}{3\chi}\,\dfrac{T_m^3}{K_f}$ is radiation parameter. The other parameters are defined in the earlier chapter.

The corresponding conditions on boundary (3.5) become

$$\begin{aligned} S = 0, \quad \theta = 0, \quad f = 0 \quad \text{at} \quad \eta = -1 \\ S = 1, \quad \theta = 1, \quad f = 0 \quad \text{at} \quad \eta = 1 \end{aligned} \tag{3.11}$$

3.3 Solution of the problem

The governing Eqs. (3.8) - (3.10) along with the boundary conditions (3.11) are solved by using homotopy analysis method (HAM) [47, 48, 49, 50]. This method is explained in detail in the previous chapter.

As explained in chapter-2, the rate of convergence of approximation for the HAM solution strongly depends on the values of auxiliary parameter h. Hence, the h-curves are plotted for 20^{th} order of approximation and presented in figure (3.1). From these figures, it is found that the admissible ranges for h_1, h_2 and h_3 are $-0.6 < h_1 < 0$, $-0.7 < h_2 < 0$ and $-1.0 < h_3 < -0.2$ respectively. In order to obtain the optimal value of the auxiliary

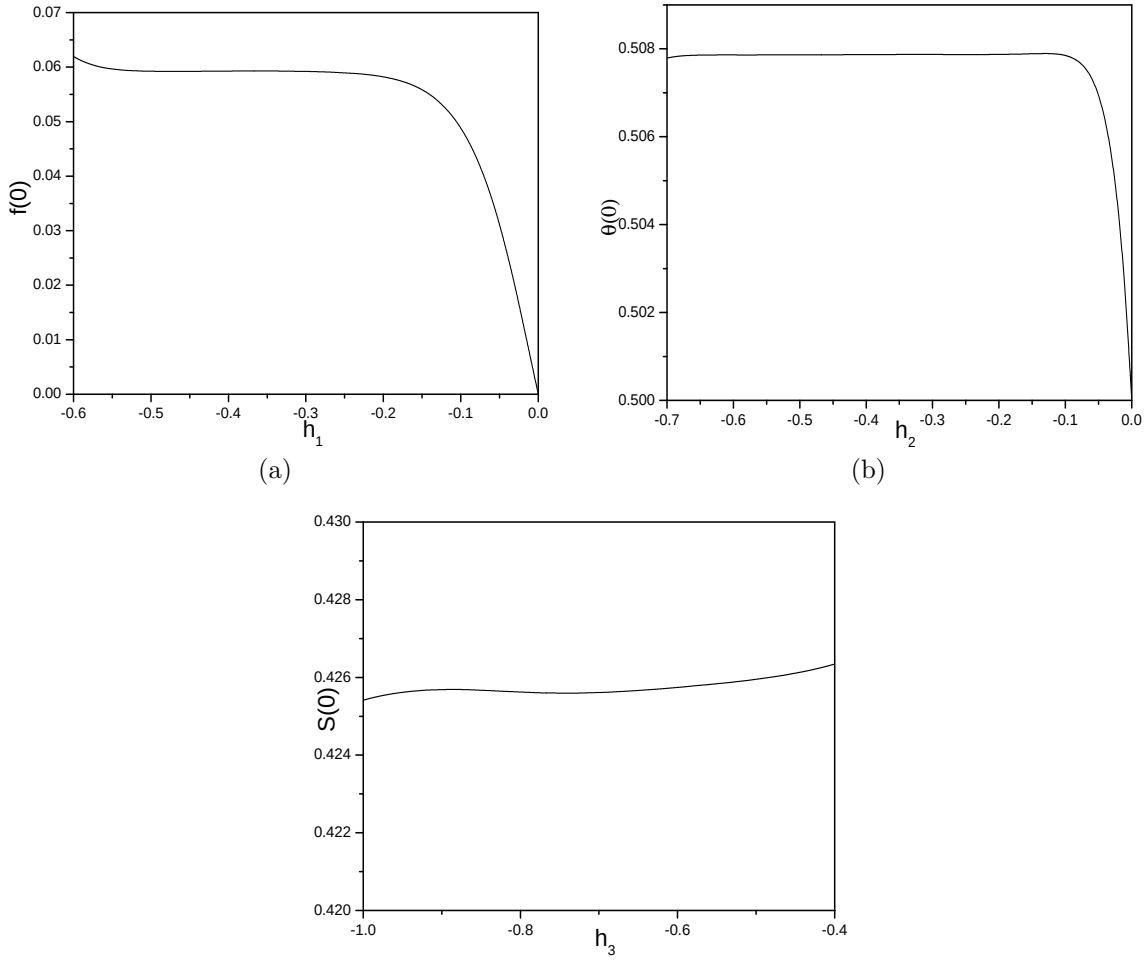

(a) (b)

(c)

Figure 3.1: "h-curves for (a) $f(\eta)$, (b) $\theta(\eta)$ and (c)$S(\eta)$ when $Nr = 1, Nt = 1, Gr = 10, R = 1, Nb = 0.5, Pr = 1, A = 1, Re = 2, Le = 1, Rd = 1.5, Ha = 2, Br = 0.5, J = 2$ and $Tp = 0.1$".

parameters, the average residual errors (given by (2.28)) are calculated and shown in table (3.1). From these average residual errors, it is noticed that the optimal value of auxiliary parameters are $h_1 = -0.3$, $h_2 = -0.64$ and $h_3 = -0.73$.

Further, the series solutions for different values of m are computed and presented in table (8.2). It is found from this table that the series solution converges in the whole region of η

	Optimal of h_1		Optimal of h_2		Optimal of h_3	
Order	h_1	Min. of E_m	h_2	Min. of E_m	h_3	Min. of E_m
10	-0.31	7.77×10^{-6}	-0.64	2.32×10^{-5}	-0.73	5.31×10^{-4}
15	-0.30	1.19×10^{-5}	-0.60	1.25×10^{-4}	-0.73	2.31×10^{-4}
20	-0.30	3.19×10^{-6}	-0.64	36.05×10^{-5}	-0.75	1.60×10^{-4}

Table 3.1: "At different order of approximations, the optimal values of h_1, h_2, and h_3".

Order	f(0)	$\theta(0)$	S(0)
05	0.0996756660	0.4756995038	0.3252773388
10	0.1055946694	0.4767324900	0.3156283339
15	0.1063916720	0.4772954862	0.3145533334
20	0.1065646732	0.4774348404	0.3145533332
25	0.1066468132	0.4775840270	0.3145353201
30	0.1066496324	0.4776434840	0.3145353198
35	0.1066546731	0.4778384021	0.3145353198
40	0.1066546732	0.4778348402	0.3145353198
45	0.1066546821	0.4778348402	0.3145353198
50	0.1066546821	0.4778348402	0.3145353198
55	0.1066546821	0.4774848402	0.3145353198

Table 3.2: "At different order of approximations, the convergence of HAM solutions".

3.4 Entropy Generation

The volumetric rate of local entropy generation of a nanofluid flow in a vertical channel can be expressed as

$$\begin{aligned} S_G &= \frac{K_f}{T_1^2}\left[\left(\frac{\partial T}{\partial y}\right)^2 + \frac{16\sigma}{3\chi}\frac{T_m^3}{K_f}\left(\frac{\partial T}{\partial y}\right)^2\right] + \frac{\sigma\, B_0^2\, u^2}{T_1} \\ &+ \frac{2\mu}{T_1}\left(\frac{\partial u}{\partial y}\right)^2 + \frac{Ru\, D}{\phi_1}\left(\frac{\partial \phi}{\partial y}\right)^2 + \frac{Ru\, D}{T_1}\left(\frac{\partial T}{\partial y}\right)\left(\frac{\partial \phi}{\partial y}\right) \end{aligned} \tag{3.12}$$

where Ru is the universal gas constant and D is the mass diffusivity through the fluid.

According to Bejan [12], entropy generation number Ns is the ratio of the volumetric entropy generation rate to the characteristic entropy generation rate. Therefore, the entropy generation number is given by

$$Ns = (1 + \frac{4}{3}Rd)\,\theta'^2 + \frac{1}{\Omega_3}\left(2\,Br f'^2 + J\,f^2\right) + \phi_3\, S'^2 + \phi_4\,\theta' S' \tag{3.13}$$

The dimensionless coefficients are ϕ_3 and ϕ_4, called irreversibility distribution ratios, which are related to diffusive irreversibility, given by

$$\phi_2 = \frac{Ru\, D}{K_f.\Omega_3}\left(\frac{\Omega_4}{\Omega_3}\right)\Delta\phi, \qquad \phi_3 = \frac{Ru\, D}{K_f.\Omega_3}.\,\Delta\phi \tag{3.14}$$

where $\Omega_4 = \frac{\Delta\phi}{\phi_1}$ and $\Omega_3 = \frac{\Delta T}{T_1}$ are the concentration and temperature ratios, respectively and $S_{Gc} = \frac{K_f\,(\Delta T)^2}{d^2\,T_1^2}$ is the characteristic entropy generation rate. The Eq.(3.13) can be formulate as

$$Ns = Nh + Nv \tag{3.15}$$

The entropy generation due to heat transfer irreversibility is denoted by the first term on the right hand side of the Eq.(3.15) and the entropy generation due to viscous dissipation is represented by second term of Eq.(3.15). The ratio of the entropy generation due to heat transfer and the total entropy generation is called Bejan number Be and to understand the entropy generation mechanisms, Bejan number Be is specified. The Bejan number for this

problem can be expressed as

$$Be = \frac{Nh}{Nh + Nv} \tag{3.16}$$

In general, the range of Bejan number varies from 0 to 1. Finally, the irreversibility due to viscous dissipation dominant is presented by $Be = 0$, whereas the dominance of heat transfer irreversibility is shown by $Be = 1$. It shows that the irreversibility due to heat transfer is equal to viscous dissipation at Be=0.5.

3.5 Results and Discussion

The effects of radiation, Joule heating and magnetic parameter on non-dimensional velocity, temperature, nanoparticle volume fraction, Bejan number Be, entropy generation Ns are presented graphically in figures (3.2) - (3.5). To study the effect of the parameters, the computations are carried out by taking $Nr = 1, Nb = 0.5, Gr = 10, Nt = 1, Re = 2, R = 1, Pr = 1, A = 1, Le = 1$ and $Tp = 0.1$.

Figure (3.2) displays the effect of radiation parameter Rd on the velocity in flow direction, temperature, nanoparticle concentration, entropy generation and Bejan number. Figure 3.2(a) reveals that the velocity is increasing with an increase in the radiation parameter Rd. This indicates that Rd has a retarding impact on the mixed convective flow. From figure 3.2(b), it is noticed that $\theta(\eta)$ is increasing with an increase in the radiation parameter Rd. A rise in the radiation parameter Rd leads to release of heat energy in the flow direction, therefore the temperature of the fluid is increasing. Figure 3.2(c) depicts that the nanoparticle concentration $S(\eta)$ decays with an enhancement in the radiation parameter Rd. Figure 3.2(d) shows that the entropy generation reduces with an enhancement in the radiation parameter Rd. It is noticed from figure 3.2(e) that Be (Bejan number) increases near the left plate of the channel, while away from the plate the trend is reversed due to more contribution of the heat transfer irreversibility on Ns and Be is decreasing near the right plate of the channel with an enhancement in Rd.

The variations of velocity in flow direction, temperature, nanoparticle concentration, Ns

and Be with magnetic parameter Ha are presented in figure (3.3). It is noticed from figure 3.3(a) that, the dimensionless velocity decreases with an increase in the magnetic parameter Ha. Figure 3.3(b) reveals that $\theta(\eta)$ decreases with a rise in the magnetic parameter Ha. There is a rise in the nanoparticle concentration $S(\eta)$ with a rise in the magnetic parameter Ha as depicted in figure 3.3(c). Figure 3.3(d) shows that entropy generation decreases with an enhancement in the magnetic parameter Ha. It is clear from figure 3.3(e) that, Be is decreasing near the left plate of the channel, while away from the plate the trend is reversed due to more contribution of the heat transfer irreversibility on Ns and Be is decreasing near the right plate of the channel with an increase in Ha.

The influence of Brinkman number Br on $f(\eta)$, $\theta(\eta)$, $S(\eta)$, Ns and Be is depicted in figure (3.4). The dimensionless velocity $f(\eta)$ is increasing with a rise in Brinkman number Br as shown in figure 3.4(a). Figure 3.4(b) reveals that the $\theta(\eta)$ increases with a raise in Br. From figure 3.4(c), it is noticed that nanoparticle concentration $S(\eta)$ decays with an increment in Brinkman number Br. Figure 3.4(d) shows that the increase in Brinkman number Br causes a increment in the entropy generation.

The influence of the Joule heating parameter on $f(\eta)$, $\theta(\eta)$, $S(\eta)$, Ns and Be is shown in figure (3.5). The velocity in the flow direction increases with a rise in the Joule heating parameter J as shown in figure 3.5(a). Figure 3.5(b) explains that the temperature $\theta(\eta)$ rises with an enhancement in the Joule heating parameter J. From figure 3.5(c), it is noticed that nanoparticle concentration $S(\eta)$ decreases with an enhancement in the Joule heating parameter J. Figure 3.5(d) shows that the increment in the Joule heating parameter J rises the entropy generation. As the Joule heating parameter J increases, the Bejan number is decreasing near the left plate of the channel and increasing near the right plate of the channel as presented in figure 3.5(e).

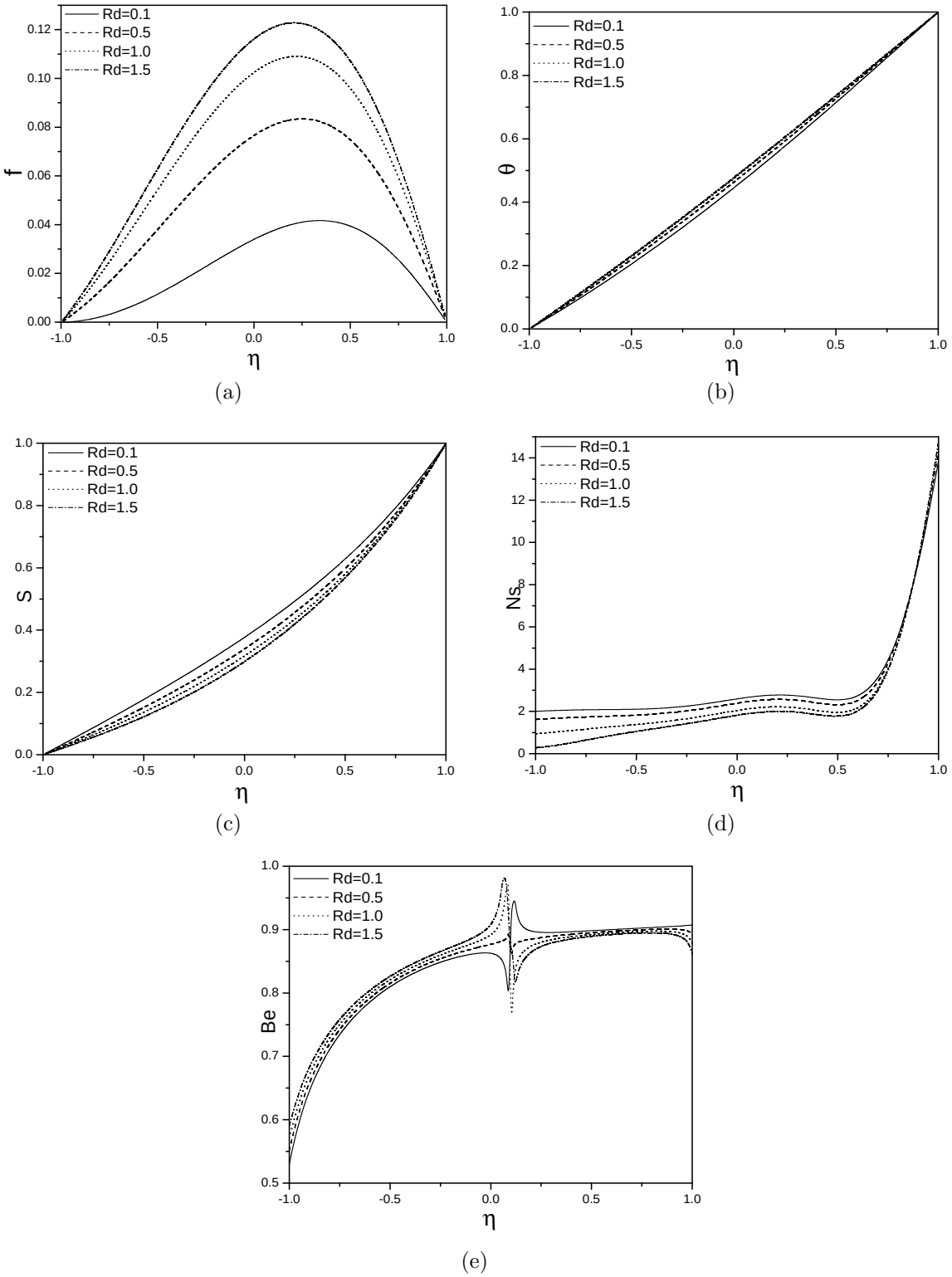

Figure 3.2: "Effec of radiation Rd on (a) $f(\eta)$, (b) $\theta(\eta)$, (c) $S(\eta)$ (d) Ns and (e) Be".

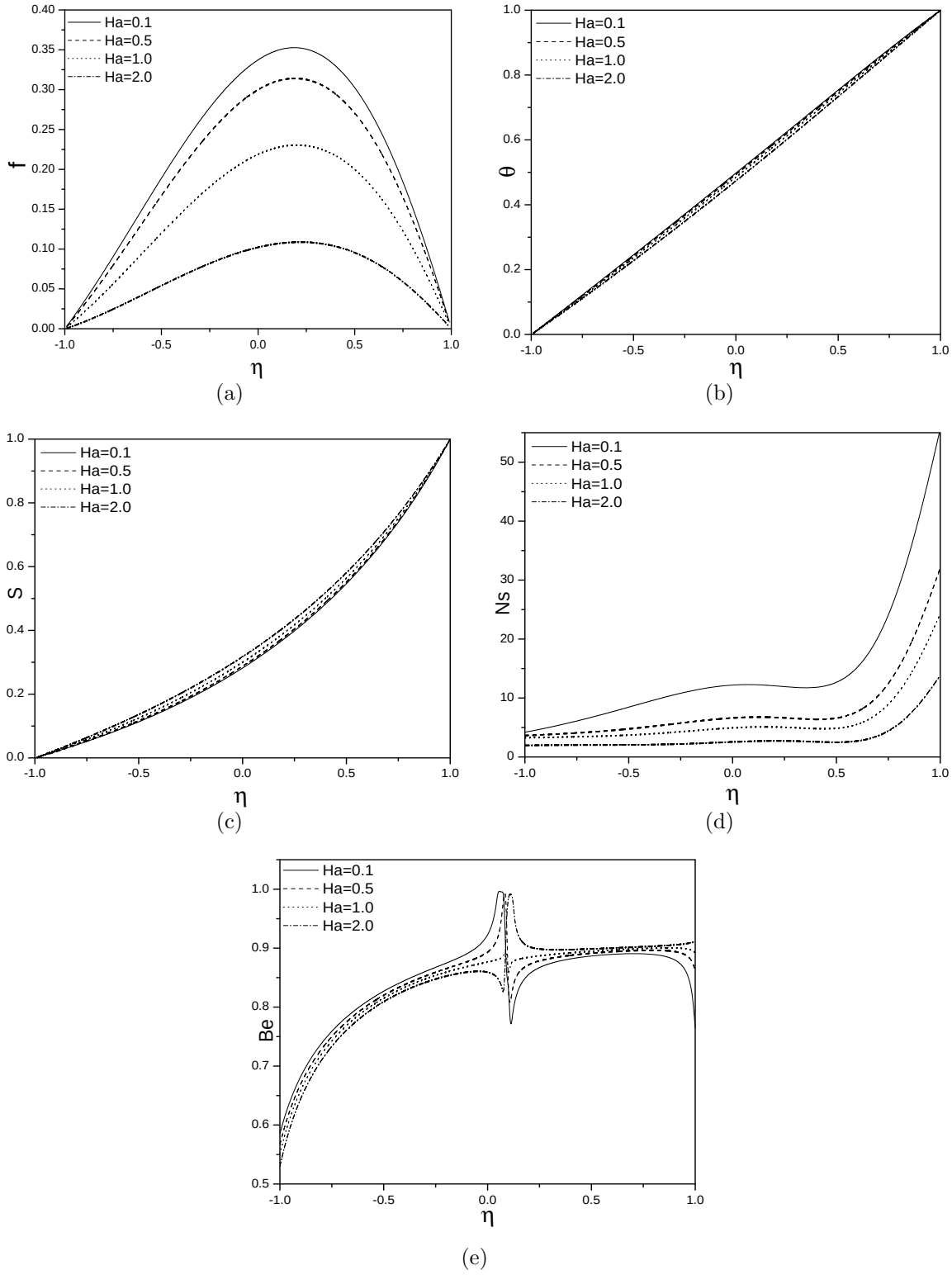

Figure 3.3: " Effec of magnetic parameter Ha on (a) $f(\eta)$, (b) $\theta(\eta)$, (c) $S(\eta)$ (d) Ns and (e) Be".

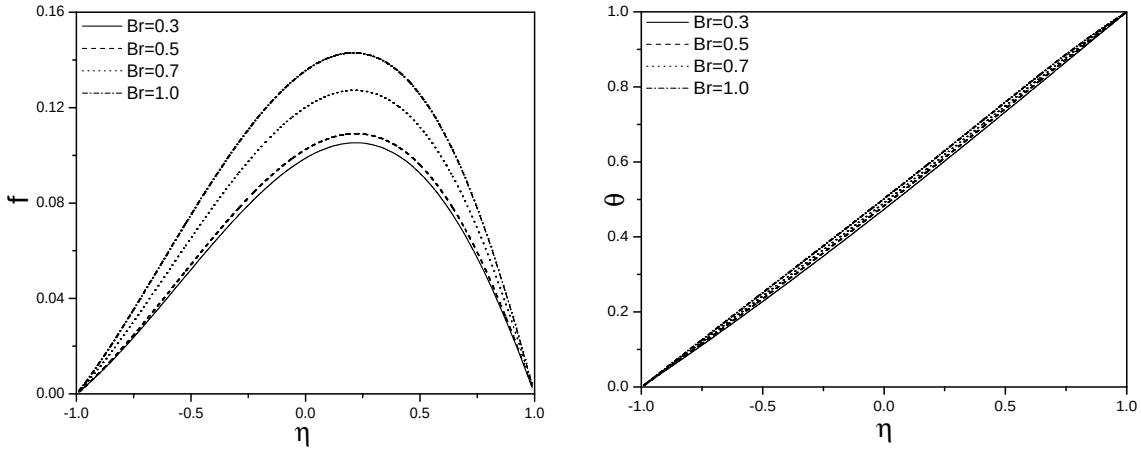

(a)

(b)

4

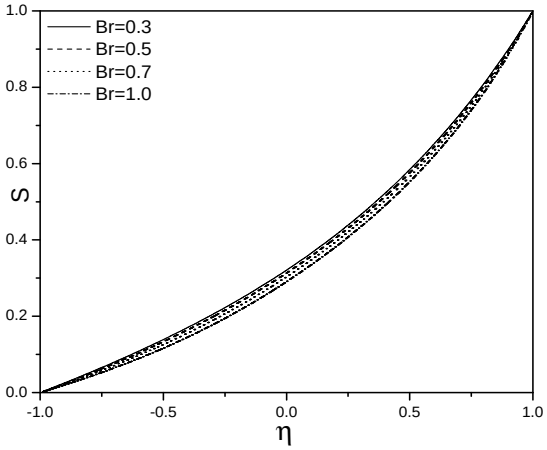

(c)

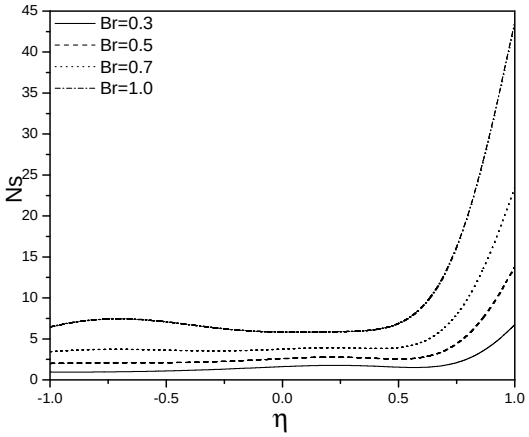

(d)

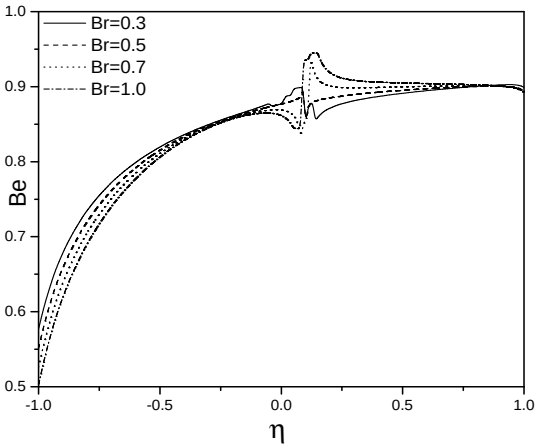

(e)

Figure 3.4: "Effect of Brinkman number Br on (a) $f(\eta)$, (b) $\theta(\eta)$, (c) $S(\eta)$ (d) Ns and (e) Be".

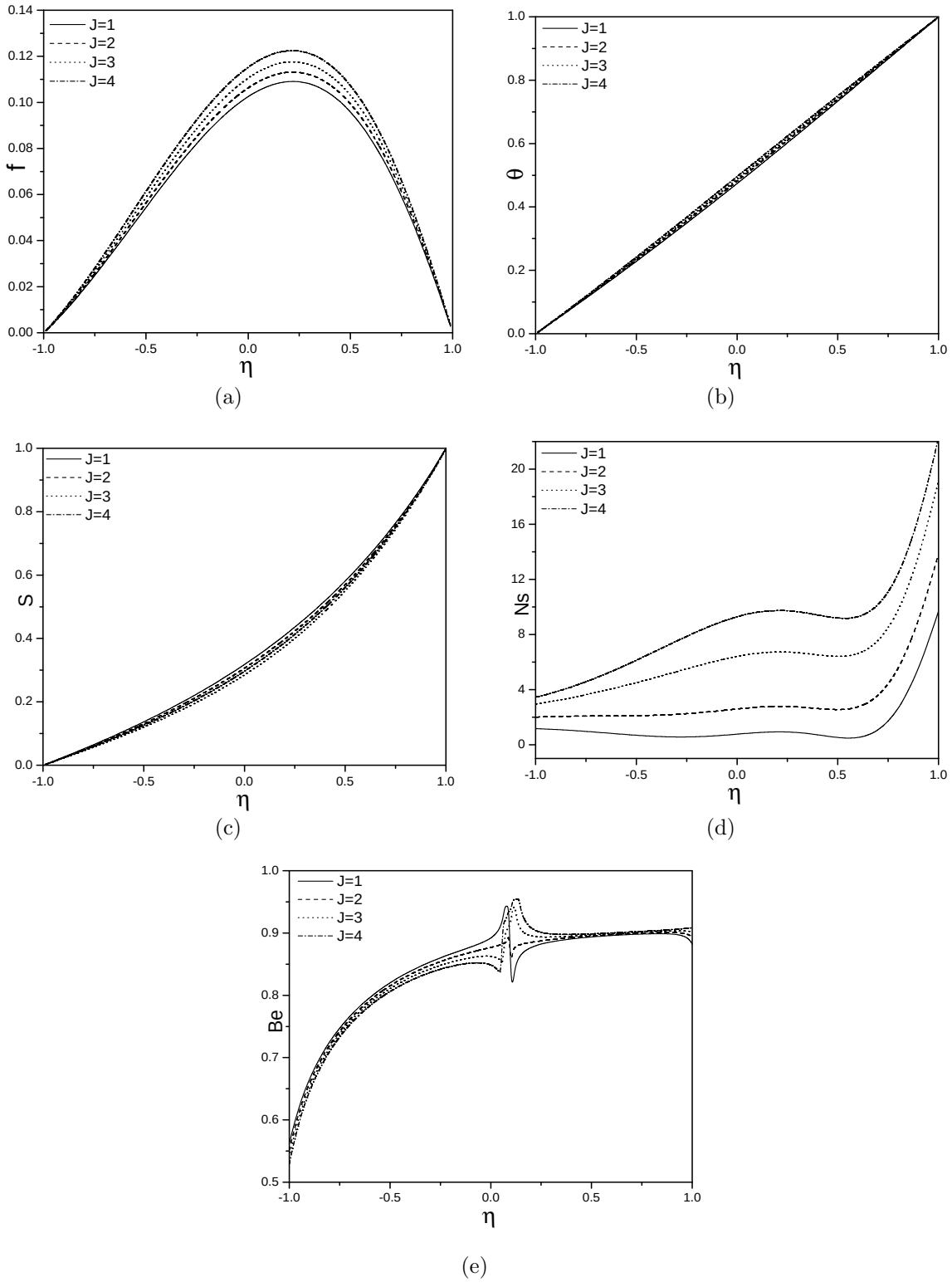

Figure 3.5: " Effec of Joule heating parameter J on (a) $f(\eta)$, (b) $\theta(\eta)$, (c) $S(\eta)$ (d) Ns and (e) Be".

3.6 Conclusions

In this chapter, the entropy generation on a mixed convective nanofluid flow in a vertical channel has been investigated by including magnetic, Joule heating and radiation effects. The non-dimensional non-linear equations are solved by HAM method. The following are the main observations

The velocity in flow direction and temperature increase, whereas the nanoparticle concentration and entropy generation decrease with a rise in the thermal-radiation Rd. As the Joule heating parameter increases, the dimensionless temperature, velocity and entropy generation increase, while the nanoparticle concentration decreases. The maximum values of Bejan number are observed at the right plate of the channel due to more heat transfer irreversibility on entropy generation and minimum value near the left plate of channel due to more contribution of the fluid friction irreversibility on entropy generation with an increase in Rd, Ha and J.

Chapter 4

Joule heating effect on entropy generation in MHD mixed convective flow of a chemically reacting nanofluid in a vertical channel [1]

4.1 Introduction

The impact of chemical reaction on heat and mass transfer has received great importance in chemical technology and hydrometallurgy industry. Chemically reacting nanofluid may play an important role in many processing systems and materials. It is well known that Joule heating is produced by inter communication among the atomic ions that composes the body of the conductor and moving charged particles that form the current. Joule heating effect on the fluid flow and heat transfer at various conditions are analyzed and found that, it plays a notable effect on MHD flow and heat transfer. Babulal and Dulalpal [26] studied the combination of chemical reaction and Joule heating effects on MHD mixed convective flow of viscous dissipating fluid through a vertical channel.

[1] Communicated to "**Chemical Industry and Chemical Engineering Quarterly, (2017)**"

The amount of irreversibility associated with the real processes is measured by entropy generation. The entropy generation destroys the system energy. Hence, the performance of the system can be improved by decreasing the entropy generation. Therefore, a powerful and useful optimization tool for a high range of thermal applications is minimization of entropy generation. Bejan [11, 12] developed the entropy generation minimization method and introduced its applications in engineering sciences. Since then several researchers have been studying the entropy generation analysis for different types of geometries with diverse fluids. Gyftopoulos and Beretta [37] discussed the entropy generation rate in a chemically reacting system.

The objective of this chapter is to analyse the combined effect of chemical reaction and Joule heating on the entropy generation due to MHD mixed convective nanofluid flow in a vertical channel. The governing equations are solved using HAM. The effect of pertinent parameters on the velocity, temperature, nanoparticle concentration, Bejan number and entropy generation are investigated and shown graphically.

4.2 Mathematical Formulation

Consider a steady, laminar, incompressible, an electrically conducting nanofluid flow through a vertical channel of width $2d$. The physical model and coordinate system is given in figure (2.1). In addition to suction/injection and magnetic field, Joule heating along with chemical reaction effects are taken into consideration. Further, all the properties of the fluid are assumed to be constant except the density in buoyancy term. The governing equations of the fluid flow, under the above assumptions, are given by

$$\frac{\partial v}{\partial y} = 0 \tag{4.1}$$

$$\rho_f \, v \frac{\partial u}{\partial y} = -\frac{\partial p}{\partial x} + \mu \frac{\partial^2 u}{\partial y^2} + (1-\phi_m)\rho_{f_0} g^* \, \beta_T (T - T_1) - (\rho_s - \rho_{f_0}) \, g^* (\phi - \phi_1) - \sigma \, B_0^2 \, u \tag{4.2}$$

$$v\frac{\partial T}{\partial y} = \alpha\frac{\partial^2 T}{\partial y^2} + \frac{2\mu}{\rho c_p}\left(\frac{\partial u}{\partial y}\right)^2 + \tau\left[D_B\frac{\partial T}{\partial y}\frac{\partial \phi}{\partial y} + \frac{D_T}{T_m}\left(\frac{\partial T}{\partial y}\right)^2\right] + \frac{1}{\rho c_p}\,\sigma\, B_0^2\, u^2 \tag{4.3}$$

$$\frac{\partial \phi}{\partial y}v = \frac{D_T}{T_m}\frac{\partial^2 T}{\partial y^2} + D_B\frac{\partial^2 \phi}{\partial y^2} - k_1(\phi - \phi_1) \tag{4.4}$$

along with the boundary conditions are

$$\begin{aligned} u = 0, \quad v = v_0, \quad T = T_1, \quad \phi = \phi_1 \quad \text{on} \quad y = -d, \\ u = 0, \quad v = v_0, \quad T = T_2, \quad \phi = \phi_2 \quad \text{on} \quad y = d. \end{aligned} \tag{4.5}$$

Introducing the following non-dimensional variables

$$\eta = \frac{y}{d},\ f = \frac{u}{u_0},\ p = \frac{\mu\, u_0}{d^2}\, P,\ \theta = \frac{T - T_1}{T_2 - T_1},\ S = \frac{\phi - \phi_1}{\phi_2 - \phi_1} \tag{4.6}$$

in Eqs. (4.1) - (4.4), we get the nonlinear differential equations as

$$f'' - Rf' + \frac{Gr}{Re}\,(\theta - NrS) + Ha^2\, f - A = 0 \tag{4.7}$$

$$\theta'' - R\,Pr\,\theta' + PrNb\theta' S' + PrNt\,\theta'^2 + 2\,Br(f')^2 + J\,f^2 = 0 \tag{4.8}$$

$$S'' - R\,Le\,S' + \frac{Nt}{Nb}\theta'' - K\,Le\,S = 0 \tag{4.9}$$

where $K = \frac{k_1\, d^2}{\upsilon}$ is the chemical reaction parameter and $J = \dfrac{{u_0}^2 \sigma\, B_0^2\, d^2}{(T_2 - T_1)k_f}$ is the Joule heating parameter. Remaining parameters are defined in the earlier chapters.

The corresponding non-dimensional boundary conditions are

$$\begin{aligned} S = 0, \quad \theta = 0, \quad f = 0 \quad \text{at} \quad \eta = -1 \\ S = 1, \quad \theta = 1, \quad f = 0 \quad \text{at} \quad \eta = 1 \end{aligned} \tag{4.10}$$

	Optimal of h_1		Optimal of h_2		Optimal of h_3	
Order	h_1	Min. of E_m	h_2	Min. of E_m	h_3	Min. of E_m
10	-0.44	8.67×10^{-6}	-0.38	7.31×10^{-5}	-1.18	3.54×10^{-4}
15	-0.43	1.18×10^{-5}	-0.36	7.65×10^{-4}	-1.16	3.81×10^{-5}
20	-0.43	1.02×10^{-5}	-0.38	7.64×10^{-4}	-1.16	3.84×10^{-4}

Table 4.1: "At different order of approximations, the optimal values of h_1, h_2, and h_3".

Order	f(0)	$\theta(0)$	S(0)
05	0.1388039967	0.4890064756	0.1928253252
10	0.1304585594	0.4785814767	0.1932333156
15	0.1193821063	0.4697395477	0.1997383124
20	0.1084391065	0.4614794434	0.2056582531
25	0.0981478164	0.4614791477	0.2056583145
30	0.0981478129	0.4614791275	0.2056583124
35	0.0981478125	0.4614791275	0.2056583124
40	0.0981478106	0.4614791275	0.2056583124
45	0.0981478106	0.4614791047	0.2056583124
50	0.0981478106	0.4614791047	0.2056583124
55	0.0981478106	0.4614791047	0.2056583124

Table 4.2: "At different order of approximations, the convergence of HAM solutions".

4.3 Solution of the problem

The governing Eqs. (4.7) - (4.9) along with the boundary conditions (4.10) are solved by using HAM. As this method is explained in chapter - 2, the details are not presented here. However, the convergence of homotopy solution is discussed. To determine the admissible range of auxiliary parameters, the h-curves are plotted for 20^{th} order of approximation and presented in figure (4.1). It is found that the admissible ranges for h_1, h_2 and h_3 are $-0.6 < h_1 < -0.2$, $-0.5 < h_2 < -0.1$ and $-1.4 < h_3 < -0.2$ respectively. In order to obtain the optimal value of the auxiliary parameter, the average residual errors (given by (2.28)) are calculated and shown in table (4.1). From this table, it is noticed that the optimal value of auxiliary parameters are $h_1 = -0.43$, $h_2 = -0.38$ and $h_3 = -1.16$. Further, the series solutions for different values of m are computed and displayed in table (4.2). From table (4.2), it is found that the series solution converges in the whole region of η.

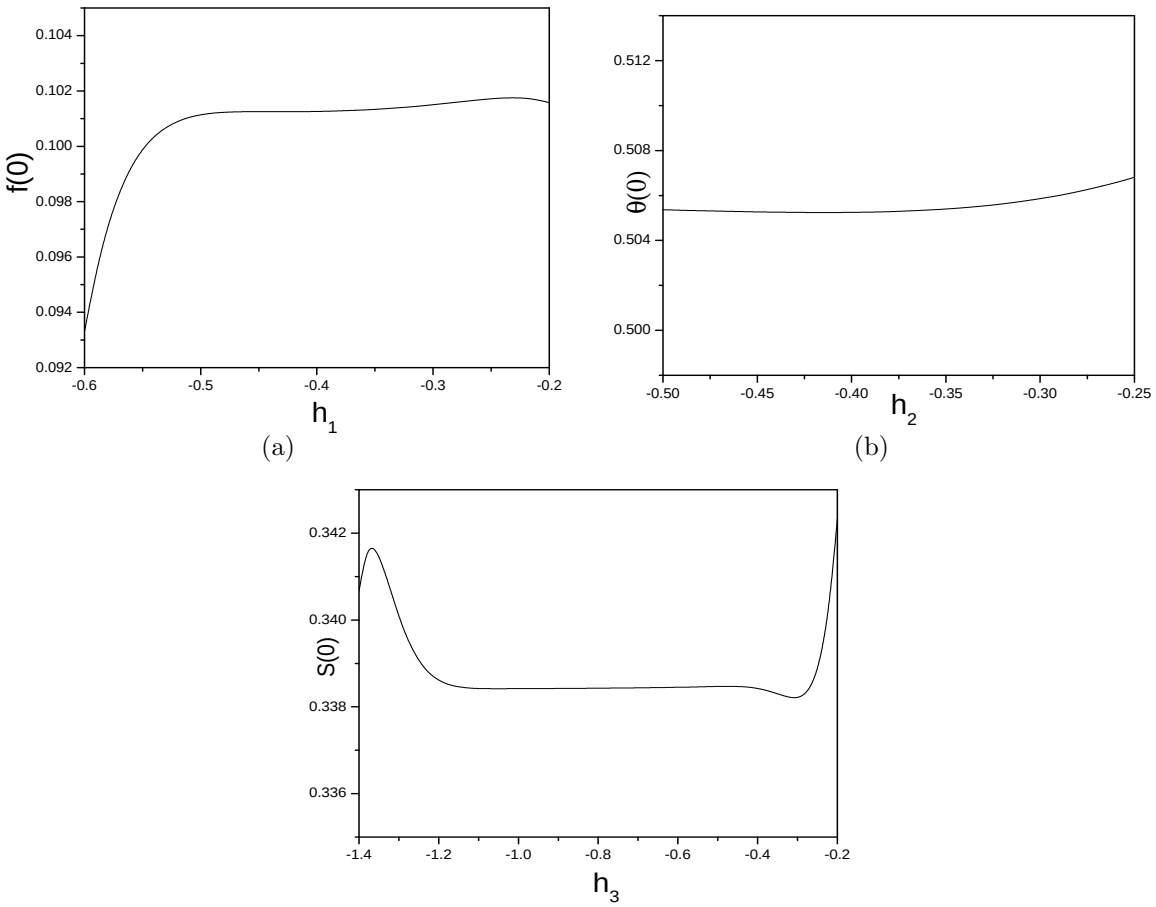

Figure 4.1: "h-curves for (a) $f(\eta)$, (b) $\theta(\eta)$ and (c) $S(\eta)$ when $Nr = 1, Nt = 1, Gr = 10, R = 1, Nb = 0.5, Pr = 1, A = 1, Re = 2, Le = 1, Ha = 2, Br = 0.5, J = 2$ and $Tp = 0.1$".

4.4 Entropy generation

The nanofluid flow through a vertical channel is naturally irreversible. The non-equilibrium condition arises due to the exchange of energy and momentum within the nanofluid and at the solid boundaries, that leads to continuous entropy generation in a vertical channel. For the present study, the volumetric rate of local entropy generation of a nanofluid in a vertical channel can be expressed as

$$S_G = \frac{K_f}{T_1^2}\left(\frac{\partial T}{\partial y}\right)^2 + \frac{\sigma\, B_0^2\, u^2}{T_1} + \frac{2\mu}{T_1}\left(\frac{\partial u}{\partial y}\right)^2 + \frac{RD}{\phi_1}\left(\frac{\partial \phi}{\partial y}\right)^2 + \frac{RD}{T_1}\left(\frac{\partial T}{\partial y}\right).\left(\frac{\partial \phi}{\partial y}\right) \Bigg\} \quad (4.11)$$

The dimensionless entropy generation number Ns is given by

$$Ns = \theta'^2 + \frac{1}{\Omega_3}\left(2\, Br f'^2 + J\, f^2\right) + \phi_3\, S'^2 + \phi_4\, \theta' S' \quad (4.12)$$

Here ϕ_3 and ϕ_4 are the dimensionless coefficients, called irreversibility distribution ratios which are related to diffusive irreversibility as given in the earlier chapter.

To produce the entropy generation profiles Eq. (4.12) is useful, but it fails to give an idea about the relative importance of fluid friction and heat transfer effects. Therefore, an alternative parameter Bejan number (Be), is introduced. It is defined as the ratio of entropy generation due to heat transfer to the overall entropy generation, which is given below

$$Be = \frac{Nh}{Nh + Nv} \quad (4.13)$$

4.5 Results and Discussion

The effects of chemical reaction, Joule heating, magnetic parameters and Brinkman number on non-dimensional velocity, temperature, nanoparticle volume fraction, Bejan number Be and entropy generation Ns are presented graphically in figures (4.2) - (4.3). To study the effect of these parameters, other parameters are taken as $Nr = 1, Nb = 0.5, Nt = 1, Gr =$

$10, Re = 2, R = 1, Pr = 1, A = 1, Le = 1$ and $Tp = 0.1$.

Figure 4.2 displays the role of chemical reaction K on velocity, temperature and nanoparticle volume fraction. Figure 4.2(a) reveals that the velocity increases as the rate of chemical reaction K increases. This indicates that K has a retarding impact on the mixed convective flow. From figure 4.2(b), it is noticed that $\theta(\eta)$ increases with an increase in K. The influence of the parameter K is to rise the temperature extremely in the flow field. From the flow region, the heat energy is released because of rise in chemical reaction, therefore the fluid temperature increases. It is evident from figure 4.2(c) that the nanoparticle concentration $S(\eta)$ decays with a rise in K. Figure 4.2(d) shows that the entropy generation increases with an enhancement in K. It is shown in figure 4.2(e) that, Be (Bejan number) is increasing near the left plate of the channel, while away from the plate the trend is reversed due to more contribution of the heat transfer irreversibility on Ns and Be is decreasing at the right plate of the channel as K increases.

The influence of the Joule heating parameter J on velocity $f(\eta)$, temperature $\theta(\eta)$ and nanoparticle volume fraction $S(\eta)$ are shown in figure (4.3). The dimensionless velocity $f(\eta)$ rises with a rise in the Joule heating parameter J as shown in figure 4.3(a). Figure 4.3(b) reveals that the temperature increases with an increase in the Joule heating parameter J. From figure 4.3(c), it is noticed that nanoparticle concentration $S(\eta)$ decays with a growth in the Joule heating pameter J. Figure 4.3(d) shows that an enhancement in J causes an increase in entropy generation. With an increase in the Joule heating parameter J, the Bejan number is observed to be increases near the end plate of the channel, while the trend is reversed at the center of the channel due to more contribution of heat transfer irreversibility on Ns, therefore, Be increases near the right plate of the channel as represented in figure 4.3(e).

The influence of magnetic parameter Ha on the velocity in flow direction, dimensionless temperature, nanoparticle concentration, Bejan number and entropy generation is presented in figure (4.4). It is noticed from the figure 4.4(a) that the dimensionless velocity in flow direction decreases with an increase in magnetic parameter Ha. Figure 4.4(b) reveals that the temperature $\theta(\eta)$ decays with a rise in magnetic parameter Ha. There is a rise in

the nanoparticle concentration $S(\eta)$ with a rise in magnetic parameter Ha as depicted in figure 4.4(c). Figure 4.4(d) shows that entropy generation decays with a growth in magnetic parameter Ha. From the figure 4.4(e), it is clear that Be increases near the lower plate of the channel, while away from the plate the trend is reversed due to more contribution of the heat transfer irreversibility on Ns with Be is decreasing near the upper plate of the channel as Ha reports an increase in value.

The effects of Brinkman number Br on $f(\eta)$, $\theta(\eta)$, $S(\eta)$, Be and Ns is displayed in figure (4.5). The dimensionless velocity $f(\eta)$ rises with a rise in Brinkman number Br as shown in figure 4.5(a). Figure 4.5(b) reveals that $\theta(\eta)$ increases with a rise in Br. From the figure 4.5(c), it is noticed that the nanoparticle concentration $S(\eta)$ decays with an enhancement in Brinkman number Br. Figure 4.5(d) shows that an enhancement in Br causes an increment in the entropy generation. With an increase in Brinkman number Br, the Bejan number is observed to be increasing near the end plate of the channel, while the trend is reversed at center of the channel due to more contribution of heat transfer irreversibility on Ns and Be increases near the right plate of the channel as presented in figure 4.5(e).

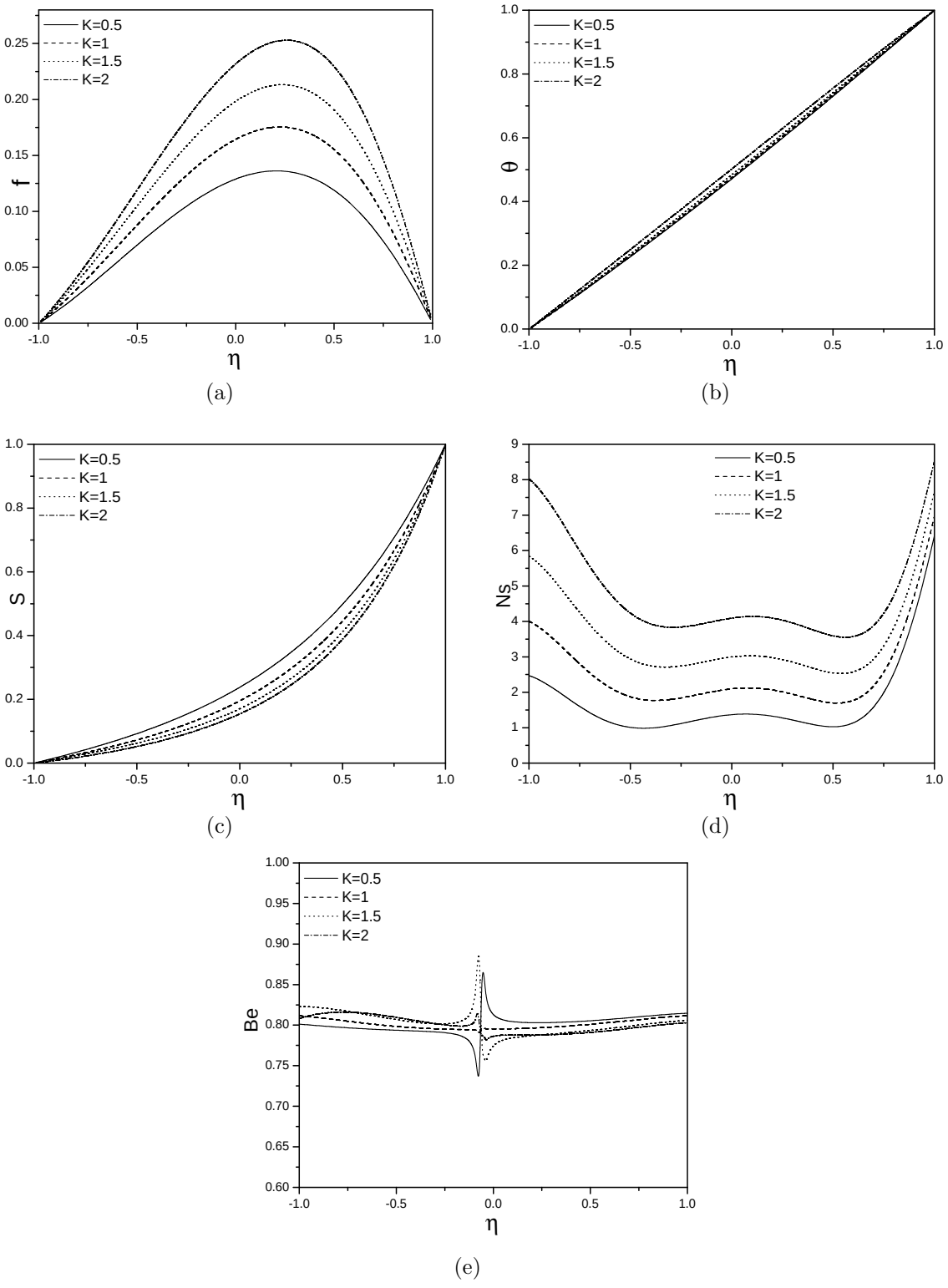

Figure 4.2: "Effect of the chemical reaction K on (a) $f(\eta)$, (b) $\theta(\eta)$, (c) $S(\eta)$, (d) Ns and (e) Be".

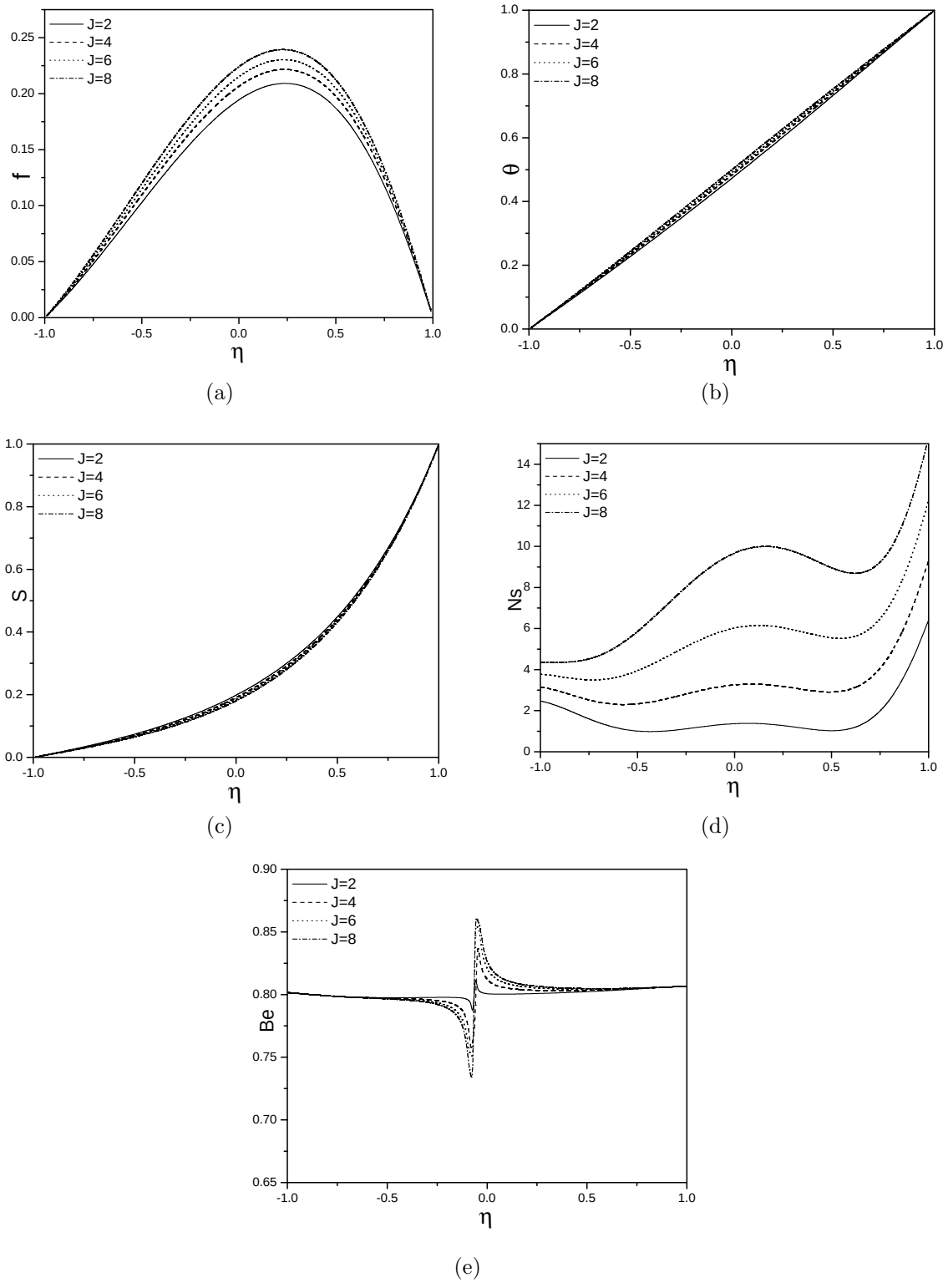

(a) (b) (c) (d) (e)

Figure 4.3: "Effect of the Joule heating parameter J on (a) $f(\eta)$, (b) $\theta(\eta)$, (c) $S(\eta)$, (d) Ns and (e) Be".

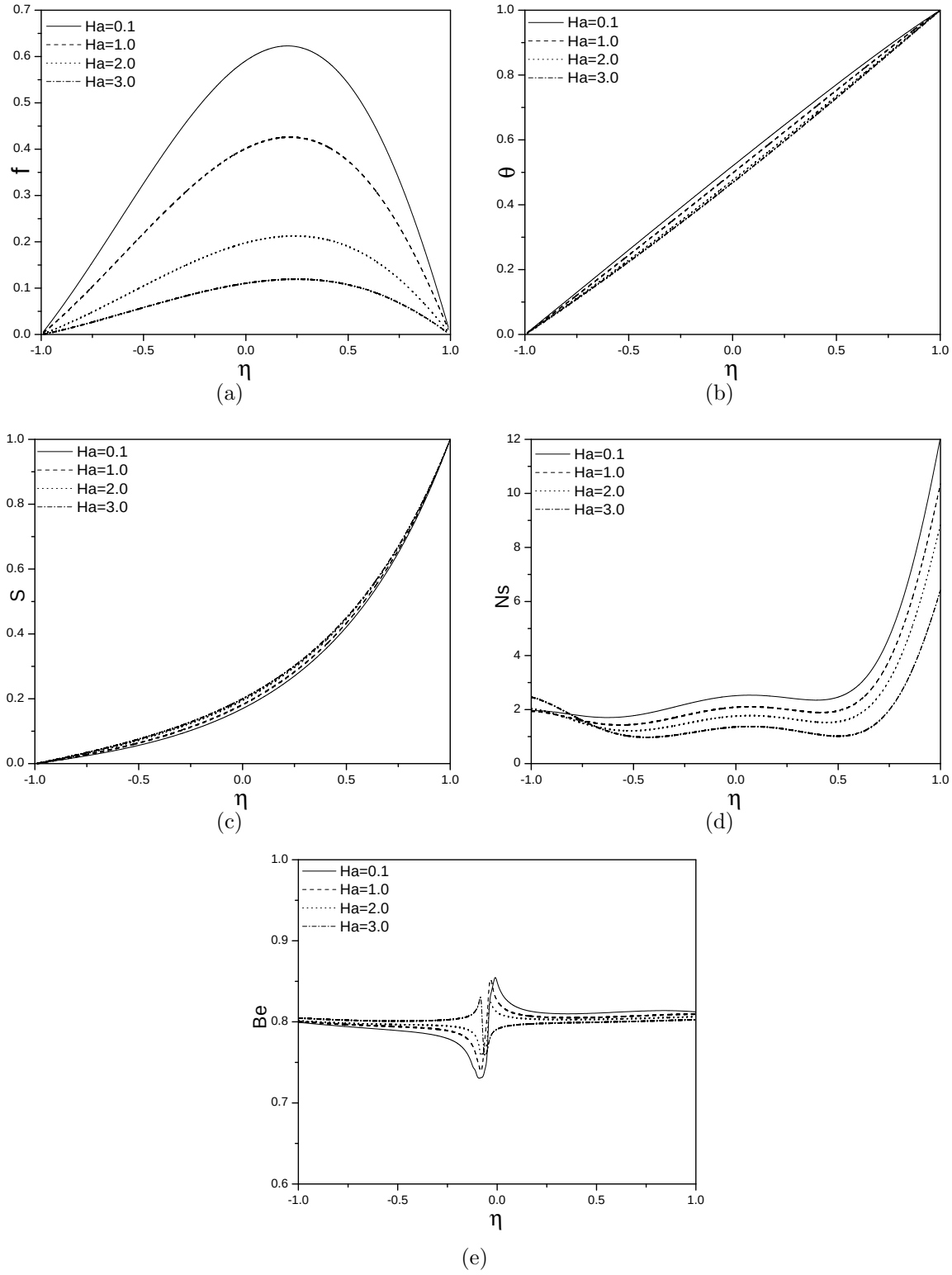

Figure 4.4: "Effect of the magnetic parameter Ha on (a) $f(\eta)$, (b) $\theta(\eta)$, (c) $S(\eta)$, (d) Ns and (e) Be".

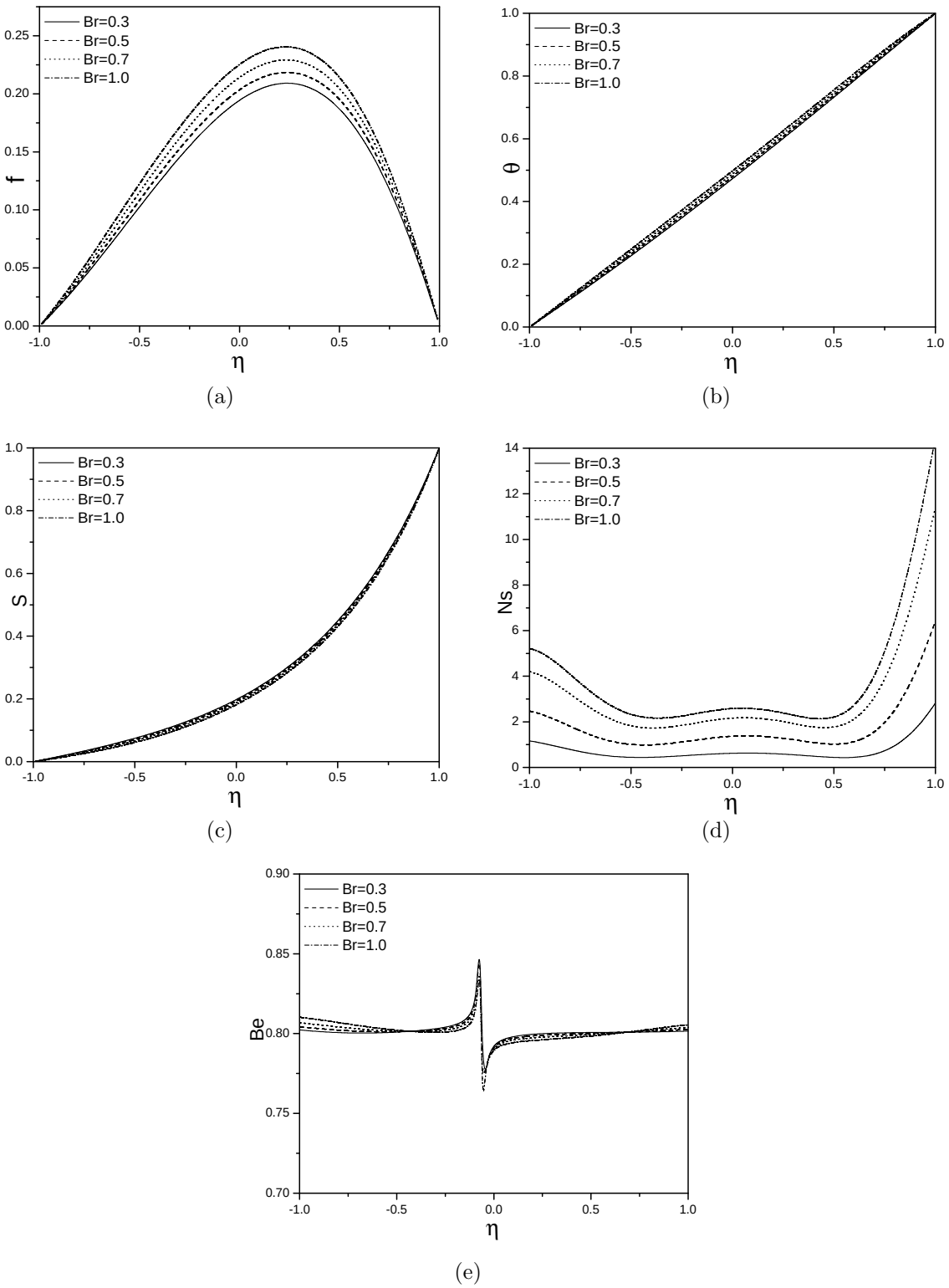

Figure 4.5: "Effect of Brinkman number Br on (a) $f(\eta)$, (b) $\theta(\eta)$, (c) $S(\eta)$, (d) Ns and (e) Be".

4.6 Conclusions

In this chapter, the effect of the Joule heating parameter on laminar mixed convective flow of an incompressible chemically reacting nanofluid in vertical channel is studied. The entropy generation rate and Bejan number are calculated numerically. The effect of Joule heating and chemical reaction parameters on the dimensionless velocity, temperature, nanoparticle concentration, entropy generation and Bejan number are investigated and represented graphically. From the analysis, the following are the observations

The dimensionless velocity, temperature and entropy generation increase, whereas the nanoparticle concentration decreases with a rise in the chemical reaction parameter K. The dimensionless temperature, velocity and entropy generation increase but the nanoparticle concentration decreases with an increase in J. The maximum values of Bejan number are observed at upper and lower plate of the channel due to more contribution of heat transfer irreversibility on entropy generation Ns with an increase in Ha, K, J and Br.

Part III

ENTROPY GENERATION DUE TO MIXED CONVECTIVE FLOW OF A NANOFLUID BETWEEN TWO CONCENTRIC CYLINDERS

Chapter 5

Mixed convective flow of a nanofluid in an annulus with Hall and ion-slip effects [1]

5.1 Introduction

The convective heat exchange and problems of fluid flow with the interaction of magnetic field have increased enormously due to several astrophysics and industrial applications. Mozayyeni and Rahimi [60] discussed the effect of the magnetic field applied in the radial direction on mixed convective flow in a cylindrical annulus with rotating outer cylinder. Ashorynejad *et al* [5] studied numerically the problem of mixed convective heat transfer in an annuli of horizontal cylinders filled with a nanofluid considering constant radial magnetic field. In the investigations concerned with the MHD convective flows, the Hall current and ion-slip terms in Ohms law were neglected in order to simplify the mathematical analysis of the problem. However, the significance of Hall current and ion-slip are essential for the existence of strong magnetic field. Srinivasacharya and Kaladhar [79] examined the effects of Hall current and

[1] Type - I: Published in "**Journal of the Association of Arab Universities for Basic and Applied Sciences,Vol. 24(2017), 223–231**", Type - II: Communicated to "**Propulsion and Power Research**"

ion-slip on mixed convection in a couple stress fluid flow between two circular cylinders.

The aim of this chapter is to study the magnetic, Hall and ion-slip effects on steady, laminar mixed/natural convective heat transfer flow between two concentric cylinders in a nanofluid. The effect of Hall and ion-slip and magnetic parameters on the velocity, temperature and nanoparticle concentration are investigated.

5.2 Mathematical Formulation

Consider a nanofluid flow in an annular space between two infinitely long concentric cylinders of radius a and b ($a < b$) and kept at temperatures T_a and T_b respectively. Assume that the outer cylinder is rotating with a constant angular velocity Ω whereas the inner cylinder is at rest. The flow is induced by the rotation of the exterior cylinder. The flow is subjected to a uniform magnetic field B_0 in an axial direction as shown in figure (5.1). The assumption of very small magnetic Reynolds number leads to neglect of the induced magnetic field. Assume relatively high electron-atom collision frequency so that the impact of Hall and ion-slip cannot be omitted. Thermo-physical characteristics of a nanofluid are taken as constant. The velocity component along ψ direction is u, temperature is T and nanoparticle volume fraction is ϕ. Under the assumptions of steady state, laminar, incompressible, boundary layer and Boussinesq approximation, the governing equations with Brownian motion and the thermophoresis effects [18] in polar coordinates (r, ψ, z) (z-axis along the common axis of the cylinders) become

$$\frac{\partial u}{\partial \psi} = 0 \tag{5.1}$$

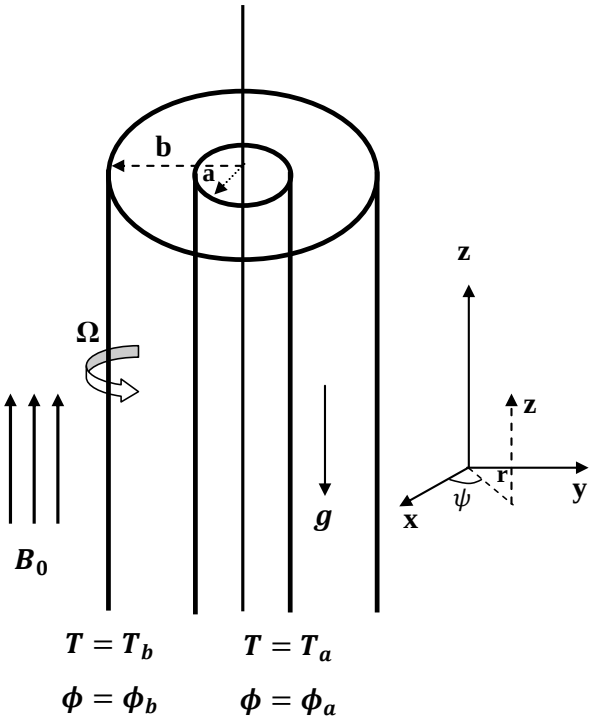

Figure 5.1: Physical model and coordinate system.

$$\frac{\partial p}{\partial r} = \frac{u}{r^2} - \frac{\sigma\, B_0^2\, \beta h\, u}{(\alpha e^2 + \beta h^2)} \tag{5.2}$$

$$\mu \nabla_1^2\, u + (1-\phi)\rho_f g^*\, \beta_T (T - T_a) - (\rho_s - \rho_f)\, g^* (\phi - \phi_a) - \frac{\sigma\, B_0^2\, \alpha e\, u}{(\alpha e^2 + \beta h^2)} - \frac{1}{r}\, \frac{\partial p}{\partial \psi} = 0 \tag{5.3}$$

$$\begin{aligned} \alpha \left[\frac{\partial^2 T}{\partial r^2} + \frac{1}{r}\, \frac{\partial T}{\partial r} \right] + \frac{\mu}{(\rho c)_p} \left[\left(\frac{\partial u}{\partial r} \right)^2 - 2\, \frac{u}{r}\, \frac{\partial u}{\partial r} + \left(\frac{u}{r} \right)^2 \right] \\ + \tau \left[D_B \frac{\partial T}{\partial r} \frac{\partial \phi}{\partial r} + \frac{D_T}{T_m} \left(\frac{\partial T}{\partial r} \right)^2 \right] = 0 \end{aligned} \tag{5.4}$$

$$D_B \left[\frac{\partial^2 \phi}{\partial r^2} + \frac{1}{r}\, \frac{\partial \phi}{\partial r} \right] + \frac{D_T}{T_m} \left[\frac{\partial^2 T}{\partial r^2} + \frac{1}{r}\, \frac{\partial T}{\partial r} \right] = 0 \tag{5.5}$$

where ρ is the density, p is the pressure, C_p is the specific heat capacity, μ is the viscosity coefficient, g^* is the acceleration due to gravity, σ is the electrical conductivity, βi is the ion-slip parameter, βh is the Hall parameter, D_B is the Brownian diffusion coefficient, β_T is

the coefficients of thermal expansion, D_B is the thermophoretic diffusion coefficient, α is the effective thermal diffusivity, $K_f = \alpha\,(\rho\,C)_p$ is the coefficient of thermal conductivity, D is the mass diffusivity, T_m is the mean fluid temperature, $\nabla_1^2 u = \frac{\partial}{\partial r}\left[\frac{1}{r}\,\frac{\partial}{\partial r}(r\,u)\right]$ and $\alpha_e = 1 + \beta h\,\beta i$ is a constant.

The conditions on the boundary are

$$\begin{aligned} u = 0,\ T = T_a,\ \phi = \phi_a \ \text{ at } \ r = a, \\ u = b\Omega,\ T = T_b,\ \phi = \phi_b \ \text{ at } \ r = b, \end{aligned} \tag{5.6}$$

In this chapter, two types of convection i.e., mixed (type - I) and natural (type - II) convection are considered.

5.2.1 Mixed Convection

Assume that the mixed convective flow is taking place in the presence of thermal buoyancy and the uniform axial pressure gradient.

Introducing the following non-dimensional variables

$$\lambda = \frac{r^2}{b^2},\ f(\lambda) = \frac{ub\sqrt{\lambda}}{\Omega}, \theta = \frac{T - T_a}{T_b - T_a},\ S = \frac{\phi - \phi_a}{\phi_b - \phi_a},\ P = \frac{p}{\mu\,\Omega} \tag{5.7}$$

in Eqs.(5.3) - (5.5), we get the nonlinear differential equations as

$$4\,f''\lambda + \sqrt{\lambda}\frac{Gr}{Re}\,(\theta - NrS) - \frac{Ha^2\,\alpha e\,f}{(\alpha e^2 + \beta h^2)} - A = 0 \tag{5.8}$$

$$\lambda^3\theta'' + \lambda^2\theta' + Br\,\left[\lambda^2(f')^2 - 2\,\lambda\,f\,f' + (f)^2\right] + Pr\,Nb\,\lambda^3\,\theta'\,S' + Pr\,Nt\,\lambda^3\,(\theta')^2 = 0 \tag{5.9}$$

$$\lambda\,S'' + S' + \frac{Nt}{Nb}(\lambda\,\theta'' + \theta') = 0 \tag{5.10}$$

where the prime indicates derivative corresponding to λ, $Pr = \dfrac{\mu\,C_P}{k_f}$ is Prandtl number, $Gr = \dfrac{(1-\phi)\,g^*\,\beta_T(T_b - T_a)b^3}{\nu^2}$ is Grashof number, $Re = \dfrac{\rho\Omega b}{\mu}$ is Reynold's number, $A = \dfrac{1}{r}\,\dfrac{\partial p}{\partial \psi}$

is a constant pressure gradient, $Ha^2 = \dfrac{\sigma {B_0}^2 b^2}{\mu}$ is Hartman number, $Br = \dfrac{\mu \Omega^2}{k_f (T_b - T_a)}$ is Brinkman number, $Nb = \dfrac{\tau D_B(\phi_b - \phi_a)}{\nu}$ is the Brownian motion parameter, $Nt = \dfrac{\tau D_T(T_b - T_a)}{T_a \nu}$ is the thermophoresis parameter and $Nr = \dfrac{(\rho_p - \rho_f)(\phi_b - \phi_a)}{\rho_f \beta_T (T_b - T_a)(1 - \phi)}$ is the buoyancy ratio.

The corresponding dimensionless boundary conditions are

$$\begin{aligned} S = 0,\ \theta = 0,\ f = 0 \ \text{ at } \lambda = \lambda_0 \\ S = 1,\ \theta = 1,\ f = b \ \text{ at } \quad \lambda = 1 \end{aligned} \tag{5.11}$$

5.2.2 Natural convection

In this case, we assume the flow is free convective which is caused by buoyancy forces and assume that there is no external pressure gradient ($\frac{1}{r}\frac{\partial p}{\partial \psi} = 0$). The non-dimensional form of governing equations takes the form

$$4\, f''\lambda + \sqrt{\lambda}\,(\theta - NrS) - \frac{Ha^2\, \alpha e\, f}{(\alpha e^2 + \beta h^2)} = 0 \tag{5.12}$$

$$\lambda^3\theta'' + \lambda^2\theta' + Br\,\left[\lambda^2 (f')^2 - 2\,\lambda\, f\, f' + (f)^2\right] + Pr\, Nb\, \lambda^3\, \theta'\, S' + Pr\, Nt\, \lambda^3\, (\theta')^2 = 0 \tag{5.13}$$

$$\lambda\, S'' + S' + \frac{Nt}{Nb}(\lambda\, \theta'' + \theta') = 0 \tag{5.14}$$

The corresponding dimensionless boundary conditions are

$$\begin{aligned} f = 0,\ S = 0,\ \theta = 0 \ \text{ at } \quad \lambda = \lambda_0 \\ f = b,\ S = 1,\ \theta = 1 \ \text{ at } \quad \lambda = 1 \end{aligned} \tag{5.15}$$

5.3 Solution of the Problem

5.3.1 Mixed convection

The governing Eqs. (5.8) - (5.10) along with the boundary conditions (5.11) are solved by using homotopy analysis method (HAM). (For more details on HAM, see the works of Liao [47, 48, 49, 50]). The initial values of $f(\lambda)$, $\theta(\lambda)$ and $S(\lambda)$ and auxiliary linear operators are chosen as

$$f_0(\lambda) = \frac{b\,(\lambda - \lambda_0)}{1 - \lambda_0}, \quad \theta_0(\lambda) = \frac{\lambda - \lambda_0}{1 - \lambda_0} \quad \text{and} \quad S_0(\lambda) = \frac{\lambda - \lambda_0}{1 - \lambda_0} \tag{5.16}$$

and

$$L_i = \frac{\partial^2}{\partial \lambda^2} \quad \text{for} \quad i = 1, 2, 3 \tag{5.17}$$

such that

$$L_1(c_1 + c_2\lambda) = 0,\ L_2(c_3 + c_4\lambda) = 0 \quad \text{and} \quad L_3(c_5 + c_6\lambda) = 0 \tag{5.18}$$

where $c_i, (i = 1, 2, \cdots 6)$, are constants. The second step in HAM is to define the zeroth order deformation, which is given by

$$(1 - p)L_1[f(\lambda; p) - f_0(\lambda)] = ph_1N_1[f(\lambda; p)] \tag{5.19}$$

$$(1 - p)L_2[\theta(\lambda; p) - \theta_0(\lambda)] = ph_2N_2[\theta(\lambda; p)] \tag{5.20}$$

$$(1 - p)L_3[S(\lambda; p) - S_0(\lambda)] = ph_3N_3[S(\lambda; p)] \tag{5.21}$$

where

$$N_1[f(\lambda, p), \theta(\lambda, p), S(\lambda, p)] = 4\, f''\lambda + \sqrt{\lambda}\frac{Gr}{Re}\,(\theta - NrS) - \frac{Ha^2\,\alpha e\, f}{(\alpha e^2 + \beta h^2)} - A \tag{5.22}$$

$$N_2[f(\lambda, p), \theta(\lambda, p), S(\lambda, p)] = \lambda^3\theta'' + \lambda^2\theta' + Br\,\left[\lambda^2(f')^2 - 2\,\lambda\, f\, f' + (f)^2\right] + Pr\, Nb\,\lambda^3\,\theta'\,S' + Pr\, Nt\,\lambda^3\,(\theta')^2 \tag{5.23}$$

$$N_3[f(\lambda,p),\theta(\lambda,p),S(\lambda,p)] = S'' + S' + \frac{Nt}{Nb}(\lambda\,\theta'' + \theta') \tag{5.24}$$

where $p \in [0,1]$ is the embedded parameter and h_i, $(i = 1,2,3)$, are auxiliary parameters which are not vanish.

The equivalent boundary conditions are

$$\begin{aligned} f(0;p) = 0, \quad \theta(0;p) = 0, \quad S(0;p) = 0, \\ f(1;p) = b, \quad \theta(1;p) = 1, \quad S(1;p) = 1 \end{aligned} \tag{5.25}$$

From $p = 0$ to $p = 1$, we have

$$\begin{aligned} f(\lambda;0) = f_0, \quad f(\lambda;1) = f(\lambda), \\ \theta(\lambda;0) = \theta_0, \quad \theta(\lambda;1) = \theta(\lambda), \\ S(\lambda;0) = S_0, \quad S(\lambda;1) = S(\lambda) \end{aligned} \tag{5.26}$$

Thus, as p varying from 0 to 1, f, θ and S varies continuously from f_0, θ_0 and S_0 to final value $f(\lambda)$, $\theta(\lambda)$ and $S(\lambda)$ respectively. Using Taylor's series and Eq.(5.26), f, θ and S can be written as

$$\begin{aligned} f(\lambda;p) &= f_0 + \sum_{m=1}^{\infty} f_m(\lambda)p^m, \quad f_m(\lambda) = \frac{1}{m!}\frac{\partial^m f(\lambda;p)}{\partial p^m}\bigg|_{p=0} \\ \theta(\lambda;p) &= \theta_0 + \sum_{m=1}^{\infty} \theta_m(\lambda)p^m, \quad \theta_m(\lambda) = \frac{1}{m!}\frac{\partial^m \theta(\lambda;p)}{\partial p^m}\bigg|_{p=0} \\ S(\lambda;p) &= S_0 + \sum_{m=1}^{\infty} S_m(\lambda)p^m, \quad S_m(\lambda) = \frac{1}{m!}\frac{\partial^m S(\lambda;p)}{\partial p^m}\bigg|_{p=0} \end{aligned} \tag{5.27}$$

We have to choose the values of auxiliary parameters for which the series (5.27) is converges at $p = 1$ i.e.,

$$f(\lambda) = f_0 + \sum_{m=1}^{\infty} f_m(\lambda), \quad \theta(\lambda) = \theta_0 + \sum_{m=1}^{\infty} \theta_m(\lambda), \quad S(\lambda) = S_0 + \sum_{m=1}^{\infty} S_m(\lambda) \tag{5.28}$$

Next, the deformation equations of m^{th}-order are given by

$$L_1[f_m(\lambda) - \chi_m f_{m-1}(\lambda)] = h_1 R_m^f(\lambda) \tag{5.29}$$

$$L_2[\theta_m(\lambda) - \chi_m \theta_{m-1}(\lambda)] = h_2 R_m^\theta(\lambda) \tag{5.30}$$

$$L_3[S_m(\lambda) - \chi_m S_{m-1}(\lambda)] = h_3 R_m^S(\lambda) \tag{5.31}$$

where

$$\left.\begin{aligned} R_m^f(\lambda) &= 4\, f''\lambda + \sqrt{\lambda}\frac{Gr}{Re}\,(\theta - NrS) - \frac{Ha^2\,\alpha e\, f}{(\alpha e^2 + \beta h^2)} - A \\ R_m^\theta(\lambda) &= \lambda^3\theta'' + \lambda^2\theta' + Br\ [\lambda^2(f')^2 - 2\,\lambda\, f\, f' + (f)^2] + Pr\, Nb\, \lambda^3\, \theta'\, S' + Pr\, Nt\, \lambda^3\, (\theta')^2 \\ R_m^S(\lambda) &= S'' + S' + \frac{Nt}{Nb}(\lambda\,\theta'' + \theta') \end{aligned}\right\} \tag{5.32}$$

and

$$\begin{aligned} \chi_m &= 0 \quad \text{for} \quad m \leq 1, \\ &= 1 \quad \text{for} \quad m > 1 \end{aligned}$$

for any integer m

5.3.2 Natural convection

In this case also, the governing Eqs. (5.12) - (5.14) along with the boundary conditions (5.15) are solved by using homotopy analysis method (HAM). The procedure is similar to that of mixed convection case and hence details of the method for this case are not presented to avoid repetition.

5.4 Convergence

5.4.1 Mixed convection

In HAM, it is essential to see that the series solution converges. Also, the rate of convergence of approximation for the HAM solution depends mainly on the values of h. To find the admissible range of the auxiliary parameters, h-curves are plotted for 16^{th}-order approximation and shown in figure (5.2). It is visible from this figure that the permissible interval for h_1, h_2 and h_3 are $-0.5 < h_1 < 0$, $-1.8 < h_2 < -0.5$ and $-1.8 < h_3 < -0.6$, respectively.

The following average residual errors (Ref. Liao [49]) are computed to obtain the optimal value of auxiliary parameter

$$E_{f,m} = \frac{1}{2K} \sum_{i=-K}^{K} \left(N_1 \left[\sum_{j=0}^{m} f_j(i\triangle t) \right] \right)^2 \tag{5.33}$$

$$E_{\theta,m} = \frac{1}{2K} \sum_{i=-K}^{K} \left(N_2 \left[\sum_{j=0}^{m} \theta_j(i\triangle t) \right] \right)^2 \tag{5.34}$$

$$E_{S,m} = \frac{1}{2K} \sum_{i=-K}^{K} \left(N_3 \left[\sum_{j=0}^{m} S_j(i\triangle t) \right] \right)^2 \tag{5.35}$$

where $\triangle t = 1/K$ and $K = 5$. At various level of approximations (m), least average residual errors are represented in table (5.4). From this, we see that the average residual errors are least at $h_1 = -0.43$, $h_2 = -0.67$ and $h_3 = -1.60$. Therefore, the optimality of convergence control parameters are taken as $h_1 = -0.43$, $h_2 = -0.67$ and $h_3 = -1.60$. For different values of m, the series solutions are calculated and presented in table (5.5). It is noticed from this table that, the series (5.28) converges in the total area of λ. The graphs of the following ratio

$$\beta f = \left| \frac{f_m(h)}{f_{m-1}(h)} \right|, \quad \beta\theta = \left| \frac{\theta_m(h)}{\theta_{m-1}(h)} \right|, \quad \beta S = \left| \frac{S_m(h)}{S_{m-1}(h)} \right| \tag{5.36}$$

versus the number of terms m in the homotopy series is presented in figure (5.3). These

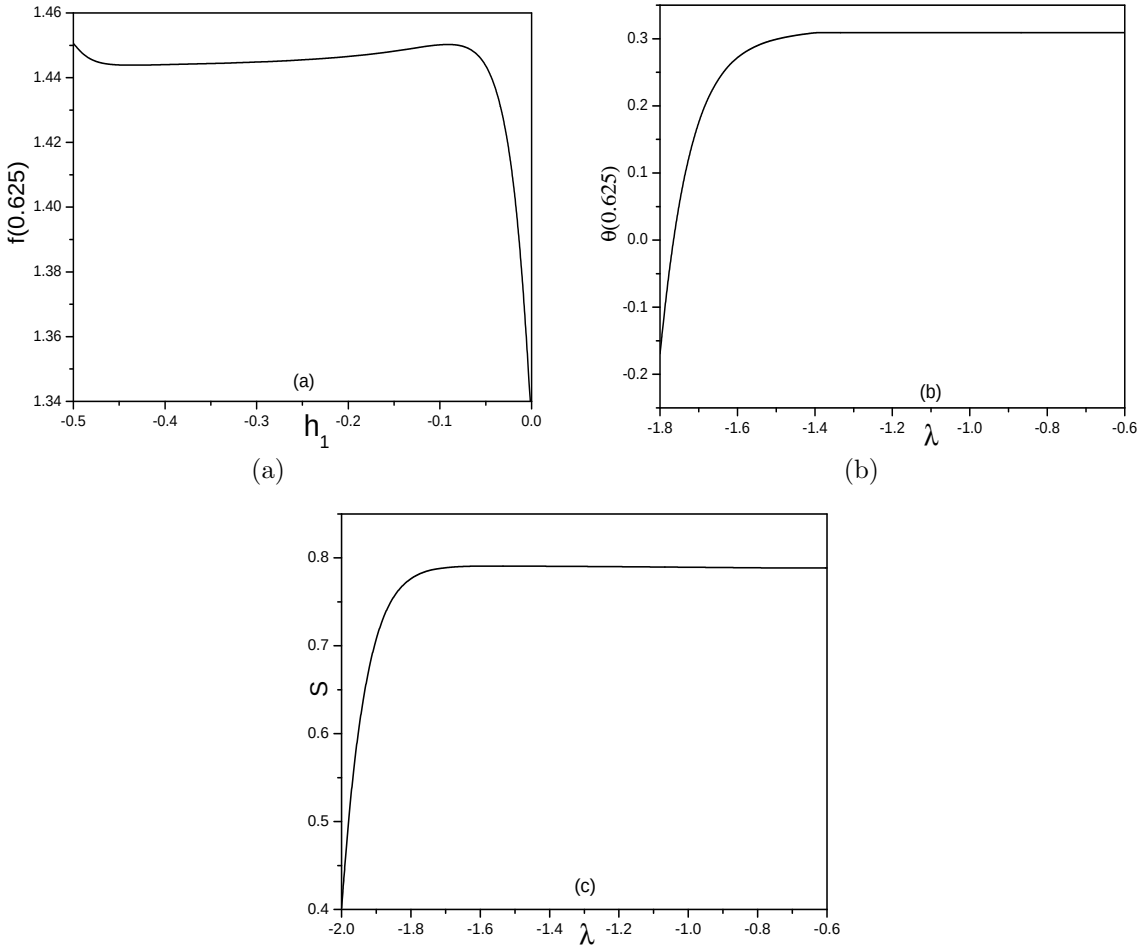

Figure 5.2: "h-curves of (a) $f(\lambda)$, (b) $\theta(\lambda)$ and (c) $S(\lambda)$ when $Nr = 1.0, Nt = 0.5, Nb = 0.5, Gr = 10.0, Ha = 5.0, A = 1.0, Re = 2.0, Pr = 1.0, \beta i = 5.0, \beta h = 2.0$ and $Br = 0.5$ (mixed convection case)".

figures indicate that the series (5.28) converges to the exact solution.

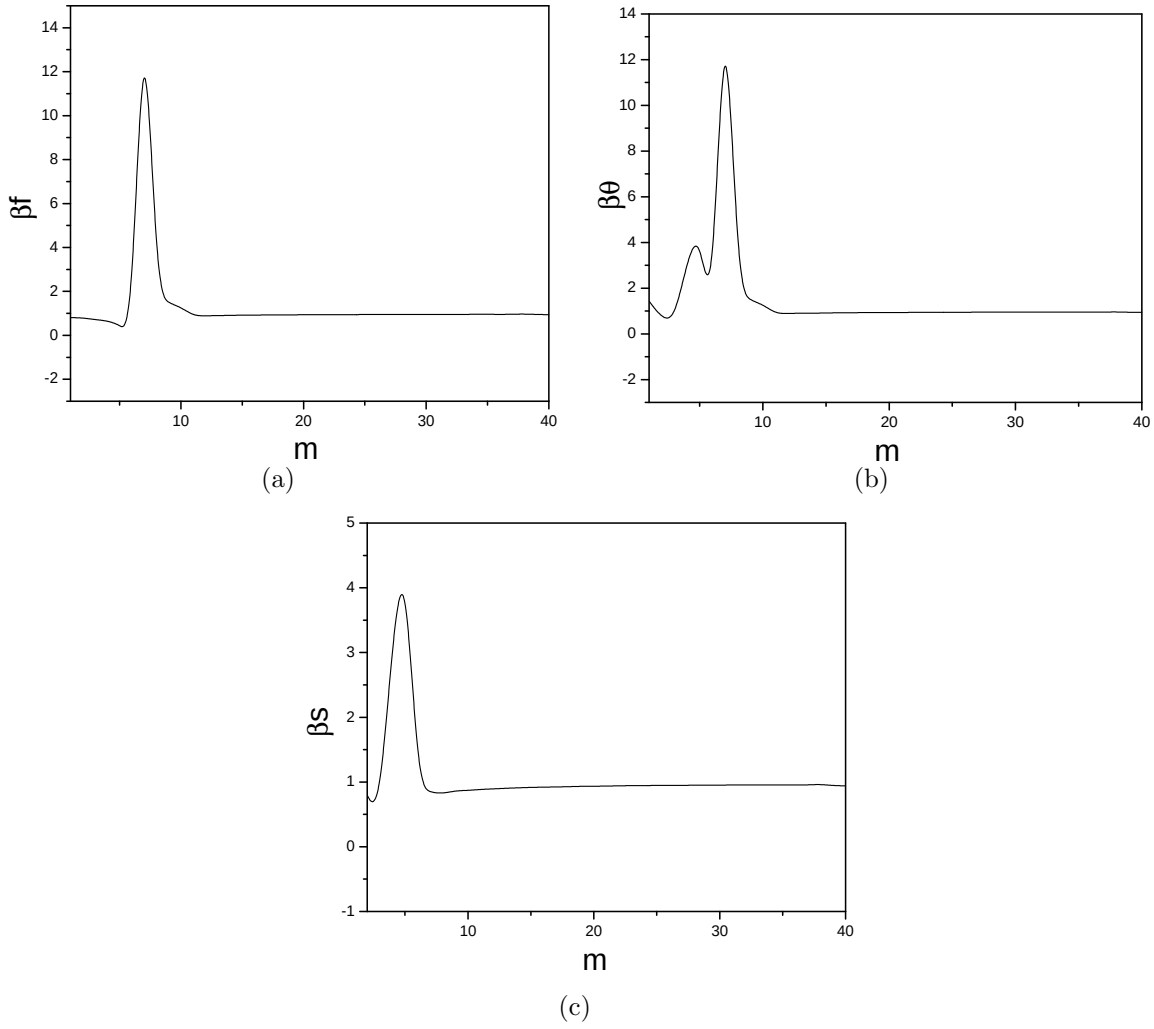

Figure 5.3: "Ratios of (a) βf, (b) $\beta\theta$ and (c) βs verses m to reveal the convergence of HAM solutions (mixed convection case)".

	Optimal of h_1		Optimal of h_2		Optimal of h_3	
Order	h_1	Min. of E_m	h_2	Min. of E_m	h_3	Min. of E_m
12	-0.42	1.49×10^{-6}	-0.67	2.92×10^{-4}	-1.56	7.16×10^{-5}
14	-0.43	1.08×10^{-6}	-0.67	7.90×10^{-4}	-1.60	1.23×10^{-5}
16	-0.43	8.03×10^{-7}	-0.65	2.89×10^{-5}	-1.60	3.53×10^{-5}

Table 5.1: "Optimal values of h_1, h_2 and h_3 at different order of approximations (mixed convection case)".

Table 5.2: "Convergence of HAM solutions for different order of approximations (mixed convection case)".

Order	f(0.625)	$\theta(0.625)$	S(0.625)
05	0.45201062040	0.80760004656	0.65436658412
10	0.45166547215	0.80760008211	0.65415106427
15	0.45133062142	0.80720010397	0.64106428731
20	0.44120618062	0.80720010598	0.64106337319
25	0.44120612487	0.80724016788	0.64105463192
30	0.44120612495	0.80722102382	0.64105463293
35	0.44120564124	0.80719025837	0.64105463524
40	0.44120564128	0.80719025389	0.64105467933
45	0.44120563244	0.80719024879	0.64105437932
50	0.44120563244	0.80719024689	0.64105437932
55	0.44120563244	0.80719024689	0.64105437932

Table 5.3: "Comparison of HAM for the velocity against analytical and SQLM solutions for $Gr = 0$, $Ha = 0$, $A = 0$, $Pr = 0$, $Nt = 0$ and $Nb = 0$ (mixed convection case)".

λ	Sinha and Chaudhary[74]	Srinivasacharya and Himabindu[77]	Present
	analytical solution	SQLM	HAM
0.25	0	0	0
0.2684	0.02453	0.024532	0.0245333
0.3216	0.09546	0.095462	0.0954667
0.4046	0.20613	0.206127	0.206133
0.5091	0.34546	0.345462	0.345467
0.625	0.5	0.5	0.5
0.7409	0.65453	0.654539	0.654533
0.8454	0.793867	0.793863	0.793867
0.9284	0.90453	0.904529	0.904533
0.9816	0.97546	0.975468	0.975467
1	1	1	1

	Optimal of h_1		Optimal of h_2		Optimal of h_3	
Order	h_1	Min. of E_m	h_2	Min. of E_m	h_3	Min. of E_m
12	-0.42	1.68×10^{-5}	-0.67	2.95×10^{-4}	-1.38	5.19×10^{-5}
14	-0.43	1.21×10^{-5}	-0.64	6.58×10^{-4}	-1.40	5.14×10^{-5}
16	-0.44	7.83×10^{-5}	-0.65	2.92×10^{-4}	-1.40	4.53×10^{-5}

Table 5.4: "Optimal values of h_1, h_2 and h_3 at different order of approximations (natural convection case)".

5.4.2 Natural convection

To find the admissible range of the auxiliary parameters, h-curves are plotted for 16^{th}-order approximation and shown in figure (5.4). It is evident from this figure that, the admissible ranges for h_1, h_2 and h_3 are $-0.5 < h_1 < 0$, $-1.8 < h_2 < -0.5$ and $-1.8 < h_3 < -0.6$ respectively. The average residual errors given by (5.33)-(5.35), at different order of approximations (m), are computed. It is found that the average residual errors are least at $h_1 = -0.43$, $h_2 = -0.64$ and $h_3 = -1.4$. Therefore, the optimum values of convergence control parameters are taken as $h_1 = -0.43$, $h_2 = -0.64$ and $h_3 = -1.4$. Further, the series solutions for different values of m are computed. It is observed from these computed values that the series (5.28) converges in the whole region of η. The graphs of the ratio given by figure (5.5) against the number of terms m in homotopy series indicate that the series (5.28) converges to the exact solution.

5.5 Results and Discussion

5.5.1 Mixed convection

In order to determine the accuracy of HAM, we have compared present solution with the analytical solution [74], as well as the solution obtained by spectral quasi-linearization method (SQLM) [77] in absence of Gr, Ha, A, Pr, Nt and Nb. The comparisons are found to be in good agreement, as shown in table (5.3).

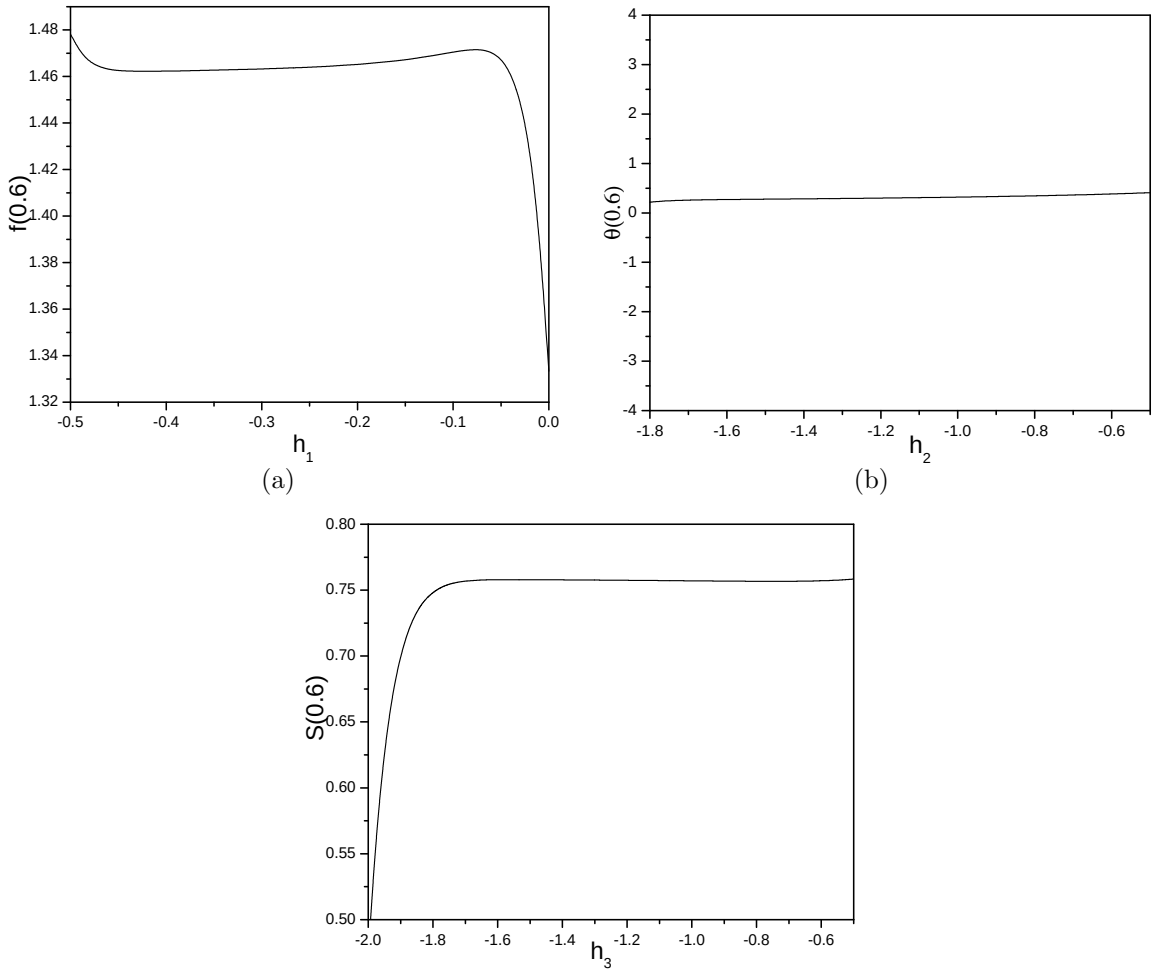

(a) (b)

(c)

Figure 5.4: "h-curves of (a) $f(\lambda)$, (b) $\theta(\lambda)$ and (c) $S(\lambda)$ when $Nr = 1.0, Nt = 0.5, Nb = 0.5, Gr = 10.0, Ha = 5.0, Re = 2.0, Pr = 1.0, \beta i = 5.0, \beta h = 2.0$ and $Br = 0.5$ (natural convection case)".

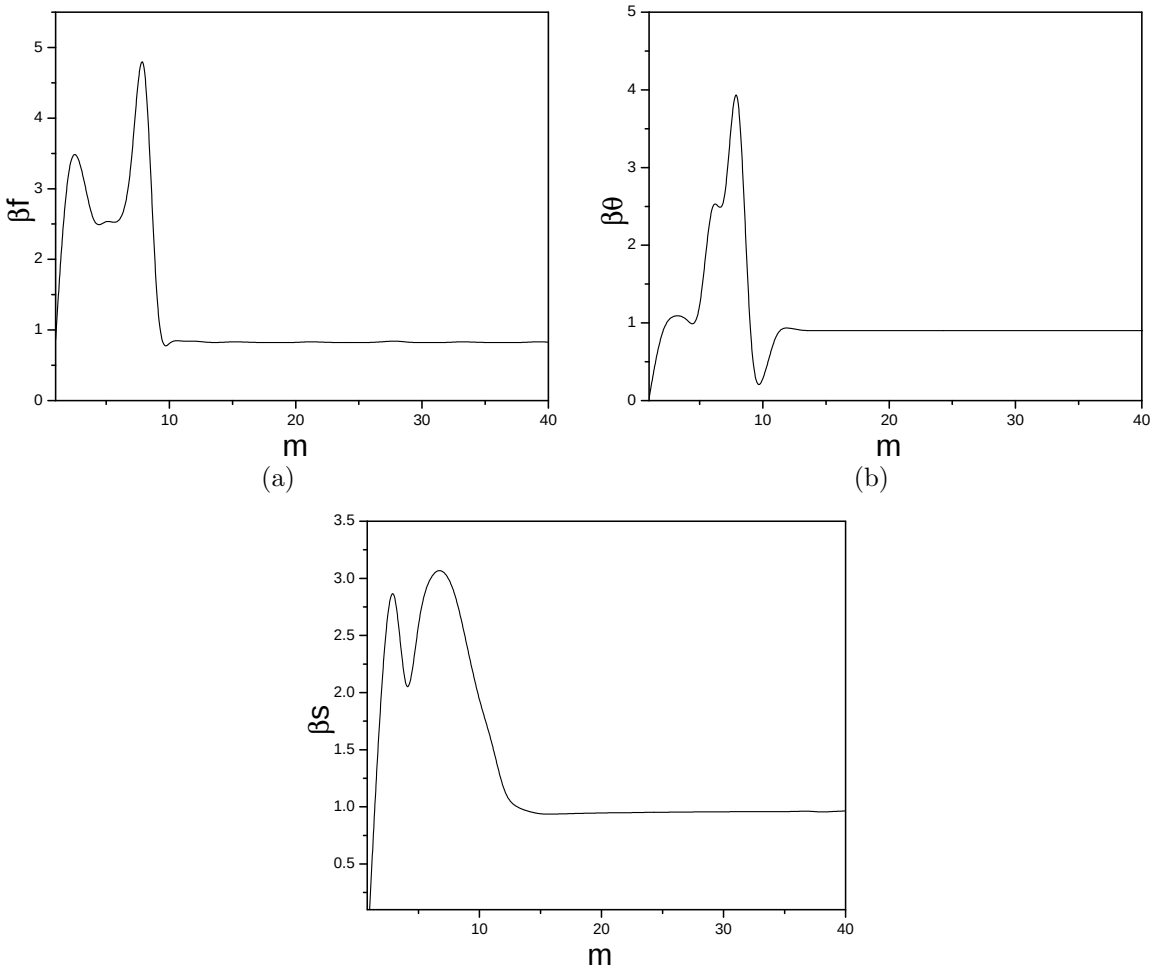

Figure 5.5: "Ratios of (a) βf, (b) $\beta\theta$ and (c) βs versus m to reveal the convergence of HAM solutions (natural convection case)".

Table 5.5: "Convergence of HAM solutions for different order of approximations (natural convection case)".

Order	f(0.625)	$\theta(0.625)$	S(0.625)
05	0.4897195201	0.6703748076	0.6552164366
10	0.4977435164	0.6738914807	0.6476354151
15	0.5021085133	0.6776065807	0.6429961064
20	0.5092824541	0.6807795200	0.6410633722
25	0.5129294412	0.6808724016	0.6409112546
30	0.5144120618	0.6809872210	0.6408546329
35	0.5151205641	0.6810719025	0.6405463524
40	0.5157220364	0.6810731902	0.6400754680
45	0.5164120763	0.6810751902	0.6400554379
50	0.5164125634	0.6810756190	0.6400549913
55	0.5164126324	0.6810756190	0.6400549913

The influence of magnetic parameter Ha, thermophoresis Nt, Brownian motion Nb, Hall parameter βh, ion-slip βi on the non-dimensional velocity $f(\lambda)$, temperature $\theta(\lambda)$ and nanoparticle volume fraction $S(\lambda)$ are shown graphically in figures (5.6) - (5.10) by taking $Br = 0.5$, $Pr = 1.0$, $Gr = 10$, $A = 1$, $Re = 2$ and $Nr = 1.0$.

Figure (5.6) presents the impact of the magnetite parameter Ha on the dimensionless velocity in flow direction, temperature and nanoparticle volume fraction. Figure 5.6(a) reveals that the dimensionless velocity decays with a rise in Ha. The transverse magnetic field, which is applied orthogonally to the direction of flow gives a resistive force, known as Lorentz force. This Lorentz force resists the flow of a nanofluid and therefore, the velocity decreases. Figure 5.6(b) illustrates that the dimensionless temperature $\theta(\lambda)$ increases with a rise in Ha. Figure 5.6(c) depicts that the nanoparticle volume fraction $S(\lambda)$ reduces as Ha increases. This is due to the perpendicular effect of magnetic field on the flow direction.

The variations of velocity $f(\lambda)$, temperature $\theta(\lambda)$ and nanoparticle volume fraction $S(\lambda)$ with Hall-parameter βh are presented in figure (5.7). It is observed from figure 5.7(a) that the velocity increases with an increase in the parameter βh. From figure 5.7(b), it is noticed that the dimensionless temperature $\theta(\lambda)$ decreases with a rise in βh. There is an enhancement in the nanoparticle concentration $S(\lambda)$ with a rise in βh as depicted in figure 5.7(c). The

inclusion of Hall parameter reduces the effective conductivity and hence drops the magnetic resistive force. Therefore, increase in βh rises the velocity component $f(\lambda)$ and nanoparticle volume fraction $S(\lambda)$, whereas decreases temperature $\theta(\lambda)$.

The variations of velocity in flow direction $f(\lambda)$, temperature $\theta(\lambda)$ and nanoparticle volume fraction $S(\lambda)$ with ion-slip parameter βi are presented in figure (5.8). It is observed from the figure 5.8(a) that the velocity increases with a rise in βi. Figure 5.8(b) reports that $\theta(\lambda)$ decreases with a rise in βi. There is an increment in the nanoparticle concentration $S(\lambda)$ with an increase in βi as depicted in figure 5.8(c). The effective conductivity increases as increase in βi, hence the damping force on the dimensionless velocity decreases due to increase in the velocity .

The impact of thermophoresis parameter Nt on the dimensionless velocity $f(\lambda)$, temperature $\theta(\lambda)$ and nanoparticle concentration $S(\lambda)$ are depicted in figure (5.9). The dimensionless velocity $f(\lambda)$ rises with a rise in Nt as shown in figure 5.9(a). Figure 5.9(b) reveals that $\theta(\lambda)$ rises with a rise in Nt. Increase of Nt leads to increase in the effective-conductivity. It is recognized from figure 5.9(c) that the nanoparticle concentration $S(\lambda)$ decays with an enhancement in Nt.

The influence of Brownian motion Nb on the dimensionless velocity $f(\lambda)$, temperature $\theta(\lambda)$ and nanoparticle concentration $S(\lambda)$ are presented in figure (5.10). The velocity $f(\lambda)$ rises with rise in Nb as shown in figure 5.10(a). Figure 5.10(b) reveals that the dimensionless temperature $\theta(\lambda)$ increases with an enhancement in Nb. The nanoparticle volume fraction $S(\lambda)$ decreases with an increase in Nb as shown in figure 5.10(c).

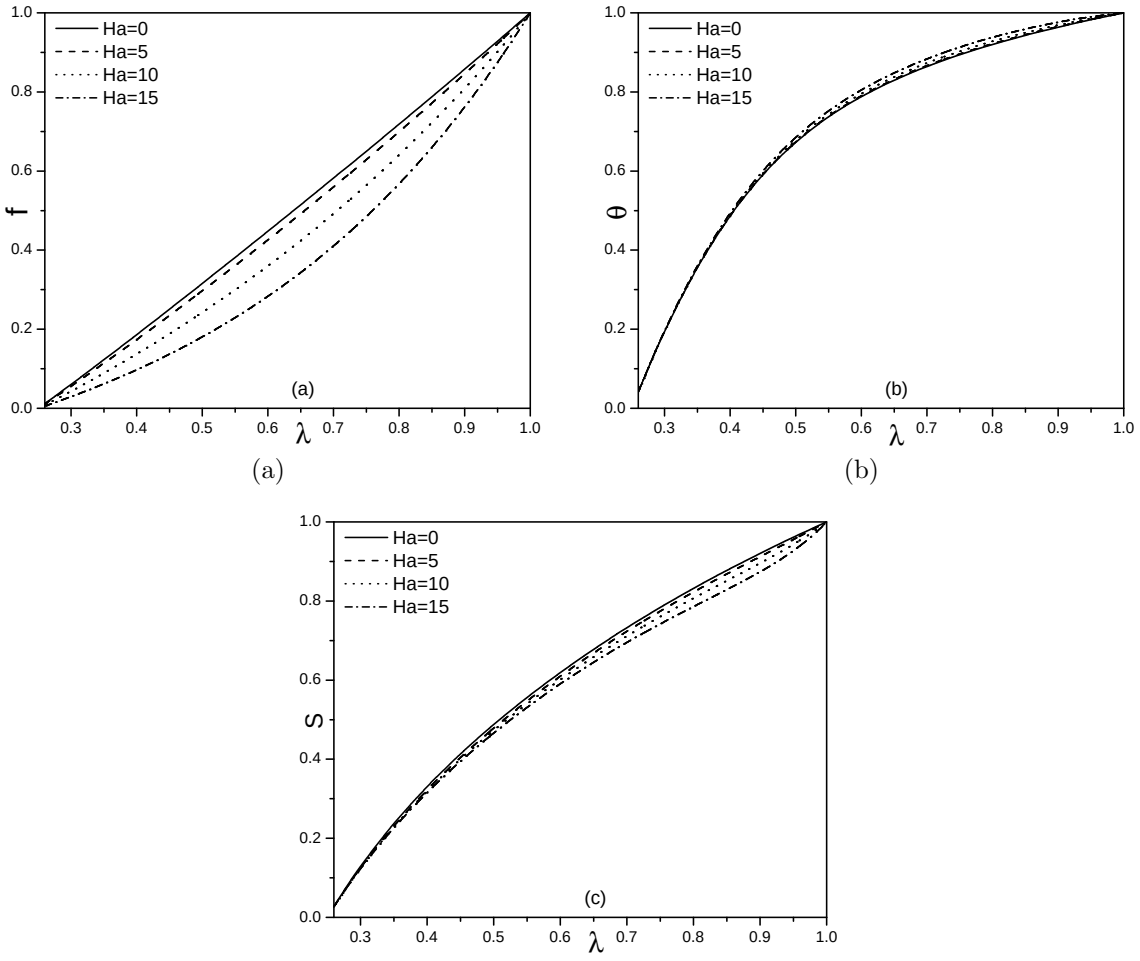

Figure 5.6: "Effect of Ha on (a) velocity, (b) temperature and (c) nanoparticle concentration profiles (mixed convection case)".

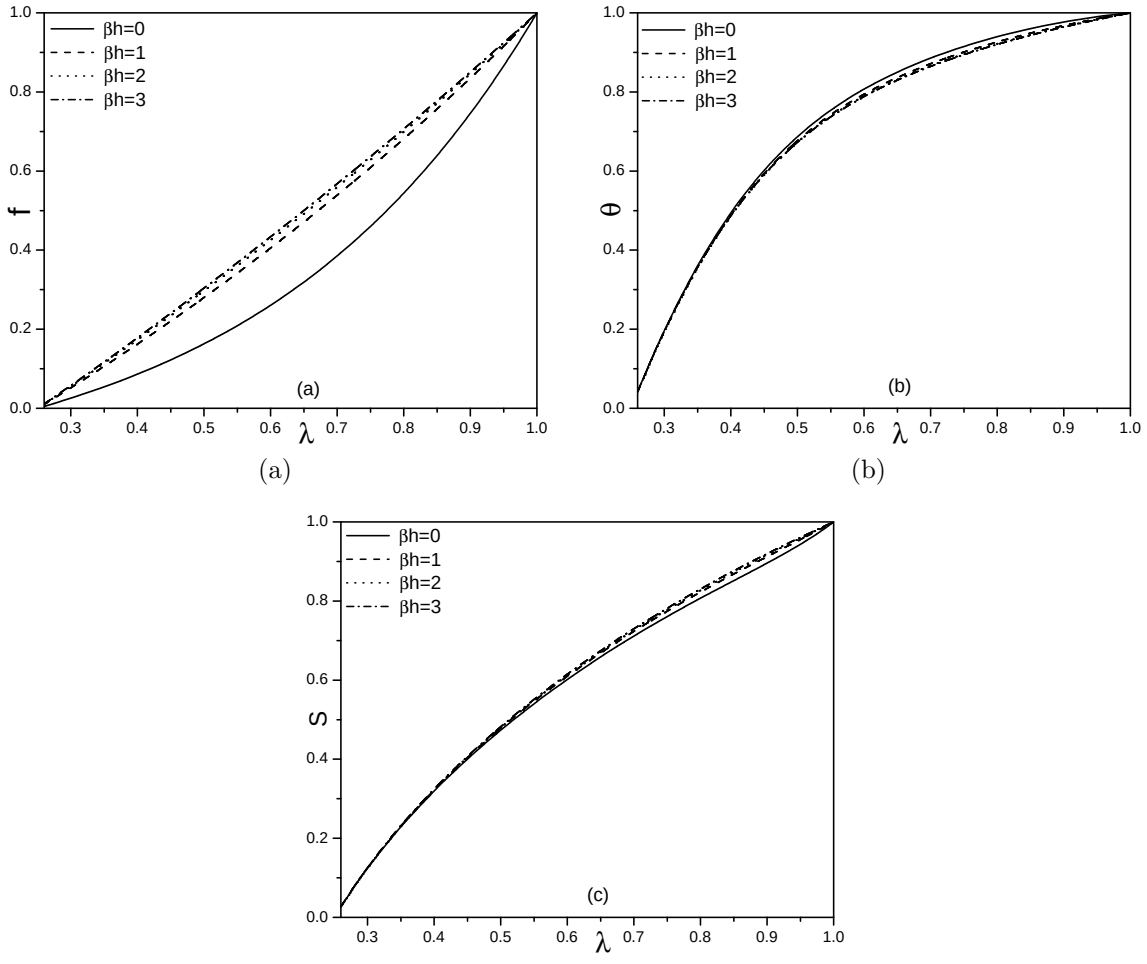

Figure 5.7: "Effect of βh on (a) velocity, (b) temperature and (c) nanoparticle concentration profiles (mixed convection case)".

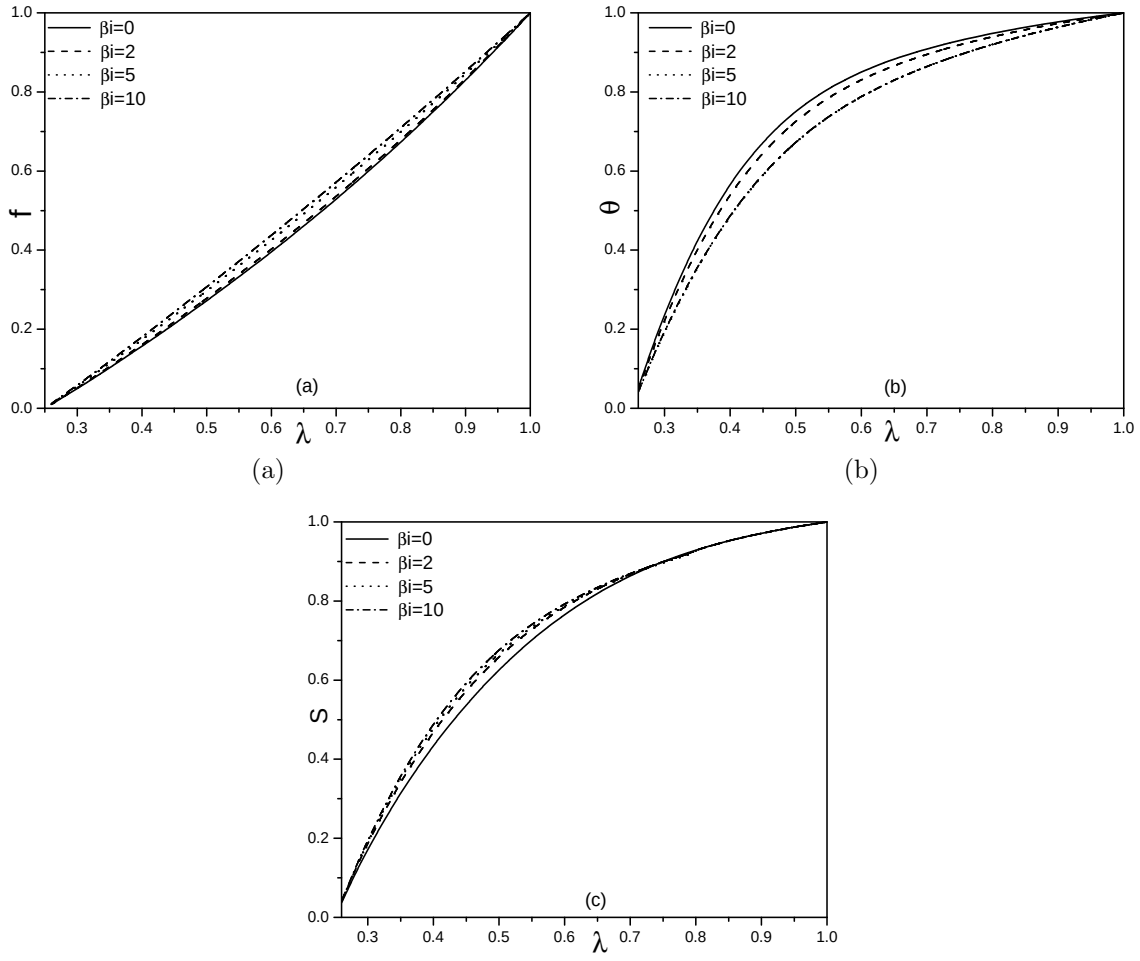

Figure 5.8: "Effect of βi on (a) velocity, (b) temperature and (c) nanoparticle concentration profiles (mixed convection case)".

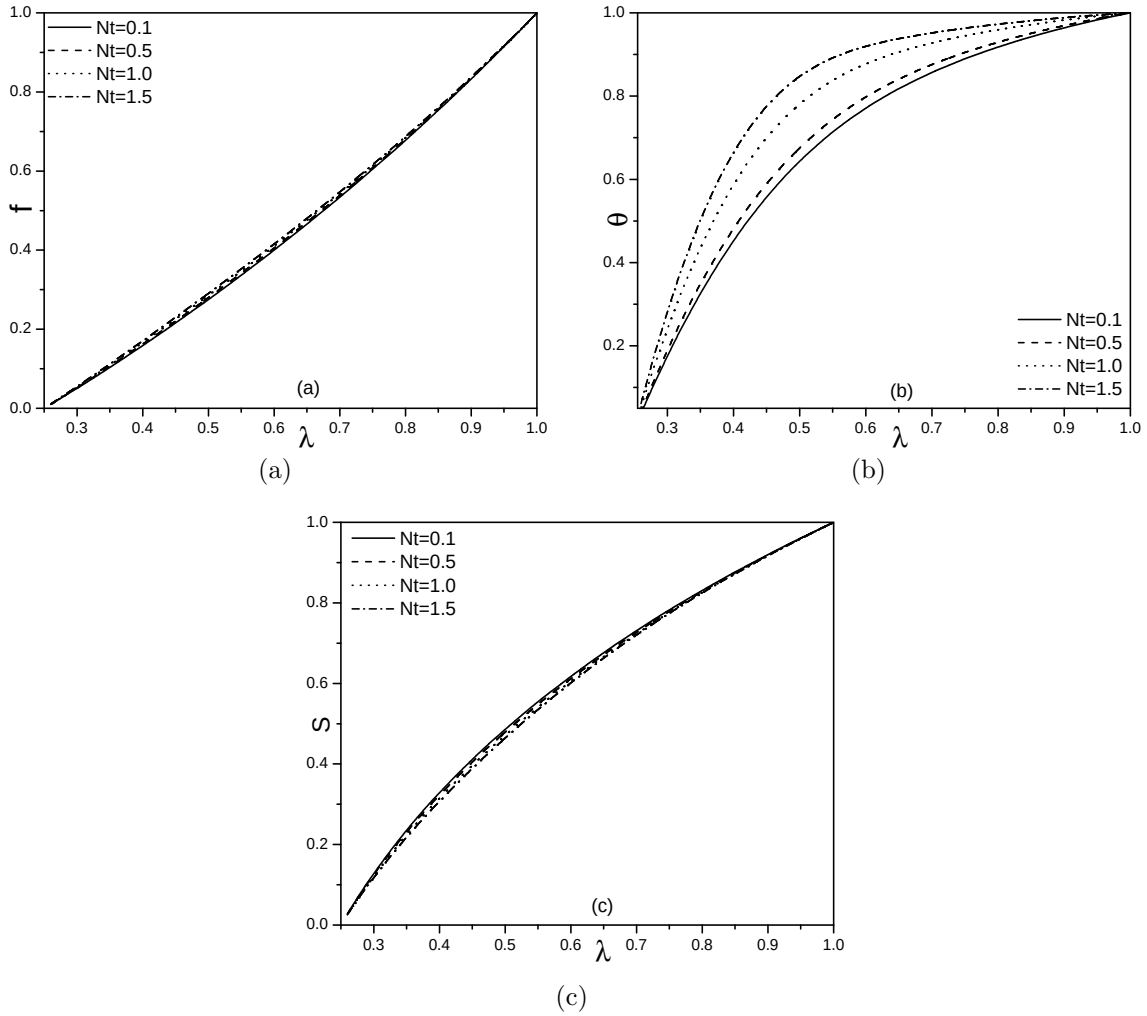

Figure 5.9: "Effect of Nt on (a) velocity, (b) temperature and (c) nanoparticle concentration profiles (mixed convection case)".

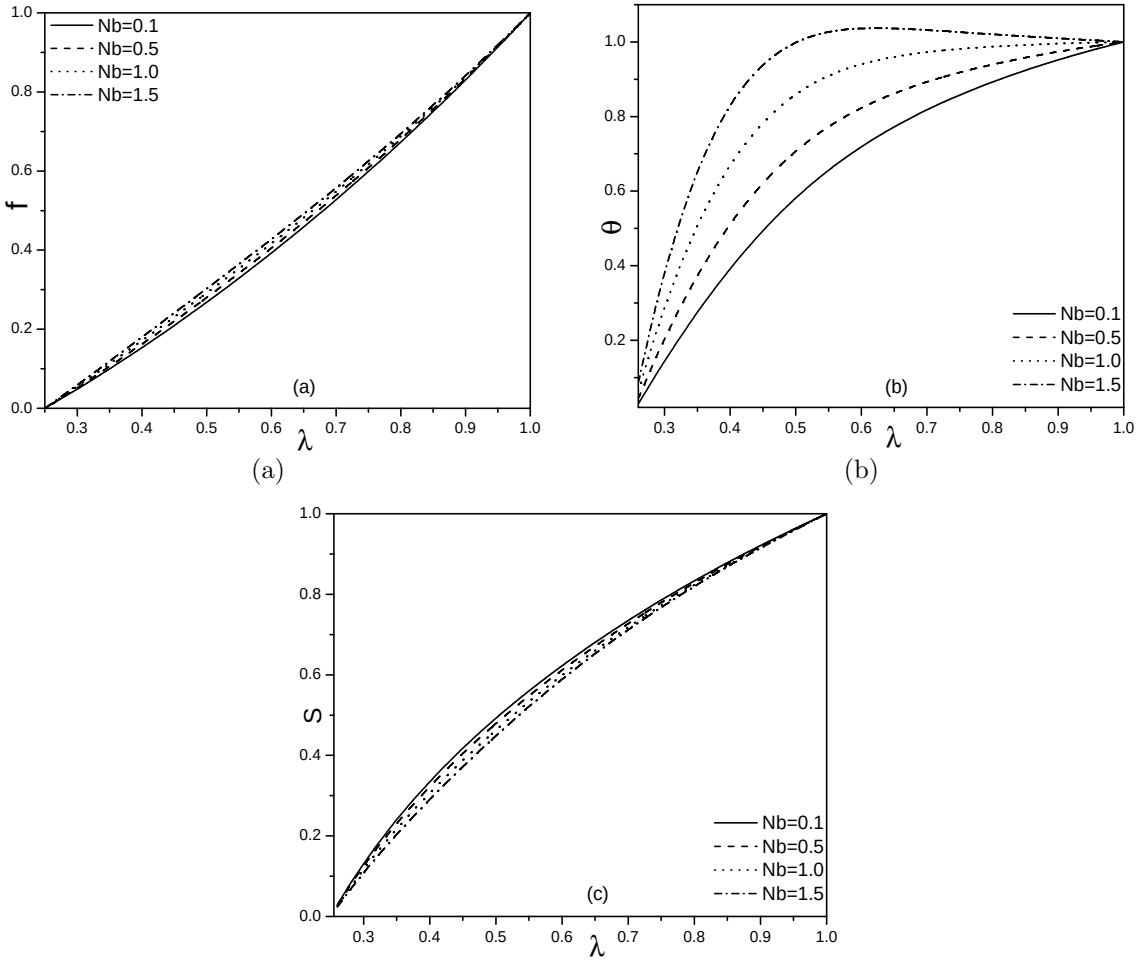

Figure 5.10: "Effect of Nb on (a) velocity, (b) temperature and (c) nanoparticle concentration profiles (mixed convection case)".

5.5.2 Natural convection

The influence of magnetic parameter Ha, Hall parameter βh and ion-slip parameter βi on the velocity $f(\lambda)$, temperature $\theta(\lambda)$ and nanoparticle volume fraction $S(\lambda)$ are shown graphically in figure (5.11) - (5.13). To study the effect of these parameters, the remaining parameters, are taken as $Br = 0.5$, $Pr = 1.0$ and $Nr = 1.0$.

Figure (5.11) represents the influence of magnetic parameter Ha on dimensionless velocity, temperature and nanoparticle volume fraction. Figure 5.11(a) reveals that the dimensionless velocity decays with a rise in Ha. The magnetic field which is applied orthogonally to the flow direction gives a resistive force, known as Lorentz force. This Lorentz force resists the flow of a nanofluid leading to decrease in the velocity. Figure 5.11(b) presents the variations in dimensionless temperature with Ha. From this figure, it observed that the temperature $\theta(\lambda)$ is increasing with an increase in Ha. Figure.5.11(c) depicts the variations of $S(\lambda)$ with Ha. A decay in a nanoparticle volume fraction $S(\lambda)$ is noticed as magnetic parameter Ha increases.

The variation of the velocity $f(\lambda)$, temperature $\theta(\lambda)$ and nanoparticle volume fraction $S(\lambda)$ with hall parameter βh is presented in figure (5.13). It is noticed from figure 5.12(a) that the velocity is increasing with a rise in the value of Hall parameter βh . From the figure 5.12(b), it is observed that the dimensionless temperature $\theta(\lambda)$ is decreasing with an increase in βh. There is an increase in a nanoparticle volume fraction $S(\lambda)$ with an increase in the value of βh as depicted in figure 5.12(c). The inclusion of Hall parameter reduces the effective conductivity and drops the magnetic resistive force. Hence, increase in βh, rises the velocity $f(\lambda)$ and nanoparticle volume fraction $S(\lambda)$, but decreases temperature $\theta(\lambda)$.

The variation of velocity in flow direction $f(\lambda)$, temperature $\theta(\lambda)$ and nanoparticle volume fraction $S(\lambda)$ with ion-slip parameter βi is depicted in figure (5.13). Figure 5.13(a) reveals that the velocity in flow direction is increases with an enhancement in βi . From the figure 5.13(b), it is seen that the temperature $\theta(\lambda)$ decreases with an increase in βi. The nanoparticle volume fraction $S(\lambda)$ is enhanced with an increase in βi as shown in figure 5.13(c). The effective conductivity increases as βi increases, hence the damping force on the

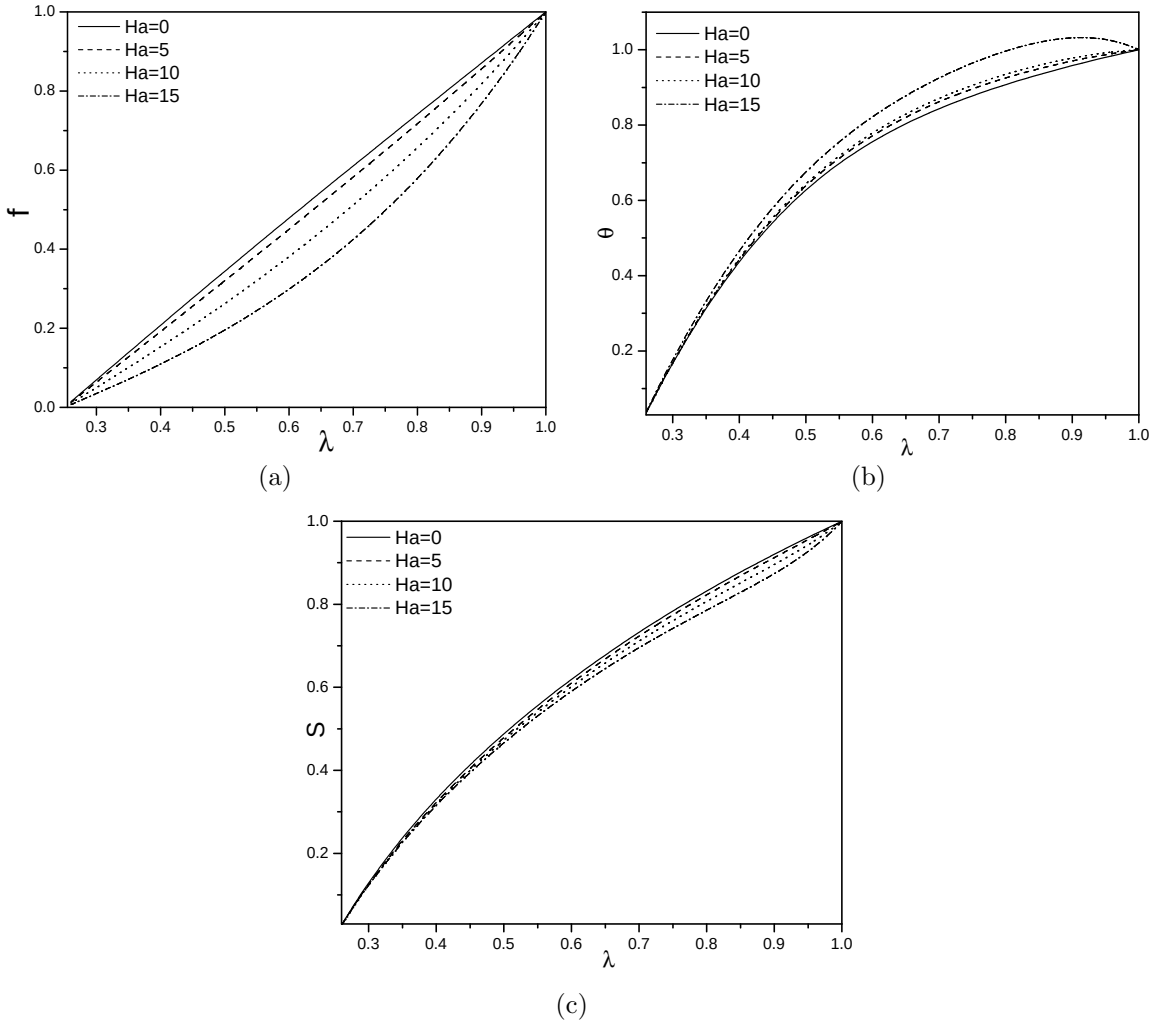

Figure 5.11: "Effect of Ha on (a) velocity, (b) temperature and (c) nanoparticle concentration profiles (natural convection case)".

dimensionless velocity decreases and due to this, the dimensionless velocity increases.

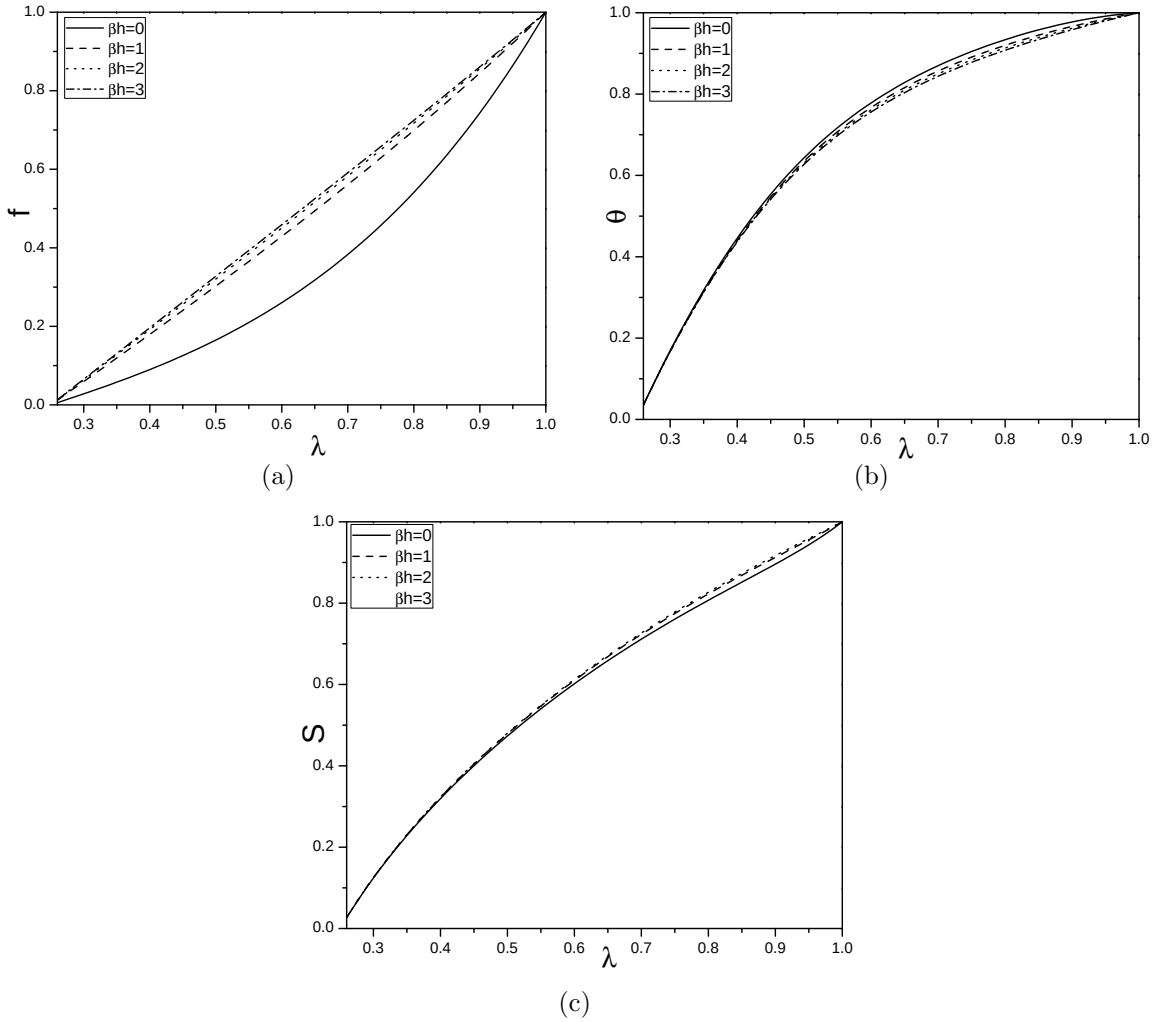

(a) (b)

(c)

Figure 5.12: "Effect of βh on (a) velocity, (b) temperature and (c) nanoparticle concentration profiles (natural convection case)".

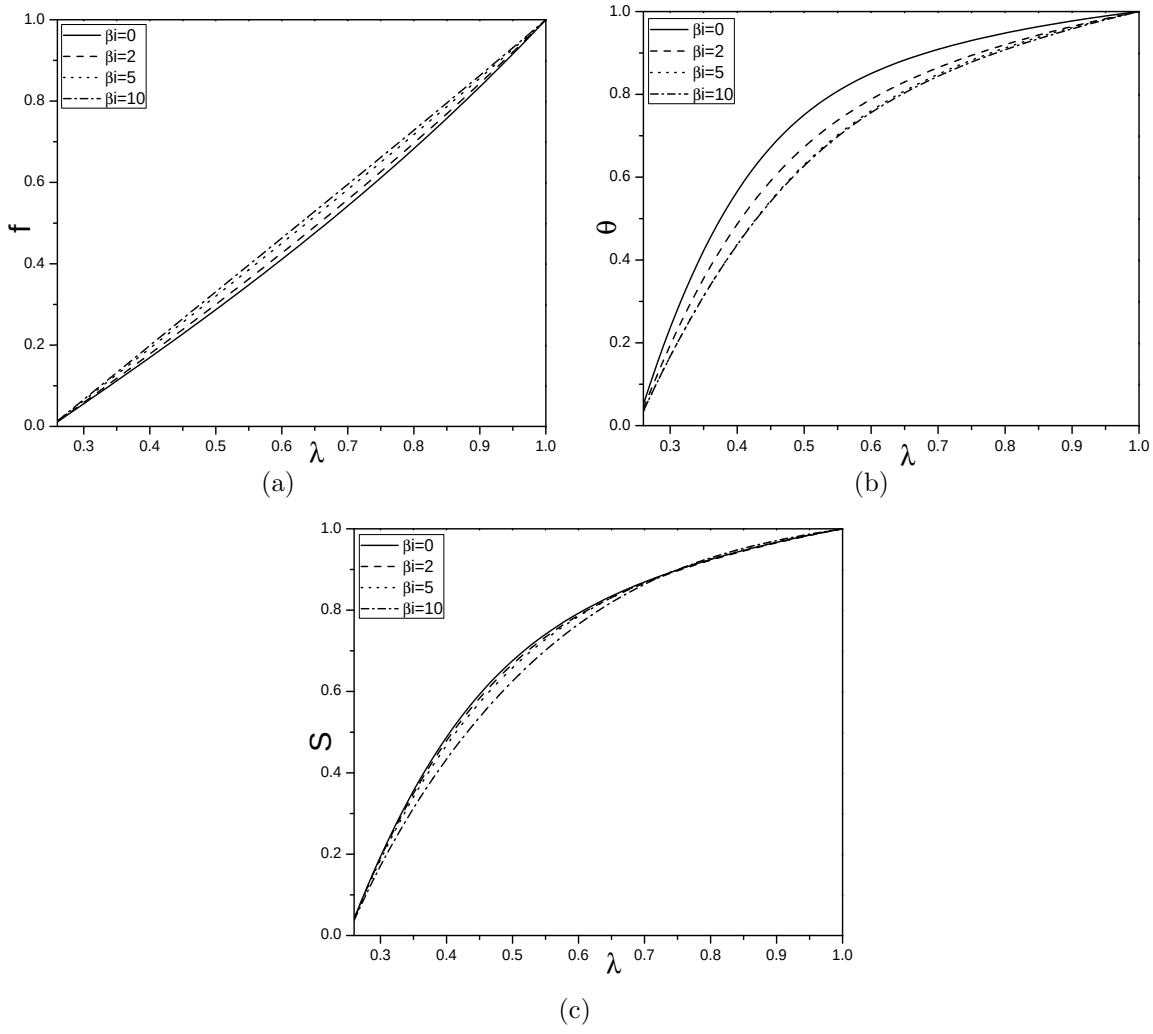

Figure 5.13: "Effect of βi on (a) velocity, (b) temperature and (c) nanoparticle concentration profiles (natural convection case)".

5.6 Conclusions

In this chapter, the steady, laminar, an incompressible nanofluid flow passing through the concentric cylinders has been investigated in presence of Hall and ion-slip effects. In addition, two types of convection namely, natural and mixed convective flows are considered. From this analysis, the following are the main observations in both cases.

With an increase in magnetic parameter, the velocity and nanoparticle concentration decrease, whereas the temperature increases in both the cases. As the Hall parameter increases, the velocity and nanoparticle concentration increase, whereas the temperature decreases in both the cases. The velocity and nanoparticle concentration increase, whereas the temperature decreases in both the cases as ion-slip parameter increases. As Brownian motion parameter increases, the dimensionless temperature and velocity in the flow direction increase, but the nanoparticle concentration decreases. The dimensionless temperature, velocity in the flow direction increase, but the nanoparticle concentration decreases as thermophoresis parameter increases.

Chapter 6

Entropy generation due to MHD mixed convective flow of a nanofluid between two concentric cylinders with radiation and Joule heating [1]

6.1 Introduction

The entropy generation plays an important role in the design and development of thermal machines. As irreversibility destroys the system's energy, its minimization has been considered as the optimal design criteria for thermal systems to utilize maximum available energy. Hence, efficient utilization of energy can be achieved by entropy generation minimization. Chen *et al* [19] analyzed the entropy generation due to natural convection in a vertically concentric annular space. Eegunjobi and Makinde [28] studied the entropy generation rate in transient couette flow of variable viscosity fluid between two concentric pipes where inner pipe is moving and outer pipe is fixed. Srinivasacharya and Hima bindu [77] investigated the entropy generation in a micropolar fluid flow between concentric cylinders.

[1] Published in "**Journal of Nanofluids, Vol. 6(2017), 1227–1237**"

In this chapter, the mixed convective flow of a nanofluid passing through a concentric cylinders with thermal radiation and Joule heating effects is considered. The homotopy analysis method is used to solve the governing nonlinear differential equations. The effects of pertinent parameters on the velocity along the fluid direction, temperature, nanoparticle concentration, Bejan number and entropy generation are investigated and presented graphically.

6.2 Mathematical Formulation

Consider steady, laminar and incompressible nanofluid flow in an annular space between two infinitely long concentric cylinders of radius a and $b\,(a < b)$. The inner cylinder and outer cylinders are kept at temperatures T_a and T_b respectively. The physical model and coordinate system is given in figure (5.1). The flow is induced due to the rotation of the exterior cylinder. A strong magnetic field B_0 is taken in an axial direction. The magnetic Reynolds number is assumed to be very small so that the induced magnetic field is negligible compared to the applied radial field. The fluid is considered to be a gray, absorbing/emitting radiation, but non-scattering medium so that the Rosseland approximation [76] can be used to describe the radiative heat flux in the energy equation. Further, the Joule heating effect is considered.

The equations of the governing flow are as follows

$$\frac{\partial u}{\partial \psi} = 0 \tag{6.1}$$

$$\frac{\partial p}{\partial r} = \frac{u}{r^2} \tag{6.2}$$

$$\mu \nabla_1^2 \, u + (1-\phi)\rho_f g^* \beta_T (T - T_a) - (\rho_s - \rho_f)\, g^* (\phi - \phi_a) - \sigma \, B_0^2 \, u - \frac{1}{r}\,\frac{\partial p}{\partial \psi} = 0 \tag{6.3}$$

$$\alpha\left[\frac{\partial^2 T}{\partial r^2}+\frac{1}{r}\frac{\partial T}{\partial r}\right]-\frac{1}{\rho C_p}\nabla.q_r+\frac{\mu}{\rho c_p}\left[\left(\frac{\partial u}{\partial r}\right)^2-2\frac{u}{r}\frac{\partial u}{\partial r}+\left(\frac{u}{r}\right)^2\right]$$
$$+\tau\left[D_B\frac{\partial T}{\partial r}\frac{\partial \phi}{\partial r}+\frac{D_T}{T_m}\left(\frac{\partial T}{\partial r}\right)^2\right]+\frac{1}{\rho c_p}\sigma B_0^2 u^2=0 \tag{6.4}$$

$$D_B\left[\frac{\partial^2\phi}{\partial r^2}+\frac{1}{r}\frac{\partial\phi}{\partial r}\right]+\frac{D_T}{T_m}\left[\frac{\partial^2 T}{\partial r^2}+\frac{1}{r}\frac{\partial T}{\partial r}\right]=0 \tag{6.5}$$

The radiation heat flux q_r under the Rosseland approximation takes the form

$$q_r=-\frac{4\sigma^*}{3\chi}\frac{\partial T^4}{\partial r} \tag{6.6}$$

where σ^* is a Stefan-Boltzman constant and χ is the coefficient of mean absorption. We assume the variation in fluid phase temperature inside the flow to be appropriately minimum such that T^4 may be taken as a linearly continuous function of the temperatures and expanded in a Taylor series around T_m and removing highest order terms, we get $T^4=4T_m^3\,T-3T_m^4$.

The boundary conditions are

$$\begin{aligned} u=0,\ T=T_a,\ \phi=\phi_a\ \text{at}\ r=a,\\ u=b\Omega,\ T=T_b,\ \phi=\phi_b\ \text{at}\ r=b. \end{aligned} \tag{6.7}$$

Introducing the following non-dimensional variables

$$\lambda=\frac{r^2}{b^2},\ f(\lambda)=\frac{ub\sqrt{\lambda}}{\Omega},\theta=\frac{T-T_a}{T_b-T_a},\ S=\frac{\phi-\phi_a}{\phi_b-\phi_a},\ P=\frac{p}{\mu\,\Omega} \tag{6.8}$$

in Eqs. (6.1) to (6.5), to get the following non-linear system of differential equations

$$4\,f''\lambda+\sqrt{\lambda}\frac{Gr}{Re}\left(\theta-NrS\right)-Ha^2\ f-A=0 \tag{6.9}$$

$$\left(1+\frac{4}{3}Rd\right)\left(\lambda^3\theta''+\lambda^2\theta'\right)+Br\ \left[\lambda^2(f')^2-2\,\lambda\,f\,f'+(f)^2\right]+\frac{1}{4}J\lambda^2 f^2$$
$$+Pr\,Nb\,\lambda^3\,\theta'\,S'+Pr\,Nt\,\lambda^3\,(\theta')^2=0 \tag{6.10}$$

	Optimal of h_1		Optimal of h_2		Optimal of h_3	
Order	h_1	Min. of E_m	h_2	Min. of E_m	h_3	Min. of E_m
12	-0.37	5.81×10^{-5}	-0.53	5.78×10^{-4}	-1.2	9.75×10^{-4}
14	-0.39	1.05×10^{-4}	-0.54	6.52×10^{-4}	-1.2	1.49×10^{-3}
16	-0.39	1.62×10^{-4}	-0.53	7.73×10^{-4}	-1.19	2.24×10^{-4}

Table 6.1: "At different order of approximations, the optimal values of h_1, h_2, and h_3".

$$\lambda S'' + S' + \frac{Nt}{Nb}(\lambda \theta'' + \theta') = 0 \tag{6.11}$$

where $Rd = \dfrac{4\sigma^*}{\chi}\dfrac{T_m^3}{K_f}$ is the radiation parameter and $J = \dfrac{\sigma B_0^2 b^2 \Omega^2}{(T_b - T_a)k_f}$ is the Joule heating parameter. The remaining parameters are defined in chapter-5.

The corresponding boundary conditions in dimensionless form become

$$\begin{aligned} S = 0,\ \theta = 0,\ f = 0 \ \text{ at } \lambda = \lambda_0 \\ S = 1,\ \theta = 1,\ f = b \ \text{ at } \quad \lambda = 1 \end{aligned} \tag{6.12}$$

6.3 Solution of the problem

The governing Eqs. (6.9) - (6.11) along with the boundary conditions (6.12) are solved by using HAM [47, 48, 49, 50]. The method is explained in detail in Chapter-5.

As explained in chapter-5, the h-curves are plotted for 16^{th} order approximations and are presented in figure (6.1). It is found that the admissible ranges for h_1, h_2 and h_3 are $-0.5 < h_1 < -0.25$, $-0.6 < h_2 < 0.25$ and $-1.7 < h_3 < -0.2$, respectively. In order to obtain the optimal value of the auxiliary parameter, the average residual errors (given by (5.36)) are calculated and represented in the table (6.1). From these average residual errors, it is noticed that the optimal value of auxiliary parameters are $h_1 = -0.39$, $h_2 = -0.53$ and $h_3 = -1.12$. Further the series solutions for different values of m are computed and represented in table (6.2). From table (6.2), it is found that the series solution converge in the whole region of η.

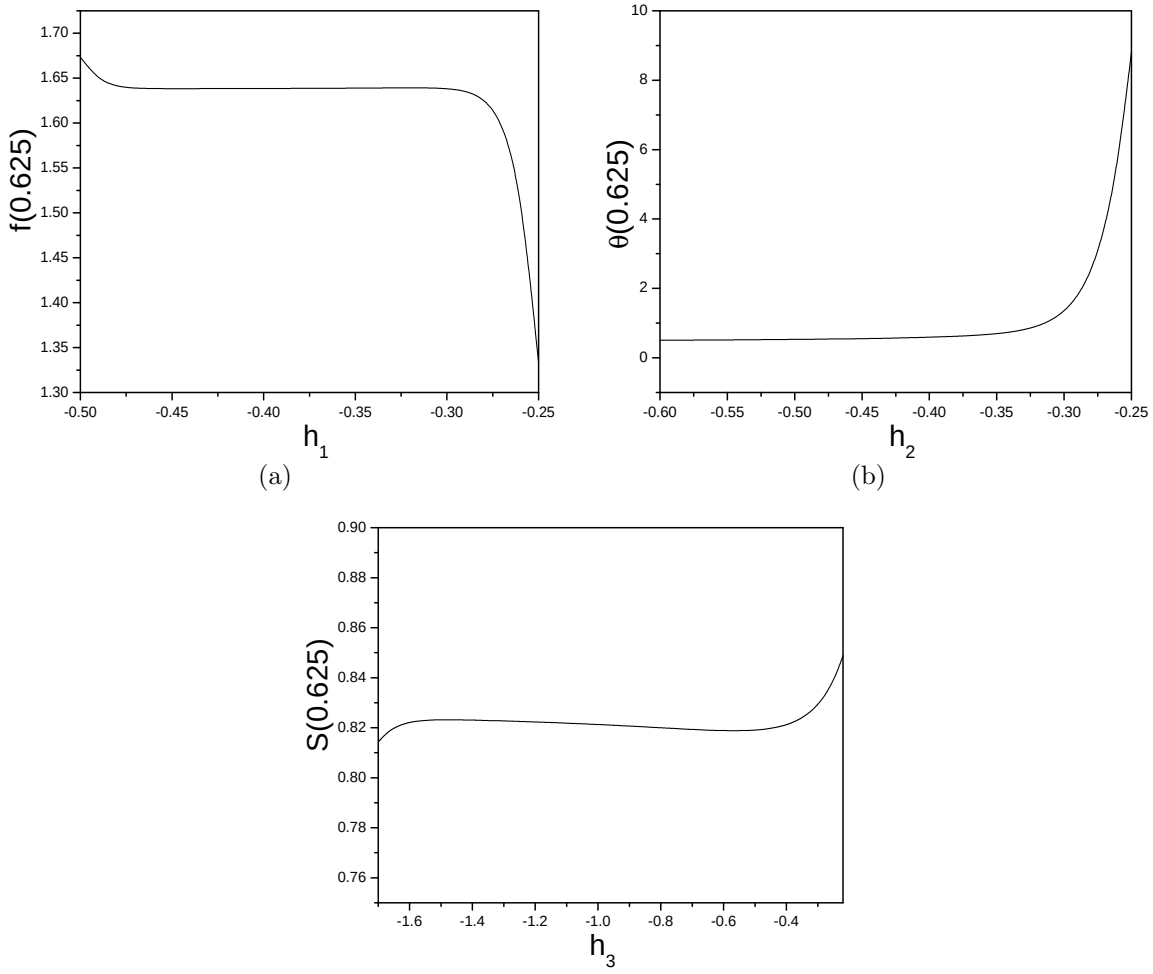

(a) (b)

(c)

Figure 6.1: "h-curves of (a) $f(\lambda)$, (b) $\theta(\lambda)$ and (c) $S(\lambda)$, when $Nr = 1.0, Nt = 0.5, Nb = 1.0, Gr = 10.0, A = 1.0, Re = 5.0, Pr = 1.0, Rd = 1.0, J = 2.0, Ha = 2.0$ and $Br = 0.5$".

Order	f(0.625)	$\theta(0.625)$	S(0.625)
05	0.4376535201	0.6737468076	0.6581184839
10	0.4406095166	0.6916338076	0.6219805748
15	0.4413595133	0.7055058072	0.6127974698
20	0.4420191206	0.7061768072	0.6020224807
25	0.4420194520	0.7172401678	0.6020226948
30	0.4420194612	0.7172472210	0.6020226464
35	0.4420194612	0.7172472807	0.6020226464
40	0.4420194612	0.7172472807	0.6020226464
45	0.4420194612	0.7172472807	0.6020226464
50	0.4420194612	0.7172472807	0.6020226464
55	0.4420194612	0.7172472807	0.6020226464

Table 6.2: "At different order of approximations, the convergence of HAM solutions".

Entropy Generation

For the present study, the volumetric rate of entropy generation reduces to

$$\left.\begin{aligned} S_G = \frac{K_f}{T_a^2}\left(\frac{\partial T}{\partial r}\right)^2 + \frac{\mu}{T_a}\left[\left(\frac{\partial u}{\partial r}\right)^2 - \frac{2\mu}{r}\frac{\partial u}{\partial r} + \left(\frac{u}{r}\right)^2\right] + \frac{\sigma\, B_0^2\, u^2}{T_a} \\ + \frac{Ru\, D}{\phi_a}\left(\frac{\partial \phi}{\partial r}\right)^2 - \frac{\nabla . q_r}{T_a} + \frac{Ru\, D}{T_a}\left(\frac{\partial T}{\partial r}\right).\left(\frac{\partial \phi}{\partial r}\right) \end{aligned}\right\} \tag{6.13}$$

The entropy generation number Ns [12] is given by

$$Ns = (1 + \frac{4}{3}Rd)\,\lambda^3\,\theta'^2 + \frac{Br}{\Omega_3}\left[\lambda^2 (f')^2 - 2\,\lambda\, f\, f' + (f)^2\right] + \phi_3\,\lambda^3\, S'^2 + \phi_4\,\lambda^3 \theta' S' + \frac{J}{4\Omega_3}\,\lambda^2 f^2 \tag{6.14}$$

The dimensionless coefficients are ϕ_3 and ϕ_4, called irreversibility distribution ratios which are related to diffusive irreversibility, given by

$$\phi_3 = \frac{Ru\, D}{K_f . \Omega_3}\left(\frac{\Omega_4}{\Omega_3}\right)\Delta\phi \qquad \phi_4 = \frac{Ru\, D}{K_f . \Omega_3} . \Delta\phi \tag{6.15}$$

where $\Omega_3 = \frac{\Delta T}{T_a}$ and $\Omega_4 = \frac{\Delta \phi}{\phi_a}$ are the concentration and temperature ratios, respectively. The Eq.(6.14) can be formulate as

$$Ns = Nh + Nv \tag{6.16}$$

The Bejan number for this problem can be expressed as

$$Be = \frac{Nh}{Nh + Nv} \tag{6.17}$$

Results and Discussion

The effects of radiation, Joule heating, magnetic parameters and Brinkman number on the velocity component $f(\lambda)$, temperature $\theta(\lambda)$, nanoparticle concentration $S(\lambda)$, entropy generation Ns and Bejan number Be are presented graphically in figures (6.2) - (6.6) by taking $Nr = 1$, $Nb = 0.5$, $Gr = 10$, $Re = 2$, $Pr = 1$, $A = 1$, $\Omega_3 = 0.1$ and $\Omega_4 = 1$.

Figure (6.2) displays the effect of the thermal-radiation Rd on the velocity in flow direction, temperature, nanoparticle concentration, entropy generation Ns and Bejan number Be. Figure 6.2(a) reveals that the velocity decays with an enhancement in Rd. The effect of Rd on the non-dimensional temperature $\theta(\lambda)$ is represented in figure 6.2(b). From this figure, it is noticed that $\theta(\lambda)$ decays with an increase in the radiation parameter Rd. The influence of the radiation parameter Rd is to get the temperature to decay extremely in the flow field. From the flow region, the heat energy is released because of a rise in the radiation Rd and therefore, the fluid temperature decreases. Figure 6.2(c) depicts the variation of nanoparticle concentration with the radiation parameter Rd. The nanoparticle concentration $S(\lambda)$ increases with a rise in the radiation parameter Rd. Figure 6.2(d) shows that entropy generation increases with an enhancement in Rd. It is clear from figure 6.2(e) that Be (Bejan number) increases near the inner cylinder of the channel, while away from the inner cylinder the trend is reversed due to more contribution of the heat transfer irreversibility on Ns and Be decreasing near the outer cylinder with enhancement in the radiation parameter Rd.

From the result, it is observed that the fluid friction dominates near the inner cylinder and heat transfer irreversibility dominates around the center of an annulus.

The variations of velocity in flow direction, temperature, nanoparticle concentration, Ns and Be with the magnetic parameter Ha is presented in figure (6.3). It is noticed from figure 6.3(a) that the dimensionless velocity in flow direction decreases with an enhancement in magnetic parameter Ha. Figure 6.3(b) reveals that, the dimensionless temperature $\theta(\lambda)$ increases with a rise in magnetic parameter Ha. There is a rise in the nanoparticle concentration $S(\lambda)$ with a rise in magnetic parameter Ha as depicted in figure 6.3(c). Figure 6.3(d) shows that entropy generation is enhanced with a growth in the magnetic parameter Ha. It is clear from figure 6.3(e) that Be decreases near the inner cylinder while away from the inner cylinder, the trend is reversed due to more contribution of the heat transfer irreversibility on entropy generation and Be increases near the outer cylinder with an enhancement in the value of Ha. It observed that the fluid friction dominated at the inner cylinder, and heat transfer irreversibility dominates around the center of an annulus.

The influence of Joule heating parameter on $f(\lambda)$, $\theta(\lambda)$, $S(\lambda)$, Ns and Be is shown in figure (6.4). The dimensionless velocity $f(\lambda)$ rises with a rise in the Joule heating pameter J as shown in figure 6.4(a). Figure 6.4(b) reveals that $\theta(\lambda)$ rises with a rise in the Joule heating parameter J. From figure 6.4(c), it is noticed that the nanoparticle concentration $S(\lambda)$ decays with a growth in the Joule heating pameter J. Figure 6.4(d) shows that the increase in Joule heating parameter J causes an increase in the entropy generation. With an increase in the Joule heating parameter J, the Bejan number is observed to decrease near the inner cylinder, while away from the inner cylinder, the trend is reversed due to more contribution of heat transfer irreversibility on entropy generation and Be increasing near the outer cylinder as presented in figure 6.4(e). It observe that the fluid friction dominates near the inner cylinder and heat transfer irreversibility dominates around the center of an annulus.

The impact of Brinkman number Br on $f(\lambda)$, $\theta(\lambda)$, $S(\lambda)$, Ns and Be is depicted in figure (6.5). The dimensionless velocity $f(\lambda)$ rises with a rise in Brinkman number Br as shown in

figure 6.5(a). Figure 6.5(b) reveals that $\theta(\lambda)$ increases with an increase in Br. From figure 6.5(c), it is noticed that nanoparticle concentration $S(\lambda)$ decays with a growth in Brinkman number Br. Figure 6.5(d) shows that an increase in Br causes an increase in the entropy generation. With an increase in Br, the Bejan number is decreasing as presented in figure 6.5(e) and it is observed that the fluid friction dominated near the inner cylinder and heat transfer irreversibility dominated around the center of an annulus.

Figure (6.6) shows the effect of the thermophoresis parameter Nt on velocity in flow direction $f(\lambda)$, temperature $\theta(\lambda)$, nanoparticle concentration $S(\lambda)$, Bejan number Be and entropy generation Ns. The velocity $f(\lambda)$ increases with an enhancement in the thermophoresis parameter Nt as shown in figure 6.6(a). Figure 6.6(b) reveals that the temperature $\theta(\lambda)$ increases with an improvement in the thermophoresis parameter Nt. An increase in the thermophoresis parameter Nt leads to increase in effective-conductivity, hence the nanoparticle concentration $S(\lambda)$ decreases as recognized from figure 6.6(c). It is seen from figure 6.6(d) that the entropy generation is increasing with an enhancement in the thermophoresis parameter Nt. It is noticed from figure 6.6(d) that Be decreases as an enhancement in the thermophoresis parameter Nt. It is observed that the fluid friction dominated near the inner cylinder and heat transfer irreversibility dominated around the center of an annulus.

6.4 Conclusions

In this chapter, the entropy generation due to nanofluid in mixed convective flow between two concentric cylinders has been analyzed by considering magnetic, Joule heating, thermophoresis, radiation parameters and Brinkman number effects. The main observations are summarized below

The dimensionless velocity and temperature decrease, whereas the nanoparticle concentration and entropy generation increase with an increase in thermal-radiation Rd. As magnetic parameter increases, the dimensionless temperature, nanoparticle concentration and entropy generation increase, but the velocity decreases. As Joule heating parameter in-

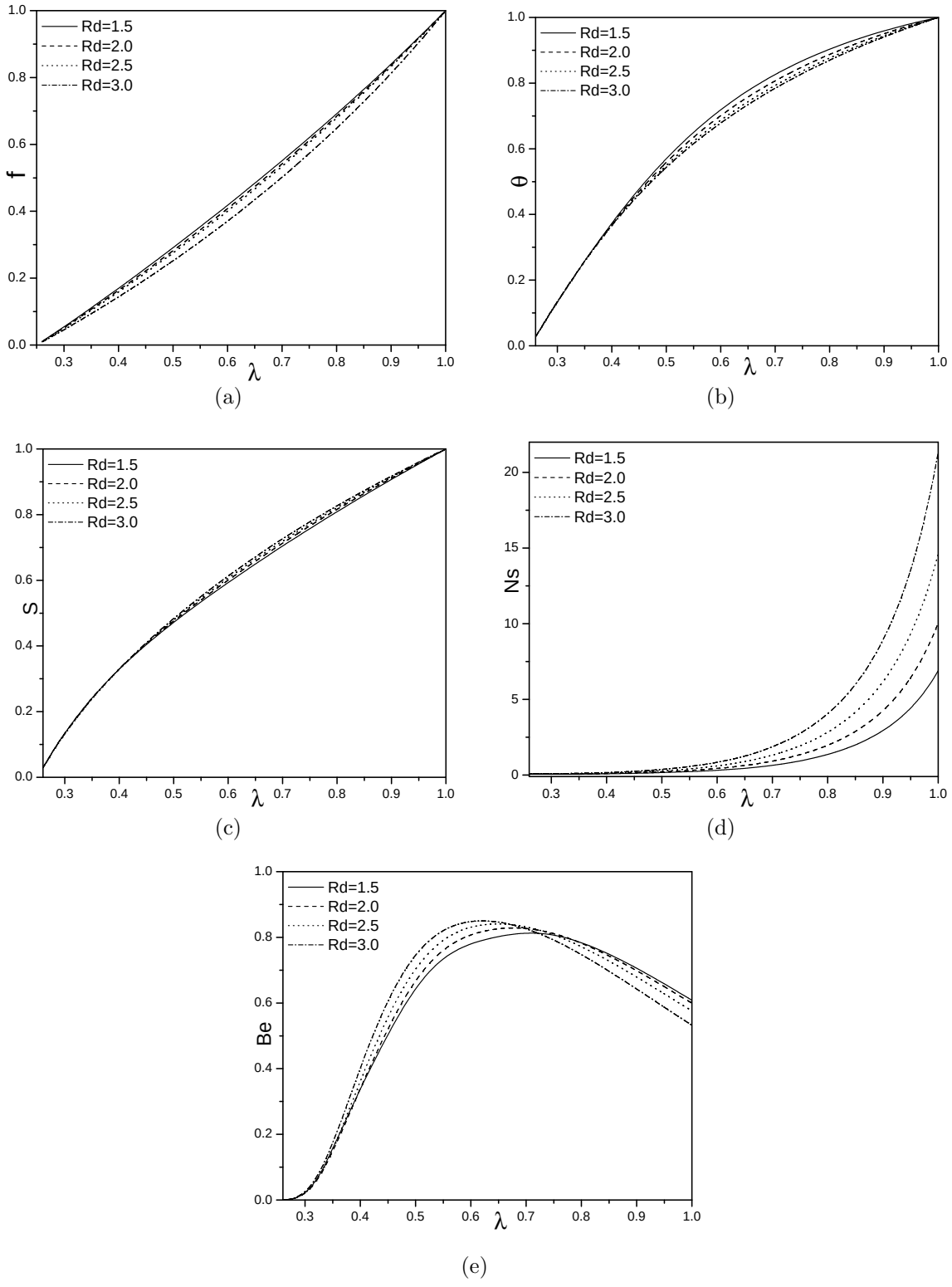

Figure 6.2: "Effect of radiation parameter Rd on (a) $f(\lambda)$, (b) $\theta(\lambda)$, (c) $S(\lambda)$, (d) Ns and (e) Be".

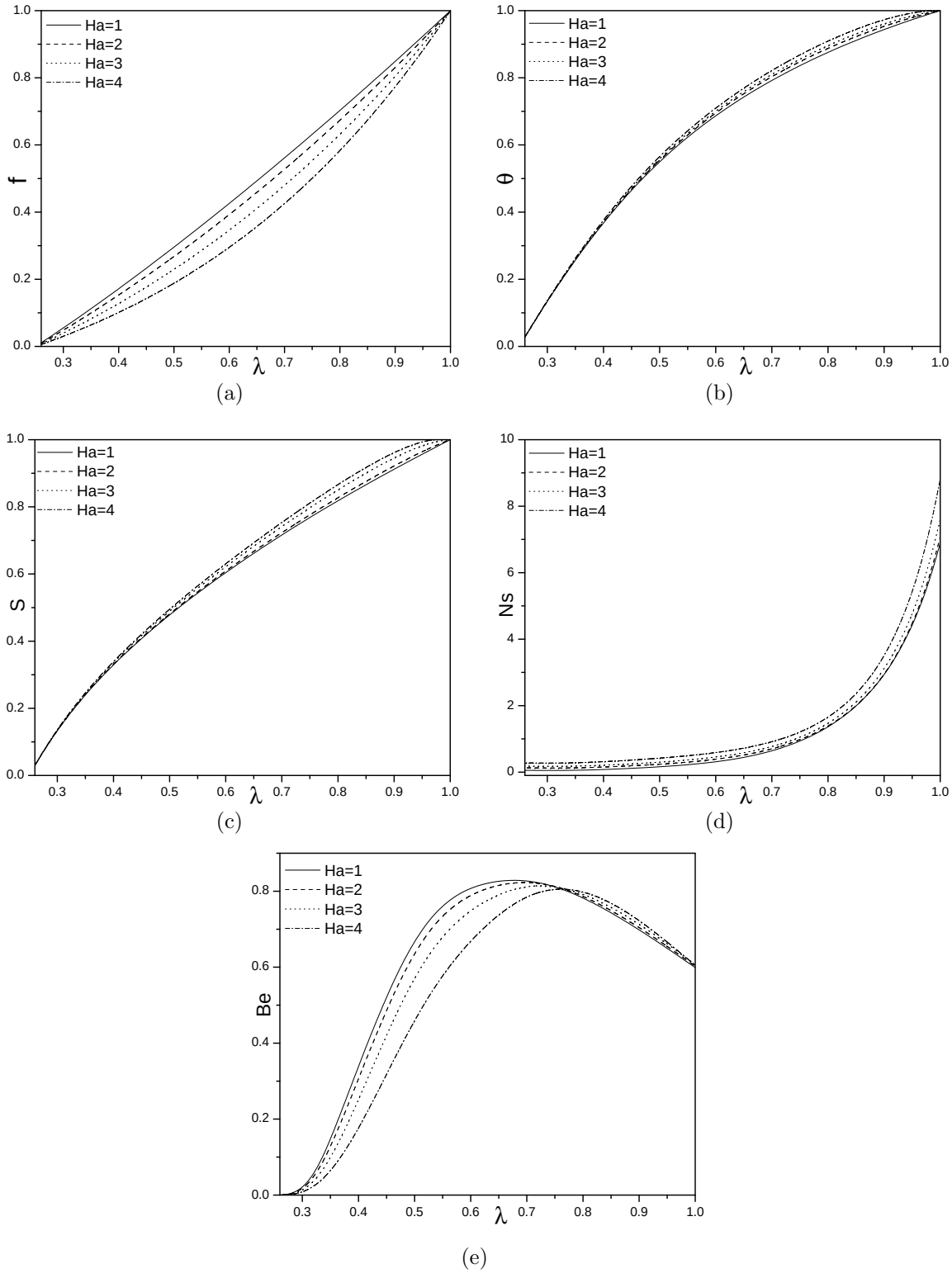

Figure 6.3: "Effect of magnetic parameter Ha on (a) $f(\lambda)$, (b) $\theta(\lambda)$, (c) $S(\lambda)$, (d) Ns and (e) Be".

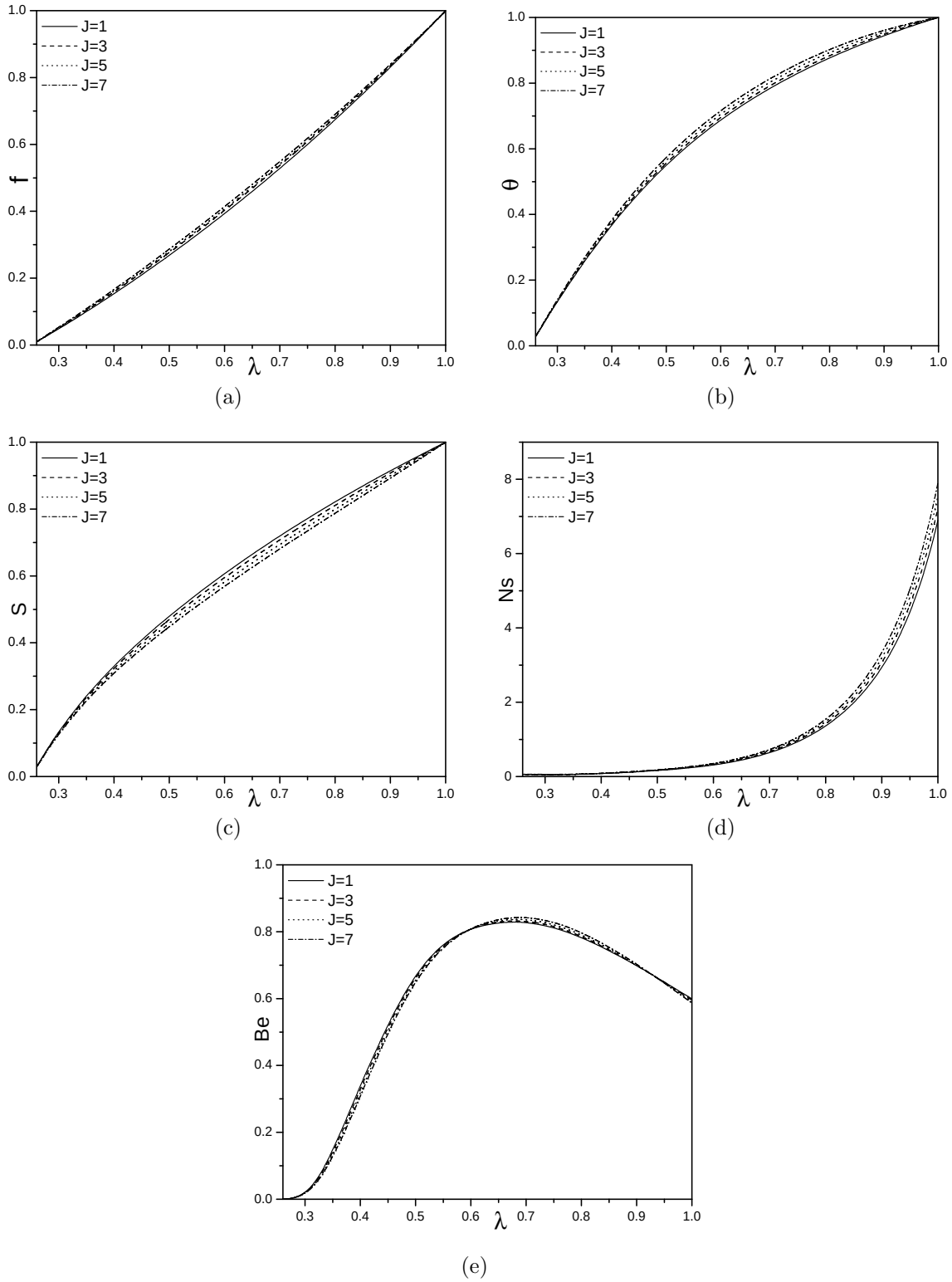

Figure 6.4: "Effect of Joule heating parameter J on (a) $f(\lambda)$, (b) $\theta(\lambda)$, (c) $S(\lambda)$, (d) Ns and (e) Be".

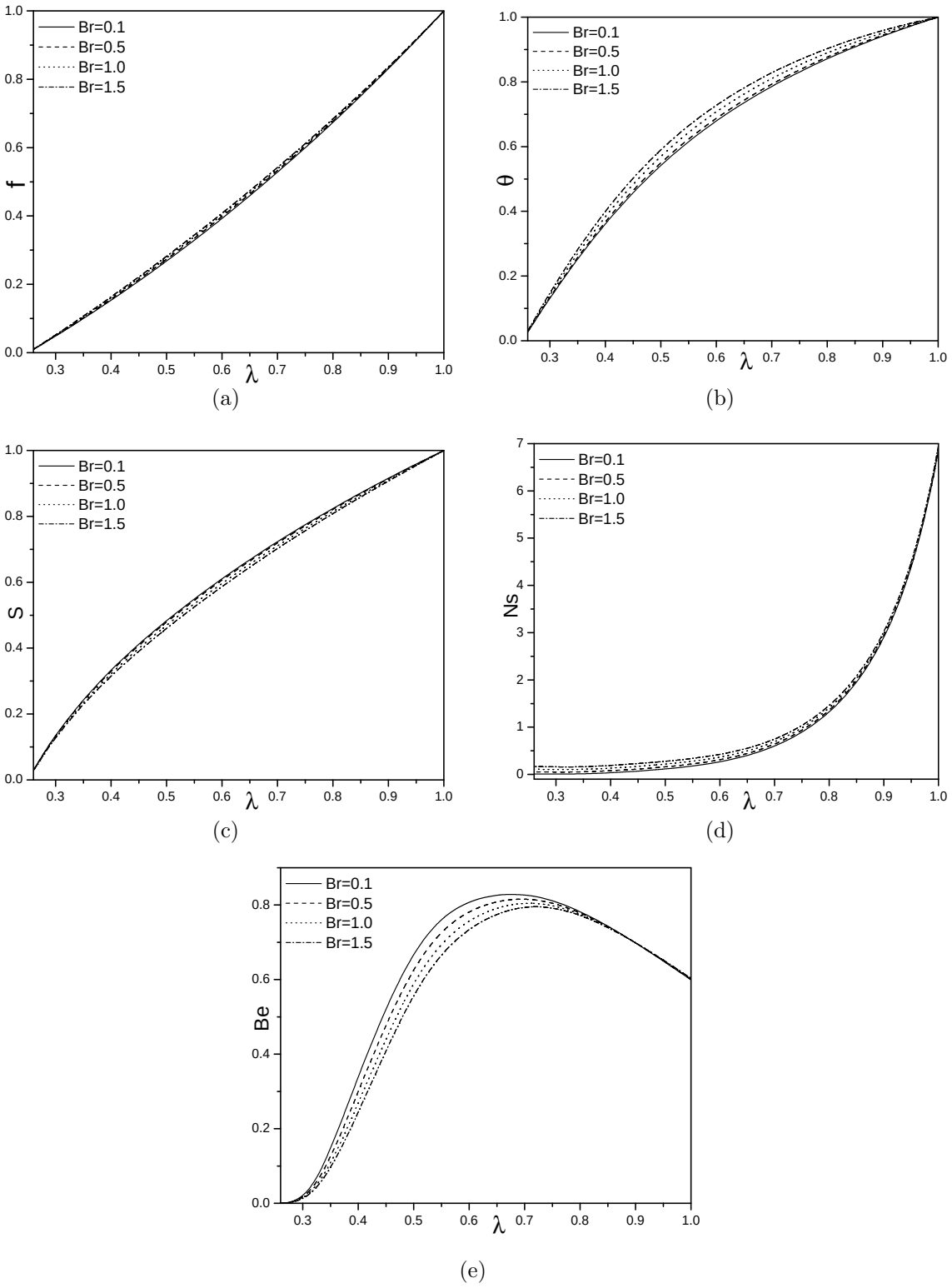

Figure 6.5: "Effect of Brinkman number Br on (a) $f(\lambda)$, (b) $\theta(\lambda)$, (c) $S(\lambda)$, (d) Ns and (e) Be".

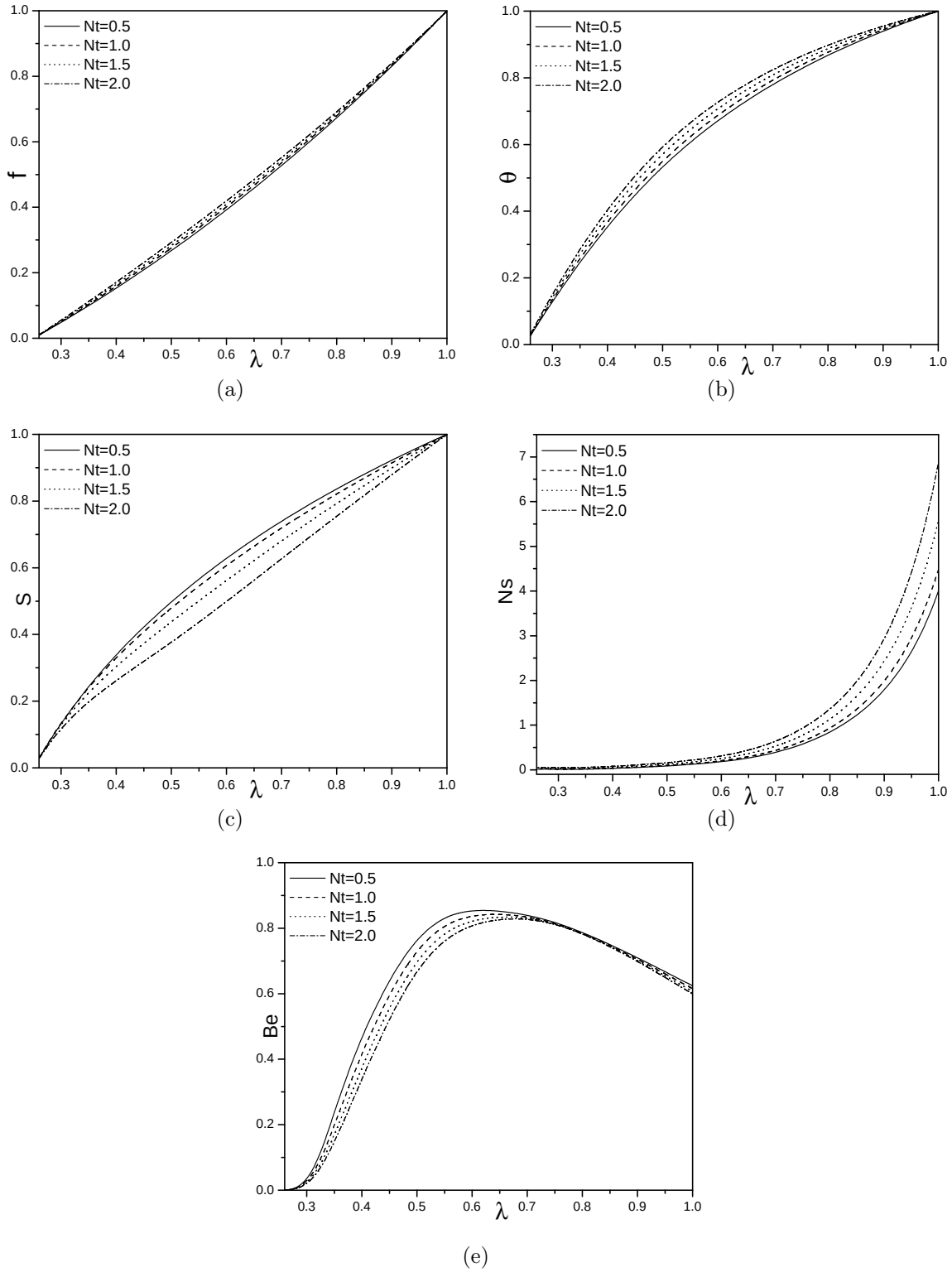

Figure 6.6: " Effect of thermophoresis parameter Nt on (a) $f(\lambda)$, (b) $\theta(\lambda)$, (c) $S(\lambda)$, (d) Ns and (e) Be".

creases, the dimensionless temperature, velocity and entropy generation increase, but the nanoparticle concentration decreases. As Brinkman number increases, the velocity, temperature and entropy generation increase, but the nanoparticle concentration and Bejan number decrease. As the thermophoresis parameter increases, the velocity, temperature and entropy generation increase, but the nanoparticle concentration and Bejan number are decrease. The maximum values of Bejan number are observed at the center of an annulus due to more contribution of heat transfer irreversibility on entropy generation and minimum value is near the inner cylinder, due to more contribution of fluid friction irreversibility on entropy generation by increasing Rd, Ha, Br, J and Nt.

Chapter 7

Joule heating effect on entropy generation due to MHD mixed convective flow of a chemically reacting nanofluid between two concentric cylinders [1]

7.1 Introduction

The influence of Joule heating on heat transfer and fluid flow, under various conditions, plays a notable effect in an engineering and industrial applications. Motsa *et al* [59] focused on the effects of viscous dissipation and Joule heating on a nanofluid flow through a shrinking/stretching sheet considering homogeneous heterogeneous reactions. On the otherhand, entropy generation is directly proportion to the thermodynamic irreversibility in a system. Bejan [9, 10] examined the different aspects behind the entropy generation in applied thermal engineering. Assad and Oztop [6] presented the influence of internal heat generation

[1] Published in "**International Journal of Heat and Technology, Vol. 35, No. 3(2017), 487–497**"

on entropy generation between two rotating cylinders. Mazgar *et al* [57] investigated the interaction between thermal radiation and mixed convection on the entropy generation in a semi-transparent and non-gray gas, bounded by two vertical coaxial cylinders. Specifically, the investigations focused on the effect of different parameters on the components of velocity, temperature, nanoparticle concentration, entropy generation and Bejan number.

In this chapter, the mixed convective flow of an incompressible chemically reacting nanofluid in an annulus between two concentric cylinders is investigated by considering the Joule heating effect.

7.2 Mathematical Formulation

Consider the steady, laminar, incompressible nanofluid flow in an annular space between two infinitely long concentric cylinders as shown in figure (5.1). It is assumed that

- The outer cylinder is rotates with a constant angular velocity Ω, whereas the inner cylinder is at rest. The flow is induced due to the rotation of the exterior cylinder.
- The velocity component along ψ direction, temperature and nanoparticle concentration are denoted by u, T and ϕ , respectively.
- The radii of the inner and outer cylinders are a and b $(a < b)$ and kept at temperatures T_a and T_b respectively.
- A strong magnetic field B_0 is taken in an axial direction. The conductivity of fluid is chosen to be small so that the magnetic Reynolds number is smaller than one unit and hence the induced magnetic field is removable compared to the applied radial field.
- Thermophysical characteristics of the nanofluid are taken as constant except density in the buoyancy term of the balance of momentum equation.

The equations which govern the present flow [13] with Boussinesq approximation are

$$\frac{\partial u}{\partial \psi} = 0 \tag{7.1}$$

$$\frac{\partial p}{\partial r} = \frac{u}{r^2} \tag{7.2}$$

$$\mu \nabla_1^2 \, u + (1-\phi)\rho_f g^* \beta_T (T - T_a) - (\rho_s - \rho_f)\, g^* (\phi - \phi_a) - \sigma \, B_0^2 \, u - \frac{1}{r} \frac{\partial p}{\partial \psi} = 0 \tag{7.3}$$

$$\begin{aligned} \alpha \left[\frac{\partial^2 T}{\partial r^2} + \frac{1}{r} \frac{\partial T}{\partial r} \right] + \frac{\mu}{\rho C_p} \left[\left(\frac{\partial u}{\partial r} \right)^2 - 2 \frac{u}{r} \frac{\partial u}{\partial r} + \left(\frac{u}{r} \right)^2 \right] + \frac{1}{\rho C_p} \sigma \, B_0^2 \, u^2 \\ + \tau \left[D_B \frac{\partial T}{\partial r} \frac{\partial \phi}{\partial r} + \frac{D_T}{T_m} \left(\frac{\partial T}{\partial r} \right)^2 \right] = 0 \end{aligned} \tag{7.4}$$

$$D_B \left[\frac{\partial^2 \phi}{\partial r^2} + \frac{1}{r} \frac{\partial \phi}{\partial r} \right] + \frac{D_T}{T_m} \left[\frac{\partial^2 T}{\partial r^2} + \frac{1}{r} \frac{\partial T}{\partial r} \right] - k_1 (\phi - \phi_a) = 0 \tag{7.5}$$

$$\begin{aligned} u = 0, \;\; T = T_a, \;\; \phi = \phi_a \;\; \text{at} \;\; r = a, \\ u = b\Omega, \;\; T = T_b, \;\; \phi = \phi_b \;\; \text{at} \;\; r = b \end{aligned} \tag{7.6}$$

Introducing the following non-dimensional variables

$$\lambda = \frac{r^2}{b^2}, \; f(\lambda) = \frac{ub\sqrt{\lambda}}{\Omega}, \theta = \frac{T - T_a}{T_b - T_a}, \; S = \frac{\phi - \phi_a}{\phi_b - \phi_a}, \; P = \frac{p}{\mu \, \Omega} \tag{7.7}$$

in Eqs. (7.1) to (7.5), to get the following non-linear system of differential equations

$$4 \, f'' \lambda + \sqrt{\lambda} \frac{Gr}{Re} \left(\theta - Nr S \right) - Ha^2 \; f - A = 0 \tag{7.8}$$

$$\lambda^3 \theta'' + \lambda^2 \theta' + Br \; \left[\lambda^2 (f')^2 - 2 \, \lambda \, f \, f' + (f)^2 \right] + \frac{1}{4} \, J \lambda^2 f^2 + Pr \, Nb \, \lambda^3 \, \theta' \, S' + Pr \, Nt \, \lambda^3 \, (\theta')^2 = 0 \tag{7.9}$$

$$\lambda \, S'' + S' + \frac{Nt}{Nb} (\lambda \, \theta'' + \theta') - \frac{K}{4} \, Le \, S = 0 \tag{7.10}$$

	Optimal of h_1		Optimal of h_2		Optimal of h_3	
Order	h_1	Min. of E_m	h_2	Min. of E_m	h_3	Min. of E_m
12	-0.41	7.82×10^{-5}	-0.58	6.24×10^{-5}	-1.11	6.46×10^{-4}
14	-0.41	5.35×10^{-4}	-0.59	8.42×10^{-6}	-1.12	1.95×10^{-5}
16	-0.40	2.42×10^{-4}	-0.58	7.99×10^{-4}	-1.12	2.45×10^{-5}

Table 7.1: "At different order of approximations, the optimal values of h_1, h_2, and h_3".

where $K = \dfrac{k_1\, b^2}{\nu}$ is the chemically reacting parameter and the other parameters are defined in the earlier chapters.

The corresponding boundary conditions (7.6) are

$$\begin{aligned} S = 0,\ \theta = 0,\ f = 0 \ \text{ at } \lambda = \lambda_0 \\ S = 1,\ \theta = 1,\ f = b \ \text{ at } \quad \lambda = 1 \end{aligned} \tag{7.11}$$

7.3 Solution of the problem

The governing Eqs. (7.8) - (7.10) along with the boundary conditions (7.11) are solved by using HAM [47, 48, 49, 50]. The method is explained in detail in chapter-5.

As explained in chapter-5, the h-curves are plotted for 16^{th} order approximation and presented in figure (7.1). It is found that the admissible ranges for h_1, h_2 and h_3 are $-0.6 < h_1 < -0.05$, $-1.5 < h_2 < 0$ and $-1.5 < h_3 < 0$, respectively. In order to obtain the optimal value of the auxiliary parameter, the average residual errors (given by (5.36)) are calculated and presented in the table (7.1). From these average residual errors, it is noticed that the optimal value of auxiliary parameters are $h_1 = -0.41$, $h_2 = -0.58$ and $h_3 = -1.12$. Further, the series solutions for different values of m are computed and represented in table (7.2). From table (7.2), it is found that the series solution converges in the whole region of λ.

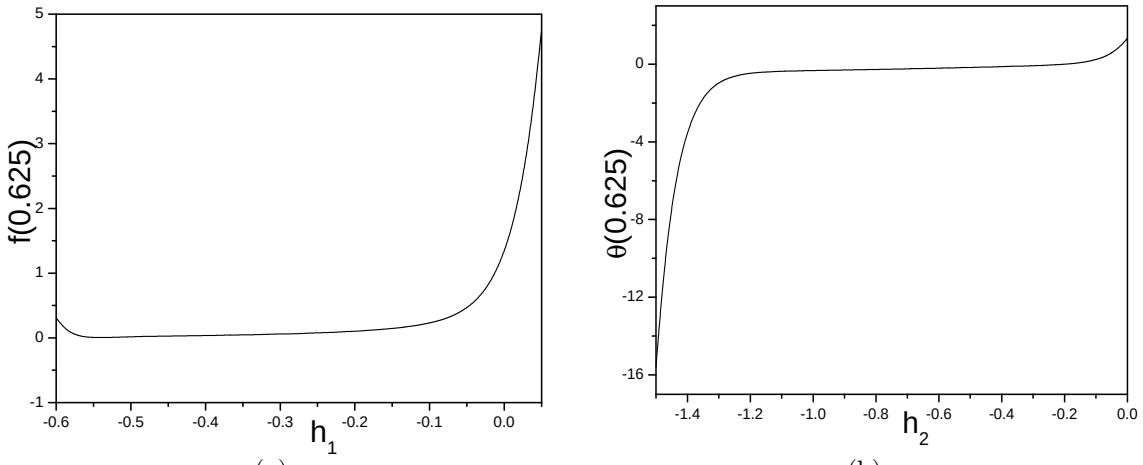

(a) (b)

(c)

Figure 7.1: "h-curves of (a) $f(\lambda)$, (b) $\theta(\lambda)$ and (c) $S(\lambda)$, when $Nr = 1.0, Nt = 0.1, Nb = 0.5, Gr = 10.0, A = 1.0, Re = 2.0, Pr = 1.0, B = 1.0, K = 1.0, J = 1.0, Ha = 2.0, Le = 1$ and $Br = 0.5$".

Order	f(0.625)	$\theta(0.625)$	S(0.625)
05	0.4290765352	0.6847374680	0.6480435436
10	0.4310609516	0.6901633807	0.6367595415
15	0.4321359513	0.7055058007	0.6340344106
20	0.4332019120	0.7016176807	0.6301234106
25	0.4342019452	0.7010724018	0.6283910546
30	0.4342019461	0.7017247220	0.6283964105
35	0.4352019461	0.7017247280	0.6283964641
40	0.4352019461	0.7017247280	0.6283964664
45	0.4352019461	0.7017247280	0.6283964664
50	0.4352019461	0.7017247280	0.6283964664
55	0.4352019461	0.7017247280	0.6283964664

Table 7.2: "At different order of approximations, the convergence of HAM solutions".

Entropy Generation

The mechanisms of entropy generation are the heat transfer, fluid friction and magnetic effect. The volumetric rate of entropy generation for incompressible nanofluid is given as

$$\left.\begin{aligned} S_G = \frac{k_f}{T_a^2}\left(\frac{\partial T}{\partial r}\right)^2 + \frac{\mu}{T_a}\left[\left(\frac{\partial u}{\partial r}\right)^2 - \frac{2\mu}{r}\frac{\partial u}{\partial r} + \left(\frac{u}{r}\right)^2\right] + \frac{\sigma\, B_0^2\, u^2}{T_a} \\ + \frac{Ru\, D}{\phi_a}\left(\frac{\partial \phi}{\partial r}\right)^2 + \frac{Ru\, D}{T_a}\left(\frac{\partial T}{\partial r}\right).\left(\frac{\partial \phi}{\partial r}\right) \end{aligned}\right\} \tag{7.12}$$

For the present study, the dimensionless entropy generation number is given by

$$Ns = \lambda^3\,\theta'^2 + \frac{Br}{\Omega_3}\left[\lambda^2 (f')^2 - 2\,\lambda\, f\, f' + (f)^2\right] + \phi_3\,\lambda^3\, S'^2 + \phi_4\,\lambda^3 \theta' S' + \frac{J}{4\Omega_3}\,\lambda^2 f^2 \tag{7.13}$$

The Eq.(7.13) can be expressed, alternatively, as follows

$$Ns = Nh + Nv \tag{7.14}$$

The dominant effect of either heat transfer irreversibility or fluid friction irreversibility can be investigated using Bejan number (Be). The Bejan number is defined as follows

$$Be = \frac{Nh}{Nh + Nv} \tag{7.15}$$

Results and Discussion

The effects of the chemical reaction, Joule heating and magnetic parameters on non-dimensional velocity $f(\lambda)$, temperature $\theta(\lambda)$, nanoparticle volume fraction $S(\lambda)$, Bejan number Be and entropy generation Ns are presented graphically in figures (7.2) - (7.4). To study the effect of these parameters, calculations were carried out by taking $Nr = 1.0, Nb = 0.5, \Omega_3 = 0.1, Gr = 10, Re = 2.0, Pr = 1.0, A = 1.0$ and $Le = 1.0$.

The variation of velocity in flow direction, temperature, nanoparticle concentration, Ns and Be with magnetic parameter Ha is presented in figure (7.2). It is identified from figure 7.2(a) that the dimensionless velocity in flow direction decreases with an enhancement in magnetic parameter Ha . Figure 7.2(b) reveals that $\theta(\lambda)$ is rising with a rise in magnetic parameter Ha. There is a rise in the nanoparticle concentration $S(\lambda)$ with a rise in magnetic parameter Ha as depicted in figure 7.2(c). Figure 7.2(d) shows that the entropy generation decays with a growth in magnetic parameter Ha. It is clear from figure 7.2(e) that Be increases with an enhancement in the value of Ha. The maximal values of Be are observed at the center of an annulus region due to more contribution of heat transfer irreversibility on entropy generation and it is observed that the fluid friction dominates near the cylinders.

The influence of Joule heating pameter on $f(\lambda)$, $\theta(\lambda)$, $S(\lambda)$, Ns and Be is shown in figure (7.3). The dimensionless velocity $f(\lambda)$ rises with a rise in the Joule heating parameter J as shown in figure 7.3(a). Figure 7.3(b) reveals that $\theta(\lambda)$ increase with an increase in the Joule heating pameter J. From figure 7.3(c) it is noticed that nanoparticle concentration $S(\lambda)$ decays with a growth in the Joule heating parameter J. Figure 7.3(d) shows that an increase in the Joule heating parameter J causes an increase in entropy generation. With an increase in the Joule heating parameter J the Bejan number is observed to be increasing near the inner cylinder, while away from the inner cylinder the trend is reversed due to more contribution of heat transfer irreversibility on Ns as presented in figure 7.3(e). It observed that the fluid friction dominates near the end points of the cylinder and heat transfer irreversibility dominates around the center of an annulus.

Figure (7.4) displays the impact of chemical reaction parameter K on velocity in flow direction, temperature, nanoparticle concentration, entropy generation and Bejan number. Figure 7.4(a) reveals that the velocity is increasing as the chemical reaction parameter increases. The effect of K

on the non-dimensional temperature $\theta(\lambda)$ is represented in figure 7.4(b). From this figure, it is observed that $\theta(\lambda)$ decays with an enhancement in the chemical reaction parameter K. The influence of K is to reduce the temperature extremely in the flow field. From the flow region the heat energy is released because of a rise in the chemical reaction K, therefore the fluid temperature decreases. Figure 7.4(c) depicts the variation of nanoparticle concentration with K. The nanoparticle concentration $S(\lambda)$ decreases with an increase in the chemical reaction K. Figure 7.4(d) shows that the entropy generation decays with an enhancement in K. It is clear from figure 7.4(e) that Be increases with an enhancement in the value of K. The maximal value of Bejan number is noticed at the center of an annular region due to more contribution of heat transfer irreversibility on Ns and it is noticed that the fluid friction dominated near the cylinders.

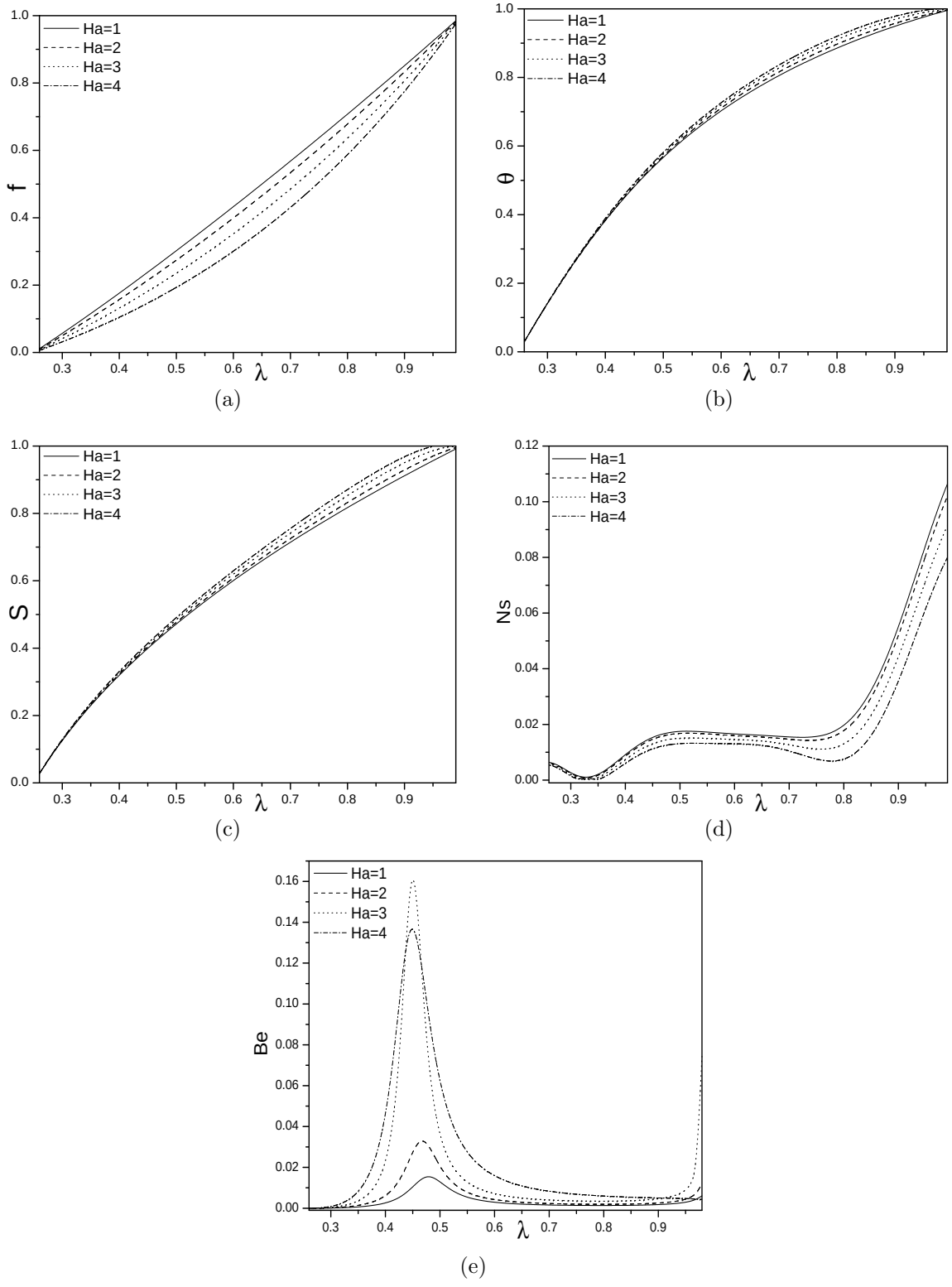

Figure 7.2: " Effect of the magnetic parameter Ha on (a) $f(\lambda)$, (b) $\theta(\lambda)$, (c) $S(\lambda)$, (d) Ns and (e) Be".

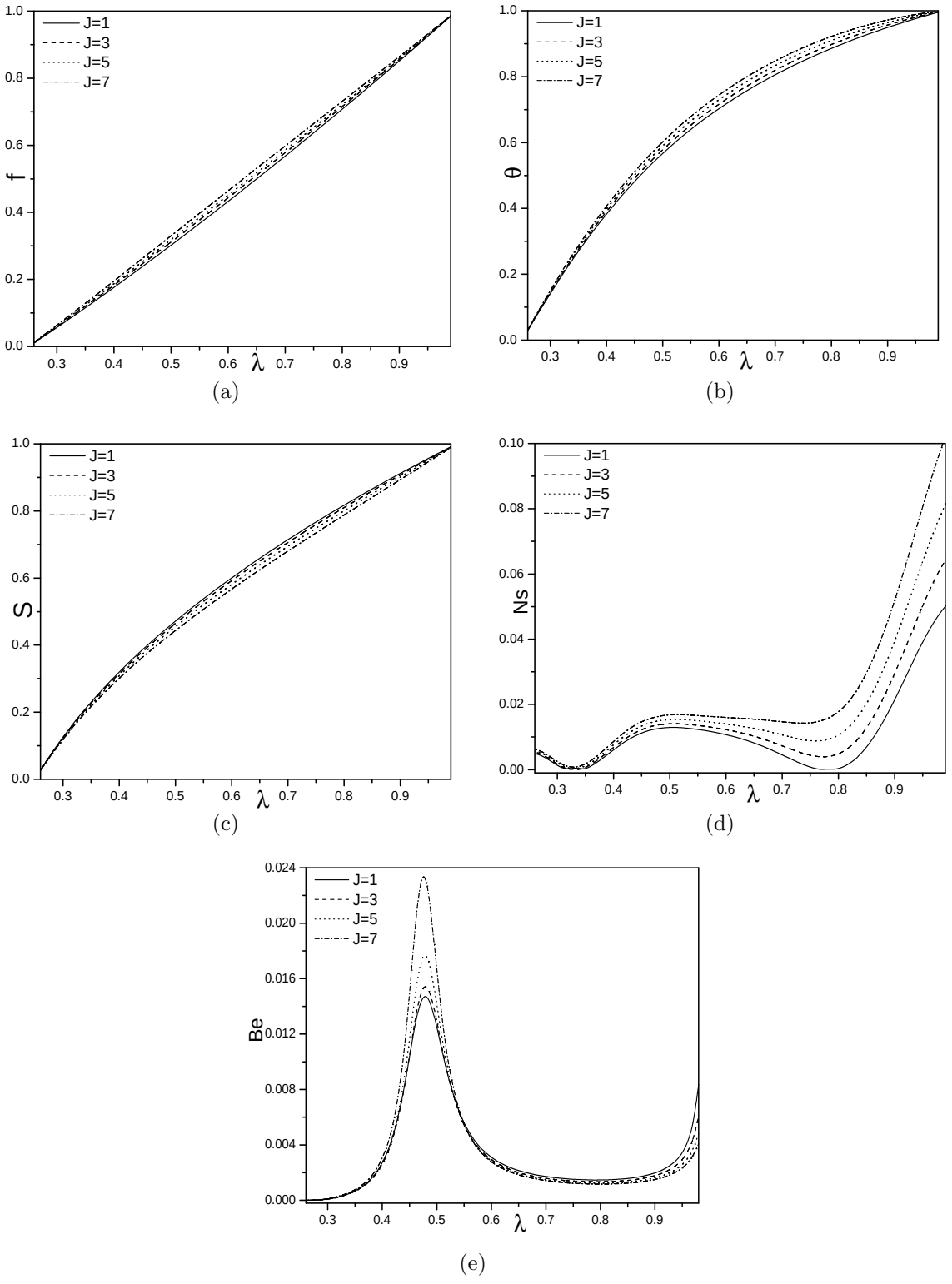

Figure 7.3: "Effect of the Joule heating parameter J on (a) $f(\lambda)$, (b) $\theta(\lambda)$, (c) $S(\lambda)$, (d) Ns and (e) Be".

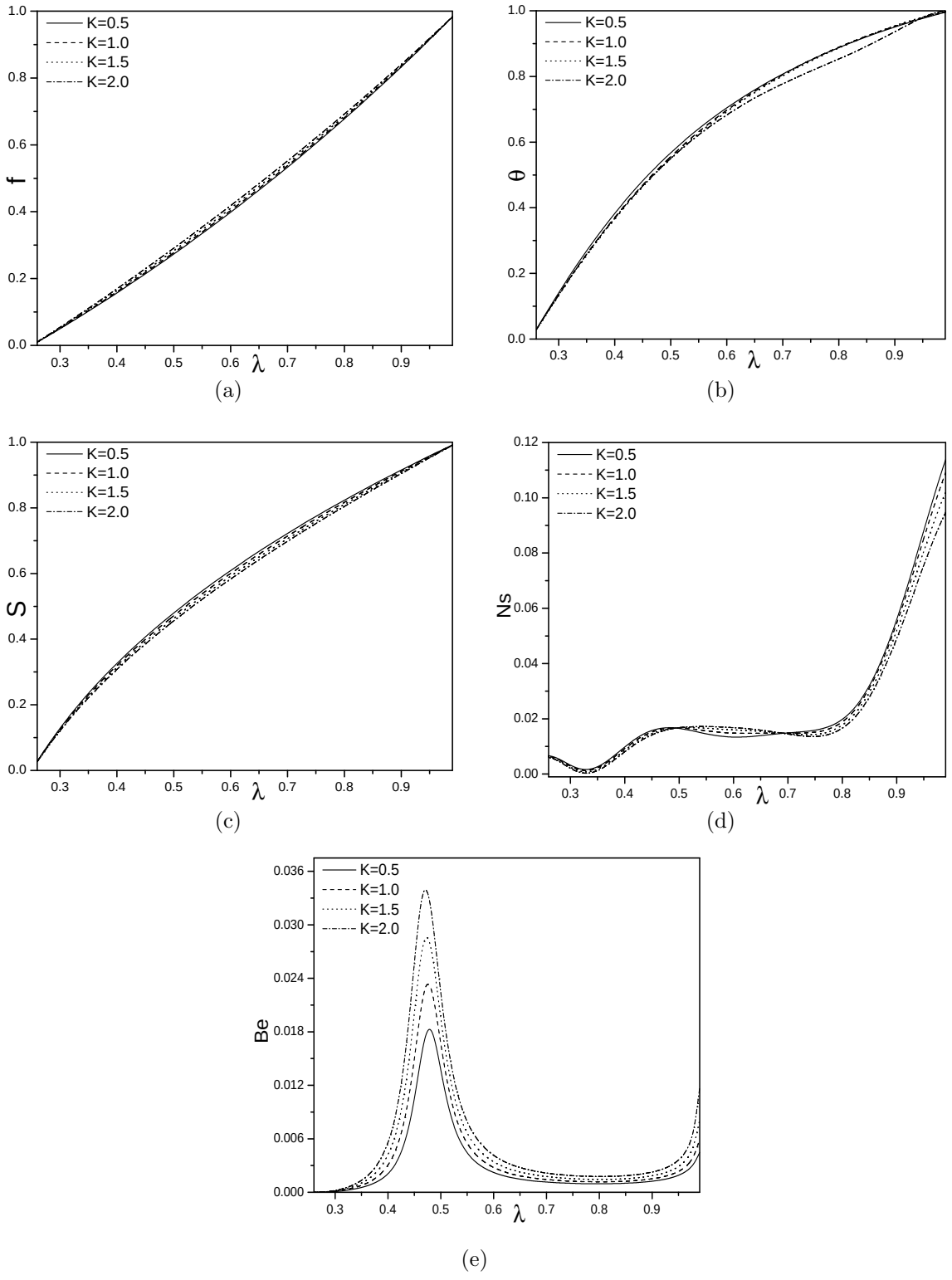

Figure 7.4: "Effect of the chemical reaction parameter K on (a) $f(\lambda)$, (b) $\theta(\lambda)$, (c) $S(\lambda)$, (d) Ns and (e) Be".

7.4 Conclusions

In this chapter, the entropy generation due to a chemically reacting nanofluid flow between two concentric cylinders has been analyzed by considering MHD and Joule heating effects. The main observations are summarized below:

As magnetic parameter increases, the velocity and entropy generation decrease, but the nanoparticle concentration, temperature and Bejan number increase. As the Joule heating parameter increases, the dimensionless temperature, velocity and entropy generation increase, but the nanoparticle concentration decreases. The dimensionless velocity and Bejan number increase, whereas the temperature, nanoparticle concentration and entropy generation are decrease with a rise in chemical reaction K.

The maximum values of Bejan number Be are observed at the center of an annulus due to more contribution of heat transfer irreversibility on entropy generation and minimum value is near the cylinders, due to more contribution of fluid friction irreversibility on entropy generation by increasing the values of K, Ha and J.

Part IV

ENTROPY GENERATION DUE TO MIXED CONVECTIVE FLOW OF A NANOFLUID BETWEEN PARALLEL DISKS

Chapter 8

Entropy generation in MHD mixed convective flow of a nanofluid between parallel disks with Joule heating, Hall and ion-slip effects [1]

8.1 Introduction

Heat transfer and fluid flow between rotating disks is an important topic in view of its wider applications in rotating machinery, crystal growth processes, lubrication and computer storage devices. Further, the analysis of magnetohydrodynamics (MHD) flow of a nanofluids has gained much attention due to its an engineering and industrial applications. Hatami and Ganji [43] analyzed the influence of magnetite field on the heat transfer and nanofluid flow in between two parallel disks considering the lower plate is stationary and the upper disk moves away from the lower disk or towards the lower disk, using least square method. Azimi and Riazi [7] investigated the MHD flow of grapheme oxide water nanofluids between parallel coaxial disks. In most of the investigations concerned with the MHD convective flows, the Hall current and ion-slip effects in Ohms law were neglected in order to simplify the problem. However, the impact of the Hall current and ion-slip

[1] Communicated to "**Journal of the Brazilian Society of Mechanical Sciences and Engineering**"

effects are an essential in a strong magnetic field. Srinivasacharya and Kaladhar [81] analyzed the role of Hall current and ion-slip parameters on mixed convection in a couple stress fluid between parallel disks.

Entropy generation analysis is vital for optimizing the thermal systems. Entropy generation is directly proportion to the thermodynamic irreversibility in a system. The quality of energy decreases when entropy generation takes place i.e. the entropy generation destroys the system energy. Hence, the performance of the system can be improved by decreasing the entropy generation. Therefore, a powerful and useful optimization tool for a high range of thermal applications is minimization of entropy generation. Bejan [11, 12] introduced the entropy generation optimization method and developed its applications in science and engineering field.

In this chapter, we analysed the effects of Joule heating, Hall and ion-slip parameters on entropy generation due to mixed convective flow of a nanofluid between parallel disks. The effect of Hall and ion-slip, Joule heating and magnetic parameters on the temperature, velocity, nanoparticle concentration, Bejan number and entropy generation are investigated.

8.2 Mathematical Formulation

Consider the steady, laminar and incompressible nanofluid between two horizontal coaxial parallel disks separated by a spacing d. The lower and upper disks are rotating with rotational speeds Ω_1 and Ω_2. The temperature and nanoparticle volume fraction of the lower disk are T_1 and ϕ_1 while for the upper disk, they are T_2 and ϕ_2. The cylindrical coordinate system (r, φ, z) is taken on the lower disk and the center of the disk is considered as a pole. It is assumed that the stress work effects and the gravitational force are negligibly small. Uniform magnetic filed of strength B_0 is applied normal to the disk. Consider a very small magnetic Reynolds number for which the induced magnetite field can be omitted in comparison with the applied magnetic field. Assume relatively high electron atom collision frequency, so that the Hall and ion-slip parameters cannot be omitted. The Boussinesq approximation can be easily applied because the Coriolis force $(2\rho\overline{\Omega} \times \overline{q})$ and centrifugal forces $(\rho\overline{\Omega} \times (\overline{\Omega} \times \overline{r}))$, appear in the momentum balance explicitly due to disk-rotation. Hence, the Coriolis force, centrifugal force, curvilinear flow of the fluids and the density correlated with the terms of gravitation are all treated as variables. To account for the rotational buoyancy

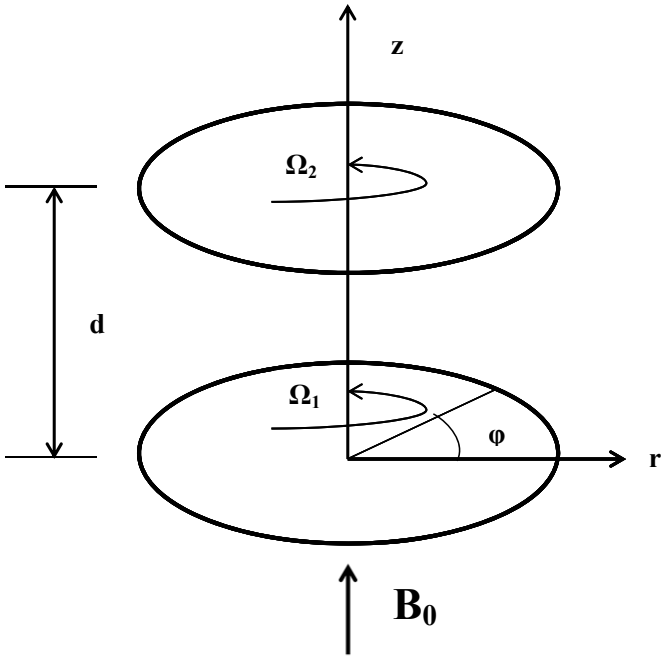

Figure 8.1: "Physical model and coordinate system".

induced by the body forces, a linear density-temperature-nanoparticle concentration relation is employed. Under the uniform axial pressure gradient and thermal buoyancy, the flow is mixed convective. Let u, v and w be the components of velocities along r, φ and z directions, T and ϕ are the temperature and nanoparticle volume fraction respectively.

Under these assumptions, equations governing the nanofluid flow in the presence of uniform transverse magnetic field are given by

$$\frac{\partial u}{\partial r} + \frac{\partial w}{\partial z} + \frac{u}{r} = 0 \tag{8.1}$$

$$\begin{aligned}
\rho_f \,(u\frac{\partial u}{\partial r} + w\frac{\partial u}{\partial z}) = \frac{v^2\rho_f}{r}(1-(1-\phi_0)\rho_f\, g^*\,\beta_T(T-T_1) - (\rho_s-\rho_f)\, g^*(\phi-\phi_1)) - \frac{\partial p^*}{\partial r} \\
-\rho_f\, r\Omega_1^2((1-\phi_0)\rho_f\, g^*\,\beta_T(T-T_1) - (\rho_s-\rho_f)\, g^*(\phi-\phi_1)) + \mu\left[\frac{\partial}{\partial r}\left(\frac{1}{r}\frac{\partial}{\partial r}(r\,u)\right) + \frac{\partial^2 u}{\partial z^2}\right] \\
-2\rho_f\, v\Omega_1(1-(1-\phi_0)\rho_f\, g^*\,\beta_T(T-T_1) - (\rho_s-\rho_f)\, g^*(\phi-\phi_1)) - \frac{\sigma\, B_0^2}{(\alpha e^2+\beta h^2)}\,(\alpha e\, u - \beta h\, v)
\end{aligned} \tag{8.2}$$

$$\begin{aligned}\rho_f\,(u\frac{\partial v}{\partial r}+w\frac{\partial v}{\partial z}) &= -\frac{uv\rho_f}{r}(1-(1-\phi_0)\rho_f\,g^*\,\beta_T(T-T_1)-(\rho_s-\rho_f)\,g^*(\phi-\phi_1))\\ &- 2\rho_f\,u\Omega_1(1-(1-\phi_0)\rho_f\,g^*\,\beta_T(T-T_1)-(\rho_s-\rho_f)\,g^*(\phi-\phi_1))\\ &+ \mu\left[\frac{\partial}{\partial r}\left(\frac{1}{r}\,\frac{\partial}{\partial r}(r\,v)\right)+\frac{\partial^2 v}{\partial z^2}\right]-\frac{\sigma\,B_0^2}{(\alpha e^2+\beta h^2)}\,(\alpha e\,v+\beta h\,u)\end{aligned} \tag{8.3}$$

$$\begin{aligned}\rho_f\,(u\frac{\partial w}{\partial r}+w\frac{\partial w}{\partial z}) &= \rho_f((1-\phi_0)\rho_f\,g^*\,\beta_T(T-T_1)-(\rho_s-\rho_f)\,g^*(\phi-\phi_1))-\frac{\partial p^*}{\partial z}\\ &+ \mu\left[\frac{1}{r}\,\frac{\partial}{\partial r}\left(r\,\frac{\partial w}{\partial z}\right)+\frac{\partial^2 w}{\partial z^2}\right]\end{aligned} \tag{8.4}$$

$$\begin{aligned}u\frac{\partial T}{\partial r}+w\frac{\partial T}{\partial z} &= \frac{2\mu}{\rho C_p}\left[\left(\frac{\partial u}{\partial r}\right)^2+\left(\frac{u}{r}\right)^2+\left(\frac{\partial w}{\partial z}\right)^2\right]+\alpha\left[\frac{\partial^2 T}{\partial z^2}+\frac{\partial^2 T}{\partial r^2}+\frac{1}{r}\,\frac{\partial T}{\partial r}\right]\\ &+ \frac{\mu}{\rho C_p}\left[\left(r\,\frac{\partial}{\partial r}\,\left(\frac{v}{r}\right)\right)^2+\left(\frac{\partial v}{\partial z}\right)^2+\left(\frac{\partial u}{\partial z}+\frac{\partial w}{\partial r}\right)^2\right]\\ &+ \frac{\sigma\,B_0^2}{\rho C_p(\alpha e^2+\beta h^2)}\,(u^2+v^2)\\ &+ \tau\left[\frac{D_T}{T_m}\left(\left(\frac{\partial T}{\partial z}\right)^2+\left(\frac{\partial T}{\partial r}\right)^2\right)+D_B\left(\frac{\partial\phi}{\partial r}\frac{\partial T}{\partial r}+\frac{\partial\phi}{\partial z}\frac{\partial T}{\partial z}\right)\right]\end{aligned} \tag{8.5}$$

$$u\frac{\partial\phi}{\partial r}+w\frac{\partial\phi}{\partial z}=\frac{D_T}{T_m}\,\left[\frac{1}{r}\,\frac{\partial T}{\partial r}+\frac{\partial^2 T}{\partial z^2}+\frac{\partial^2 T}{\partial r^2}\right]+D_B\,\left[\frac{\partial^2\phi}{\partial z^2}+\frac{1}{r}\,\frac{\partial\phi}{\partial r}+\frac{\partial^2\phi}{\partial r^2}\right] \tag{8.6}$$

where ρ_f is the density, the difference between reference pressure and local pressure is $P^*=P-P_r$.

The boundary conditions are

$$\begin{aligned}&u=0,\quad v=r\Omega_1,\quad w=0,\quad T=T_1,\quad \phi=\phi_1\quad\text{on}\quad z=0\\ &u=0,\quad v=r\Omega_2,\quad w=0,\quad T=T_2,\quad \phi=\phi_2\quad\text{on}\quad z=d\end{aligned} \tag{8.7}$$

Introducing the following non-dimensional variables

$$\eta=\frac{z}{d},\ F=\frac{u}{r\Omega_1},\ g=\frac{v}{r\Omega_1},\ f=\frac{w}{\sqrt{\nu\Omega_1}},\ \theta=\frac{T-T_1}{T_2-T_1},\ S=\frac{\phi-\phi_1}{\phi_2-\phi_1} \tag{8.8}$$

in Eqs. (8.1) to (8.6), we get

$$f^{iv} - \sqrt{Re}\left[4Re(g' - gg') + 2ff'' + ff''' - 2/\sqrt{Re}f' + 2Gr(2gg'\theta - 2g'\theta + g^2\theta' - 2g\theta' + \theta')\right]$$
$$+\sqrt{Re}Nr(2gg'S - 2g'S + g^2S' - 2gs' + s') - \frac{Ha^2\alpha e\, f''}{(\alpha e^2 + \beta h^2)} + \frac{2\sqrt{Re}Ha^2\beta h\, g'}{(\alpha e^2 + \beta h^2)} = 0 \quad (8.9)$$

$$2\sqrt{Re}g'' - 2Re(f'g + fg' + f) + Gr\left[f'g\theta + 2f'\theta - Nrf'gS - 2Nrf'S\right]$$
$$- \frac{Ha^2\beta h\, f'}{(\alpha e^2 + \beta h^2)} - \frac{2\sqrt{Re}Ha^2\alpha e\, g}{(\alpha e^2 + \beta h^2)} = 0 \quad (8.10)$$

$$\theta'' - \sqrt{Re}\, Pr\, \theta' f + PrNb\theta' S' + PrNt\, \theta'^2 + \frac{Br}{4Re}\left[10f'^2 + f''^2\right] + Br\left[2g^2 + g'^2\right]$$
$$+\frac{J}{(\alpha e^2 + \beta h^2)}\frac{(f'^2 + 4Re\, g^2)}{4Re} = 0 \quad (8.11)$$

$$S'' - \sqrt{Re}\, Le\, f\, S' + \frac{Nt}{Nb}\theta'' = 0 \quad (8.12)$$

in which the continuity equation $f' = 2\sqrt{Re}F(\eta)$ is used to solve the system to eliminate the function $F(\eta)$ of radial velocity. $Re = \dfrac{\Omega_1 d^2}{\nu}$ is Reynold's number and $J = \dfrac{\sigma B_0^2 \Omega_1^2 d^2}{(T_2 - T_1)\, k_f}$ is the Joule heating parameter.

The rate of relative rotation of the disk 2 with respect to disk 1 is denoted by the parameter $\gamma = \frac{\Omega_1 - \Omega_2}{\Omega_1}$. For example, $\gamma = 0$ and $\gamma = 1$ values corresponding to the cases of rotating disks ($\Omega_1 = \Omega_2$) and rotorstator ($\Omega_1 \neq \Omega_2$), respectively.

The corresponding conditions on boundary (8.7) are

$$\begin{aligned} &S = 0 \quad f = f' = 0, \quad g = 1, \quad \theta = 0, \quad \text{at} \quad \eta = 0 \\ &S = 1 \quad f = f' = 0, \quad g = \gamma, \quad \theta = 1, \quad \text{at} \quad \eta = 1 \end{aligned} \quad (8.13)$$

8.3 Solution of the Problem

The governing Eqs. (8.8) - (8.12) together with(8.13) are solved by using HAM. (For more details on homotopy analysis method see the works of Liao [47, 48, 49, 50]). The initial approximations of

$f(\eta)$, $g(\eta)$, $\theta(\eta)$ and $S(\eta)$ and auxiliary linear operators are chosen as

$$f_0(\eta) = 0, \quad g_0(\eta) = 1 + (\gamma - 1)\eta, \quad \theta_0(\eta) = \eta \quad \text{and} \quad S_0(\eta) = \eta \tag{8.14}$$

and

$$L_1 = \frac{\partial^4}{\partial \eta^4}, \quad L_i = \frac{\partial^2}{\partial \eta^2} \quad \text{for} \quad i = 2, 3, 4 \tag{8.15}$$

such that

$$L_1(c_1 + c_2\eta + c_3\eta^2 + c_4\eta^3) = 0,\ L_2(c_5 + c_6\eta) = 0,\ L_3(c_7 + c_8\eta) = 0 \text{ and } L_4(c_9 + c_{10}\eta) = 0 \tag{8.16}$$

where $c_i, (i = 1, 2, \cdots 10)$, are constants.

The zeroth order deformation, which is given by

$$\begin{aligned}(1-p)L_1[f(\eta;p) - f_0(\eta)] = ph_1N_1[f(\eta;p)],\ (1-p)L_2[g(\eta;p) - g_0(\eta)] = ph_2N_2[g(\eta;p)],\\ (1-p)L_3[\theta(\eta;p) - \theta_0(\eta)] = ph_3N_3[\theta(\eta;p)],\ (1-p)L_4[S(\eta;p) - S_0(\eta)] = ph_4N_4[S(\eta;p)]\end{aligned} \tag{8.17}$$

where

$$\begin{aligned}N_1[f(\eta,p), g(\eta,p), \theta(\eta,p), S(\eta,p)] = f^{iv} - \sqrt{Re}\left[4Re(g' - gg') + 2ff'' + ff''' - 2/\sqrt{Re}f'\right]\\ -2\sqrt{Re}Gr(2gg'\theta - 2g'\theta + g^2\theta' - 2g\theta' + \theta') + \sqrt{Re}Nr(2gg'S - 2g'S + g^2S' - 2gs' + s')\\ -\frac{Ha^2\alpha e\, f''}{(\alpha e^2 + \beta h^2)} + \frac{2\sqrt{Re}Ha^2\beta h\, g'}{(\alpha e^2 + \beta h^2)}\end{aligned} \tag{8.18}$$

$$\begin{aligned}N_2[f(\eta,p), g(\eta,p), \theta(\eta,p), S(\eta,p)] = 2\sqrt{Re}g'' - 2Re(fg' + f'g + f)\\ +Gr\left(f'g\theta + 2f'\theta - Nrf'gS - 2Nrf'S\right) - \frac{Ha^2\beta h\, f'}{(\alpha e^2 + \beta h^2)} - \frac{2\sqrt{Re}Ha^2\alpha e\, g}{(\alpha e^2 + \beta h^2)}\end{aligned} \tag{8.19}$$

$$\begin{aligned}N_3[f(\eta,p), g(\eta,p), \theta(\eta,p), S(\eta,p)] = \theta'' - \sqrt{Re}\, Pr\, \theta' f + PrNb\theta'S' + PrNt\, \theta'^2\\ +\frac{Br}{4Re}\left[10(f')^2 + (f'')^2\right] + Br\left[2(g)^2 + (g')^2\right] + \frac{J}{(\alpha e^2 + \beta h^2)}\frac{(f'^2 + 4Re\, g^2)}{4Re}\end{aligned} \tag{8.20}$$

$$N_4[f(\eta,p), g(\eta,p), \theta(\eta,p), S(\eta,p)] = S'' - \sqrt{Re}\, Le\, f\, S' + \frac{Nt}{Nb}\theta'' \tag{8.21}$$

where $p \in [0, 1]$ is the embedded parameter and h_i, $(i = 1, 2, 3, 4)$, are auxiliary parameters which

are not vanish. From $p = 0$ to $p = 1$, we have

$$f(\eta;0) = f_0(\eta), \quad f(\eta;1) = f(\eta), \qquad g(\eta;0) = g_0(\eta), \quad g(\eta;1) = g(\eta) \tag{8.22}$$

$$\theta(\eta;0) = \theta_0(\eta), \quad \theta(\eta;1) = \theta(\eta), \qquad S(\eta;0) = S_0(\eta), \quad S(\eta;1) = S(\eta) \tag{8.23}$$

Thus, as p varies from 0 to 1, f_0, g_0, θ_0 and S_0 approach $f(\eta)$, $g(\eta)$, $\theta(\eta)$ and $S(\eta)$, respectively. Using Taylor's series, one can write them as

$$\begin{aligned}
f(\eta;p) &= f_0 + \sum_{m=1}^{\infty} f_m(\eta)p^m, \quad f_m(\eta) = \frac{1}{m!}\frac{\partial^m f(\eta;p)}{\partial p^m}\bigg|_{p=0}, \\
g(\eta;p) &= g_0 + \sum_{m=1}^{\infty} g_m(\eta)p^m, \quad g_m(\eta) = \frac{1}{m!}\frac{\partial^m g(\eta;p)}{\partial p^m}\bigg|_{p=0}, \\
\theta(\eta;p) &= \theta_0 + \sum_{m=1}^{\infty} \theta_m(\eta)p^m, \quad \theta_m(\eta) = \frac{1}{m!}\frac{\partial^m \theta(\eta;p)}{\partial p^m}\bigg|_{p=0}, \\
S(\eta;p) &= S_0 + \sum_{m=1}^{\infty} S_m(\eta)p^m, \quad S_m(\eta) = \frac{1}{m!}\frac{\partial^m S(\eta;p)}{\partial p^m}\bigg|_{p=0}.
\end{aligned} \tag{8.24}$$

We have to choose the values of auxiliary parameters for which the series (8.24) converges at $p = 1$ i.e.,

$$f(\eta) = f_0 + \sum_{m=1}^{\infty} f_m(\eta),\ g(\eta) = g_0 + \sum_{m=1}^{\infty} g_m(\eta),\ \theta(\eta) = \theta_0 + \sum_{m=1}^{\infty} \theta_m(\eta),\ S(\eta) = S_0 + \sum_{m=1}^{\infty} S_m(\eta). \tag{8.25}$$

Next, m^{th}-order deformation is given by

$$\begin{aligned}
L_1[f_m(\eta) - \chi_m f_{m-1}(\eta)] &= h_1 R_m^f(\eta), \quad L_2[g_m(\eta) - \chi_m g_{m-1}(\eta)] = h_2 R_m^g(\eta), \\
L_3[\theta_m(\eta) - \chi_m \theta_{m-1}(\eta)] &= h_3 R_m^\theta(\eta), \quad L_4[S_m(\eta) - \chi_m S_{m-1}(\eta)] = h_4 R_m^S(\eta).
\end{aligned} \tag{8.26}$$

where

$$R_m^f(\eta) = f^{iv} - \sqrt{Re}\left[4Re(g' - \sum_{n=0}^{m-1} g_{m-1-n}g'_n) + 2\sum_{n=0}^{m-1} f'_{m-1-n}f''_n + \sum_{n=0}^{m-1} f_{m-1-n}f'''_n \right.$$
$$\left. -2/\sqrt{Re}f'\right] - 2\sqrt{Re}Gr\left[2\sum_{n=0}^{m-1}\theta_{m-1-n}\sum_{l=0}^{n} g_l g'_{n-l} - 2\sum_{n=0}^{m-1} g'_{m-1-n}\theta_n + \sum_{n=0}^{m-1}\theta'_{m-1-n}\sum_{l=0}^{n} g_l g_{n-l}\right.$$
$$\left. -2\sum_{n=0}^{m-1} g_{m-1-n}\theta'_n + \theta'\right] + \sqrt{Re}Nr\left[2\sum_{n=0}^{m-1} S_{m-1-n}\sum_{l=0}^{n} g_l g'_{n-l} - 2\sum_{n=0}^{m-1} g'_{m-1-n}S_n\right.$$
$$\left. + \sum_{n=0}^{m-1} S'_{m-1-n}\sum_{l=0}^{n} g_l g_{n-l} - 2\sum_{n=0}^{m-1} g_{m-1-n}S'_n + S'\right] - \frac{Ha^2\alpha e\, f''}{(\alpha e^2 + \beta h^2)} + \frac{2\sqrt{Re}Ha^2\beta h\, g'}{(\alpha e^2 + \beta h^2)} \quad (8.27)$$

$$R_m^g(\eta) = 2\sqrt{Re}g'' - 2Re\left[\sum_{n=0}^{m-1} f_{m-1-n}g'_n + \sum_{n=0}^{m-1} f'_{m-1-n}g_n + f\right] - \frac{Ha^2\beta h\, f'}{(\alpha e^2 + \beta h^2)} - \frac{2\sqrt{Re}Ha^2\alpha e\, g}{(\alpha e^2 + \beta h^2)}$$
$$+Gr\left[\sum_{n=0}^{m-1} f'_{m-1-n}\sum_{l=0}^{n} g_l\theta_{n-l} + 2\sum_{n=0}^{m-1} f'_{m-1-n}\theta_n - Nr\sum_{n=0}^{m-1} f'_{m-1-n}\sum_{l=0}^{n} g_l S_{n-l} - 2Nr\sum_{n=0}^{m-1} f'_{m-1-n}S_n\right] \quad (8.28)$$

$$Rm^\theta(\eta) = \theta'' - \sqrt{Re}\,Pr\sum_{n=0}^{m-1}\theta'_{m-1-n}f_n + PrNb\sum_{n=0}^{m-1}\theta'_{m-1-n}S'_n + PrNt\sum_{n=0}^{m-1}\theta'_{m-1-n}\theta'_n$$
$$+\frac{Br}{4Re}\left[10\sum_{n=0}^{m-1} f'_{m-1-n}f'_n + \sum_{n=0}^{m-1} f''_{m-1-n}f''_n\right] + Br\left[2\sum_{n=0}^{m-1} g_{m-1-n}g_n + \sum_{n=0}^{m-1} g'_{m-1-n}g'_n\right]$$
$$+\frac{J}{4Re(\alpha e^2 + \beta h^2)}\left[\sum_{n=0}^{m-1} f'_{m-1-n}f'_n + 4\,Re\sum_{n=0}^{m-1} g_{m-1-n}g_n\right] \quad (8.29)$$

$$R_m^S(\eta) = S'' - \sqrt{Re}\,Le\,f\,S' + \frac{Nt}{Nb}\,\theta'' \quad (8.30)$$

for integer m, we take

$$\chi_m = 0 \quad \text{for} \quad m \le 1$$
$$= 1 \quad \text{for} \quad m > 1.$$

8.4 Convergence

To find the admissible range of the auxiliary parameters, h-curves are drawn for 12^{th}-order approximation and shown in figure (8.2). It is visible from this figure that the permissible interval for h_1, h_2, h_3 and h_4 are $-1.0 < h_1 < -0.5$, $-1.8 < h_2 < -0.6$, $-1.5 < h_3 < -0.5$ and $-2.0 < h_4 < -0.5$, respectively. In order to obtain the optimal values of the auxiliary parameters, the following average residual errors (Ref. Liao [49]) are computed

$$\begin{aligned} E_{f,m} &= \frac{1}{2K}\sum_{i=-K}^{K}\left(N_1\left[\sum_{j=0}^{m} f_j(i\triangle t)\right]\right)^2, \quad E_{g,m} = \frac{1}{2K}\sum_{i=-K}^{K}\left(N_2\left[\sum_{j=0}^{m} g_j(i\triangle t)\right]\right)^2, \\ E_{\theta,m} &= \frac{1}{2K}\sum_{i=-K}^{K}\left(N_3\left[\sum_{j=0}^{m} \theta_j(i\triangle t)\right]\right)^2, \quad E_{S,m} = \frac{1}{2K}\sum_{i=-K}^{K}\left(N_4\left[\sum_{j=0}^{m} S_j(i\triangle t)\right]\right)^2. \end{aligned} \tag{8.31}$$

where $\triangle t = 1/K$ and $K = 5$. At different order of approximations (m), the least average residual errors are shown in table (8.1).

From this, we see that the average residual errors are least at $h_1 = -0.76$, $h_2 = -1.26$, $h_3 = -0.65$ and $h_4 = -0.85$. Therefore, the optimum values of convergence control parameters are taken as $h_1 = -0.76$, $h_2 = -1.26$, $h_3 = -0.65$ and $h_4 = -0.85$. The series solutions for different values of m are computed and presented in table (8.2). It is found from this table that the series (8.25) converges in the whole region of η.

Further, the ratios

$$\beta f = \left|\frac{f_m(h)}{f_{m-1}(h)}\right|, \quad \beta g = \left|\frac{g_m(h)}{g_{m-1}(h)}\right|, \quad \beta\theta = \left|\frac{\theta_m(h)}{\theta_{m-1}(h)}\right|, \quad \beta S = \left|\frac{S_m(h)}{S_{m-1}(h)}\right|. \tag{8.32}$$

against the number of terms m in homotopy series are calculated and observed that the series (8.25) converges to the exact solution.

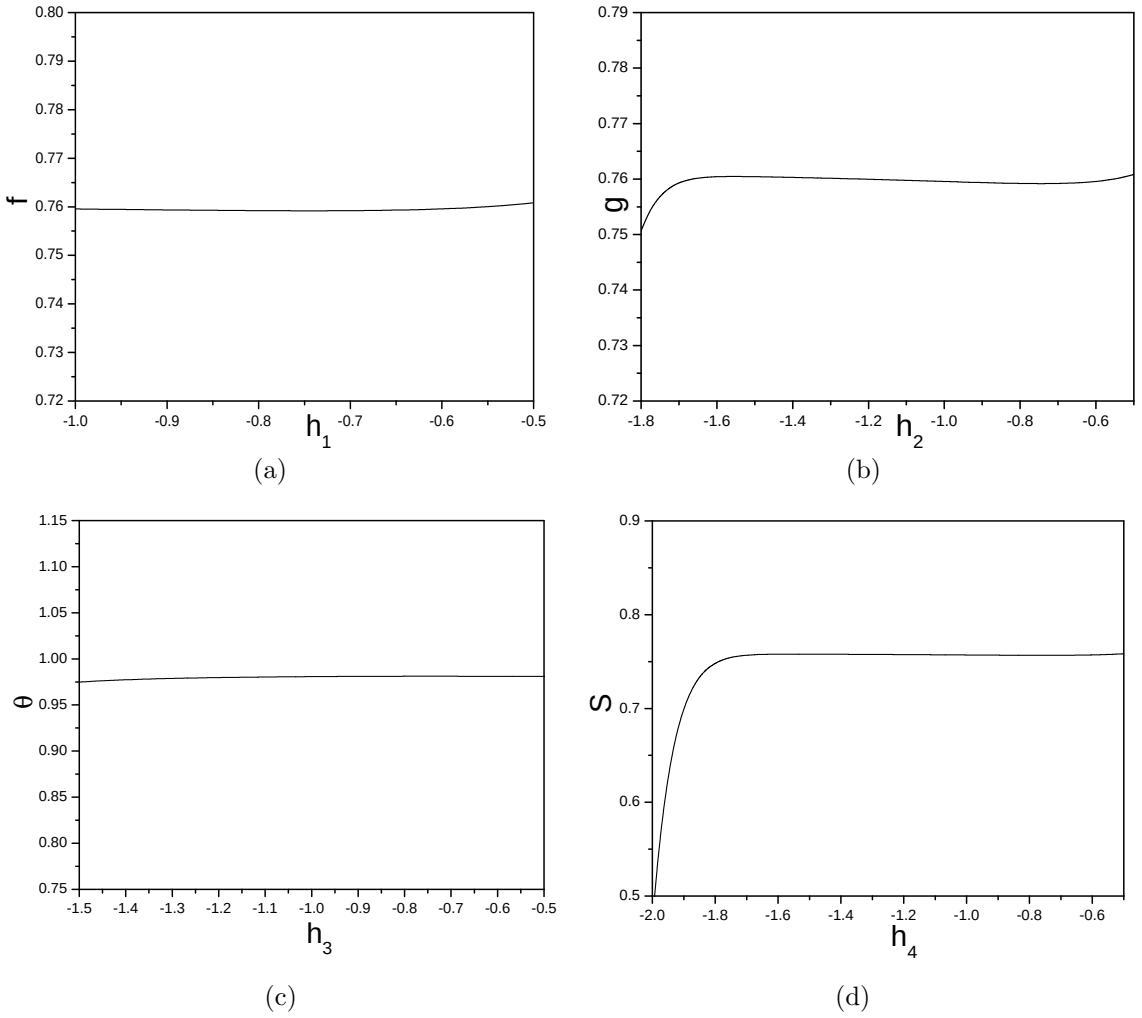

Figure 8.2: "h-curve for (a) axial velocity, (b) tangential velocity, (c) temperature and (d) nanoparticle concentration when $Nr = 1.0, Nt = 0.5, Gr = 10.0, Ha = 1.0, Nb = 0.5, Pr = 1.0, \beta i = 2.0, Re = 50, Le = 1.0, \beta h = 2.0$ and $Br = 0.5$".

	Optimal of h_1		Optimal of h_2		Optimal of h_3		Optimal of h_4	
Order	h_1	Min. of E_m	h_2	Min. of E_m	h_3	Min. of E_m	h_4	Min. of E_m
10	-0.76	3.29×10^{-5}	-1.26	2.68×10^{-4}	-0.65	8.39×10^{-5}	-0.83	6.76×10^{-5}
12	-0.76	5.13×10^{-5}	-1.24	1.10×10^{-5}	-0.64	7.47×10^{-6}	-0.85	3.12×10^{-5}
14	-0.78	7.22×10^{-4}	-1.26	5.10×10^{-6}	-0.65	8.25×10^{-5}	-0.85	6.88×10^{-6}

Table 8.1: "At different order of approximations, the optimal values of h_1, h_2, h_3 and h_4".

Order	f(0.5)	g(0.5)	$\theta(0.5)$	S(0.5)
5	-0.1145800106	-0.7237400046	0.1804538436	0.6047344904
10	-0.1171206547	-0.6548700082	0.2004254151	0.6571454270
15	-0.1211306214	-0.6384600103	0.2011424106	0.6872366455
20	-0.1212140618	-0.6375800105	0.2024264103	0.6893354554
25	-0.1212380612	-0.6375500240	0.2025124105	0.6894564673
30	-0.1212390612	-0.6375350290	0.2025174105	0.6894615346
35	-0.1212410624	-0.6375339025	0.2025174105	0.6894615346
40	-0.1212411206	-0.6375339028	0.2025174105	0.6894615467
45	-0.1212411206	-0.6375339029	0.2025174105	0.6894615467
50	-0.1212411206	-0.6375339029	0.2025174105	0.6894615467
55	-0.1212411206	-0.6375339029	0.2025174105	0.6894615467

Table 8.2: "At different order of approximations, the convergence of HAM solutions".

8.5 Entropy generation

The entropy generation volumetric rate of nanofluid in between parallel disks can be expressed as

$$\begin{aligned} S_G &= \frac{K_f}{T_1^2}\left[\left(\frac{\partial T}{\partial r}\right)^2+\frac{1}{d^2}\left(\frac{\partial T}{\partial z}\right)^2\right]+\frac{2\mu}{T_1}\left[\left(\frac{\partial u}{\partial r}\right)^2+\left(\frac{u}{r}\right)^2+\left(\frac{\partial w}{\partial z}\right)^2\right] \\ &+ \frac{\mu}{T_1}\left[\left(r\,\frac{\partial}{\partial r}\left(\frac{v}{r}\right)\right)^2+\left(\frac{\partial v}{\partial z}\right)^2+\left(\frac{\partial u}{\partial z}+\frac{\partial w}{\partial r}\right)^2\right]+\frac{\sigma\,B_0^2}{T_1(\alpha e^2+\beta h^2)}\left(u^2+v^2\right) \end{aligned} \tag{8.33}$$

The entropy generation Ns ([12]) is given by

$$Ns=\theta'^2+\frac{Br}{Tp}\left(\frac{1}{4Re}\left[10(f')^2+(f'')^2\right]+2(g)^2+(g')^2\right)+\frac{J}{(\alpha e^2+\beta h^2)}\,\frac{(f'^2+4Re\,g^2)}{4Tp\,Re} \tag{8.34}$$

where the dimensionless temperature difference is $Tp=\frac{\Delta T}{T_1}$, and the characteristic entropy generation rate is $S_{Gc}=\frac{K_f\,(\Delta T)^2}{d^2\,T_1^2}$. The Eq.(8.34) can be formulate as

$$Ns=Nh+Nv \tag{8.35}$$

The ratio of entropy generation due to heat transfer and the total entropy generation is called Bejan number Be, to understand the mechanisms of entropy generation, Be is specified. The Bejan

number for this problem can be expressed as

$$Be = \frac{Nh}{Nh + Nv} \tag{8.36}$$

8.6 Results and discussion

Effects of Hall βh, ion-slip βi, magnetic Ha, relative rotating rate γ and Joule heating parameters on non-dimensional axial velocity component $f(\eta)$, tangential velocity component $g(\eta)$, temperature $\theta(\eta)$, nanoparticle volume fraction $S(\eta)$, Bejan number Be and entropy generation Ns are presented graphically in Figures (8.3) - (8.8). The effect of these parameter values are established by choosing $Le = 1.0$, $Br = 0.5$, $Pr = 1.0$, $Tp = 1.0$, $Gr = 10$, $Re = 50$, $Nb = 0.5$ and $Nr = 1.0$.

Figure (8.3) displays the impact of magnetite parameter Ha on the axial and tangential velocities, temperature, nanoparticle concentration, entropy generation and Bejan number. Figure 8.3(a) reveals that the axial velocity decays with an enhancement in Ha. This is because of the fact that the induction of a magnetic field, normal to the flow direction has a tendency to develope the drag known as Lorentz force which leads to resist the flow. Hence, the velocity decays as a growth in Ha. It is realized from figure 8.3(b) that $g(\eta)$ increases with an enhancement in Ha. The non-dimensional temperature is increasing with an enhancement in the magnetic parameter Ha as shown in figure 8.3(c). The resistance, created by Lorentz force, increases the fluid friction between layers of fluid and hence the temperature increases. From figure 8.3(d), it is observed that the nanoparticle concentration $S(\eta)$ is decreasing with a rise in Ha. Figure 8.3(e) shows that entropy generation is increasing with an increase in Ha. The significance of Ha on Be is presented in figure 8.3(f). An increase in Bejan number is examined from lower disk to the center of the disks due to more contribution of the heat transfer irreversibility on Ns, while away from the center of the disk, the trend is reversed and there is no effect on the end points of disks with an enhancement in Ha.

The variations of $f(\eta)$, $g(\eta)$, $\theta(\eta)$, $S(\eta)$, Be and Ns with βh are presented in figure (8.4). It is seen from figure 8.4(a) that the axial velocity in flow direction decreases with an enhancement in βh. Figure 8.4(b) reveals that the tangential velocity $g(\eta)$ increases with an enhancement in βh. Hall current tends to stimulate secondary fluid velocity. From figure 8.4(c), it is noticed that the dimensionless temperature $\theta(\eta)$ is increasing with an enhancement in the Hall parameter βh. There

is a decay in the nanoparticle volume fraction $S(\eta)$ with an enhancement in βh as depicted in figure 8.4(d). The involvement of Hall parameter decays the resistive force demand by the magnetic field due to its effect in minimizing the effective conductivity. Figure 8.4(e) shows the entropy generation increased with growth in βh. It is clear from figure 8.4(f) that Be decays from lower disk to the center of the disks, while far away from the center of the disk the trend is reversed due to more contribution of the heat transfer irreversibility on Ns and there is no effect on the end points of disks with an enhancement in βh.

The changes in axial velocity, tangential velocity, temperature, nanoparticle concentration, entropy generation and Bejan number with βi are represented in figure (8.5). From figure 8.5(a), it is noticed that the dimensionless axial velocity in flow direction increases with an enhancement in βi. Figure 8.5(b) reveals that the tangential velocity flow $g(\eta)$ decays with a rise in βi. The effective conductivity also increases as βi increases, while it decreases the damping force on the velocity component in the direction of the flow, due to which velocity increases. The non-dimensional temperature increases with an increase in βi as shown in figure 8.5(c). It is observed that the nanoparticle concentration $S(\eta)$ increases with a rise in βi as depicted in figure 8.5(d). The effect of βi on Bejan number and entropy generation is similar to that of βh.

The variation of $f(\eta)$, $\theta(\eta)$, $g(\eta)$, $S(\eta)$, Be and Ns with Nt are presented in figure (8.6). From figure 8.6(a), it is examined that the axial velocity in flow direction rises with a rise in parameter Nt . Figure 8.6(b) reveals that the tangential velocity $g(\eta)$ increases as an increase in Nt. From figura 8.6(c), it is noticed that the dimensionless temperature $\theta(\eta)$ increases with an increase in Nt. There is a decrease in the nanoparticle concentration $S(\eta)$ with an enhancement in thermoporesis parameter Nt as depicted in figure 8.6(d). Figure 8.6(e) shows that the entropy generation increases at the center of the disks, the trend is reversed at the end point of the disks with an increase in Nt. Figure 8.6(f) shows that Be diminishes with a rise in the value of Nt and Bejan number is not much effected with increase in the value of Nt at the center of the disks.

Figure (8.7) displays the role of relative rotating rate parameter γ on the non-dimensional axial and tangential velocities, temperature, nanoparticle concentration, entropy generation and Bejan number. Figure 8.7(a) reveals that the axial velocity decreases with a rise in γ. It is observed from figure 8.7(b) that $g(\eta)$ rises with a rise in γ. The non-dimensional temperature is increases with an increase in γ as shown in figure 8.7(c). Figure 8.7(d) reveals that the nanoparticle concentration $S(\eta)$ decreases with a rise in γ. Figure 8.7(e) shows that the entropy generation increases at the

center of the disks, and at the end point of the disks, the trend is reversed with an enhancement in γ. Increasing Bejan number is observed from lower disk to the center of the disks because of more contribution of the heat transfer irreversibility on Ns, while away from the center of the disk the trend is reversed and there is no effect at the end points of the disks with an enhancement in Be (Bejan number), as shown in figure 8.7(f).

Figure (8.8) expiores the importance of Joule heating parameter J on $f(\eta)$, $\theta(\eta)$, $g(\eta)$, $S(\eta)$, Be and Ns. Figure 8.8(a) reveals that the axial velocity rises with a rise in J . It is observed from figure 8.8(b) that $g(\eta)$ rises with a rise in J. It is clear from figure 8.8(c) that the temperature increases with an increase in J. Nanoparticle concentration $S(\eta)$ decreases with a rise in J, as presented in figure 8.8(d). Figure 8.8(e) shows that the entropy generation increases with an enhancement in J. Increasing Bejan number is observed from lower disk to the center of the disks due to more contribution of the heat transfer irreversibility on Ns, while away from the center of the disks, the trend is reversed and there is no effect at the end points of the disks with an enhancement in J, as shown in figure 8.8(f).

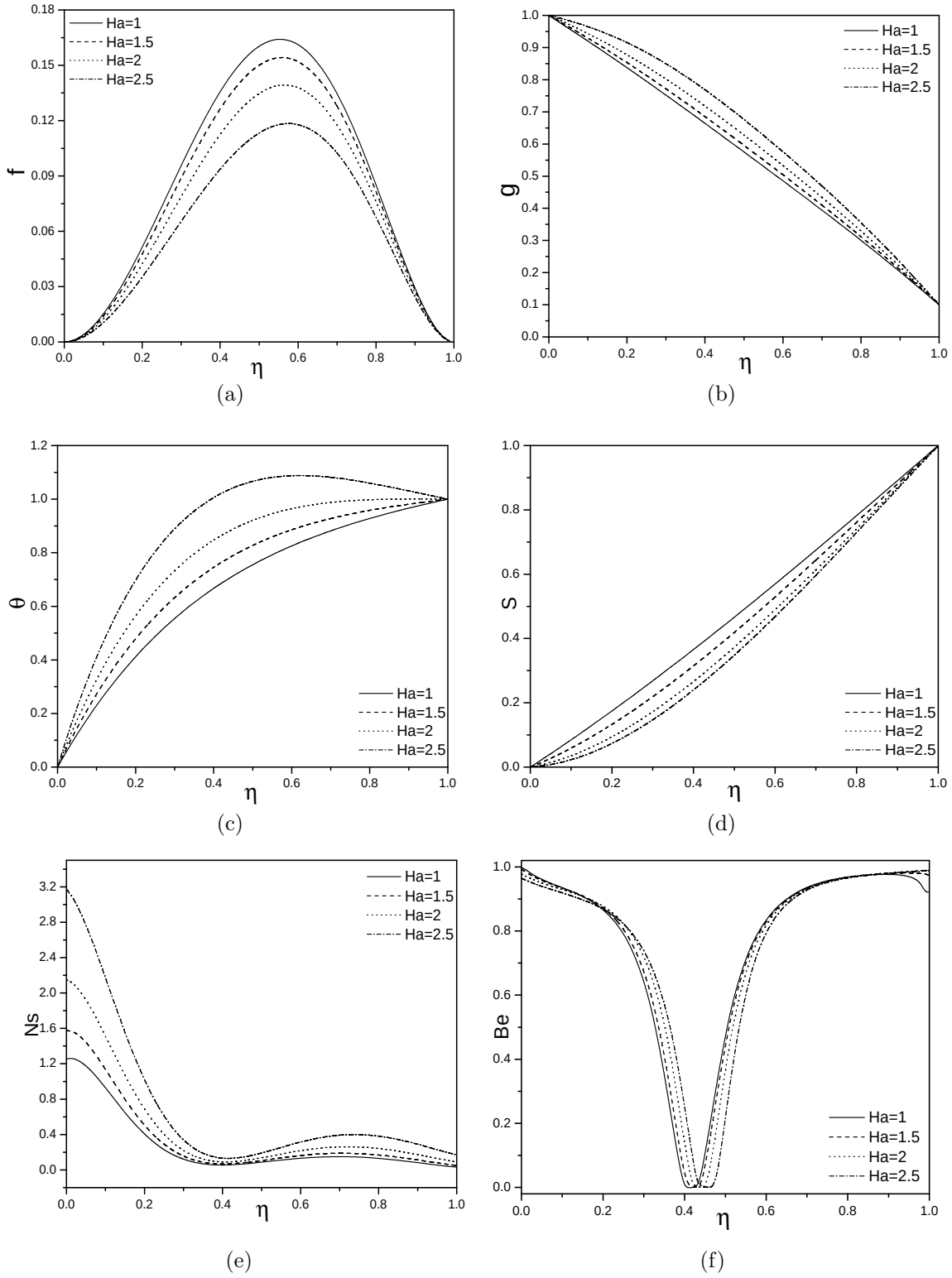

Figure 8.3: "Effect of Ha on (a) axial velocity, (b) tangential velocity, (c) temperature, (d) nanoparticle concentration, (e) entropy generation and (f) Bejan number".

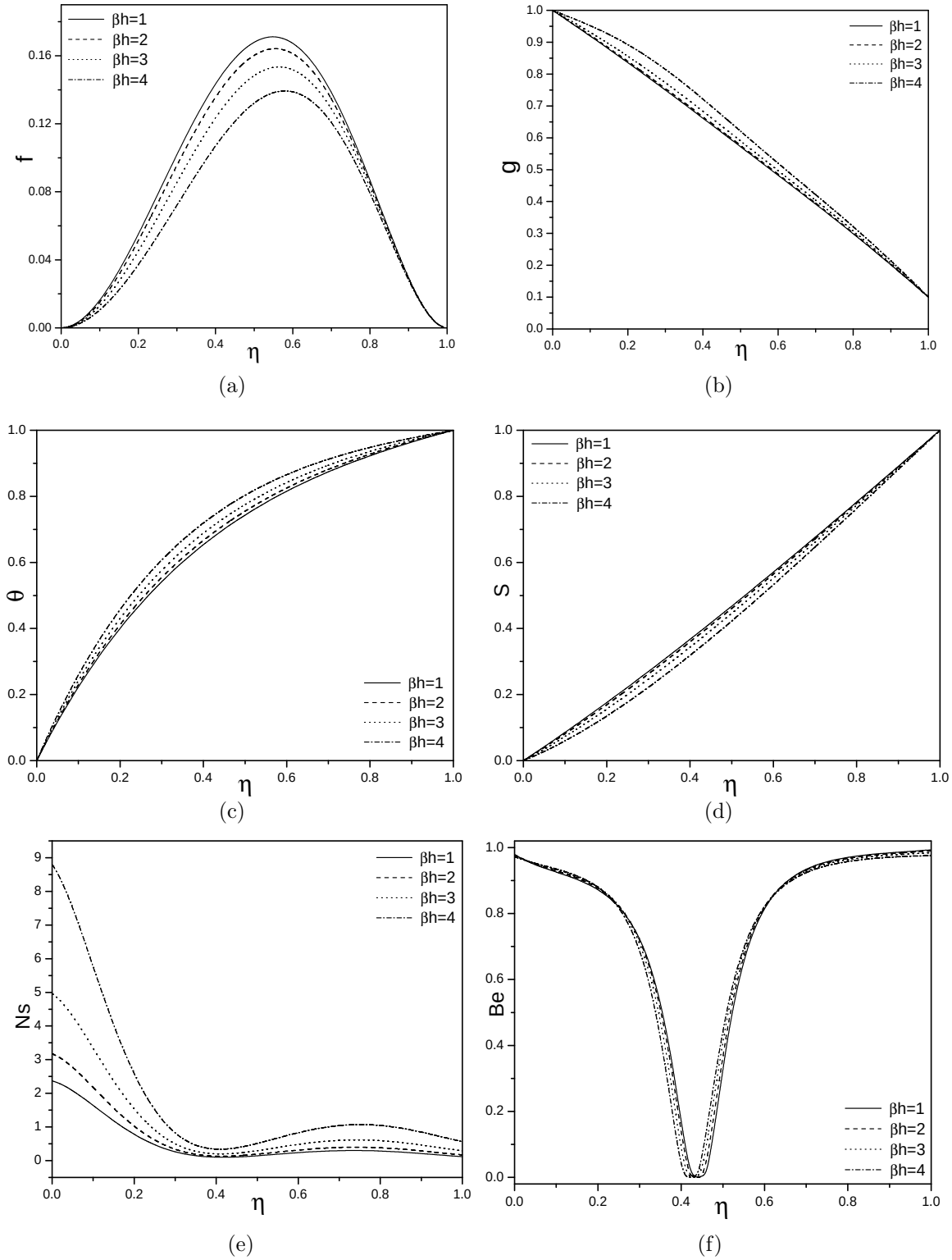

Figure 8.4: "Effect of βh on (a) axial velocity, (b) tangential velocity, (c) temperature, (d) nanoparticle concentration, (e) entropy generation and (f) Bejan number".

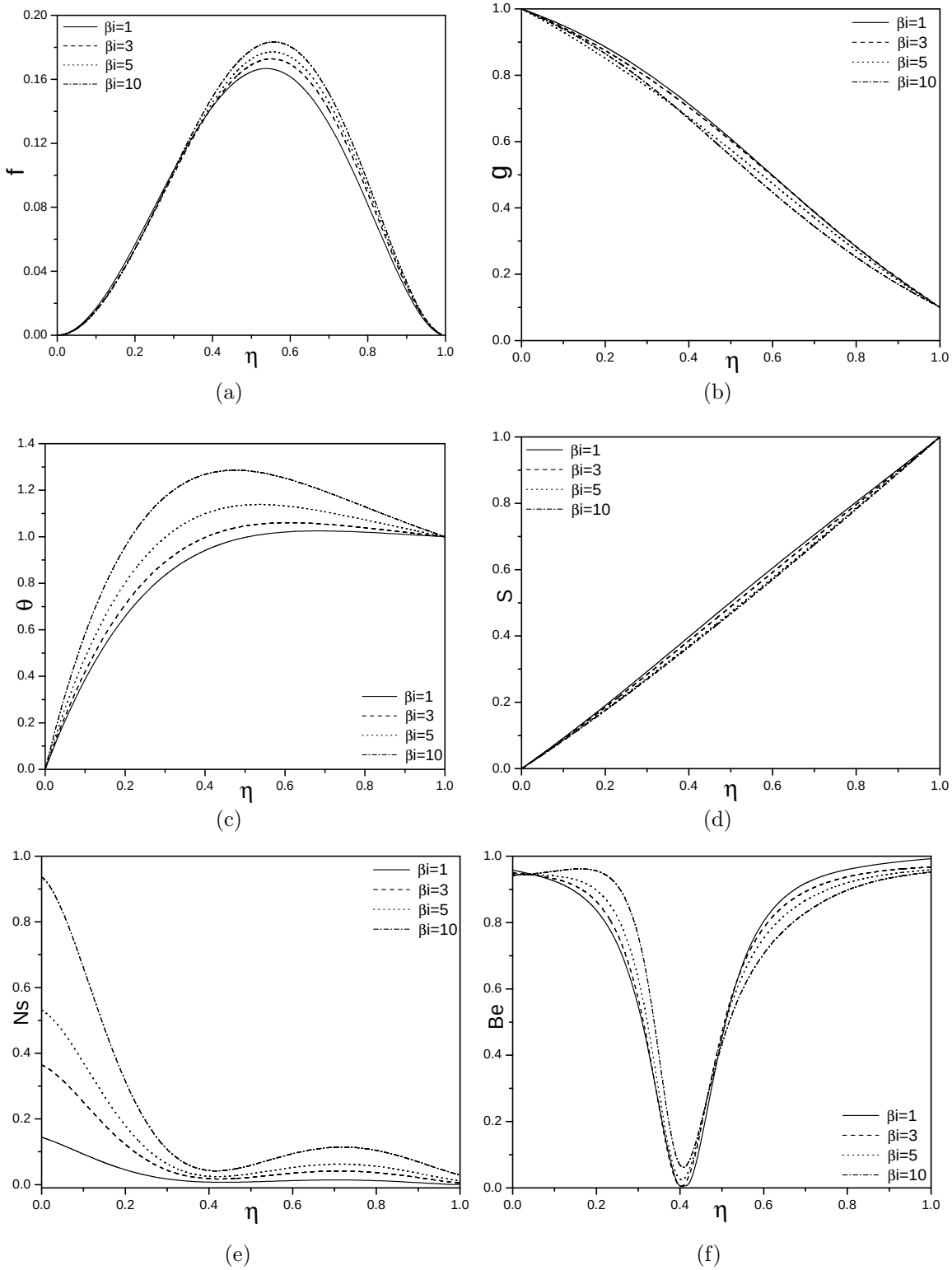

Figure 8.5: "Effect of βi on (a) axial velocity, (b) tangential velocity, (c) temperature, (d) nanoparticle concentration, (e) entropy generation and (f) Bejan number".

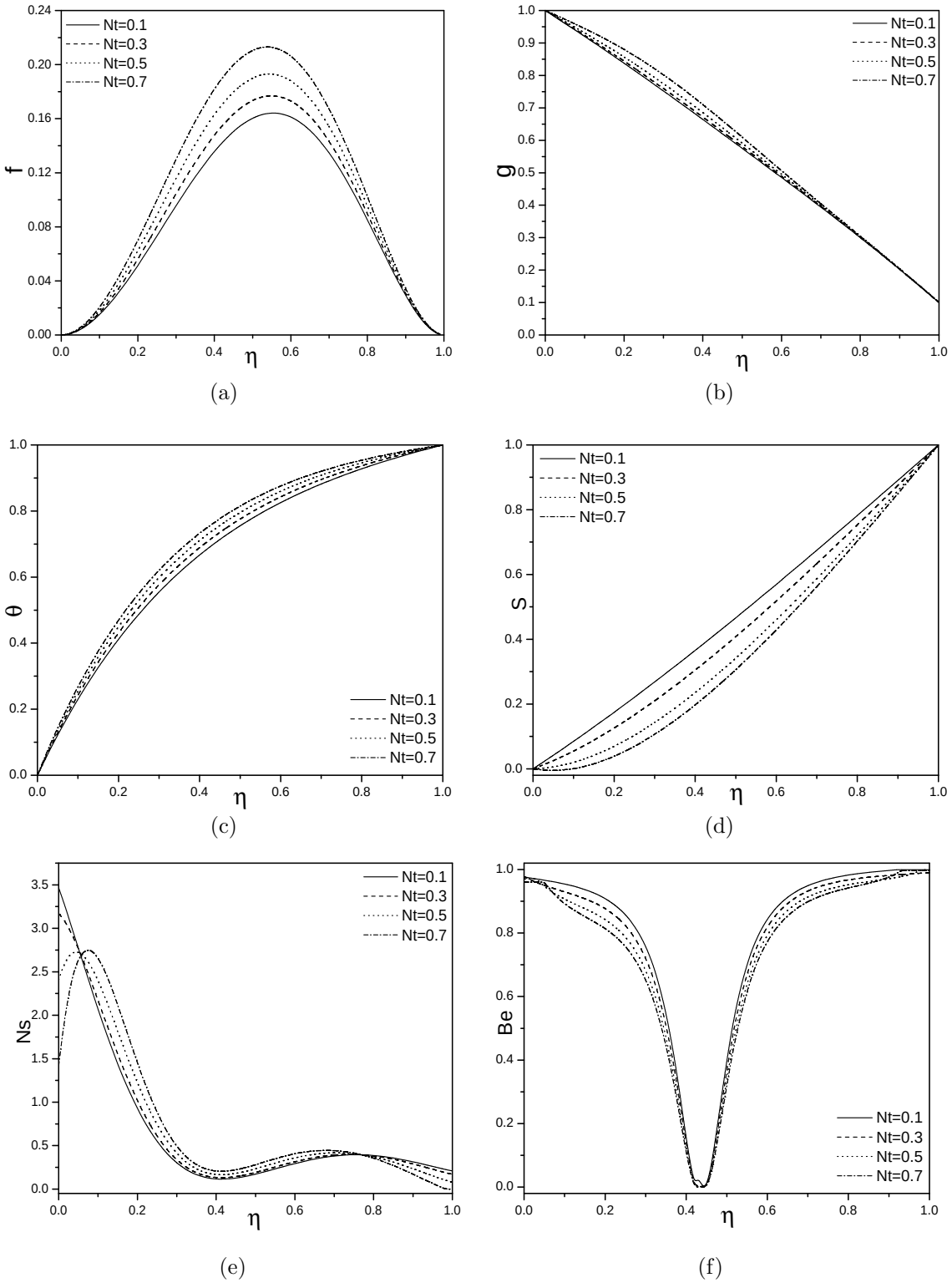

Figure 8.6: "Effect of Nt on (a) axial velocity, (b) tangential velocity, (c) temperature, (d) nanoparticle concentration, (e) entropy generation and (f) Bejan number".

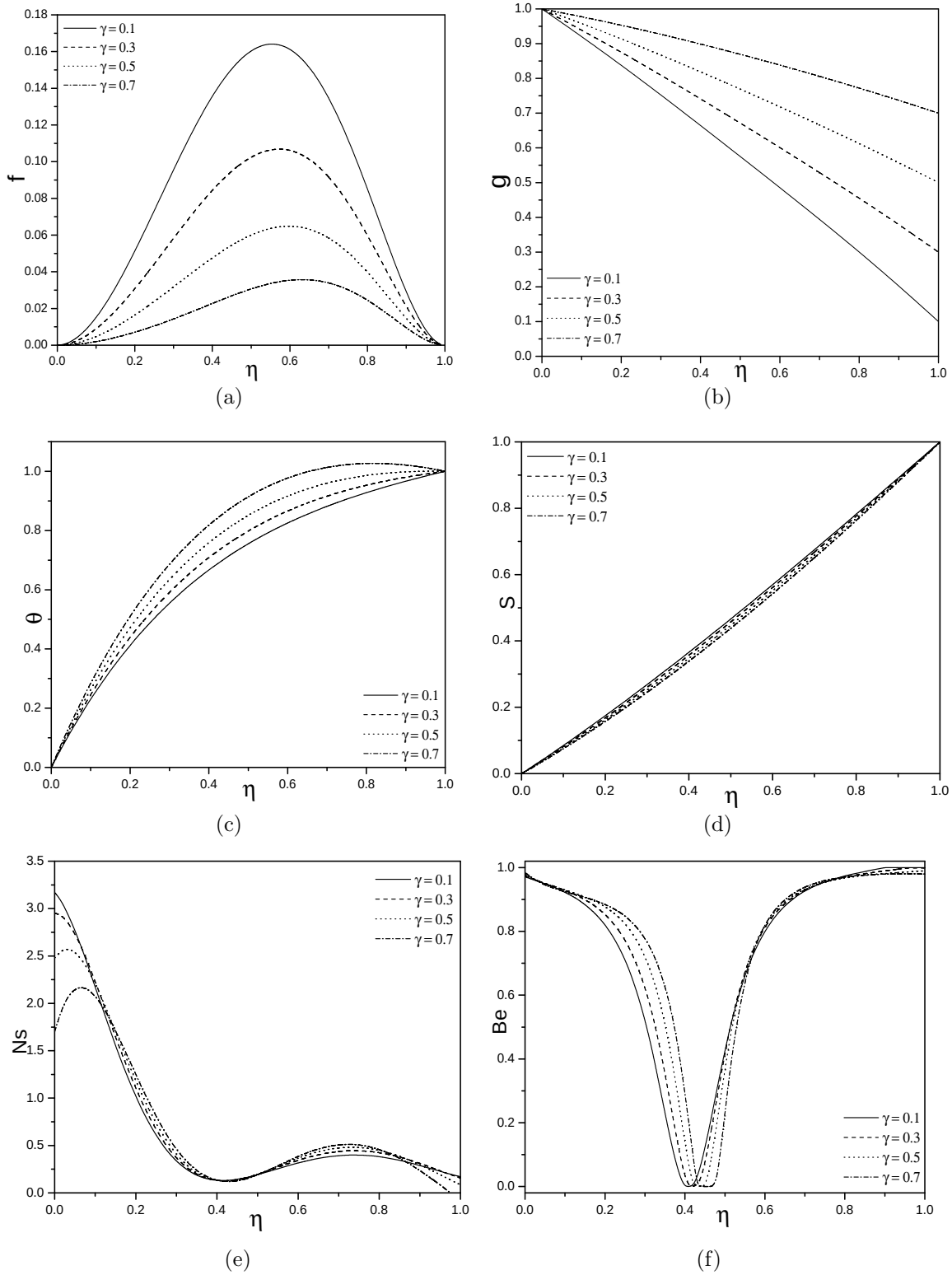

Figure 8.7: "Effect of γ on (a) axial velocity, (b) tangential velocity, (c) temperature, (d) nanoparticle concentration, (e) entropy generation and (f) Bejan number".

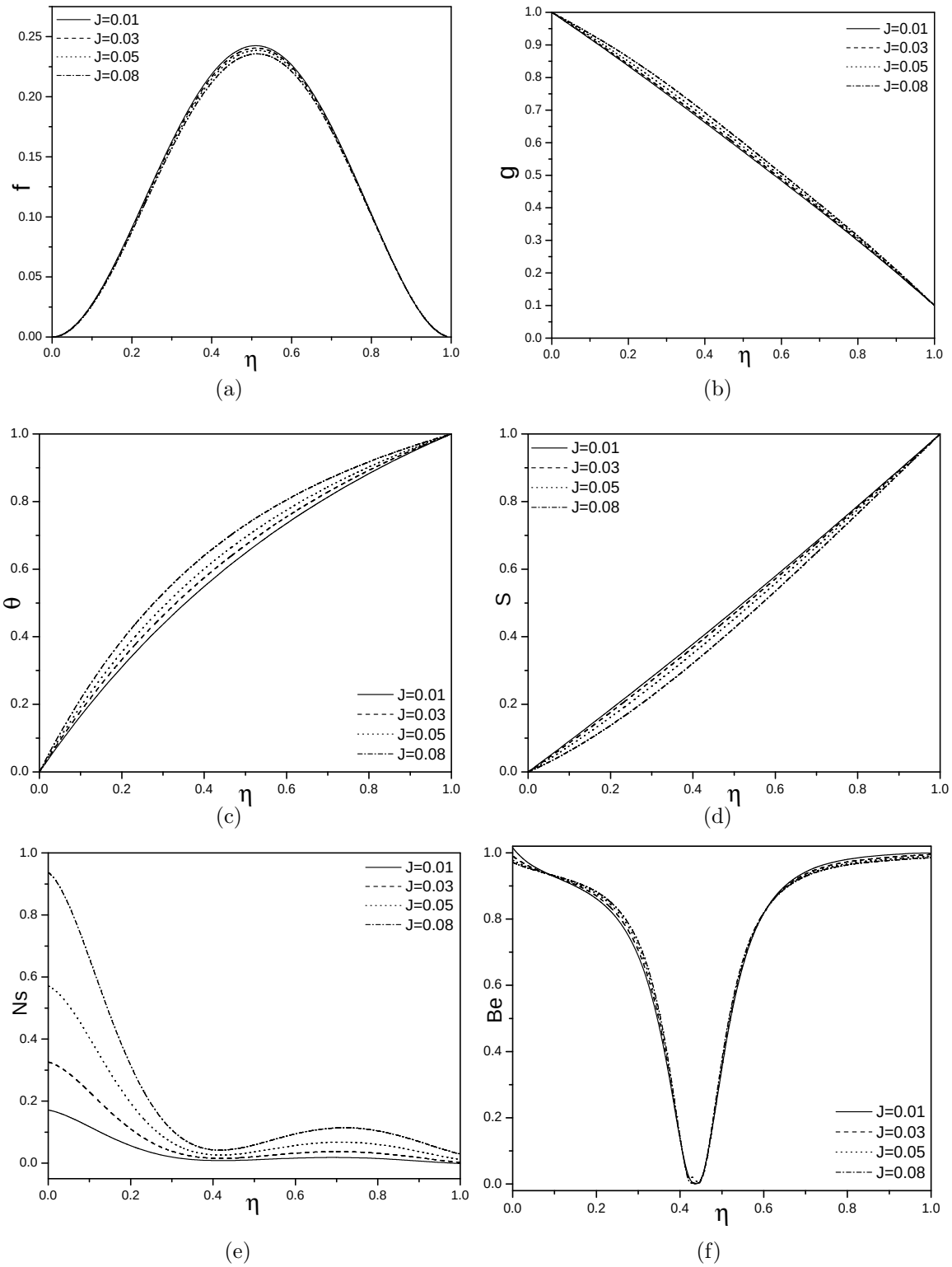

Figure 8.8: "Effect of J on (a) axial velocity, (b) tangential velocity, (c) temperature, (d) nanoparticle concentration, (e) entropy generation and (f) Bejan number".

8.7 Conclusions

In this chapter, the entropy generation due to mixed convective nanofluid flow between the horizontal parallel infinite coaxial disks has been investigated by considering the effects of Joule, Hall and ion-slip parameters. The following are the observations:

As Hall current increases, the tangential velocity, axial velocity, temperature and entropy generation increase, but the nanoparticle concentration decreases. The axial velocity, temperature and nanoparticle concentration increase, whereas the tangential velocity decreases with an increase in ion-slip parameter. The axial velocity, temperature and entropy generation increase, whereas the tangential velocity and nanoparticle concentration decrease with a rise in γ. The tangential, axial velocities, temperature and entropy generation increase, whereas the nanoparticle concentration decreases with a rise in Joule heating parameter J. The maximum values of Bejan number Be are observed at the end point of the disks due to more contribution of the heat transfer irreversibility on the entropy generation and minimum value at the center of the disks due to more contribution of the fluid friction irreversibility on the entropy generation with an enhancement in $Ha, \beta h, \beta i, \gamma$ and J.

Chapter 9

Entropy generation in mixed convective flow of a chemically reacting nanofluid between parallel disks with radiation effect [1]

9.1 Introduction

Rotating disk flow has long been an interesting research topic in the thermal fluid field for its importance in fluid physics. From the practical point of view, one of the important areas in mechanical engineering is the rotating machinery, in which thermal fluid plays a very significant role in design and performance analysis. Especially, rotating disk configuration is the most common one in real time applications, e.g. gas turbine disks, hard disk driver in desk top computers, rotating heat exchangers, disk-type contactor, rotating disk reactors for epitaxy of thin film, etc.

The effect of radiation on mixed convective flow of a nanofluid over different surface geometries has vast applications involving high temperatures such as satellites, gas turbines missiles, nuclear power plant, aircraft, space vehicles, etc. Sheikholeslami and Davood [71] investigated the effects

[1] Communicated to "**Journal of King Saud University - Science**"

of radiation on the unsteady flow of the nanofluid flow and heat transfer. On the other hand, the impact of chemical reaction on heat and mass transfer is of great influence in chemical technology and industries of hydrometallurgy. Chemically reacting nanofluid may play a significant role in many processing systems and materials. These include flow in packed bed electrodes and co-current buoyant upward gas-liquid [85]. Poulomi *et al* [64] analysed the significance of mixed convective chemically reacting nanofluid flow with a thermal radiation effect.

Entropy generation destroys the available energy of a system and as a result imposes considerable extra costs to any thermal system. In order to improve the efficiency in all types of thermal systems, it is important to minimize the entropy generation and thus optimizing the energy resources. Gyftopoulos and Beretta [37] studied the rate of entropy generation in a chemically reacting system. Rashidi *et al*[67] analysed the magnetohydrodynamic nanofluid flow due to entropy generation in a rotating porous disk.

In this chapter, the effect of thermal radiation on entropy generation due to mixed convective chemically reacting nanofluid flow between parallel disks is investigated. The effects of thermal radiation and chemical reaction on the temperature, velocity, nanoparticle concentration and entropy generation are investigated.

9.2 Mathematical Formulation

Consider the steady, laminar and incompressible nanofluid flow between two horizontal coaxial parallel disks (see figure 8.1). We assume that

- The distance between two horizontal coaxial parallel disks is d.
- The lower and upper disks are rotating with angular velocities Ω_1 and Ω_2 respectively.
- T_1 and ϕ_1 are the temperature and nanoparticle volume fraction of the lower disk whereas T_2 and ϕ_2 are at the upper disk.
- The cylindrical coordinate system (r, φ, z) is taken on the lower disk and the center of the disk is considered as pole.
- Uniform magnetic field of strength B_0 is applied normal to the disk.

The governing equations of the flow are given by

$$\frac{\partial u}{\partial r}+\frac{\partial w}{\partial z}+\frac{u}{r}=0 \tag{9.1}$$

$$\begin{aligned}\rho_f\,(u\frac{\partial u}{\partial r}+w\frac{\partial u}{\partial z}) = \frac{v^2\rho_f}{r}(1-(1-\phi_0)\rho_f\,g^*\,\beta_T(T-T_1)-(\rho_s-\rho_f)\,g^*(\phi-\phi_1))-\frac{\partial p^*}{\partial r}\\ -\rho_f\,r\Omega_1^2((1-\phi_0)\rho_f\,g^*\,\beta_T(T-T_1)-(\rho_s-\rho_f)\,g^*(\phi-\phi_1))+\mu\left[\frac{\partial}{\partial r}\left(\frac{1}{r}\,\frac{\partial}{\partial r}(r\,u)\right)+\frac{\partial^2 u}{\partial z^2}\right]\\ -2\rho_f\,v\Omega_1(1-(1-\phi_0)\rho_f\,g^*\,\beta_T(T-T_1)-(\rho_s-\rho_f)\,g^*(\phi-\phi_1))\end{aligned} \tag{9.2}$$

$$\begin{aligned}\rho_f\,(u\frac{\partial v}{\partial r}+w\frac{\partial v}{\partial z}) &= -\frac{uv\rho_f}{r}(1-(1-\phi_0)\rho_f\,g^*\,\beta_T(T-T_1)-(\rho_s-\rho_f)\,g^*(\phi-\phi_1))\\ &- 2\rho_f\,u\Omega_1(1-(1-\phi_0)\rho_f\,g^*\,\beta_T(T-T_1)-(\rho_s-\rho_f)\,g^*(\phi-\phi_1))\\ &+ \mu\left[\frac{\partial}{\partial r}\left(\frac{1}{r}\,\frac{\partial}{\partial r}(r\,v)\right)+\frac{\partial^2 v}{\partial z^2}\right]\end{aligned} \tag{9.3}$$

$$\begin{aligned}\rho_f\,(u\frac{\partial w}{\partial r}+w\frac{\partial w}{\partial z}) &= \rho_f((1-\phi_0)\rho_f\,g^*\,\beta_T(T-T_1)-(\rho_s-\rho_f)\,g^*(\phi-\phi_1))-\frac{\partial p^*}{\partial z}\\ &+ \mu\left[\frac{1}{r}\,\frac{\partial}{\partial r}\left(r\,\frac{\partial w}{\partial z}\right)+\frac{\partial^2 w}{\partial z^2}\right]\end{aligned} \tag{9.4}$$

$$\begin{aligned}u\frac{\partial T}{\partial r}+w\frac{\partial T}{\partial z} &= \frac{2\mu}{\rho C_p}\left[\left(\frac{\partial u}{\partial r}\right)^2+\left(\frac{u}{r}\right)^2+\left(\frac{\partial w}{\partial z}\right)^2\right]+\alpha\left[\frac{\partial^2 T}{\partial z^2}+\frac{\partial^2 T}{\partial r^2}+\frac{1}{r}\,\frac{\partial T}{\partial r}\right]\\ &+ \frac{\mu}{\rho C_p}\left[\left(r\,\frac{\partial}{\partial r}\,\left(\frac{v}{r}\right)\right)^2+\left(\frac{\partial v}{\partial z}\right)^2+\left(\frac{\partial u}{\partial z}+\frac{\partial w}{\partial r}\right)^2\right]-\frac{1}{\rho C_p}\,\nabla.q_r\\ &+ \tau\left[\frac{D_T}{T_m}\left(\left(\frac{\partial T}{\partial z}\right)^2+\left(\frac{\partial T}{\partial r}\right)^2\right)+D_B\left(\frac{\partial\phi}{\partial r}\frac{\partial T}{\partial r}+\frac{\partial\phi}{\partial z}\frac{\partial T}{\partial z}\right)\right]\end{aligned} \tag{9.5}$$

$$u\frac{\partial\phi}{\partial r}+w\frac{\partial\phi}{\partial z}=\frac{D_T}{T_m}\left[\frac{1}{r}\,\frac{\partial T}{\partial r}+\frac{\partial^2 T}{\partial z^2}+\frac{\partial^2 T}{\partial r^2}\right]+D_B\left[\frac{\partial^2\phi}{\partial z^2}+\frac{1}{r}\,\frac{\partial\phi}{\partial r}+\frac{\partial^2\phi}{\partial r^2}\right]-k_1\,(\phi-\phi_1) \tag{9.6}$$

Under the Rosseland approximation, we assume the radiation heat flux q_r as

$$q_r=-\frac{4\sigma^*}{3\chi}\,\frac{\partial T^4}{\partial r} \tag{9.7}$$

The boundary conditions are

$$\begin{aligned} u=0, \quad v=r\Omega_1, \quad w=0, \quad T=T_1, \quad \phi=\phi_1 \quad \text{on} \quad z=0, \\ u=0, \quad v=r\Omega_2, \quad w=0, \quad T=T_2, \quad \phi=\phi_2 \quad \text{on} \quad z=d \end{aligned} \tag{9.8}$$

Introducing the following non-dimensional variables

$$\eta=\frac{z}{d},\ F=\frac{u}{r\Omega_1},\ g=\frac{v}{r\Omega_1},\ f=\frac{w}{\sqrt{\nu\Omega_1}},\ \theta=\frac{T-T_1}{T_2-T_1},\ S=\frac{\phi-\phi_1}{\phi_2-\phi_1} \tag{9.9}$$

in Eqs. (9.1) to (9.6), we get

$$f^{iv}-\sqrt{Re}\left[4Re(g'-gg')+2ff''+ff'''-\frac{2}{\sqrt{Re}}f'+2Gr(2gg'\theta-2g'\theta+g^2\theta'-2g\theta'+\theta')\right] \\ +\sqrt{Re}GrNr(2gg'S-2g'S+g^2S'-2gs'+s')=0 \tag{9.10}$$

$$2\sqrt{Re}g''-2Re(f'g+fg'+f) \quad + \quad Gr\left[f'g\theta+2f'\theta-Nrf'gS-2Nrf'S\right]=0 \tag{9.11}$$

$$(1+\frac{4}{3}Rd)\theta''-\sqrt{Re}\,Pr\,\theta'f+PrNb\theta'S'+PrNt\,\theta'^2+\frac{Br}{Re}\left[3f'^2+\frac{f''^2}{4}+Reg'^2\right]=0 \tag{9.12}$$

$$S''-\sqrt{Re}\,Le\,f\,S'+\frac{Nt}{Nb}\,\theta''-KLeS=0 \tag{9.13}$$

where $Rd=\dfrac{4\sigma^*}{\chi}\,\dfrac{T_m^3}{K_f}$ is the thermal radiation parameter and $K=\frac{k_1\,d^2}{\nu}$ is the chemically reacting parameter. The remaining parameters are already defined in chapter-8.

The corresponding conditions on boundary (9.8) are

$$\begin{aligned} S=0 \quad f=f'=0, \quad g=1, \quad \theta=0, \quad \text{at} \quad \eta=0 \\ S=1 \quad f=f'=0, \quad g=\gamma, \quad \theta=1, \quad \text{at} \quad \eta=1 \end{aligned} \tag{9.14}$$

Order	Optimal of h_1		Optimal of h_2		Optimal of h_3		Optimal of h_4	
	h_1	Min. of E_m	h_2	Min. of E_m	h_3	Min. of E_m	h_4	Min. of E_m
10	-0.41	4.39×10^{-4}	-1.02	7.67×10^{-6}	-0.34	7.69×10^{-5}	-1.18	7.62×10^{-5}
12	-0.39	6.31×10^{-5}	-1.01	3.12×10^{-7}	-0.34	7.43×10^{-6}	-1.16	8.42×10^{-5}
14	-0.40	1.42×10^{-4}	-1.01	5.41×10^{-6}	-0.34	6.12×10^{-6}	-1.18	9.68×10^{-5}

Table 9.1: "At different order of approximations, the optimal values of h_1, h_2, h_3 and h_4 ".

Order	f(0.5)	g(0.5)	$\theta(0.5)$	S(0.5)
5	0.1545800106	0.6523740006	0.0453843627	0.6047344904
10	0.1871206547	0.4654870002	0.0425415168	0.6571454270
15	0.2011306214	0.4563846001	0.1126424106	0.6752366455
20	0.2112140618	0.4463758001	0.2412264103	0.6973354554
25	0.2120380612	0.4426375500	0.2532124105	0.6984564673
30	0.2123906124	0.4426375350	0.2532174105	0.6984615346
35	0.2124106248	0.4426137533	0.2532174105	0.6984615346
40	0.2124112065	0.4426137532	0.2532174105	0.6984615467
45	0.2124112065	0.4426137532	0.2532174105	0.6984615467
50	0.2124112065	0.4426137532	0.2532174105	0.6984615467
55	0.2124112065	0.4426137532	0.2532174105	0.6984615467

Table 9.2: "At different order of approximations, the convergency of HAM solutions".

9.3 Solution of the problem

The governing Eqs. (9.10) - (9.13) along with the boundary conditions (9.14) are solved by using HAM. As this method is already explained in the chapter - 8, the details are not provided here. However, the convergence of homotopy solution is discussed. To determine the admissible range of auxiliary parameters, the h-curves are plotted for 12^{th} order approximation and presented in figure (9.1). It is found that the admissible ranges for h_1, h_2, h_3 and h_4 are $-1.4 < h_1 < -0.2$, $-1.5 < h_2 < -0.5$, $-0.6 < h_3 < -0.2$ and $-1.6 < h_4 < -0.4$ respectively. The average residual errors (given by (8.31)) are calculated to get the optimum values of h_1, h_2, h_3 and h_4 and presented in the table (9.1). From this table, it is noticed that the optimal value of auxiliary parameters are $h_1 = -0.4$, $h_2 = -1.01$, $h_3 = -0.34$ and $h_4 = -1.18$. Further, the series solutions for different values of m are computed and represented in table (9.2). From table (9.2), it is found that the series solution converges in the whole region of η.

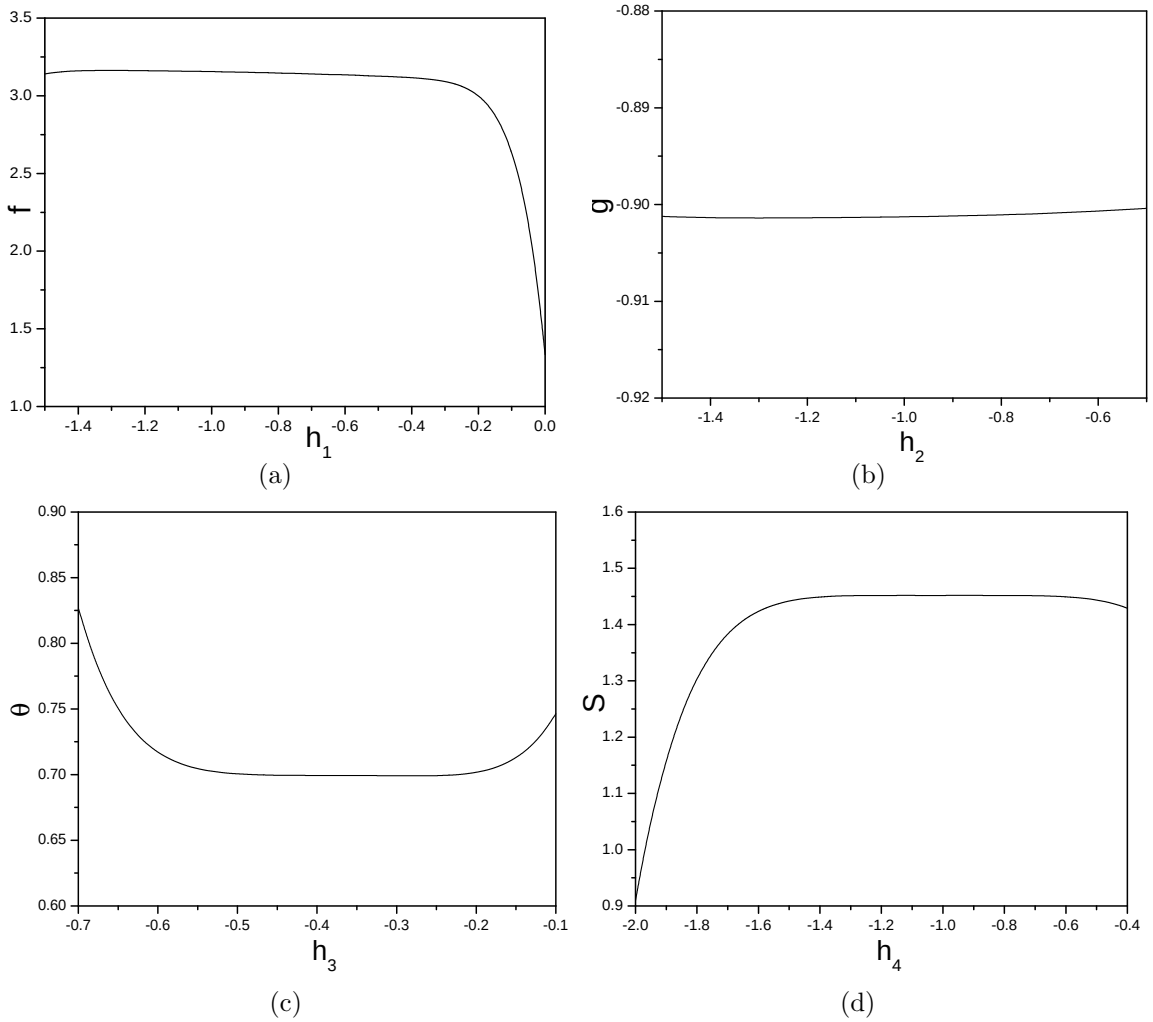

Figure 9.1: "h-curves for (a) axial velocity, (b) tangential velocity, (c) temperature and (d) nanoparticle concentration when $Nr = 1.0, Nt = 0.5, Gr = 10.0, Nb = 0.5, Pr = 1.0, Re = 20, Le = 1.0, K = 1.0, Br = 0.5$ and $Rd = 1.0$".

9.4 Entropy generation

The entropy generation volumetric rate of nanofluid between parallel disks can be expressed as

$$\begin{aligned} S_G &= \frac{K_f}{T_1^2}\left[\left(\frac{\partial T}{\partial r}\right)^2+\frac{1}{d^2}\left(\frac{\partial T}{\partial z}\right)^2\right]+\frac{2\mu}{T_1}\left[\left(\frac{\partial u}{\partial r}\right)^2+\left(\frac{u}{r}\right)^2+\left(\frac{\partial w}{\partial z}\right)^2\right] \\ &+ \frac{\mu}{T_1}\left[\left(r\,\frac{\partial}{\partial r}\left(\frac{v}{r}\right)\right)^2+\left(\frac{\partial v}{\partial z}\right)^2+\left(\frac{\partial u}{\partial z}+\frac{\partial w}{\partial r}\right)^2\right]-\frac{1}{T_1}\nabla.q_r \end{aligned} \tag{9.15}$$

The entropy generation Ns (Bejan [12]) is given by

$$Ns=(1+\frac{4}{3}Rd)\theta'^2+\frac{Br}{ReTp}\left[3f'^2+\frac{f''^2}{4}+Reg'^2\right] \tag{9.16}$$

The Eq.(9.16) can be formulate as

$$Ns=Nh+Nv \tag{9.17}$$

To understand the mechanisms of entropy generation, Be is specified and defined as

$$Be=\frac{Nh}{Nh+Nv} \tag{9.18}$$

9.5 Results and discussion

Effects of radiation parameter Rd, chemical reaction parameter K, Brinkman number Br and thermophSoresis parameters Nt on the non-dimensional axial velocity $f(\eta)$, tangential velocity $g(\eta)$, temperature $\theta(\eta)$, nanoparticle volume fraction $S(\eta)$ and the entropy generation Ns are presented geometrically in Figures. (9.2) - (9.5). The effects of these parameters are found by choosing $Le=1.0$, $Pr=1.0$, $Tp=1.0$, $Gr=10$, $Re=20$, $Nb=0.5$ and $Nr=1.0$.

Figure (9.2) displays the impact of radiation parameter Rd on the axial and tangential velocities, temperature, nanoparticle concentration and the entropy generation. Figure 9.2(a) reveals that the axial velocity is decreasing with an increase in Rd. It is realized from figure 9.2(b) that $g(\eta)$ is decreasing with an increase in Rd. The non-dimensional temperature is decreasing with an enhancement in Rd as shown in figure 9.2(c). From figure 9.2(d), it is noticed that the nanoparticle concentration $S(\eta)$ is increasing with a rise in Rd. Figure 9.2(e) depicts that the entropy generation

is decreasing with an increase in Rd.

The variation of $f(\eta)$, $g(\eta)$, $\theta(\eta)$, $S(\eta)$ and Ns with chemical reaction parameter K is presented in figure (9.3). It is examined from figure 9.3(a) that the axial velocity in flow direction increases with an increase in K. Figure 9.3(b) reveals that the tangential velocity $g(\eta)$ decreases with an enhancement in K. From figure 9.3(c), it is noticed that the dimensionless temperature $\theta(\eta)$ is decreasing with an enhancement in K. There is a decay in the nanoparticle volume fraction $S(\eta)$ with an enhancement in K as show in figure 9.3(d). Figure 9.3(e) presents that the entropy generation increases with an increase in K.

The changes in the axial velocity, tangential velocity, temperature, nanoparticle concentration and the entropy generation with Br are represented in figure (9.4). From figure 9.4(a), it is observed that the dimensionless axial velocity in flow direction increases with an enhancement in Br. Figure 9.4(b) reveals that the tangential velocity $g(\eta)$ is increasing with a rise in Br. The non-dimensional temperature increases with an increase in Br as shown in figure 9.4(c). It is noticed that the nanoparticle concentration $S(\eta)$ decreases with a rise in Br as depicted in figure 9.4(d). Figure 9.4(e) presents that the entropy generation is increasing with an enhancement in Br.

The variations of $f(\eta)$, $\theta(\eta)$, $g(\eta)$, $S(\eta)$ and Ns with Nt are presented in figure (9.5). From figure 9.5(a), it is revealed that the axial velocity in the flow direction is increasing with a rise in Nt. Figure 9.5(b) reveals that the tangential velocity $g(\eta)$ increases as the thermophoresis parameter Nt increases. From figure 9.5(c), it is noticed that the dimensionless temperature $\theta(\eta)$ is increasing as the thermophoresis parameter Nt increases. There is a decrease in the nanoparticle concentration $S(\eta)$ with an enhancement in the thermophoresis parameter Nt as depicted in figure 9.5(d). Figure 9.5(e) shows that the entropy generation increases with an enhancement in Nt.

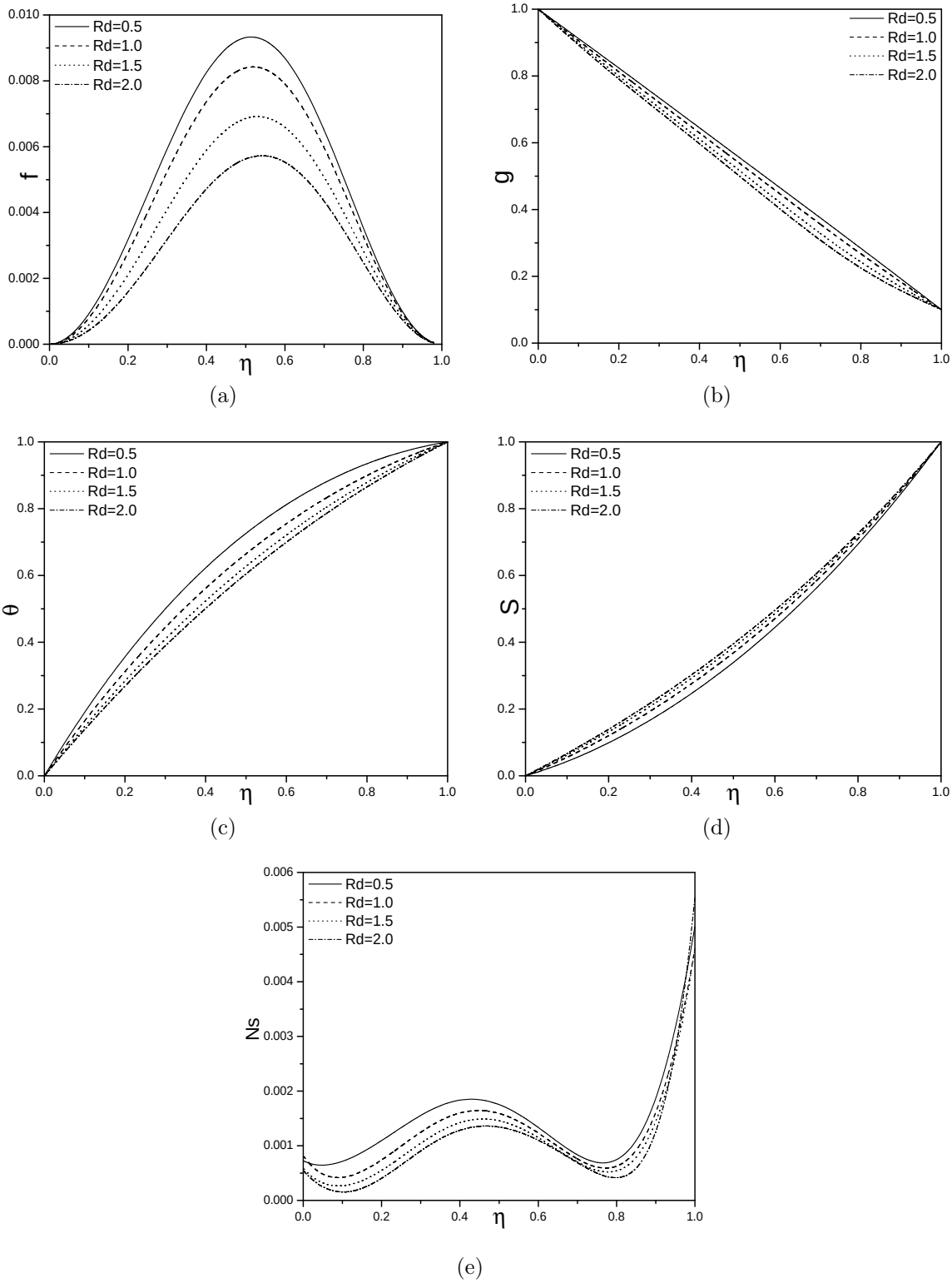

Figure 9.2: "Effect of *Rd* on (a) axial velocity, (b) tangential velocity, (c) temperature, (d) nanoparticle concentration and (e) entropy generation".

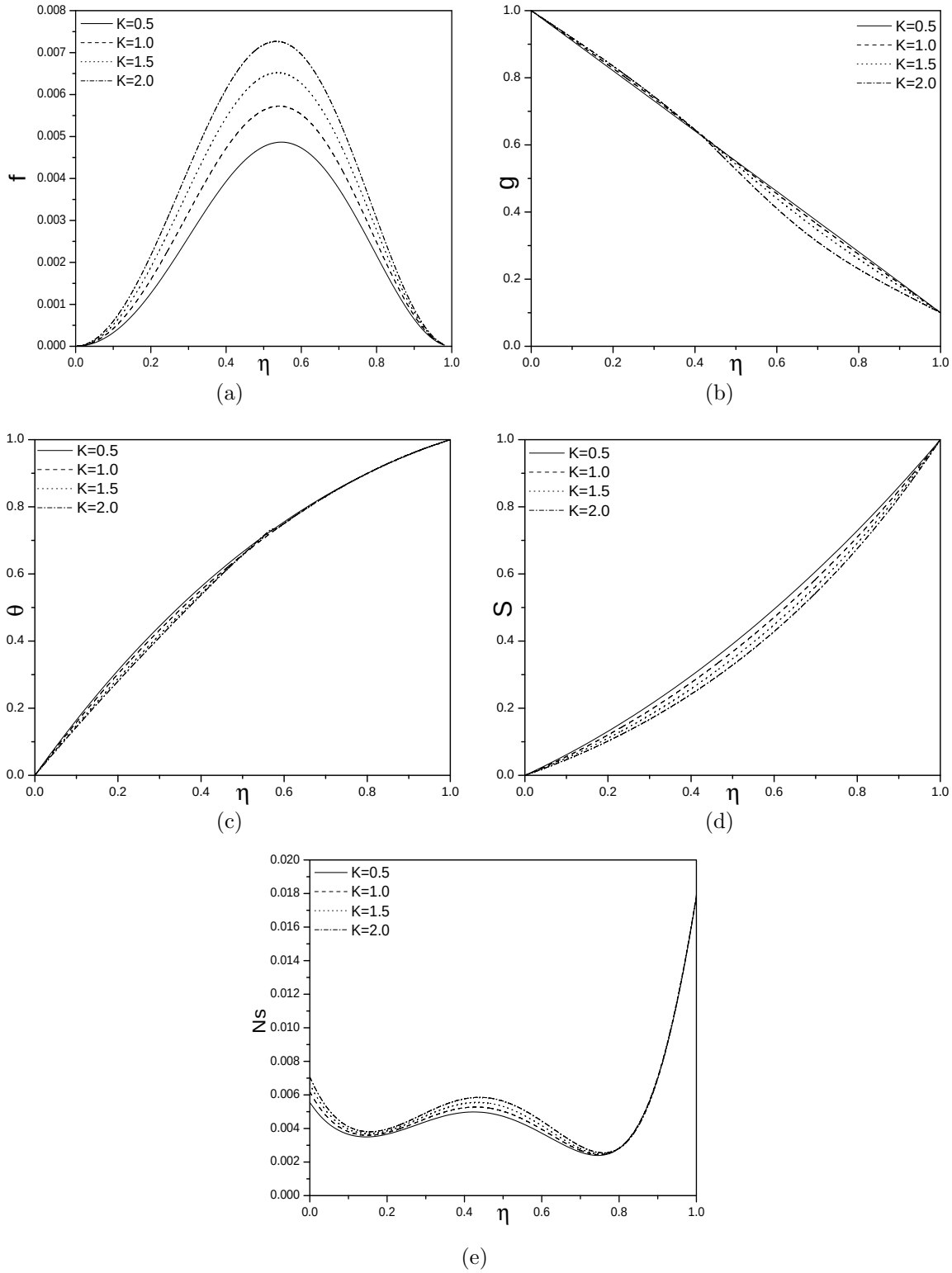

Figure 9.3: "Effect of K on (a) axial velocity, (b) tangential velocity, (c) temperature, (d) nanoparticle concentration and (e) entropy generation".

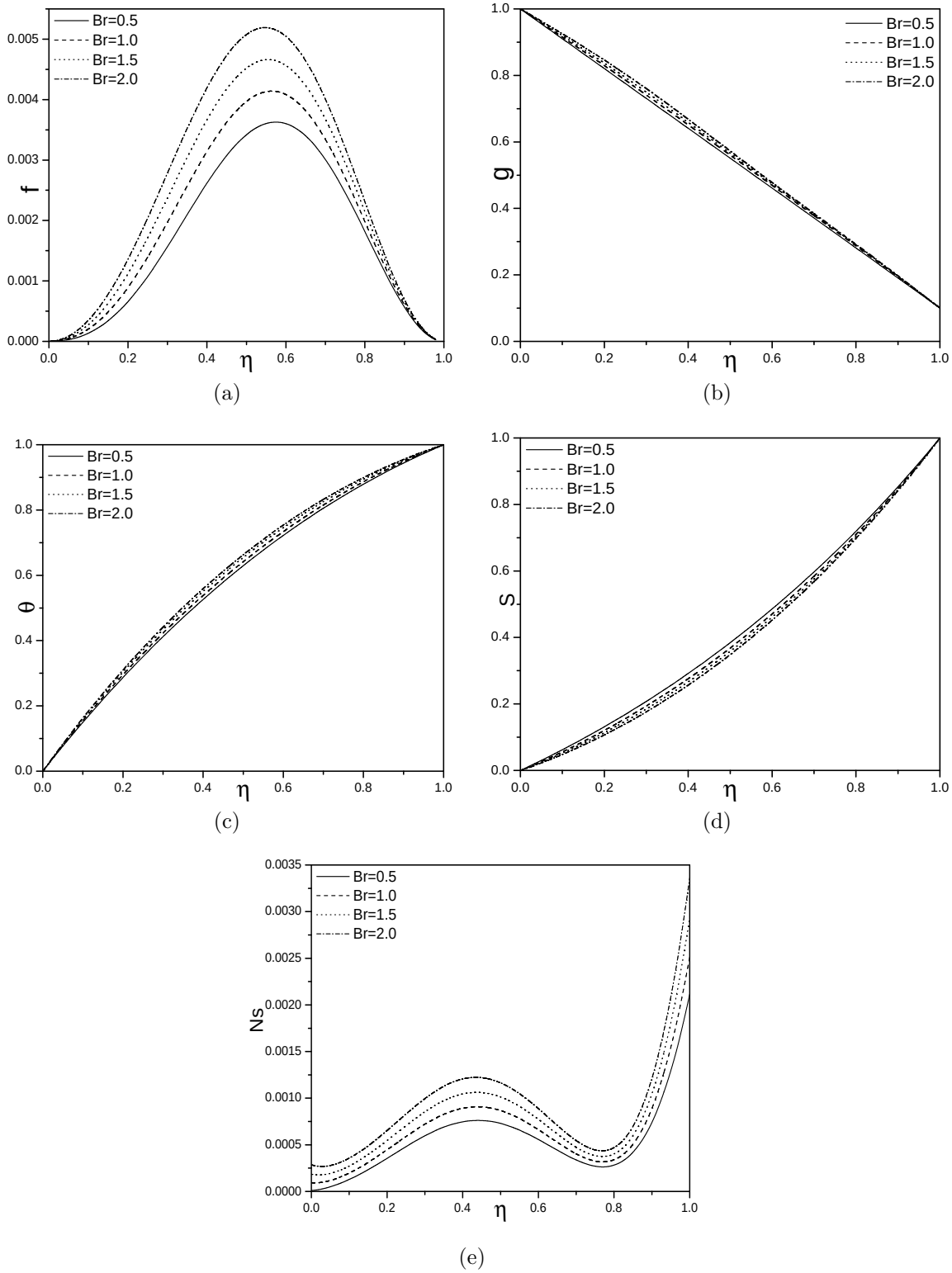

Figure 9.4: "Effect of Br on (a) axial velocity, (b) tangential velocity, (c) temperature, (d) nanoparticle concentration and (e) entropy generation".

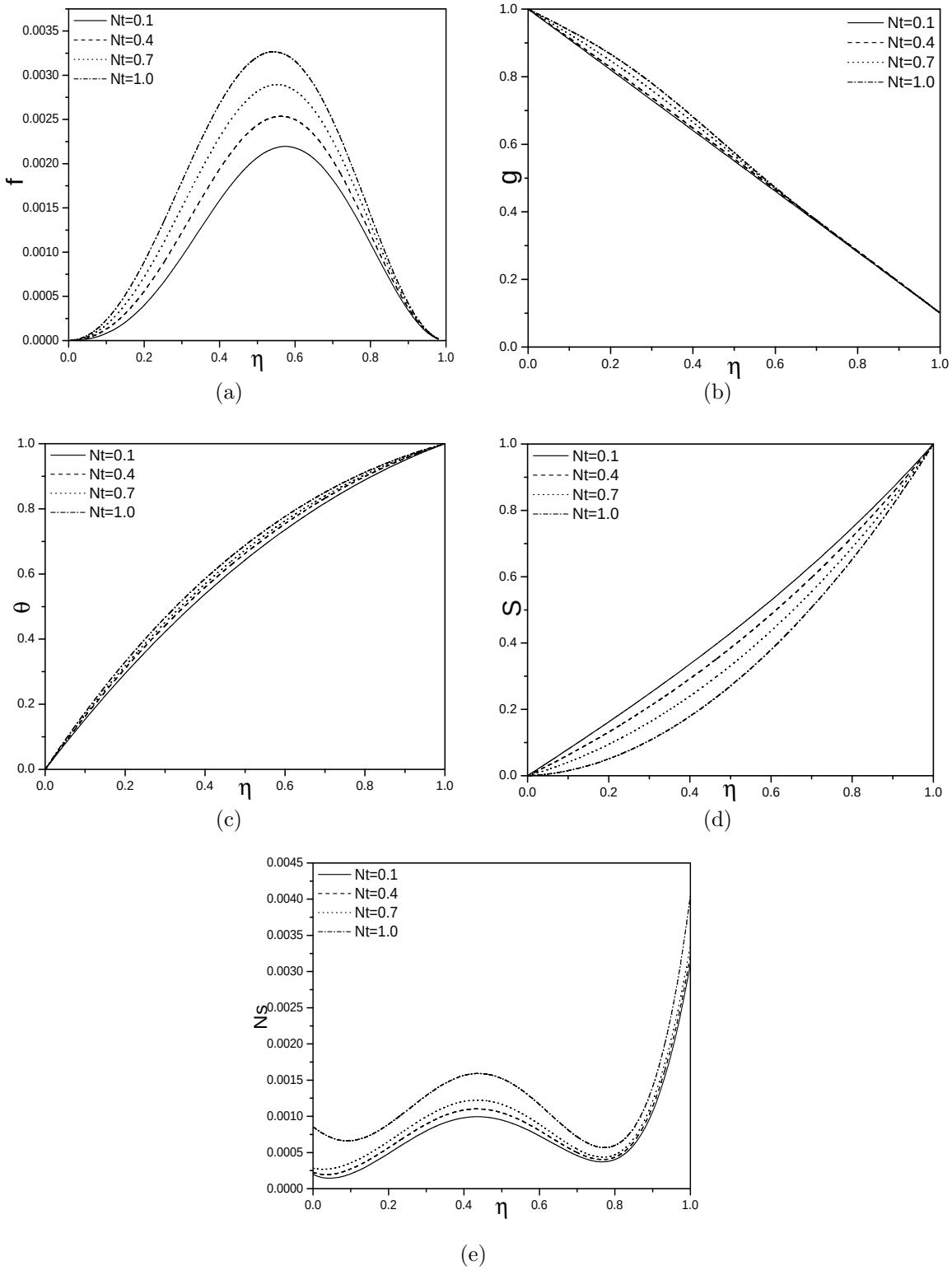

Figure 9.5: "Effect of Nt on (a) axial velocity, (b) tangential velocity, (c) temperature, (d) nanoparticle concentration and (e) entropy generation".

9.6 Conclusions

In this chapter, the entropy generation in a mixed convective chemically reacting nanofluid flow between the horizontal parallel infinite coaxial disks have been investigated by considering the effects of radiation and Brinkman number. The non-dimensional nonlinear equations are solved using HAM method. The main conclusions are given below

With an increase in radiation parameter Rd, the tangential velocity, axial velocity, temperature and the entropy generation decrease, but nanoparticle concentration increases. The axial velocity and the entropy generation increase, whereas the tangential velocity, temperature and nanoparticle concentration decrease with an enhancement in chemical reaction parameter. As Brinkman number and thermophoresis parameters increase, the axial, tangential velocity, temperature and the entropy generation increase, whereas the nanoparticle concentration decreases.

Part V

SUMMARY AND CONCLUSIONS

Chapter 10

Summary and Conclusions

In this thesis, the steady, laminar convective flow of an incompressible nanofluid and the entropy generation under the influence of transverse magnetic field through vertical channel, concentric cylinders and parallel discs is studied. The entropy generation rate and Bejan number are calculated numerically. Nanofluids are studied because of their heat transfer properties, they enhance thermal conductivity and convective properties over the properties of the base fluid.

The steady convective flow and the entropy generation of nanofluid in vertical channel has been investigated in part-II. The aim of this part is to analyze the effects of magnetic parameter, Hall, ion-slip, Joule heating, radiation and chemical reaction parameter on the velocity in flow direction, temperature, nanoparticle concentration, These findings are used to compute the entropy generation and Bejan number in a vertical channel. The governing equations and the corresponding boundary conditions are changed into a dimensionless form using suitable transformations. The obtained system of equations is then solved using the Homotopy Analysis method (HAM). The main findings of the analysis carried in part-II are

- As the Hall parameter increases, the dimensionless temperature and velocity in the flow direction increase, whereas the induced flow velocity decreases, but the nanoparticle concentration increases in case of natural convection, whereas it decreases in the case of mixed convection.
- The dimensionless temperature and velocity in the flow direction increase, but the nanoparticle concentration and the flow velocity in z-direction decrease as ion-slip parameter increases.

- With an increase in the magnetic parameter, the velocity in flow direction and temperature decrease, whereas the velocity in z-direction increases, whereas the nanoparticle concentration increases in case of natural convection and decreases in case of mixed convection.
- The dimensionless velocity and temperature increase, whereas the nanoparticle concentration and the entropy generation decrease with a rise in thermal-radiation.
- As the Joule heating parameter increases, the dimensionless temperature, velocity and the entropy generation increase, but the nanoparticle concentration decreases.
- The dimensionless velocity, temperature and the entropy generation increase, whereas the nanoparticle concentration decreases with a rise in chemical reaction parameter K.

Part-III deals with free and mixed convective flow of nanofluid passing through the annulus between two concentric cylinders in the presence of a magnetic field. Studying the effects of Hall, ion-slip, Joule heating, radiation and chemical reaction parameter on the velocity in flow direction, temperature, nanoparticle concentration are the objectives of this section. The important observations from these investigations are

- As the Hall parameter increases, the dimensionless temperature decreases whereas the velocity and nanoparticle concentration increase.
- The dimensionless temperature decreases, but the nanoparticle concentration and the velocity in flow direction increase as ion-slip parameter increases.
- As an increase in the magnetic parameter, the velocity in flow direction, nanoparticle concentration decrease, whereas the temperature increases.
- The dimensionless velocity and temperature decrease, whereas the nanoparticle concentration and entropy generation increase with a rise in thermal radiation Rd.
- As the Joule heating parameter increases, the dimensionless temperature, velocity and entropy generation increase, whereas the nanoparticle concentration decreases.
- The dimensionless velocity and Bejan number are found to be increasing, whereas the temperature, nanoparticle concentration and the entropy generation are decreasing with a rise in chemical reaction K.

In Part-IV, the entropy generation in a mixed convective electrically conducting nanofluid flow between the horizontal parallel infinite coaxial disks has been investigated by considering the effects of Joule, radiation, chemical reaction, Hall and ion-slip parameters. The non-dimensional nonlinear equations are solved using HAM procedure. The main conclusions figure below

- With an increment in Hall current, the tangential velocity, axial velocity, temperature and the entropy generation increase, but the nanoparticle concentration decreases. The axial velocity, temperature and the nanoparticle concentration increase, whereas the tangential velocity decreases as ion-slip increases.

- The axial velocity, temperature and the entropy generation increase, whereas the tangential velocity and nanoparticle concentration decrease with a rise in relative rotating rate parameter γ. The tangential, axial velocities, temperature and the entropy generation increase, whereas nanoparticle concentration decreases with a rise in Joule heating parameter J.

- As an increment in radiation, the tangential velocity, axial velocity, temperature and the entropy generation decrease, but the nanoparticle concentration increases. The axial velocity and entropy generation increase, whereas the tangential velocity, temperature and nanoparticle concentration decrease as chemical reaction increases.

- The maximum values of Bejan number Be are observed at the end point of the disks due to more contribution of heat transfer irreversibility on entropy generation Ns and minimum value at the center of the disks due to more contribution of the fluid friction irreversibility on the entropy generation Ns with an enhancement of $Ha, \beta h, Nt, \gamma$ and J.

The work presented in the thesis can be extended to analyze the effect of heat and mass transfer, viscosity variation and it can also be extended to study the effect of porosity variation, effect of wall channeling, effect of stratification, double diffusion, conjugate convection etc. In this thesis, we have used nanofluid model. These problems can be extended to other fluid models like Jeffery fluid, micropolar fluid, viscoelastic fluid model, etc. Such an exhaustive study can be a rewarding experience though it is challenging as well as time consuming.

Bibliography

[1] G. M. Abdel-Rahman. Thermal radiation and unsteady magnetohydrodynamic flow of nanofluid in stretching porous medium. *Journal of Thermophysics and Heat Transfer.*, 27:142–150, 2013.

[2] E. Abu-Nada. Application of nanofluids for heat transfer enhancement of separated flows encountered in a backward facing step. int j heat fluid flow. *Transp Porous Med.*, 29:242–249, 2008.

[3] H. A. Agha, M. N. Bouaziz, and S. Hanini. Free convection boundary layer flow from a vertical flat plate embedded in a darcy porous medium filled with a nanofluid: Effects of magnetic field and thermal radiation. *Arab. J. Sci. Eng.*, 39:8331–8340, 2014.

[4] G. Anand, R. J. Vasumathi and J. Mounica. Joule heating and thermal radiation effects on mhd boundary layer flow of a nanofluid over an exponentially stretching sheet in a porous medium. *World Journal of Mechanics*, 5:151–164, 2015.

[5] A.M. Ashorynejad, H.R. Abdulmajeed and S. Mohsen. Mixed convection in cylindrical annulus with rotating outer cylinder and constant magnetic field with an effect in the radial direction. *Scientia Iranica*, 64:240–250, 2013.

[6] M.E.H. Assad and H.F. Oztop. Parametric study of entropy generation in a fluid with internal heat generation between two rotating cylinders subjected to convective cooling at the surface. *ISRN Chemical Engineering*, 2012:1–9, 2012.

[7] M. Azimi and R. Riazi. Heat transfer analysis of go-water nanofluid flow between two parallel disks. *Propulsion and Power Research*, 4:23–30, 2015.

[8] A. C. Baytas. Entropy generation for natural convection in an inclined porous cavity. *International Journal of Heat and Mass Transfer*, 43:2089–2099, 2000.

[9] A. Bejan. A study of entropy generation in fundamental convective heat transfer. *Journal of Heat Transfer*, 101:718–725, 1979.

[10] A. Bejan. Second law analysis in heat transfer. *Energy*, 5(8):720–732, 1980.

[11] A. Bejan. Second law analysis in heat transfer and thermal design. *Advances in Heat Transfer*, 15:1–58, 1982.

[12] A. Bejan. *Entropy Generation Minimization*. CRC Press, New York, 1996.

[13] J. Buongiorno. Convective transport in nanofluids. *ASME J. Heat Transfer.*, 128:240–250, 2006.

[14] A. J. Chamkha, S. Abbasbandy, A. M. Rashad, and K. Vajravelu. Radiation effect on mixed convection about a cone embedded in a porous medium filled with a nanofluid. *Meccanica.*, 48:275–285, 2013.

[15] S. K. Chamkha, A. J. Jena and S. K. Mahapatra. Mhd convection of nanofluids: A review. *Journal of Nanofluids,*, 4:271 – 292, 2015.

[16] D. S. Chauhan and V. Kumar. Entropy analysis for third-grade fluid flow with temperature-dependent viscosity in annulus partially filled with porous medium. *Theoretical and Applied Mechanics*, 40:441–464, 2013.

[17] B. S. Chen and C.C. Liu. Heat transfer and entropy generation in fully-developed mixed convection nanofluid flow in vertical channel. *International Journal of Heat and Mass Transfer*, 79:750–758, 2014.

[18] C.-K. Chen, Y.-T. Yang, and K.-H. Chang. Entropy generation of radiation effect on laminar-mixed convection along a wavy surface. *Heat and Mass Transfer.*, 47:385–395, 2011.

[19] S. Chen, Z. Liu, S. Bao, and C. Zheng. Natural convection and entropy generation in a vertically concentric annular space. *International Journal of Thermal Sciences*, 49:2439–2452, 2010.

[20] H. S. Cheng, C.H. Kou and Huang. W. H. Flow reversal and heat transfer of fully developed mixed convection in vertical channels. *J. Thermophys Heat Transfer*, 4:375–383, 1990.

[21] S. U. S. Choi. *Enhancing thermal conductivity of fluids with nanoparticles.* American Society of Mechanical Engineers, New York, 1995.

[22] S. Das, A. S. Banu, R. N. Jana, and O. D. Makinde. Entropy analysis on mhd pseudo-plastic nanofluid flow through a vertical porous channel with convective heating. *Alexandria Engineering Journal*, 54:325–337, 2015.

[23] S. K. Das, S. U. S. Choi, W. Yu, and T. Pradeep. *Nanofluids: Science and Technology.* Wiley Interscience, New Jersey, 2007.

[24] W. Daungthongsuk and S. Wongwises. A critical review of convective heat transfer nanofluids. *Renewable and Sustainable Energy Reviews*, 11:797–817, 2007.

[25] D. Dehsara, M. Nemat and R.H.N. Mohammad. Numerical analysis of entropy generation in nanofluid flow over a transparent plate in porous medium in presence of solar radiation, viscous dissipation and variable magnetic field. *Journal of Mechanical Science and Technology*, 28:1819–1831, 2014.

[26] P. Dulal and T. Babulal. Combined effects of joule heating and chemical reaction on unsteady magneto hydrodynamic mixed convection of a viscous dissipating fluid over a vertical plate in porous media with thermal radiation. *Mathematical and Computer Modelling*, 54, 2011.

[27] J. A. Eastman, S. U. S. Choi, S. Li, W. Yu, and L. J. Thompson. Anomalously increased effective thermal conductivities of ethylene glycolbased nanofluids containing copper nanoparticles. *Appl. Phys. Lett.*, 878:718–720, 2001.

[28] A. S. Eegunjobi and O. Makinde. Entropy generation analysis in transient variable viscosity couette flow between two concentric pipes. *Journal of Thermal Science and Technology*, 9, 2014.

[29] A. S. Eegunjobi and O. D. Makinde. Combined effect of buoyancy force and navier slip on entropy generation in a vertical porous channel. *Entropy*, 14:1028–1044, 2012.

[30] S. M. M. El-Kabeir, A. J. Chamkha, and A. M. Rashad. Effect of thermal radiation on non-darcy natural convection from a vertical cylinder embedded in a nanofluid porous media. *J. Porous Med.*, 17:269–278, 2014.

[31] A. C. Eringen. Zhang, j. k., li,b. w. and chen, y. y. *The Joule Heating Effects on Natural Convection of Participating Magnetohydrodynamics Under Different Levels of Thermal Radiation in a Cavity,*, 137:1–10, 2015.

[32] J. A. Esfahani and P. B. Shahabi. Effect of non-uniform heating on entropy generation for the laminar developing pipe flow of a high prandtl number fluid. *Energy Conversion and Management*, 51:2087–2097, 2010.

[33] Yu. Feng and C. Kleinstreuer. Nanofluid convective heat transfer in a parallel-disk system. *International Journal of Heat and Mass Transfer*, 53:4619–4628, 2010.

[34] H. Fersadou, I. Kahalerras and M. El Ganaoui. Mhd mixed convection and entropy generation of a nanofluid in a vertical porous channel. *Computers and Fluids*, 121:164–179, 2015.

[35] D. D. Ganji, H. R. Ashory Nezhad, and A. Hasanpour. Effect of variable viscosity and viscous dissipation on the hagen-poiseuille flow and entropy generation. *Numerical Methods for Partial Differential Equations*, 27:529–540, 2009.

[36] T. Grosan and I. Pop. Fully developed mixed convection in a vertical channel filled by a nanofluid. *J. Heat Transfer*, 134:482–501, 2012.

[37] E.P. Gyftopoulos and G.P. Beretta. Studied the entropy generation rate in a chemically reacting system. *Journal of Egy Resources Tech.,*, 115, 1993.

[38] O.M. Haddad, M.K. Alkam, and M.T. Khasawneh. Entropy generation due to laminar forced convection in the entrance region of a concentric annulus. *Energy*, 29:35–55, 2004.

[39] F. M. Hady, F. S. Ibrahim, S. M. Abdel-Gaied, and M. R. Eid. Radiation effect on viscous flow of a nanofluid and heat transfer over a nonlinearly stretching sheet. *Nanoscale Res. Lett.*, 7:1–13, 2012.

[40] F. Hang, X. Tao and I. Pop. Analysis of mixed convection flow of a nanofluid in a vertical channel with the buongiorno mathematical model. *International Communications in Heat Mass Transfer*, 44:15–22, 2013.

[41] X. Hang and I. Pop. Fully developed mixed convection flow in a vertical channel filled with nanofluids. *International Communications in Heat Mass Transfer*, 39:1086–1092, 2012.

[42] J. Hartmann and F. Lazarus. Theory of the laminar flow of an electrically conductive liquid in a homogeneous magnetic field. *Kgl. Danske Videnskab. Selskab.Mat-Fys Medd.*, 15:1–28, 1937.

[43] M. Hatami and D. D. Ganji. Heat transfer and nanofluid flow in suction and blowing process between parallel disks in presence of variable magnetic field. *J. Mol. Liq.*, 190:159 – 168, 2014.

[44] H. Heidary, M. Pirmohammadi, and M. Davoudi. Control of free convection and entropy generation in inclined porous media. *Heat Transfer Engineering*, 33:565–573, 2012.

[45] H. Imen, Ch. Nejib and B.B. Ammar. entropy generation analysis of a chemical reaction process. *J. of Heat and Transfer*, 136, 2014.

[46] S. Lee, S. U. S. Choi, and J. A. Eastman. Measuring thermal conductivity of fluids containing oxide nanoparticles. *ASME J. Heat Transfer.*, 121:280–289, 1999.

[47] S.J. Liao. *Beyond Perturbation Introduction to the Homotopy Analysis Method*. Chapman and Hall-CRC Press, Boca Raton, 2003.

[48] S.J. Liao. On the homotopy analysis method for nonlinear problems. *Appl. Math. Comput.*, 147:499 – 513, 2004.

[49] S.J. Liao. An optimal homotopy-analysis approach for strongly nonlinear differential equations. *Commun. Nonlinear Sci. Numer. Simulat.*, 15:200–316, 2010.

[50] S.J. Liao. *Advances in the Homotopy Analysis Method*. World Scientific Publishing Company, Singapore, 2013.

[51] C. C. Liu and C. Y. Lo. Numerical analysis of entropy generation in mixed-convection mhd flow in vertical channel. *International Communications in Heat and Mass Transfer*, 39:1354–1359, 2012.

[52] Kothandapani M. and Prakash J. Effects of thermal radiation and chemical reactions on peristaltic flow of a newtonian nanofluid under inclined magnetic field in a generalized vertical channel using homotopy perturbation method. *Asia-Pac. J. Chem. Eng.*, 10:259–272, 2015.

[53] O. Mahian, S. Mahmud, and S. Z. Heris. Analysis of entropy generation between co-rotating cylinders using nanofluids. *Energy*, 44:438–446, 2012.

[54] O. Mahian, S. Mahmud, and S. Wongwises. Entropy generation between two rotating cylinders with magnetohydrodynamic flow using nanofluids. *Journal of Thermophysics and Heat Transfer*, 27:161–169, 2012.

[55] O. Mahian, I. Pop, A. Z. Sahin, H. F. Oztop, and S. Wongwises. Irreversibility analysis of a vertical annulus using tio 2/water nanofluid with mhd flow effects. *International Journal of Heat and Mass Transfer*, 64:671–679, 2013.

[56] J. C. Maxwell. *Treatise on Electricity and Magnetism*. Clarendon Press, Oxford, 1873.

[57] A. Mazgar, F. Ben Nejma, and K. Charrada. Second law analysis of coupled mixed convection and non-grey gas radiation within a cylindrical annulus. *International Journal of Mathematical models and methods in applied sciences*, 7:265–276, 2013.

[58] M. H. Mkwizu and O. D. Makinde. Entropy generation in a variable viscosity channel flow of nanofluids with convective cooling. *Comptes Rendus Mecanique*, 343:38–56, 2015.

[59] R. Motsa, S. S. Nandkeolyar and P. Sibanda. Viscous and joule heating in the stagnation point nanofluid flow through a stretching sheet with homogenousheterogeneous reactions and nonlinear convection. *Journal of Nanotechnology in Engineering and Medicine*, 4:1–9, 2013.

[60] H.R. Mozayyeni and A.B. Rahimi. Mixed convection in cylindrical annulus with rotating outer cylinder and constant magnetic field with an effect in the radial direction. *Scientia Iranica*, 19:91105, 2012.

[61] G. Mridulkumar. Effects of chemical reaction on mhd boundary layer flow over an exponentially stretching sheet with joule heating and thermal radiation. *International Research Journal of Engineering and Technology*, 2:768–773, 2015.

[62] K. Clement K. AlNimr M.A. Ioan P. Sahin A.Z. Omid, M. Ali and W. Somchai. A review of entropy generation in nanofluid flow. *International Journal of Heat and Mass Transfer*, 65:514–532, 2013.

[63] S. Omid, M. Mahmud and Z.H. Saeed. Analysis of entropy generation between co-rotating cylinders using nanofluids. *Energy*, 44:438–446, 2012.

[64] M. Poulomi, De. Hiranmoy and B. Uttamkumar. Effects of mixed convective flow of a nanofluid with internal heat generation, thermal radiation and chemical reaction. *Journal of Nanofluids*, 4:375–384, 2015.

[65] D. Ramakrishna, T. Basak, S. Roy, and E. Momoniat. Analysis of thermal efficiency via analysis of heat flow and entropy generation during natural convection within porous trapezoidal cavities. *International Journal of Heat and Mass Transfer*, 77:98–113, 2014.

[66] M. M. Rashid and N. F. Mehr. Effects of velocity slip and temperature jump on the entropy generation in magnetohydrodynamic flow over a porous rotating disk. *Journal of Mechanical Engineering*, 1:4–14, 2005.

[67] M. M. Rashidi, N. Kavyani, and S. Abelman. Investigation of entropy generation in mhd and slip flow over a rotating porous disk with variable properties. *International Journal of Heat and Mass Transfer*, 70:892–917, 2014.

[68] M.M. Munawwar A. A. Rashidi, M.M. Bhatti and M.E.S. Ali. Entropy generation on mhd blood flow of nanofluid due to peristaltic waves. *Entropy*, 18, 2016.

[69] H. Saleh, H. Ishak and S. Basriati. Flow reversal of fully developed mixed convection in a vertical channel with chemical reaction. *International Journal of Chemical Engineering*, 2013.

[70] M. Hayat T. Shehzad, S.A. Waqas and A. Alsaedi. A model of solar radiation and joule heating in magnetohydrodynamic(mhd) convective flow of thixotropic nanofluid. *Journal of Molecular Liquids*, 215:704–710, 2016.

[71] M. Sheikholeslami and S. Abelman. Two-phase simulation of nanofluid flow and heat transfer in an annulus in the presence of an axial magnetic field. *IEEE Transactions on Nanotech.*, 14:561569., 2015.

[72] M. Sheikholeslami and D.D. Ganji. Unsteady nanofluid flow and heat transfer in presence of magnetic field considering thermal radiation,. *J Braz. Soc. Mech. Sci. Eng.*, 37:895–902, 2015.

[73] H. Sheikhzadeh, G. A. Teimouri and M. Mahmoodi. Numerical study of mixed convection of nanofluid in a concentric annulus with rotating inner cylinder. *Trans. Phenom. Nano Micro Scales*, 1:26–36, 2013.

[74] K. D. Sinha and R. C. Chaudhary. Viscous incompressible flow between two coaxial rotating porous cylinders. *Proc. Nat. Inst. Sci.*, 32:81–88, 1966.

[75] C.Y. Soong. Theoretical analysis for axisymmetric mixed convection between rotating coaxial disks. *Int. J. Heat Mass Transfer*, 39:1569–1583, 1996.

[76] E. M. Sparrow and RD. Cess. *Radiation Heat Transfer,*. DC: Hemisphere, Washington, 1978.

[77] D. Srinivasacharya and K. Himabindu. Entropy generation due to micropolar fluid flow between concentric cylinders with slip and convective boundary conditions. *Ain Shams Engineering Journal*, 2016.

[78] D. Srinivasacharya and K. Kaladhar. Analytical solution of mhd free convective flow of couple stress fluid in an annulus with hall and ion-slip effects. *Nonlinear Analysis:Modelling and Control*, 16:477–487, 2011.

[79] D. Srinivasacharya and K. Kaladhar. Analytical solution of mixed convection flow of couple stress fluid between two circular cylinders with hall and ion-slip effects. *Turkish. J. Eng. Environ. Sci.*, 36:226235, 2012.

[80] D. Srinivasacharya and K. Kaladhar. Mixed convection flow of couple stress fluid between parallel vertical plates with hall and ion-slip effects. *Commun Nonlinear Sci Numer Simulat*, 17:2447–2462, 2012.

[81] D. Srinivasacharya and K. Kaladhar. Analytical solution for hall and ion-slip effects on mixed convection flow of couple stress fluid between parallel disks. *Mathematical and Computer Modelling*, 57:2494–2509, 2013.

[82] D. Srinivasacharya and P. Vijaykumar. Mixed convection over an inclined wavy surface in a nanofluid saturated non-darcy porous medium with radiation effect. *International Journal of Chemical Engineering*, 2015.

[83] G.W. Sutton and A. Sherman. *Engineering Magnetohydrodynamics*. McGraw-Hill, New Yark, 1965.

[84] R. Ellahi T. Hayat and S. Asghar. Hall effect on the unsteady flow due to noncoaxially rotating disk and fluid at infinity. *Chem. Eng. Commun.*, 195:1–19, 2008.

[85] K. Takahashi and R. Alkire. Mass transfer in gas-sparged porous electrodes. *Chem. Eng. Commun.*, 38:209–227, 1985.

[86] I. Tani. Steady flow of conducting fluids in channels under transverse magnetic fields with consideration of hall effects. *Journal of Aerospace Science*, 29:297–305, 1962.

[87] S.H. Tasnim and S. Mahmud. Entropy generation in a vertical concentric channel with temperature dependent viscosity. *International Communications in Heat and Mass Transfer*, 39:907–918, 2002.

[88] R. K. Tiwari and M. K. Das. Heat transfer augmentation in a two-sided lid-driven differentially heated square cavity utilizing nanofluids. *Int. J. Heat Mass Transf.*, 50:2002–2018, 2007.

[89] T. Kazi S.N. Badarudin A. Kadhum A.A.H. Togun, H. Abdulrazzaq and E. Sadeghinezhad. A review of studies on forced, natural and mixed heat transfer to fluid and nanofluid flow in an annular passage. *Renewable and Sustainable Energy Reviews*, 39:835–856, 2014.

[90] D. J. Tritton. *Physical Fluid Dynamics*. Van Nostrand Reinhold(U.K.), England, 1985.

[91] M. S. Tshehla and O. D. Makinde. Analysis of entropy generation in a variable viscosity fluid flow between two concentric pipes with a convective cooling at the surface. *International Journal of Physical Sciences*, 6:6053–6060, 2011.

[92] M. Turkyilmazoglu. Numerical and analytical solutions for the flow and heat transfer near the equator of an mhd boundary layer over a porous rotating sphere. *Int. J. Therm. Sci.*, 50:831–842, 2011.

[93] M. Turkyilmazoglu. Some issues on hpm and ham methods: A convergence scheme. *Mathematical and Computer Modelling*, 53:1929–1936, 2011.

[94] M. Turkyilmazoglu and I. Pop. Heat and mass transfer of unsteady natural convection flow of some nanofluids past a vertical infinite flat plate with radiation effect. *Int. J. Heat Mass Transfer.*, 59:167–171, 2013.

[95] X. Wang, X. Xu and S. U. S. Choi. Thermal conductivity of nanoparticle-fluid mixture. *Journal of Thermophysics and Heat Transfer*, 13:474–480, 1999.

[96] G. P. Williams. Thermal convection in a rotating fluid annulus: part 1. the basic axisymmetric flow. *J. Atmos. Sci.*, 24:144–161, 1967.

[97] G. P. Williams. Thermal convection in a rotating fluid annulus: part 2. classes of axisymmetric. *J. Atmos. Sci.*, 24:162–174, 1967.

[98] B. S. Yilbas, M. Yurusoy, and M. Pakdemirli. Entropy analysis for non-newtonian fluid flow in annular pipe: constant viscosity case. *Entropy*, 6:304–315, 2004.